

# **MONOTONIC AND CYCLIC SHEAR LOADING RESPONSE OF NATURAL SILTS**

by

Achala Nishan Soysa

B.Sc. Eng. (Hons), University of Moratuwa, 2009

M.Sc., University of Moratuwa, 2011

A THESIS SUBMITTED IN PARTIAL FULFILLMENT OF

THE REQUIREMENTS FOR THE DEGREE OF

MASTER OF APPLIED SCIENCE

in

THE FACULTY OF GRADUATE AND POSTDOCTORAL STUDIES

(Civil Engineering)

THE UNIVERSITY OF BRITISH COLUMBIA

(Vancouver)

March 2015

© Achala Nishan Soysa, 2015

## **Abstract**

An experimental research program comprising constant-volume direct simple shear (DSS) tests was conducted to study the monotonic, cyclic shear and post cyclic consolidation response of natural silts. Relatively undisturbed samples of silt which were obtained from three different locations in the Lower Mainland area of British Columbia were used for this purpose. Plasticity indices of the natural silt samples which were considered for the study were 5, 7, and 34.

Monotonic shear response of the natural silt was studied with the constant volume DSS test results that were conducted with different vertical effective stresses and different over-consolidation ratios (OCRs). Stress-strain response of normally consolidated silt at different consolidation stresses were found to be stress-history-normalizable where as higher OCR and higher plasticity resulted greater shear strength.

Normally consolidated silt specimen, despite of their difference plasticity, exhibit gradual strain accumulation without abrupt loss of shear stiffness during cyclic loading with different cyclic stress ratios (CSRs) at different consolidation stress levels. The potential and rate of strain accumulation and development of excess pore-water pressure ( $\Delta u$ ) were noted to be increased with higher CSRs at all tested consolidation stress levels. The cyclic shear resistances of silt, derived from cyclic direct simple shear (CDSS) tests, were not sensitive to the tested range of different consolidation stress levels, whereas higher plasticity resulted greater cyclic shear resistance. Relative undisturbed specimens exhibit comparatively higher cyclic shear resistance

than the reconstituted specimens despite of comparatively denser particle arrangement in reconstituted specimens. However, during the constant-volume monotonic DSS tests, relative undisturbed specimens exhibit comparatively lesser shear resistance than the reconstituted specimens implying that soil fabric / microstructure plays a significant role in governing the shear loading response of silt.

The examination of consolidation responses of silt specimens that were initially normally consolidated and subjected to constant-volume CDSS loading revealed that the post cyclic consolidation volumetric strain increases with the maximum cyclic pore-water pressure ratio developed during constant volume CDSS loading for all tested silt specimens with different plasticity.

## **Preface**

I was involved in soil sample retrieval process and conducted all the tests in the laboratory experimental program in this research project. Further, I am responsible for the data collection, analysis and manuscript preparation. Dr. Wijewickreme was the supervisory author and involved in formation of concept during the conductance of experiments, organizing the content and final editing of the manuscript. Three publications arising from this research are detailed below.

Version of parts in chapter 2, 3 and 4 has been published at 2014 Canadian Geotechnical Society annual conference.

Soysa, A., & Wijewickreme D. (2014) Some observations on the cyclic shear response of natural silt with increasing coarse-grained fraction, In proceedings of the 67th Canadian Geotechnical Conference, Sep 29 – Oct 1, 2014, Regina, Saskatchewan.

It is noteworthy to acknowledge the presentation of previously published data and results extracted from other sources in following figures:

For the illustration purpose of soil response, figures from Kuerbis (1989), Vaid & Chern (1985) and Andersen (2009) are reproduced and presented in Figure 2.1, Figure 2.2 and Figure 2.3 respectively for the discussion under literature review. Similarly Figure 2.4 presents data from Sanin (2010) and Figure 2.5 comprises data from Sanin (2010) and Seidalinova (2014) for the purpose of comparison of cyclic shear resistance.



In Figure 3.10, location details of the soil sample collection are overlaid on top a Google map section of Lower Mainland area of British Columbia.

In Figure 4.37, data points obtained from the current study are plotted with the results from Sanin (2010); Sivathayalan (1994); Sriskandakumar (2004) for comparison purposes. Further, Figure 4.42, Figure 4.49 and Figure 4.54 comprise data from the current study and those reported by Sanin (2005, 2010).

All the figures were prepared by the current author with the results obtained from publication from aforementioned researchers reproduced accordingly.

## Table of Contents

<b>Abstract.....</b>	<b>ii</b>
<b>Preface.....</b>	<b>iv</b>
<b>Table of Contents .....</b>	<b>vi</b>
<b>List of Tables .....</b>	<b>x</b>
<b>List of Figures.....</b>	<b>xi</b>
<b>List of Symbols .....</b>	<b>xxiii</b>
<b>List of Abbreviations .....</b>	<b>xxv</b>
<b>Acknowledgements .....</b>	<b>xxvii</b>
<b>Dedication .....</b>	<b>xxviii</b>
<b>Chapter 1: Introduction .....</b>	<b>1</b>
1.1    Background .....	1
1.2    Objective of the Thesis .....	3
1.3    Organization of the Thesis .....	4
<b>Chapter 2: Literature Review.....</b>	<b>6</b>
2.1    Mechanical Response of Sand .....	7
2.2    Mechanical Response of Clay.....	11
2.3    Mechanical Response of Fine-grained Soils (Silt and Fine-grained Tailings) .....	14
2.4    Soil Response and Laboratory Experimental Tests .....	19
2.5    Assessment of Liquefaction Resistance of Soil under Laboratory Conditions.....	20
2.5.1    Overview of Soil Liquefaction.....	20
2.5.2    Criteria for Defining ‘Liquefaction’ and ‘Cyclic Failure’ in Laboratory Tests.....	22

vi



4.1.2	Effect of Over-Consolidation Ratio (OCR) on Monotonic Shear Loading Response..	74
4.1.3	Effect of Coarse-grained Fraction on Monotonic Shear Loading Response .....	79
4.1.4	Effect of Plasticity on Monotonic Shear Loading Response .....	82
4.1.5	Comparison of Monotonic Shear Loading Response of ‘Relatively Undisturbed’ and ‘Reconstituted’ Specimens .....	84
4.2	Cyclic Shear Loading Response .....	89
4.2.1	Cyclic Strain Accumulation and Pore-water Pressure Development .....	90
4.2.2	Typical Cyclic Stress-strain and Stress Path Response .....	91
4.2.3	Effect of Initial Effective Confining Stress .....	94
4.3	Cyclic Shear Resistance .....	100
4.3.1	Effect of Initial Effective Confining Stress on Cyclic Resistance .....	101
4.3.2	Effect of Coarse-grained Fraction on Cyclic Shear Resistance of Fine-grained Soils .	105
4.3.3	Effect of Plasticity on Cyclic Shear Resistance .....	109
4.3.4	Comparison of Cyclic Shear Resistance of ‘Relatively Undisturbed’ and ‘Reconstituted’ Specimens .....	115
4.4	Post-cyclic Consolidation Response .....	125
<b>Chapter 5: Summary and Conclusions .....</b>		<b>129</b>
5.1	Monotonic Shear Loading Response of Natural Silt .....	130
5.2	Cyclic Shear Response of Natural Silt.....	132
5.3	Post-cyclic Consolidation Response of Natural Silt .....	135

5.4	Recommendations for Future Research .....	135
<b>References</b> .....		<b>138</b>
<b>Appendices</b> .....		<b>153</b>

## List of Tables

Table 3.1 Control capacity and measurement resolution of the UBC DSS device.....	34
Table 3.2 Location details of subject sites .....	39
Table 3.3 Soil properties and index parameters.....	48
Table 3.4 Assessment of sampling quality and estimation of pre-consolidation stresses from 1-D consolidation test results .....	50
Table 3.5 Test Program.....	62
Table 4.1 Test parameters and summery of test results .....	64
Table 4.2 Index of Figures for stress path and shear stress-strain curves for silt from the Site #2 .....	94

## List of Figures

Figure 2.1 Characteristics stress-strain and stress-path response of sandy soils during undrained monotonic loading through triaxial tests [reproduced after Kuerbis (1989)] .....	9
Figure 2.2 Typical liquefaction, limited liquefaction and cyclic mobility type response during undrained cyclic loading with associated stress-strain response, stress-path response and strain development [reproduced after Vaid & Chern (1985)].....	10
Figure 2.3 Effective stress paths for undrained tests with monotonic and cyclic loading [reproduced after Andersen (2009)].....	13
Figure 2.4 Effect of confining stress ( $\sigma'_{vc}$ ) and initial static shear ratio ( $\alpha = \tau_{st} / \sigma'_{vc}$ ) on the cyclic resistance of normally consolidated Fraser River Delta silt from constant-volume CDSS tests [reproduced after Sanin (2010)].....	16
Figure 2.5 Comparison of cyclic stress ratio versus number of cycles to reach $\gamma = 3.75\%$ for laterite, copper–gold, copper–gold– zinc tailings and gold tailings [after Sanin (2010) and Seidalinova (2014) ].....	17
Figure 3.1 Main components of the UBC DSS device and DACS.....	28
Figure 3.2 Schematic diagram of UBC DSS device .....	30
Figure 3.3 Schematic of Hoisting / Rigging of Top Platen.....	31

Figure 3.4 Schematic of Horizontal Shaft.....	32
Figure 3.5 Schematic of Specimen Holder and Central Unit.....	33
Figure 3.6 Schematic of Vertical Shaft.....	33
Figure 3.7 GUI of DACS during a typical incremental loading consolidation phase .....	37
Figure 3.8 GUI of DACS during a typical cyclic shearing phase.....	37
Figure 3.9 GUI of DACS during a typical monotonic shearing phase .....	38
Figure 3.10 Locations of subject sites in the Lower Mainland BC over-layer with Map data ©2014 Google.....	40
Figure 3.11 Cone penetration test profiles at Site #1, Vulcan Way, Richmond BC.....	42
Figure 3.12 Cone penetration test profiles at Site #2, 160th Street, Surrey, BC .....	43
Figure 3.13 Cone penetration test profiles at Site #3, Telegraph Street, Surrey, BC .....	44
Figure 3.14 Dimension details of the specially fabricated thin walled samplers with no insider clearance .....	45
Figure 3.15 Conventional rotary mud drilling at Site #1, # 2, and #3 for obtaining relatively undisturbed soil samples .....	46
Figure 3.16 Particle size distribution: Upper and lower bound range of soil gradation curves for Site #1, #2 and #3.....	47



Figure 3.17 Compression characteristics from 1-D consolidation tests .....	50
Figure 3.18 Extrusion of soil specimen from thin-walled steel tube sampler .....	52
Figure 3.19 Preparation of relatively undisturbed specimen .....	52
Figure 3.20 Preparation of reconstituted specimen.....	53
Figure 3.21 Preparation of the DSS device to receive a soil specimen .....	54
Figure 3.22 Placing relatively undisturbed specimen in DSS device .....	55
Figure 3.23 Placing reconstituted specimen in DSS device .....	56
Figure 3.24 Photos of typical specimen state: (A) after the applied seating pressure prior to consolidation phase (B) after monotonic shearing upto approximately 20 % shear strain.....	58
Figure 4.1 Shear stress-strain curves of constant-volume monotonic DSS tests on relatively undisturbed specimens of natural silt retrieved from the Site #1 [Series I-A(a)], Site #2 [Series II-A] and Site #3 [Series III-A] at normally consolidated stress state at varying confining stress levels .....	69
Figure 4.2 Development of excess pore-water pressure with increasing shear strain during constant-volume monotonic DSS tests on relatively undisturbed specimens of natural silt retrieved from the Site #1 [Series I-A(a)], Site #2 [Series II-A] and Site #3 [Series III-A] at normally consolidated stress state at varying confining stress levels .....	70

Figure 4.3 Stress path curves of constant-volume monotonic DSS tests on relatively undisturbed specimens of natural silt retrieved from the Site #1 [Series I-A(a)], Site #2 [Series II-A] and Site #3 [Series III-A] at normally consolidated stress state at varying confining stress levels .... 71

Figure 4.4 Normalized stress path curves of constant-volume monotonic DSS tests on relatively undisturbed specimens of natural silt retrieved from the Site #1 [Series I-A(a)], Site #2 [Series II-A] and Site #3 [Series III-A] at normally consolidated stress state at varying confining stress levels ..... 71

Figure 4.5 Shear stress-strain curves of constant-volume monotonic DSS tests on relatively undisturbed specimens of natural silt retrieved from the Site #1 [Series I-B], Site #2 [Series II-B] and Site #3 [Series III-B] at confining stress levels of OCR 1 (NC), 2 and 4 ..... 75

Figure 4.6 Development of excess pore-water with increasing shear strain during constant-volume monotonic DSS tests on relatively undisturbed specimens of natural silt retrieved from the Site #1 [Series I-B], Site #2 [Series II-B] and Site #3 [Series III-B] at confining stress levels of OCR 1 (NC), 2 and 4 ..... 76

Figure 4.7 Stress path curves of constant-volume monotonic DSS tests on relatively undisturbed specimens of natural silt retrieved from the Site #1 [Series I-B], Site #2 [Series II-B] and Site #3 [Series III-B] at confining stress levels of OCR 1 (NC), 2 and 4 ..... 77

Figure 4.8 Normalized stress path curves of constant-volume monotonic DSS tests on relatively undisturbed specimens of natural silt retrieved from the Site #1 [Series I-B], Site #2 [Series II-B] and Site #3 [Series III-B] at confining stress levels of OCR 1 (NC), 2 and 4 ..... 77

Figure 4.9 Stress path curves of constant-volume monotonic DSS tests on relatively undisturbed specimens of natural silt with 31 %, 70 % and 23 % coarser-grained fraction respectively in Series I-A(a), I-A(b)] and I-A(c) at normally consolidated stress state at confining stress levels of 150 kPa, 300 kPa and 600 kPa.....	80
Figure 4.10 Stress-strain curves of constant-volume monotonic DSS tests on relatively undisturbed specimens of natural silt with 31 %, 70 % and 23 % coarser-grained fraction respectively at normally consolidated stress state of 150 kPa, 300 kPa and 600 kPa .....	81
Figure 4.11 Normalized shear stress-strain curves of constant-volume monotonic DSS tests on relatively undisturbed specimens of natural silt with different plasticity indices.....	83
Figure 4.12 Normalized stress path curves of constant-volume monotonic DSS tests on relatively undisturbed specimens of natural silt with different plasticity indices.....	83
Figure 4.13 Shear stress-strain curves of constant-volume monotonic DSS tests on relatively undisturbed and reconstituted specimens from the Site #1 [Series I-A(a), I-D], Site #2 [Series II-A, II-D] and Site #3 [Series III-A, III-D] at normally consolidated stress state at varying confining stress levels .....	85
Figure 4.14 Stress path curves of constant-volume monotonic DSS tests on relatively undisturbed and reconstituted specimens from the Site #1 [Series I-A(a), I-D] at normally consolidated stress levels of 150 kPa, 300 kPa and 600 kPa .....	87

Figure 4.15 Stress path curves of constant-volume monotonic DSS tests on relatively undisturbed and reconstituted specimens from the Site #2 [Series II-A, II-D] at normally consolidated stress levels of 100 kPa, 200 kPa and 400 kPa .....	88
Figure 4.16 Stress path curves of constant-volume monotonic DSS tests on relatively undisturbed and reconstituted specimens from the Site #3 [Series III-A, III-D] at normally consolidated stress levels of 100 kPa and 200 kPa .....	88
Figure 4.17 Accumulation of shear strain and development of pore water pressure ratio with respect to loading cycles in constant -volume CDSS test on relatively undisturbed specimen from the Site #2 [PI =7], normally consolidated to 100 kPa with different CSRs .....	90
Figure 4.18 Stress path and shear stress-strain curves of constant-volume CDSS test on relatively undisturbed specimen from the Site #2 [PI =7], normally consolidated to $\sigma'_{vc} = 100$ kPa and CSR of 0.196 .....	92
Figure 4.19 Stress path and shear stress-strain curves of constant-volume CDSS test on relatively undisturbed specimen from the Site #2 [PI =7], normally consolidated to $\sigma'_{vc} = 100$ kPa and CSR of 0.168 .....	92
Figure 4.20 Stress path and shear stress-strain curves of constant-volume CDSS test on relatively undisturbed specimen from the Site #2 [PI =7], normally consolidated to $\sigma'_{vc} = 100$ kPa and CSR of 0.155 .....	93

Figure 4.21 Stress path and shear stress-strain curves of constant-volume CDSS test on relatively undisturbed specimen from the Site #2 [PI =7], normally consolidated to $\sigma'_{vc} = 100$ kPa and CSR of 0.132 .....	93
Figure 4.22 Stress path and shear stress-strain curves of constant-volume CDSS test on relatively undisturbed specimen from the Site #2 [PI =7], normally consolidated to $\sigma'_{vc} = 150$ kPa and CSR of 0.199 .....	95
Figure 4.23 Stress path and shear stress-strain curves of constant-volume CDSS test on relatively undisturbed specimen from the Site #2 [PI =7], normally consolidated to $\sigma'_{vc} = 150$ kPa and CSR of 0.167 .....	95
Figure 4.24 Stress path and shear stress-strain curves of constant-volume CDSS test on relatively undisturbed specimen from the Site #2 [PI =7], normally consolidated to $\sigma'_{vc} = 150$ kPa and CSR of 0.133 .....	96
Figure 4.25 Stress path and shear stress-strain curves of constant-volume CDSS test on relatively undisturbed specimen from the Site #2 [PI =7], normally consolidated to $\sigma'_{vc} = 150$ kPa and CSR of 0.12 .....	96
Figure 4.26 Development of pore water pressure ratio with respect to loading cycles in constant - volume CDSS test on relatively undisturbed specimen from the Site #2 [PI =7], normally consolidated to 150 kPa with different CSRs .....	97

Figure 4.27 Stress path and shear stress-strain curves of constant-volume CDSS test on relatively undisturbed specimen from the Site #2 [PI =7], normally consolidated to $\sigma'_{vc} = 200$ kPa and CSR of 0.191 .....	97
Figure 4.28 Stress path and shear stress-strain curves of constant-volume CDSS test on relatively undisturbed specimen from the Site #2 [PI =7], normally consolidated to $\sigma'_{vc} = 200$ kPa and CSR of 0.169 .....	98
Figure 4.29 Stress path and shear stress-strain curves of constant-volume CDSS test on relatively undisturbed specimen from the Site #2 [PI =7], normally consolidated to $\sigma'_{vc} = 200$ kPa and CSR of 0.149 .....	98
Figure 4.30 Stress path and shear stress-strain curves of constant-volume CDSS test on relatively undisturbed specimen from the Site #2 [PI =7], normally consolidated to $\sigma'_{vc} = 200$ kPa and CSR of 0.141 .....	99
Figure 4.31 Development of pore water pressure ratio with respect to loading cycles in constant - volume CDSS test on relatively undisturbed specimen from the Site #2 [PI =7], normally consolidated to 200 kPa with different CSRs .....	99
Figure 4.32 Cyclic Stress Ratio versus Number of loading cycles to reach $\gamma=3.75\%$ curves from constant-volume CDSS tests on undisturbed silt specimens [Site #2, PI=7] at confining consolidation stress levels of 100 kPa, 150 kPa and 200 kPa.....	102

Figure 4.33 Stress path and shear stress-strain curves of constant-volume CDSS test on relatively undisturbed specimen from the Site #3 [PI =34], normally consolidated to $\sigma'_{vc} = 75$ kPa, 150 kPa and 200 kPa, where $N_{cyc(\gamma=3.75\%)}=15.8, 17.8$ and $17.8$ for different values of CSR.....	103
Figure 4.34 Cyclic Stress Ratio versus Number of loading cycles to reach $\gamma=3.75\%$ curves from constant-volume CDSS tests on undisturbed silt specimens [Site #3, PI=34] at confining consolidation stress levels of 75 kPa, 150 kPa and 200 kPa.....	104
Figure 4.35 Accumulation of shear strain and development of pore water pressure ratio with respect to loading cycles in constant -volume CDSS test on relatively undisturbed specimen from the Site #1 [PI =5], having coarse-grained fraction of 20%, 30% and 35% when tested for CSR of about 0.15 .....	106
Figure 4.36 Normalized stress path and normalized shear stress-strain curves of constant-volume CDSS test on relatively undisturbed silt specimen from the Site #1 [PI =5], having coarse-grained fraction of 20%, 30% and 35% when tested for CSR of about 0.15.....	107
Figure 4.37 Cyclic Stress Ratio versus Number of loading cycles to reach $\gamma=3.75\%$ curves from constant-volume CDSS tests on undisturbed silt specimens [Site #1, PI=5] with different coarse-grained fraction of 20%, 30% and 35% and comparison of cyclic resistance with materials with different coarse-grained fractions .....	108
Figure 4.38 Accumulation of shear strain and development of pore water pressure ratio with respect to loading cycles in constant -volume CDSS test on relatively undisturbed specimen from	

the Site #1 [PI =5], Site #2 [PI =7], and Site #3 [PI =34], normally consolidated to 200 kPa with a CSR of about 0.15 .....	110
Figure 4.39 Comparison of stress path and shear stress-strain curves of constant-volume CDSS tests on relatively undisturbed specimen from the Site #1 [PI =5], Site #2 [PI =7], and Site #3 [PI =34], normally consolidated to 200 kPa with a CSR of about 0.15.....	112
Figure 4.40 Comparison of stress path and shear stress-strain curves for selected loading cycles during constant-volume CDSS tests on relatively undisturbed specimen from the Site #1 [PI =5], Site #2 [PI =7], and Site #3 [PI =34], normally consolidated to 200 kPa with a CSR of about 0.15.....	113
Figure 4.41 Stress-strain loops for relatively undisturbed, normally consolidated silt specimens with different soil plasticity, at similar strain levels during constant-volume CDSS tests.....	114
Figure 4.42 Cyclic Stress Ratio versus Number of loading cycles to reach $\gamma=3.75\%$ curves from constant-volume CDSS tests on undisturbed specimens of fine-grained materials with different plasticity .....	115
Figure 4.43 Comparison of the accumulation of shear strain and development of pore water pressure ratio with respect to number of loading cycles in constant -volume CDSS tests of relatively undisturbed and reconstituted specimens .....	117
Figure 4.44 Comparison of stress path and shear stress-strain curves of constant-volume CDSS test on relatively undisturbed (CT 150 18.75) and reconstituted specimen (CT R 150 18.75) from the Site #1 [PI =5], normally consolidated to 150 kPa and CSR of about 0.125.....	118



Figure 4.45 Comparison of stress path and shear stress-strain curves of constant-volume CDSS test on relatively undisturbed (JS 200 30) and reconstituted specimen (JS R 200 30) from the Site #2 [PI =7], normally consolidated to 200 kPa and CSR of about 0.15.....	119
Figure 4.46 Comparison of stress path and shear stress-strain curves of constant-volume CDSS test on relatively undisturbed (MD 075 15) and reconstituted specimen (MD R 075 15) from the Site #3 [PI =34], normally consolidated to 75 kPa and CSR of about 0.2 .....	120
Figure 4.47 Comparison of stress path and shear stress-strain curves of selected loading cycles during constant-volume CDSS test on relatively undisturbed and reconstituted specimen under similar normally consolidated $\sigma'_{vc}$ and CSR from Site #1 [PI =5], Site #2 [PI =7] and Site #3 [PI =34], .....	122
Figure 4.48 Comparison of Cyclic Stress Ratio versus Number of loading cycles to reach $\gamma=3.75\%$ curves during constant-volume CDSS test on normally consolidated relatively undisturbed and reconstituted specimen .....	123
Figure 4.49 Reduction of cyclic shear resistance of reconstituted specimen with respect to relatively undisturbed specimen of different fine-grained materials .....	124
Figure 4.50 Typical post-cyclic consolidation volumetric strain ( $\epsilon_{v-pcc}$ ) versus time characteristics of normally consolidated high plastic silt (PI=34) from the Site #3.....	126
Figure 4.51 Typical post-cyclic consolidation volumetric strain ( $\epsilon_{v-pcc}$ ) versus time characteristics of normally consolidated silt with different plasticity .....	127

Figure 4.52 Comparison of post-cyclic volumetric strain ( $\epsilon_{v-pcc}$ ) versus maximum cyclic pore-water pressure ratio ( $r_{u-max}$ ) during CDSS loading of relatively undisturbed and reconstituted silt specimens with different plasticity .....	127
Figure 4.53 Characteristics of post-cyclic volumetric strain ( $\epsilon_{v-pcc}$ ) versus maximum cyclic pore-water pressure ratio ( $r_{u-max}$ ) during CDSS loading of relatively undisturbed silt specimens with different plasticity .....	128
Figure 4.54 Characteristics of post-cyclic volumetric strain ( $\epsilon_{v-pcc}$ ) versus maximum cyclic pore-water pressure ratio ( $r_{u-max}$ ) during CDSS loading from this study over-layed with Fraser River delta Silt (FRS) and Quartz Rock Powder (QRP) data from (Sanin, 2010) .....	128

## List of Symbols

$e_c$	Post-consolidation void ratio prior to the application of shearing
$e_i$	Initial void ratio after the application of the seating pressure of about 10 kPa
$e_o$	Initial void ratio
$e_{pcc}$	Void ratio of the specimen after the post cyclic consolidation phase
$F_s$	Friction sleeve stress
Hz	Hertz
kg	kilo gram
km	kilo meter
kPa	kilo pascal
m	meter
mm	milli meter
$N_{cyc}$	Number of loading cycles
$N_{cyc} [\gamma=3.75\%]$	Number of uniform loading cycles to reach double amplitude shear strain of 3.75 %
$Q_t$	Corrected tip resistance for pore water pressure effects
$R_f$	Friction ratio ( $R_f$ ),
$r_u$	Excess pore-water pressure ratio
$r_{u-max}$	Maximum cyclic pore-water pressure ratio
s	second

$S_u$	Undrained shear strength
$U_0$	Equilibrium (in-situ) pore water pressure
$U_2$	Pore water pressure (behind the tip of cone)
V	Volt
$WC_{I(avg)}$	Average water content of the test specimen computed from the available trimmings from undisturbed specimens and sample portions from reconstituted specimen.
$\alpha$	Initial static shear ratio
$\Delta e$	Change in void ratio in between the initial stage and loading up to in-situ stress level
$\Delta u$	Excess pore-water pressure
$\epsilon_{v-pcc}$	Post cyclic consolidation volumetric strain
$\sigma'_{v0}$	Initial vertical effective stress
$\sigma'_{vc}$	Vertical consolidation stress prior to the application of shearing
$\sigma_1$	Major principle stress
$\sigma_3$	Minor principle stress
$\tau_{cyc}$	Cyclic shear stress
$\tau_{st}$	Static shear stress
$\gamma$	Horizontal shear strain
$\gamma_{max}$	Maximum shear strain during the cyclic shear loading phase.
$\phi_{CV}$	Constant-volume friction angle
$\phi_{PT}$	Friction angle at the phase transformation state

## List of Abbreviations

1-D	One-dimensional
BC	British Columbia
CDSS	Cyclic Direct Simple Shear
CPT	Cone Penetration Test
CRR	Cyclic Resistance Ratio
CSR	Cyclic Stress Ratio
CTX	Cyclic Triaxial
DA	Double-amplitude
DACS	Data Acquisition and Control System
DAQ	Data acquisition
DSS	Direct Simple Shear
EPR	Electro-Pneumatic Regulator
GUI	Graphical User Interface
LVDT	Linear Variable Differential Transformer
NGI	Norwegian Geotechnical Institute
OCR	Over-Consolidation Ratio
PCC	Post cyclic consolidation
PI	Plasticity Index
SA	Single Amplitude

SHANSEP

Stress History and Normalized Soil Engineering Properties

UBC

University of British Columbia

## **Acknowledgements**

First and foremost, I would like to express my appreciation to my supervisor Dr. Dharma Wijewickreme for sacrificing his priceless time to guide, direct and advise me; to review and correct my work; and for supporting unconditionally despite the time whenever I had to contact him.

The research was conducted with the financial support provided by the Natural Sciences and Engineering Research Council of Canada (NSERC) Discovery/Accelerator Supplement Grant (Application ID 429675). ConeTec Investigations Ltd. of Richmond, B.C., generously provided full funding support for the sampling of undisturbed soils for the research testing. Those financial supports are greatly appreciated. Technical assistance of Cantech Inspection Ltd. is also thankfully admired.

The contributions of technical advices and support received from Scott Jackson, Harald Schrempp, Bill Leung, John Wong, Mark Rigolo, Paula Parkinson and UBC Civil Engineering Workshop personnel are thankfully appreciated.

Further, I want to convey my gratitude to Dr. Yogi Vaid, for his advices during the conductance of laboratory experimental test program. Special thanks are owed to my colleagues for the support and fruitful discussions throughout the research program.

This thesis is dedicated to

*All who lost their lives or properties due to soil liquefaction*



# **Chapter 1: Introduction**

## **1.1 Background**

The response of soils under monotonic and cyclic shear loading has received wide attention particularly due to the well-observed occurrence of liquefaction and associated geotechnical hazards during and after the 1960 Chile earthquake, 1964 Niigata earthquake, and 1964 Alaska earthquake. Early investigations have indicated that loose state coarse-grained materials (e.g., sands) could experience static and seismic-induced liquefaction under constrained drainage conditions. Largely due to these observations, the research work has been mainly focused to study the response of coarse-grained soils as opposed to fine grained soils such as silts. However, detailed observations after Tokachi-Oki earthquake (Kishida, 1970; Tohno & Yasuda, 1981), Haicheng earthquake and Tangshan earthquake (Wang, 1979) Izu-Ohshima-Kinkai earthquake (Ishihara, 1984), Northridge earthquake (Seed et al. 1989), Loma Prieta earthquake (Boulanger et al. 1998), Chi-Chi earthquake (Chu et al. 2004) and Kocaeli earthquake (Bray et al. 2004; Martin et al. 2004), it is now well established that fine-grained silts, clays, or mixtures of fine-grained soil also can experience loss of stiffness and strength under certain loading and initial material density and stress conditions. Unlike the extensive information on liquefaction of sand, the published literature on the findings from investigations on silt, clay, and mixtures of fine grained soil is limited (e.g., Andrews & Martin, 2000; Boulanger & Idriss, 2006; Bray & Sancio, 2006; Donahue et al. 2007; Guo & Prakash, 1999; Prakash & Sandoval, 1992; Sanin & Wijewickreme, 2006a; Wijewickreme et al. 2005). In addition to the liquefaction-induced

ground deformations such as flow-failures and lateral spreading (Seed & Idriss, 1971) due to shear stiffness degradation or shear strength reduction as a result of the development of excess pore-water pressure in soils, another geotechnical concern is the post-liquefaction ground settlements that often arise due to volumetric strain caused by the dissipation of shear-induced excess pore-water pressure. Bray et al. (2004) and Idriss & Boulanger (2008) have observed post-cyclic volumetric strains resulting settlements, foundation sliding, tilting and collapse of structures

Idriss & Boulanger (2008) noted that the shear loading response of fine-grained materials are generally different from that of coarse-grained materials, as the stress-strain loops of silt and clay generally do not develop the very flat middle portions (where the shear stiffness is essentially zero) that are observed for sands after they temporarily develop high excess pore-water pressures ( $\Delta u$ ), or excess pore-water pressure ratio ( $r_u$ ) values close to 100%; Note:  $r_u = \Delta u / \sigma'_{v0}$ , where  $\Delta u$  = excess pore-water pressure and  $\sigma'_{v0}$  = initial vertical effective stress at the point of interest. Therefore, Idriss & Boulanger (2008) have used the term ‘cyclic softening’ with reference to the observed loss of shear stiffness and strength when characterizing the response of fine-grained materials under cyclic loading, as opposed to the term ‘liquefaction’ often used with respect to the loss of shear strength in coarse-grained materials.

In the current practice, the liquefaction susceptibility of fine-grained soils is assessed using criteria that are primarily based on soil index properties – ie., the plasticity index (PI) and in situ moisture content. For example, silt with  $PI < 7$  is considered to behave in a “sand-like” manner for liquefaction assessment, while silt with  $PI > 7$  is considered to exhibit “clay-like” behavior.

This approach, however, is based on the limited available knowledge on the cyclic shear response of silts. The current published information indicates that silt has a complex transitional behavior in comparison to the commonly understood cyclic shear response of clean sand and clay.

The above background highlights that there is a strong need to study the shear stress strain response of natural silts and advance the current knowledge on this subject. In particular, such study clearly requires systematic laboratory element testing that carefully addresses the effects arising from wide ranging parameters that are known to affect the soil behaviour.

## **1.2 Objective of the Thesis**

Considering the limited available knowledge on shear loading response of fine-grained soils, a study is proposed herein to investigate the monotonic and cyclic shear loading response of natural silt. The main objective of the study is to generate and enhance the laboratory experimental database in view of improving the current understanding of the mechanical behavior of natural silt.

For this purpose, natural silts having plastic indices of 4, 7, and 34, retrieved using thin-walled sharpened-edge tube sampling methods from three different locations in the Fraser River Delta of the Lower Mainland of British Columbia (BC), Canada were investigated. The monotonic, cyclic shear loading response and post-cyclic consolidation responses of above mentioned natural silts were examined by conducting a systematic laboratory test program primarily using the direct simple shear (DSS) device at the University of British Columbia (UBC). This experimental study primarily focused particularly on following aspects:

- Constant-volume (equivalent to undrained) monotonic DSS loading response of normally consolidated and over-consolidated natural silts;
- Constant-volume cyclic DSS loading response for normally consolidated natural silts;
- Effect of initial confining stress on monotonic and cyclic DSS loading response for normally consolidated natural silts;
- Effect of over-consolidation ratio (OCR) on monotonic DSS loading response for natural silts;
- Effect of coarse-grained fraction of natural silts on its monotonic and cyclic DSS loading response;
- Effect of soil-fabric / microstructure on monotonic and cyclic DSS loading response for natural silts;
- Post-cyclic consolidation response arising from the dissipation of shear induced pore-water pressure.

In addition, effect of plasticity on the shear loading response of silts was also investigated with the use of some limited data available from the current investigation combined with previous studies at UBC.

### **1.3 Organization of the Thesis**

The thesis comprises five chapters. Chapter 1 introduces the topic of shear loading response of fine-grained materials (with the preliminary background developed from the available laboratory experimental findings), rationale for generating the thesis objectives, followed by identification of those objectives.

A survey of literature on the shear response of both coarse-grained material and fine-grained material and the assessment of cyclic shear response through laboratory experiments have been summarized in Chapter 2. A detailed description of the test apparatus used in the laboratory experimental study is presented in Chapter 3. Furthermore, details of the tested material and procedures of each test phases and outline of the test program are also presented in Chapter 3.

Results obtained from the test program conducted under this study are described in Chapter 4. This includes the findings on monotonic shear, cyclic shear and post cyclic consolidation response of tested silts.

Chapter 5 presents the summary of the findings and main conclusions arising from this study. This is followed by the list of references, and a number of appendices containing: the results of X-ray radiography, index testing and particles size distribution analysis, and one dimensional (1-D) consolidation testing.

## **Chapter 2: Literature Review**

A proper understanding of the monotonic and cyclic shear response of soils is an important consideration in the solution of geotechnical engineering problems. In this regard, laboratory element testing that can mimic/simulate the field loading conditions plays a significant role in understanding this fundamental behavioral patterns of soil. The geotechnical laboratory element test devices that were developed and the phenomena observed during testing conducted using these devices have resulted in significantly advancing the current knowledge in this field. It is of relevance to note that, while the response of sand and clay has been studied extensively over the last few decades, the investigations that have been undertaken to study the response of silt and fine-grained tailings are quite limited. This thesis presents laboratory experimental research work performed on a number of natural silt materials. In order to provide the needed background and rationale for the work proposed in the thesis, this chapter presents a review of literature on the laboratory observations with particular reference made to the fundamental shear response of soil. The Section 2.1 briefs the mechanical response of sand emphasizing the monotonic and cyclic loading response. In the Sections 2.2 and 2.3, past work on the shear loading response of clay and silts including fine-grained tailings are summarized. Aspects related to laboratory experimental tests and soil responses observed from natural and reconstituted soil specimens are briefed in Section 2.4. An overview of the topics of liquefaction and cyclic mobility considering the observed shear response of soil during laboratory experiments is presented in Section 2.5. A

review on the criteria used to evaluate the cyclic shear resistance from laboratory tests and the evolution of those criteria are also included in the same section.

## **2.1 Mechanical Response of Sand**

It has been well established that the relative density and effective confining stress are the two prominent factors that govern the shear stress-strain response of sands. As such, the concepts of critical state soil mechanics, that is based upon void ratio and effective confining stress, are commonly adopted in characterizing sand behavior (Schofield & Wroth, 1968). Based on the combination of the confining stress and the void ratio of the sand, dilative response (tendency to increase its volume during shear loading) or contractive response (tendency to decrease its volume) have been observed during monotonic shear loading. Further during shear loading, sand with dilative response exhibit reduction of shear strength after reaching a peak shear strength, whereas sand with contractive response exhibit increasing shear stress until it reaches an approximately constant peak value with increasing shear strain. Because of the difficulties in obtaining undisturbed sand specimens, in most cases, laboratory experimental studies has been conducted on reconstituted sand specimen that were prepared by different techniques as air pluviation, water pluviation or moist tamping. As sand specimen prepared by different techniques affect the initial void ratio and particle arrangement at a given confining stress level, above-mentioned contractive or dilative response have been observed when the specimen underwent shear loading.

Extensive research undertaken on the undrained response of sand under monotonic and cyclic shear loading during the last four decades [for instance Boulanger & Seed, 1995; Castro, 1969;

Chern, 1985; Finn et al. 1970; Ishihara & Yamazaki, 1980; Ishihara, 1993; Peacock & Seed, 1968; Seed & Lee, 1967a; Yamamuro & Lade, 1997 and Vaid & Chern, 1985] have resulted in a good understanding on the subject and the parameters influencing the mechanical behavior. Using this understanding of the soil response, Idriss & Boulanger (2008), Youd & Idriss (2001), and Youd et al. (2001) have proposed approaches for geotechnical earthquake engineering design works.

The typical laboratory shear response of sand when subjected to undrained monotonic loading are shown in Figure 2.1 from a viewpoint of summarizing general behavioral patterns. The noted Type (1) and Type (2) curves in Figure 2.1 illustrate the contractive response of sand; the strain-softening response Type (1) is generally associated with flow failure and Vaid & Chern (1985) termed this as ‘steady state liquefaction’. Furthermore, the post-peak minimum constant shear strength exhibited in the Type (1) response at large strain level that has been referred as steady-state undrained shear strength. The Type (2) response that also displays some strain softening behavior, is referred as ‘limited liquefaction’ by Castro (1969) – this is because of the observed increase in shear resistance that seem to develop when sheared past the initial strain softening (i.e., after a local minimum shear strength). In Type (3), a dilative strain-hardening response of the sand is clearly exhibited. The point at which the induced pore pressure transitions from an increasing trend to a decreasing trend during the monotonic loading, both in Types (2) and (3) sand behavior patterns, has been defined as the phase transformation state. The friction angle at the phase transformation state ( $\phi_{PT}$ ) has been shown to be unique for given sand, and  $\phi_{PT}$  has been shown equal to the friction angle mobilized at steady state (Vaid & Chern, 1985). Negussey



et al. (1986), using data from large displacement ring shear tests, have found that the value of  $\phi_{PT}$  is equal to the constant-volume friction angle ( $\phi_{CV}$ ).

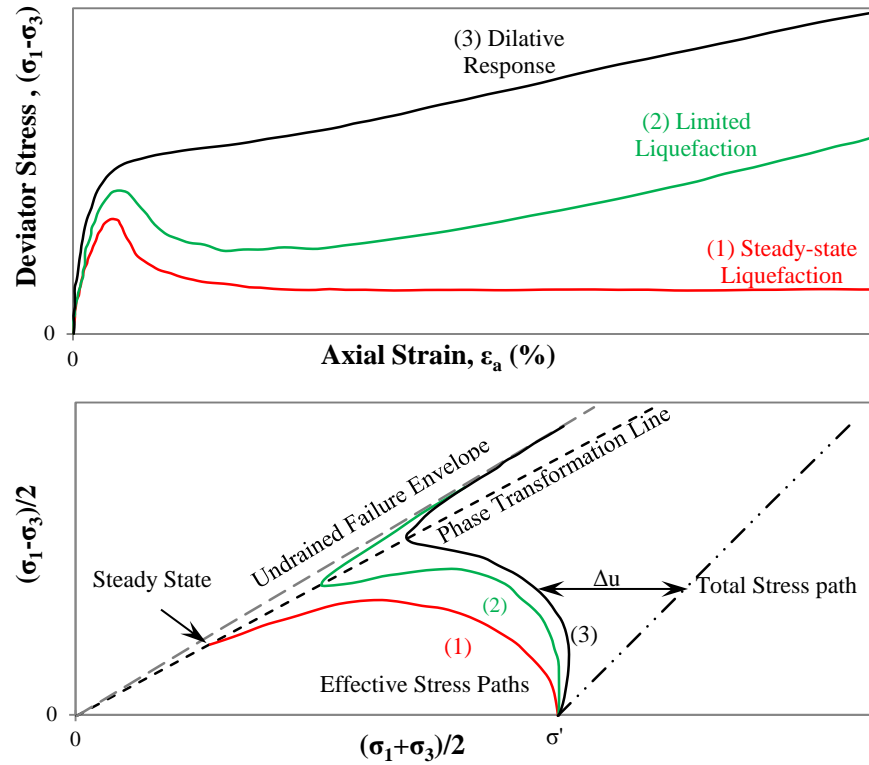


**Figure 2.1** Characteristics stress-strain and stress-path response of sandy soils during undrained monotonic loading through triaxial tests [reproduced after Kuerbis (1989)]

The resistance to liquefaction of sand under seismic loading has also been widely assessed using undrained cyclic shear loading tests [i.e. cyclic triaxial (CTX) tests and cyclic direct simple shear CDSS tests]. Similar to the responses noted in undrained monotonic loading, three typical shear response types named liquefaction, limited liquefaction and cyclic mobility have been identified by Castro (1969) and Vaid & Chern (1985). The stress-strain response, stress-path response, and strain development characteristics that distinguish the three above-mentioned behavioral types are schematized in Figure 2.2.

Sand continuously exhibits contractive deformation (i.e., increase in excess pore pressure with increasing number of cycles) in the liquefaction type response, until it finally reaches the steady state. However, in the case of limited liquefaction type response, dilative response can be observed after stress ratio reaches the phase transformation state.

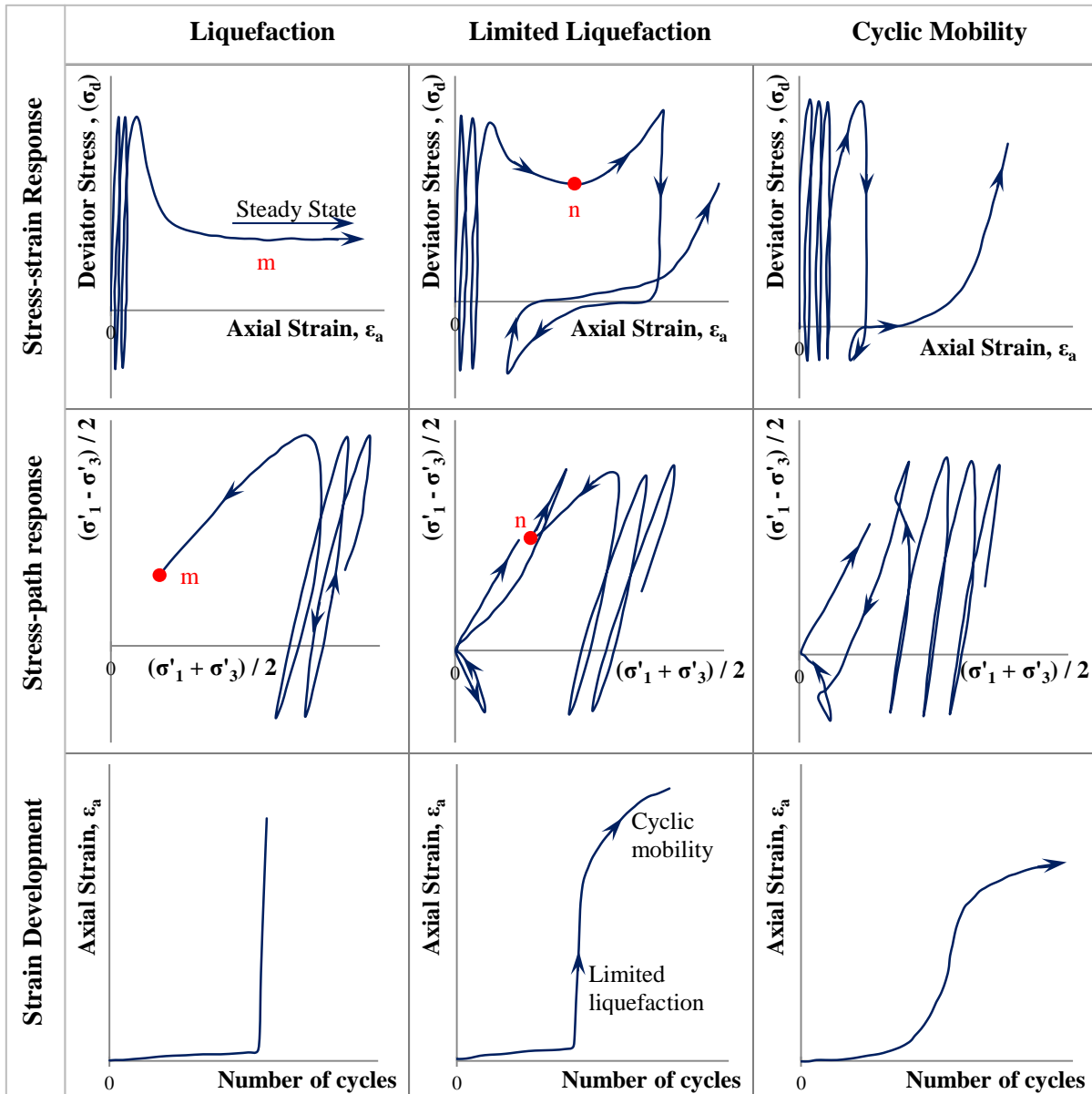


Figure 2.2 Typical liquefaction, limited liquefaction and cyclic mobility type response during undrained cyclic loading with associated stress-strain response, stress-path response and strain development [reproduced after Vaid & Chern (1985)]

Following the phase transformation state, significant development of excess pore pressure can be noted during the next loading cycle resulting effective confining stress to decrease to zero or near zero. This causes considerable amount of strain development as well. In the cyclic mobility type response, gradual development of strain and continuous buildup of pore-water pressure can be observed with increasing number of loading cycles.

## **2.2 Mechanical Response of Clay**

As indicated Chapter 1, the mechanical response of fine-grained materials such as silty and clayey soils in monotonic and cyclic shear loading has been found to be different from that of sand. With this in mind, relevant literature from works that have focused on the monotonic and cyclic shear response of fine-grained soils are presented herein.

Ladd (1964) noted that the undrained shear strength ( $S_u$ ) of fine-grained soils can be characterized by normalizing with respect to the effective vertical consolidation stress. This approach is known as the SHANSEP (Stress History and Normalized Soil Engineering Properties), and it is widely used for characterizing for fine-grained soils in engineering practice. For example, for normally consolidated simple clay, identical stress-path characteristics can be observed when stresses are divided by the initial effective consolidation stresses.

Shear loading characteristics are expected to be significantly governed by parameters other than the confining pressure and void ratio. For instance, Tanaka & Locat (1999) have indicated that different types of pores identified as inter-aggregate, intra-aggregate, skeletal, and intra-skeletal pores that can trap water could significantly influence the plastic and liquid limits of Osaka bay clay. Furthermore, it has been noted that the physio-chemical properties of fines and presence of

microfossils can significantly influence the plasticity and in turn, mechanical behavior of fine-grained soil. Similarly, Hight & Leroueil (2003) have also emphasized the difference in the responses, observed for glacio-aqueous clay, alluvial clay, temperate marine clay and tropical marine clay due to their different ageing and depositional and post-deposition environments. Although the shear response characteristics of normally consolidated and over-consolidated clay can be considered broadly similar to those of loose and dense sand, respectively, it has been established that factors such as fabric, anisotropy, mineralogy, orientations of shear planes and weathering could significantly influence the shear strength of the fine-grained material. Furthermore, several experimental studies [i.e. Crawford, 1965; Graham et al. 1983; Lefebvre & LeBoeuf, 1987; Vaid et al. 1979] have shown that soil structure in clay has an important time dependent resistance to compression. Lefebvre & LeBoeuf (1987) performed triaxial tests on Grande-Baleine clay and Olga clay with different strain rate (i.e. 0.5% per hour to 130% per hour) and reported that variation of  $S_u$  with strain rate observed in those tests varied from 7-14% per tenfold increment in strain rate. Similarly, Vaid et al. (1979) observed an increment in  $S_u$  of about 10% per tenfold increment in strain rate from the tests performed on Saint-Jean-Vianney clay with a range of strain rate from 0.04% per hour to 16.8% per hour. Based on triaxial tests performed on a wide range of clay, Graham et al. (1983) reported 10%~20% change of  $S_u$  for a tenfold change in strain rate. Cyclic shear loading responses of clay has been studied by Andersen et al. (1980), Azzouz et al. (1989); Boulanger & Idriss, (2007); Koutsoftas, (1978); Lefebvre & Pfendler, (1996); McCarron et al. (1995); and Zergoun & Vaid, (1994) from laboratory experiments.

Andersen (2009) compared the effective stress paths between monotonic and cyclic loading conditions using the data obtained during undrained monotonic and cyclic loading of Drammen clay (Figure 2.3). He postulated that the soil structure would break down during cyclic shear loading, and, in turn, this would cause a contractive tendency in the soil material, which under undrained conditions, would result in significant increase in excess pore water pressure (i.e., the effective stresses in the soil would decrease). The effects of strain rate during cyclic shear test have been investigated by Zergoun & Vaid (1994) through CTX tests on Cloverdale clay and by Lefebvre & Pfendler (1996) through CDSS tests on St. Lawrence clay. The influence of the loading rate was explicitly illustrated by the observation that the cyclic shear stresses required for failure in just one loading cycles during cyclic loading tests exceeded the value of  $S_u$  observed under relatively slow conventional monotonic loading rates (Idriss & Boulanger, 2008).

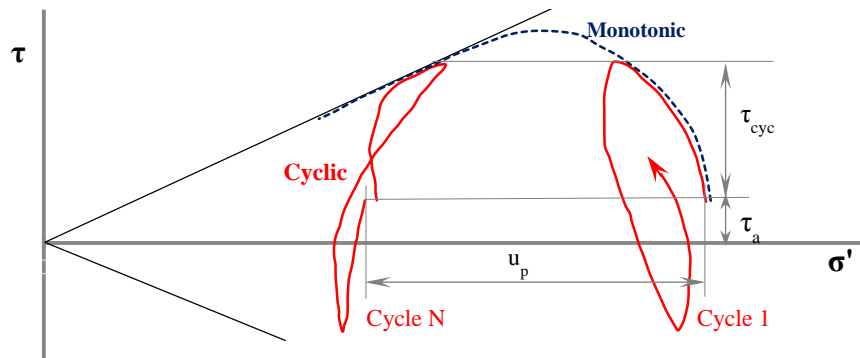


**Figure 2.3 Effective stress paths for undrained tests with monotonic and cyclic loading [reproduced after Andersen (2009)]**

$u_p$  = permanent pore-pressure component;  $\sigma'$  = effective normal stress;  $\tau$  = shear stress;  $\tau_a$  = average shear stress;  $\tau_{cyc}$ , single-amplitude cyclic shear stress

From the results of consolidated undrained CTX tests conducted on plastic clay and silty clay, Koutsoftas (1978) reported that secant and tangent moduli decrease significantly as the double

amplitude (DA) strain increases. Further, for of plastic clay, it was observed that the loss of shear strength of over-consolidated specimens was smaller than that of normally consolidated specimens; whereas for silty clay, the loss of strength for normally and over-consolidated specimens were noted to be similar.

Comparing test results obtained for plastic Drammen clay from a test program which comprised of 129 triaxial tests and 103 simple shear tests, Andersen et al. (1980) reported that simple shear test indicated good repeatability while triaxial test results exhibit some scatter. The  $S_u$  derived from triaxial compression, triaxial extension, and simple shear tests of Drammen clay were different as those tests follow different effective stress paths.

Unlike the contractive sand, gradual increments of strain and pore-water pressure have been observed for clays and plastic silts with increasing number of loading cycles. As a result of that, different forms of engineering procedures have been adapted to characterize the static and dynamic strengths (Boulanger & Idriss, 2007; Ishihara, 1996). In order to distinguish the difference of the characteristics and response of clay and plastic silt, Idriss & Boulanger (2008) have used the term ‘cyclic softening’ to refer the strength loss and associated deformation in clay and plastic silt, whereas the term ‘liquefaction’ referred the strength loss and associated deformation of contractive sand.

### **2.3 Mechanical Response of Fine-grained Soils (Silt and Fine-grained Tailings)**

The review of the literature undertaken reveals that a number of researchers have engaged in laboratory experimentation to study the response of natural silts (Bray & Sancio 2006; Donahue et al. 2007; Guo & Prakash 1999; Hyde et al. 2006; Prakash & Sandoval 1992; Sanin &

Wijewickreme 2006a). It is also of relevance to note the significant efforts placed to study the response fine-grained tailings through many laboratory studies (Ishihara et al. 1980, Troncoso 1986, Wijewickreme et al. 2005, Kim et al. 2011, Geremew & Yanful 2011 and Seidalinova, 2014).

Experimental observations of silts during cyclic shear loading (Guo & Prakash, 1999; Prakash & Sandoval, 1992) have indicated that cyclic loading resulted pore pressure build-up which becomes equal or close to the initial effective confining pressure. Similar observations were noted by Sanin & Wijewickreme (2006a) and Bray & Sancio (2006) for low-plastic Fraser River delta silt and Adapazari silt, where increase of  $r_u$  with accompanied gradual loss of shear stiffness. In general, silt during cyclic loading exhibited cyclic mobility type response as opposed to the abrupt loss of shear stiffness which has been typically observed for contractive coarse-grained soils.

The data developed from research undertaken have shown that the relationship between the cyclic stress ratio (CSR) and the number of loading cycles ( $N_{cyc}$ ) to reach a certain failure condition – determined based on a pre-defined criteria - could be conveniently examined/expressed using CSR versus  $N_{cyc}$  in linear-logarithmic type semi-log graph. Such relationships derived by Donahue et al. (2007), Guo & Prakash, (1999), Hyde et al. (2006), and Sanin & Wijewickreme (2006) seem to differ from each other likely due to the differences of the plasticity, fabric and mineralogy of tested silts. Based on the cyclic resistance obtained from the constant-volume CDSS test on normally consolidated Fraser River Delta silts, Sanin (2010) reported that the cyclic resistance of undisturbed silt found to be relatively insensitive to the

confining stresses whereas increasing initial static shear ratio ( $\alpha$ ) has found to generally decrease the cyclic resistance (Figure 2.4).

The observation of pore-water pressure development and degradation of shear stiffness noted by Ishihara et al. (1980); Troncoso et al. (1988); and Wijewickreme et al. (2005) for fine-grained tailings suggest that the cyclic shear loading response of such tailings are similar to natural silts where gradual degradation of shear strength with limited strain accumulation have been noted. From CTX tests performed on fine-grained tailings, Ishihara et al. (1980) observed that the cyclic shear resistance of fine-grained tailing is significantly influenced by the plasticity, where relatively high plastic fine-grained tailings exhibit greater shear resistance than that of non-plastic fine-grained tailings.

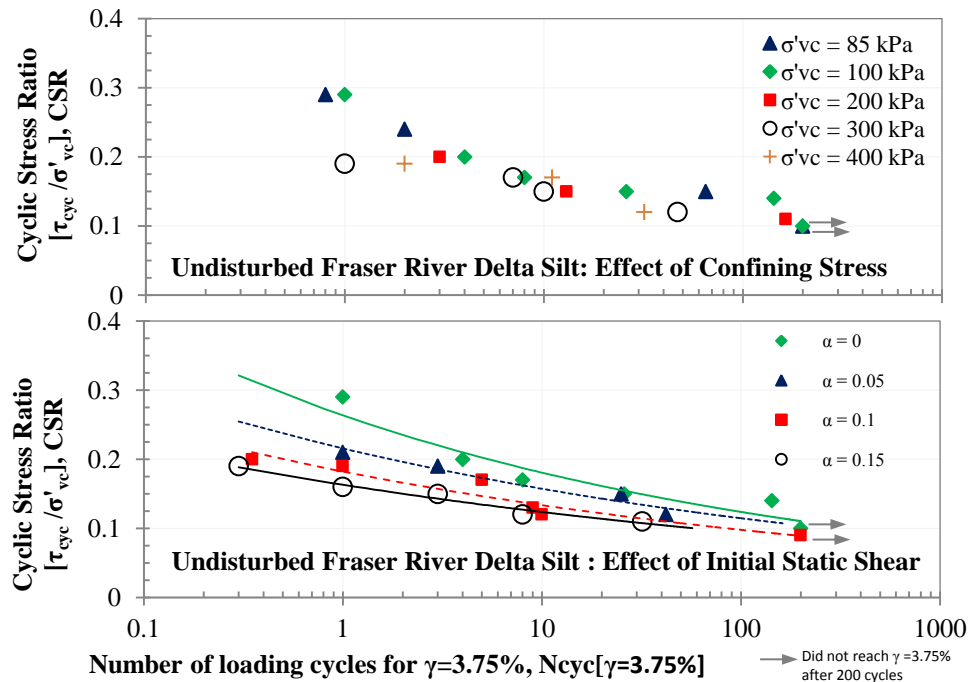


**Figure 2.4** Effect of confining stress ( $\sigma'_{vc}$ ) and initial static shear ratio ( $\alpha = \tau_{st}/\sigma'_{vc}$ ) on the cyclic resistance of normally consolidated Fraser River Delta silt from constant-volume CDSS tests [reproduced after Sanin (2010)]



Wijewickreme et al. (2005) conducted constant-volume CDSS tests to assess the cyclic shear resistance of undisturbed samples of laterite, copper–gold tailings, copper–gold– zinc tailings and reconstituted copper–gold–zinc tailings (Figure 2.5). With an increase in the confining pressure, greater cyclic shear resistance was observed for laterite tailings, implying that contractive tendency due to the increase in confining stress would be overridden by the dilative tendency arising due to stress densification. Nevertheless, the cyclic shear resistance observed for copper–gold–zinc tailings did not indicate sensitiveness to the initial density condition and confining pressure.

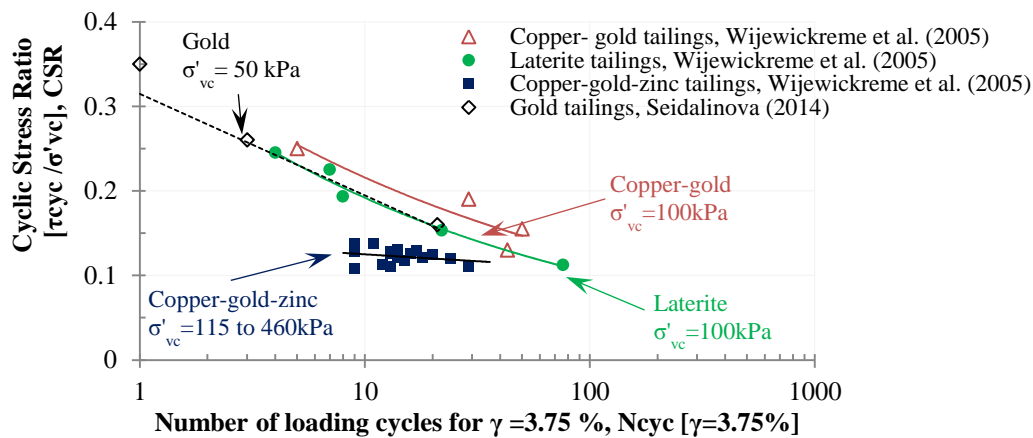


**Figure 2.5 Comparison of cyclic stress ratio versus number of cycles to reach  $\gamma = 3.75\%$  for laterite, copper–gold, copper–gold– zinc tailings and gold tailings [after Sanin (2010) and Seidalinova (2014) ]**

Based on CDSS tests conducted on fine-grained gold tailings, Seidalinova (2014) and Kim et al. (2011) have reported that cyclic shear resistance would increase with increasing over-consolidation ratio (OCR). From the CDSS tests with initial static shear stress bias conducted on gold tailings, simulating sloping ground condition, Seidalinova (2014) noted reduction in cyclic shear resistance with increasing level of initial static shear stress bias.

Høeg et al. (2000), Jung et al. (2012) and Wijewickreme & Sanin (2008) investigated the difference of shear response of natural and reconstituted specimens using Borlänge silt, Chicago clay and Fraser River delta silt respectively. It was noted that the shear response of reconstituted specimen deviated from the response of natural specimen and concluded that fabric / microstructure in natural specimens influence greater cyclic shear resistance.

The empirical Chinese criteria (Wang, 1979) to assess the liquefaction susceptibility of fine-grained soil, which was based on observed field performance of fine-grained soil during earthquakes was later modified by Koester (1992) and Finn et al. (1994) addressing the uncertainty and variation of fine-content and water content during measurements. Boulanger & Idriss (2004, 2006) and Idriss & Boulanger (2006) noted that Chinese criteria are unacceptable and their use should be discontinued. Bray & Sancio (2006) and Idriss & Boulanger (2008) have recommended alternate new criteria to assess the liquefaction susceptibility of fine-grained soil. Based on the results of laboratory CTX tests on fine-grained soil, Bray & Sancio (2006) and Donahue et al. (2007) suggested an empirical criterion to assess the liquefaction susceptibility of fine grained soil based on liquid limit, water content, and plasticity index. Idriss & Boulanger (2008) suggested that fine-grained soil with  $PI < 7$  is to be considered to behave in a “sand-like” manner, while silt with  $PI > 7$  should be considered to behave in a “clay-like” manner for the purpose of liquefaction assessment. These approaches, however, are based on the limited available knowledge on the cyclic shear response of silts and clay.

## **2.4 Soil Response and Laboratory Experimental Tests**

Many factors such as particle size, packing density, confining stress, age, micro structure, fabric, water content, drainage condition and loading mechanism have been identified as to influence the mechanical response of soil. Out of those, loading mechanism can be controlled in the laboratory testing as various test devices such as direct shear, direct simple shear, directional shear cell, ring shear, triaxial, hollow cylinder torsional and hollow cylinder triaxial are available in current practice. Further, confining stresses of the soil can be controlled depending on the loading capacities of the test device whereas drainage conditions can also be accomplished. However, it has been noted that factors such as changes of packing density, micro structure, age, fabric, water content significantly influence the soil specimen to made different responses when relatively undisturbed and reconstituted specimens are concerned. In this regard, it has been considered that the reconstituted specimens with different methods allow systematic laboratory experimental studies of the soil response with respect to packing density, particle size and gradation and other factors (Vaid & Negussey, 1988; Vaid et al., 1990; Thevanayagam, 1998). However, studies conducted by Vaid et al. (1999), Høeg et al. (2000), Donahue et al. (2007) and Wijewickreme & Sanin (2008) indicated the significant differences in mechanical response of soil specimen prepared from relatively undisturbed and reconstituted soil samples. While the effect of fabric (Oda, 1972) and anisotropy (Oda et al., 1978) of soil have been investigated as possible causes for the different type of responses, Høeg et al. (2000) stated that predicting in-situ behavior of soil based on the reconstituted specimens is a difficult and complex approach. Further, in order to understand the field response of soil, Hight & Leroueil (2003) and Leroueil & Hight (2003) emphasized the importance of testing undisturbed samples of soil as not only

void ratio and density, but also anisotropy, fabric and direction of shearing with respect to the fabric are key factors in distinguishing the different types of behavior of soil. With the limited amount of test results obtained from relatively undisturbed specimens of fine-grained soil, in most cases in practice, cone penetration resistance and shear wave velocity based estimation for undrained strength and cyclic resistance of fine-grained soil against liquefaction have been considered.

## **2.5 Assessment of Liquefaction Resistance of Soil under Laboratory Conditions**

Laboratory element testing plays an important role in complementing the in-situ testing methods and correlations developed to assess the available soil shear resistance under seismic loading for geotechnical design. As such, it is of interest to review the methods used to assess the cyclic resistance ratio (CRR) against liquefaction (or cyclic failure) from laboratory testing of soil, as one of the objectives of this study is to study the cyclic shear resistance of natural silt. The Section 2.5.1 provides an overview on the term liquefaction and cyclic mobility with particular reference to the response of soils under cyclic loading conditions. In Section 2.5.2, commonly used criteria to define liquefaction under laboratory conditions are discussed along with the criteria selected to assess the liquefaction resistance for the present laboratory study.

### **2.5.1 Overview of Soil Liquefaction**

In describing the failure of Calaveras dam in California, Hazen (1920) introduced the term “liquefied”, and it is considered as the origin of the term liquefaction. Specially after the observations made during and after the 1960 Chile earthquake, 1964 Niigata earthquake, and

1964 Alaska earthquake, the term liquefaction triggering is now often associated with earthquakes (Davis et al. 1988).

When investigating the soil behavior after Niigata earthquake 1964, Ohsaki (1966) described that the soil attains a liquid-like state due to decrease of effective grain to grain contact pressure (arising as a result of rise in excess pore water pressure) - i.e., liquefaction due to earthquake shaking. Early investigations on earthquake induced soil liquefaction by Seed & Lee (1966), Yoshimi (1967), Seed & Lee (1967a, 1967b), Terzaghi & Peck (1968), Peacock & Seed (1968), Kishida (1969) and Finn et al (1970) used broad definitions as initial liquefaction, partial liquefaction, complete liquefaction to describe the phenomenon of liquefaction. Later, when extensive laboratory experiments (Seed & Peacock, 1971; Finn et al. 1971; Shibata et al. 1972; Ishihara & Yasuda, 1972; Yoshimi & Kuwabara, 1973; Ishibashi & Sherif, 1974; Lee & Albaisa, 1974; Lee et al. 1975; Castro, 1975; Wong et al. 1975; De Alba et al. 1976; Silver et al. 1976; Mullins et al. 1977; Martin et al. 1978; Vaid & Finn, 1979; Andersen et al. 1980; Vaid & Chern, 1983; Tatsuoka et al., 1986; Toki et al., 1986) on liquefaction were performed, it was necessary to define a criterion for liquefaction in order to identify, compare and analyze the strength or resistant of soil against liquefaction.

Through laboratory experimental studies and testing, three types of stress-strain responses have been observed: liquefaction, cyclic mobility with limited liquefaction, and cyclic mobility without limited liquefaction (Castro, 1969; Vaid & Chern, 1985). In the “liquefaction” type of response, the soil experiences contractive deformation until the steady state is reached – i.e., sand behaves in a contractive strain-softening manner with abrupt loss of stiffness and/or strength with development of large strains. In the “cyclic mobility without limited liquefaction”, the

shear strains increase gradually - with increasing number of load cycles, and there is gradual buildup of pore water pressure although there is no strain-softening (Boulanger & Idriss, 2006; Bray et al., 2004; Vaid & Chern, 1985). The behavior termed “cyclic mobility with limited liquefaction” lies essentially between the above two types: i.e., some limited strain softening occurs during the part of the load cycles leading the state of phase transformation, then the soil starts to behave in a dilative manner during increasing parts of the loading cycle, and in subsequent unloading parts of the cycles, larger excess pore water pressures are developed producing a state of zero effective stress. The loading cycles that follow would cause a dilative response leading to a strain-hardening tendency.

For example, in order to distinguish the failures due to limited movements caused by earthquakes against large movements such as in flow slides, Seed & Idriss (1971) suggested the term ‘cyclic mobility’. Castro (1975) pointed out that liquefaction develops only in loose sand, but cyclic mobility can be induced in the laboratory even in dense sand. Research on the cyclic shear behavior of fine-grained soils (Sanin & Wijewickreme, 2006; Wijewickreme et al. 2005) has indicated that some natural silts and tailings display cyclic mobility type strain development during cyclic loading with no liquefaction in the form of strain softening accompanied by loss of shear strength.

### **2.5.2 Criteria for Defining ‘Liquefaction’ and ‘Cyclic Failure’ in Laboratory Tests**

The instance, where soil attains a liquid-like state during cyclic loading, as a result of the rise of shear induced excess pore-water pressure and ultimately loss of effective grain to grain contact pressure have been observed by many researchers and investigators during their laboratory experimental procedures. The most commonly used criteria to define liquefaction or cyclic

failure are either based on  $r_u$  or based on strain development during cyclic loading (i.e., double amplitude axial strain) in cyclic shear tests. Based on the observations made on cyclic loading tests for sand, Seed & Lee (1966) defined initial / partial liquefaction as the stage where pore water pressure equals to the confining stress for some short time during the loading cycle; however, the failure of the specimen was defined as the attainment of 20% double-amplitude (DA) axial strain in CTX. The criterion that pore water pressure develops and equals to the confining stress as liquefaction was identified as a transient state by Martin et al. (1975) during laboratory testing with crystal silica sand, where they noted that the condition of  $r_u = 100\%$  coincides with the point where the applied cyclic stress is zero in loading cycles. The studies considered by both Gordon et al. (1974) and Lee et al. (1975) defined liquefaction as the instance when the excess pore pressure equals the initial confining effective stress. Additionally, Poulos et al. (1985) considered that the minimum undrained strength that remains after occurrence of  $r_u = 100\%$  is the undrained steady-state strength, which was noted to be as a function of void ratio. Emphasizing that  $r_u = 100\%$  cannot be used to estimate strength, Poulos et al. (1985) suggested that consideration of a definition of liquefaction based on momentary  $r_u = 100\%$  condition is misleading and fundamentally unsound.

Although Seed & Lee (1966) defined liquefaction based on the excess pore pressure, the failure criterion used for determining the cyclic shear failure was the achievement of 20% DA axial strain during CTX testing. Gordon et al. (1974) considered 5% of single-amplitude (SA) strain as a criterion for failure, whereas Lee et al. (1975) used 5% DA, or  $\pm 2.5\%$  SA strain as a failure criterion. Castro (1975) identified that substantial loss of soil shear strength that causes the soil mass to actually flows is the condition of liquefaction, while gradual increase of strain without

entailing a loss in shear strength is cyclic mobility; in this, DA strain of 5% was considered failure. Since then, many studies have used strain criteria such as 2.5%, 5%, 10% and 20% to define cyclic failure, and in turn, to estimate cyclic shear resistance. Seed & Idriss (1982) highlighted that for dense samples of sand, the onset of liquefaction or cyclic mobility is not so abrupt and a critical condition is normally considered to develop when the pore pressure ratio builds up to a value of 100 % and cyclic shear strain is  $\pm 5$  %. National Research Council (1985) used the results of the studies from Seed (1976) and Yoshimi et al., (1984) where  $\pm 2.5$ % SA and 5% DA axial strain were used as criteria to evaluate number of loading cycles in CTX to establish cyclic resistance of certain soils. Ishihara (1996) mentions that “the occurrence of 5% double amplitude axial strain in the cyclic triaxial will be taken up as a criterion to coherently define the state of cyclic softening or liquefaction of the soils covering from clean sands to fines containing sands.” Poulos et al. (1985) noted that it had become customary to use the term liquefaction to mean 5% strain in a cyclic test. The strain levels of SA 2.5% (Mullins et al., 1977), SA 3% to 5 % (Lefebvre & Pfendler, 1996), about SA 1.4% to 2% axial strain (Boulanger & Idriss, 2004), and SA 3% strain (Bray & Sancio, 2006) have been considered as approximately corresponding to initial liquefaction which was defined as the state where the excess pore pressure would equal the confining stress. As 5% DA strain level has been considered mainly as failure of the specimen in CTX, Vaid & Sivathayalan (1996), Sriskandakumar (2004), Sanin (2005), Wijewickreme et al (2005) and Porcino et al. (2012) have used a SA shear strain of 3.75% in CDSS tests - since 3.75% SA shear strain is equivalent to reaching a 2.5% SA strain in CTX under constant volume conditions.



Based on the above consideration, as an “index” of comparison, the occurrence of single-amplitude horizontal shear strain ( $\gamma$ ) value of 3.75% during a CDSS specimen was considered as criteria for determining unacceptable performance during the present investigation of cyclic shear resistance of natural silts – i.e., 3.75% SA strain criteria is used in Section 4.3 for deriving the cyclic shear resistance and other evaluations considered in this study.

## **Chapter 3: Experimental Aspects, Material Tested and Test Program**

This chapter presents the details of the Direct Simple Shear (DSS) device and the Data acquisition and Control System (DACS) of the DSS device as the experimental setup for the present laboratory study (Section 3.1); details on the soil sampling process, interpretation of soil type, conditions and properties of material tested (Section 3.2) during the study. Latter part of the chapter describes the test procedure elaborating on the specimen preparation and performance of DSS tests (Section 3.3), which is then followed by the test program (Section 3.4) of this study.

### **3.1 Experimental Aspects**

Many types of laboratory testing devices are available for the assessment of shear strength and deformation characteristics of soil – e.g., direct shear, direct simple shear, directional shear cell, ring shear, triaxial, hollow cylinder torsional and hollow cylinder triaxial devices. Out of these, cyclic triaxial (CTX) and cyclic direct simple shear (CDSS) tests are commonly used for the research studies on the cyclic shear response of soil. Triaxial device is one of the commonly used devices in practice, and the devices ability to directly impose principal stresses and/or strains is an added advantage since it allows subjecting the test specimen to well defined stress conditions. On the other hand, the DSS device imposes continuous rotation of principle stresses during shearing (Oda & Konishi, 1974), and therefore it is considered able to simulate the field stress conditions prevalent during earthquake loading, although some limitations exist in consideration of the specimen as a single element because of the boundary conditions of the apparatus (Silver

& Seed, 1971; Wood et al. 1979). Although ideal boundary deformation conditions are not achievable in a simple shear device, Finn (1985) pointed out that the practical boundary conditions that may be achieved in a well-designed simple shear device with rigid container walls create essentially uniform simple shear stress and deformation fields over a large portion of the test specimen.

Two types of DSS devices are most commonly used in studies for characterizing the mechanical response of soil. The Cambridge type DSS device (Roscoe, 1953) accommodates a cuboidal sample, and the other type DSS device (Bjerrum & Landva, 1966) which was developed at the Norwegian Geotechnical Institute (NGI) uses a cylindrical sample that is surrounded by a wire-reinforced rubber membrane. It has been shown that cubical specimen does reasonably subject the specimens to simple shear stress conditions whereas the NGI-type specimen with wire-reinforced membrane may not be uniformly distorted during shear due to the flexibility of the membrane. However, from a photographic analysis of the specimen during shearing, Youd (1972) showed that deformed profiles for larger displacement of the specimen with wire-reinforced membrane are approximately quite close to the true simple shear condition, thereby suggested that at smaller strain excursions, the approximation is even better. More similarities and dissimilarities of stress non uniformities in these two types of DSS devices have been extensively studied (Budhu, 1984, 1985; Dabeet et al. 2012; Hanzawa et al. 2007; Lucks et al. 1972). Further, Finn & Vaid (1977) conducted constant volume cyclic loading tests that were free from many difficult and time-consuming features of undrain cyclic loading test and reported that it is quickly to perform while indicating higher reproductively in results. Over the recent past, many additional improvements to DSS devices, such as loading mechanisms to address

specific research intentions have been reported by a number of researchers (Boulanger et al. 1993; Ishihara & Nagase, 1988; Ishihara & Yamazaki, 1980; and DeGroot et al. 1991).

With the above considerations in mind, the cyclic direct simple shear apparatus at UBC was used for the experimental program herein. As a part of the work, the UBC-DSS device was upgraded with a new Data acquisition and Control System (DACS). Graphical User Interface (GUI) was introduced to operate / control the DSS device in a more systematic, efficient and user friendly manner. The DACS includes: data acquisition, device control, signal conditioning and data processing, computing stress and strain states, and live displaying of stress and strain state plots during testing. The UBC DSS device and DACS are detailed in Section 3.1.1 and Section 3.1.2 respectively. The main components of the UBC DSS device and .DACS are depicted in Figure 3.1

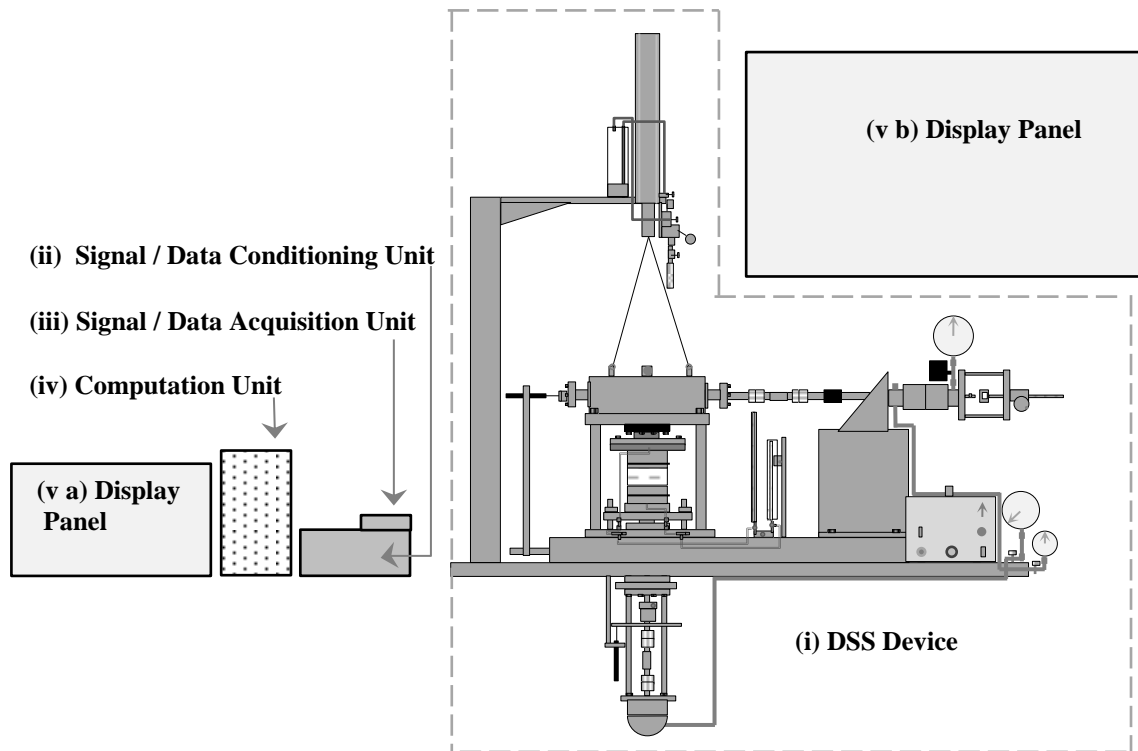


**Figure 3.1 Main components of the UBC DSS device and DACS**

### **3.1.1 UBC Direct Simple Shear (DSS) device**

The UBC-DSS device is a modified NGI-type device (Bjerrum & Landva, 1966). A schematic diagram of the device depicting main segments is given in Figure 3.2. The detailed configurations of these segments are then illustrated in Figure 3.3 to Figure 3.6 respectively.

In the DSS device, a cylindrical soil specimen of 70 mm in nominal diameter and approximately 20 mm in height is placed in a wire-reinforced rubber membrane. The specimen is laterally confined by the wire reinforced membrane that enforces an essentially constant cross sectional area and prevents the specimen from localized lateral deformations while promoting uniform shear deformation of the specimen during shear loading. By closing the top and bottom drainage lines (shown in Figure 3.5), during either monotonic or cyclic shear loading phase, undrained DSS tests can be performed. Similarly, by locking the vertical loading shaft (shown in Figure 3.6), vertical deformation of the specimen can be restricted during shearing stage. In this way, constant-volume condition can be achieved, as sample is restrained laterally by the wire-reinforced rubber membrane and vertical deformation is restricted by locking the vertical shaft. Hence, it is capable of conducting constant-volume undrained shearing in both monotonic and cyclic shear stress application. In constant-volume DSS tests, Dyvik et al. (1987) showed that the increments (or decrements) in vertical stress are equal to the measured excess pore pressures in an undrained DSS test. Hence, the increment and decrement of the vertical stress in constant-volume, undrained DSS test was interpreted as the corresponding decrement and increment of the equivalent excess pore water pressure during this study.

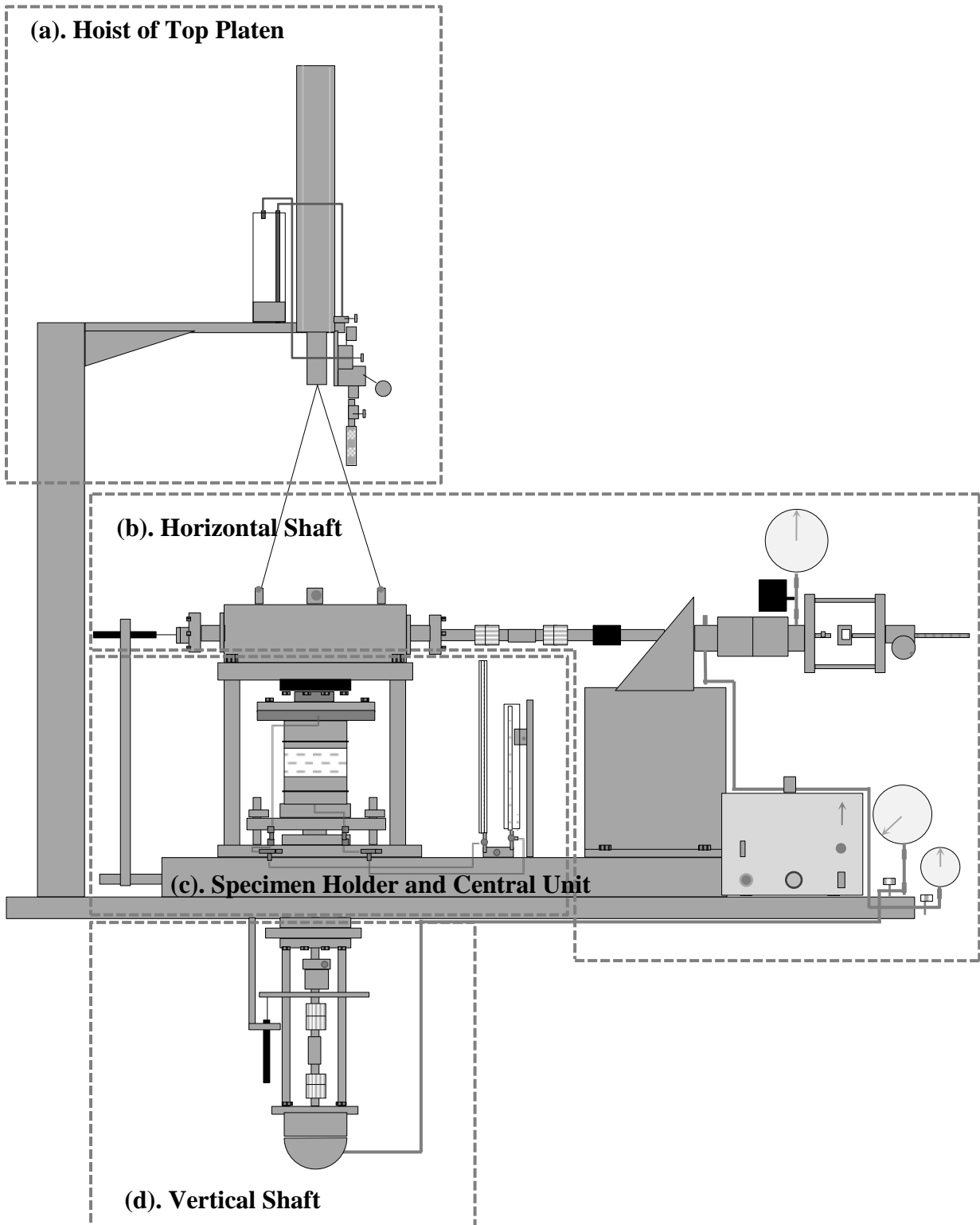


Figure 3.2 Schematic diagram of UBC DSS device

## Hoist of top platen

- (1) Air Cylinder
- (2) Oil Cylinder
- (3) Hoister Controller
- (4) Inlet Air Pressure Gauge
- (5) Air Pressure Controller
- (6) Hoister Direction Controller
- (7) Air Pressure Diffuser / Releaser Controller
- (8) Air Pressure Diffuser / Releaser

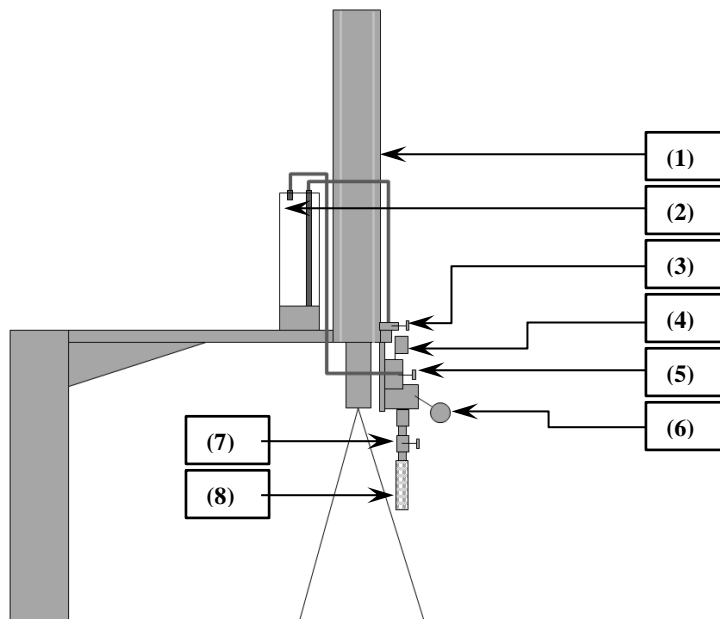
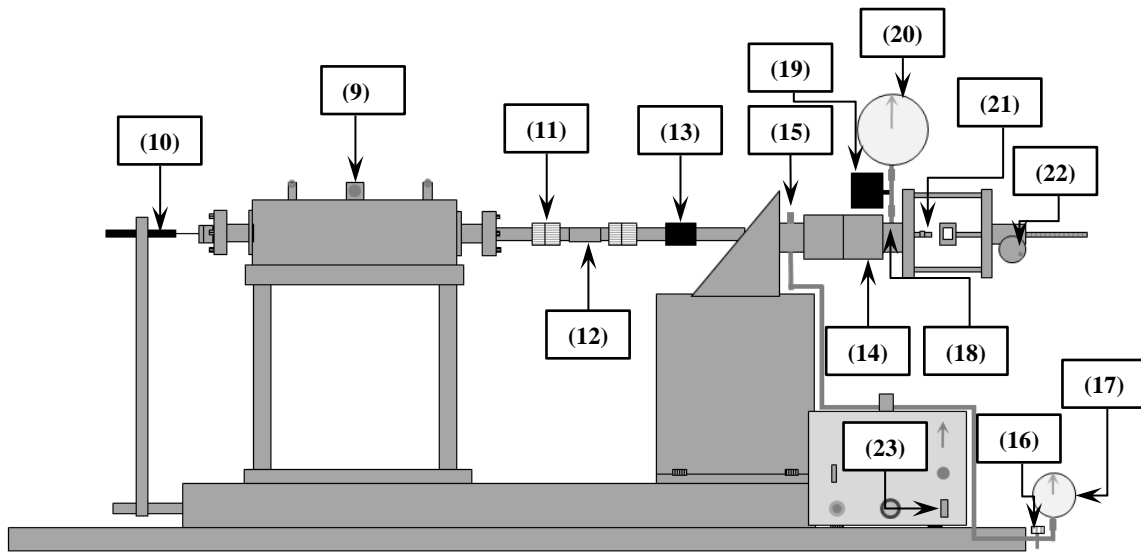


Figure 3.3 Schematic of Hoisting / Rigging of Top Platen

## Horizontal shaft

- (9) Horizontal Shaft Locker Pin
- (10) Horizontal LVDT
- (11) Horizontal Shaft and Actuator Connector
- (12) Horizontal Shaft Articulator
- (13) Horizontal Load Cell
- (14) Double Acting Pneumatic Cylinder (Static & Cyclic)
- (15) Air Pressure Inlet (Static)

- (16) Air Pressure Regulator (Static)
- (17) Air Pressure Gauge (Static)
- (18) Air Pressure Inlet (Cyclic)
- (19) Electro Pneumatic Regulator
- (20) Air Pressure Gauge (Cyclic)
- (21) Horizontal Shaft and Motomatic Motor Connector
- (22) Manual Shaft Mover (Motomatic Motor)
- (23) Motomatic Motor Controller Unit



**Figure 3.4 Schematic of Horizontal Shaft**

### **Specimen holder and central unit**

- (24) Top Platen Locator Bolts
- (25) Vertical Load Cell
- (26) Top Drainage Line
- (27) Top Porous Plate
- (28) Soil Specimen in a Wire Reinforced Rubber Membrane
- (29) Bottom Porous Plate
- (30) Bottom Drainage Line
- (31) Bottom Platen
- (32) Top Drainage Line Regulator
- (33) Bottom Drainage Line Regulator
- (34) Water Reservoir



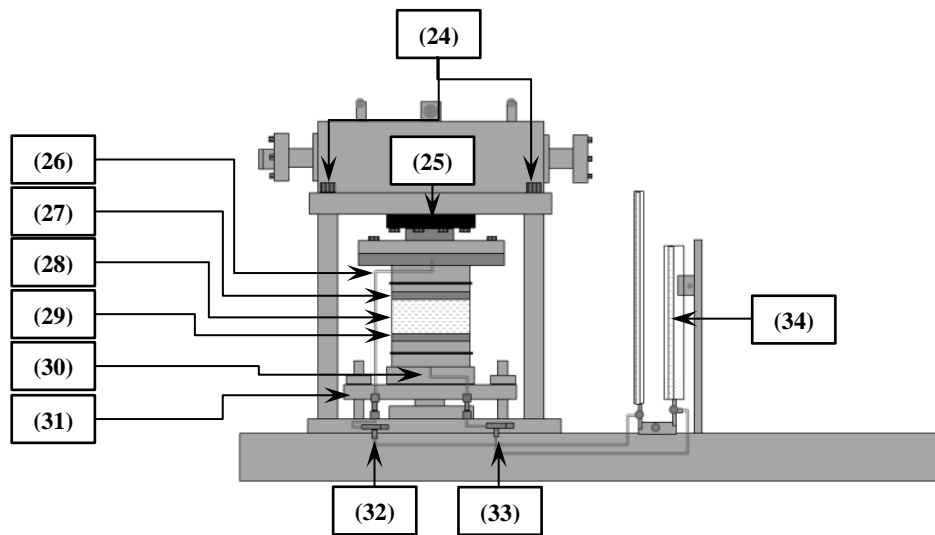


**Figure 3.5 Schematic of Specimen Holder and Central Unit**

## Vertical shaft

- (35) Vertical Shaft Locker Pin
- (36) Vertical LVDT
- (37) Single Acting Pneumatic Cylinder
- (38) Air Pressure Inlet (Single Acting Cylinder)
- (39) Air Pressure Regulator (Single Acting Cylinder)
- (40) Air Pressure Gauge (Single Acting Cylinder)

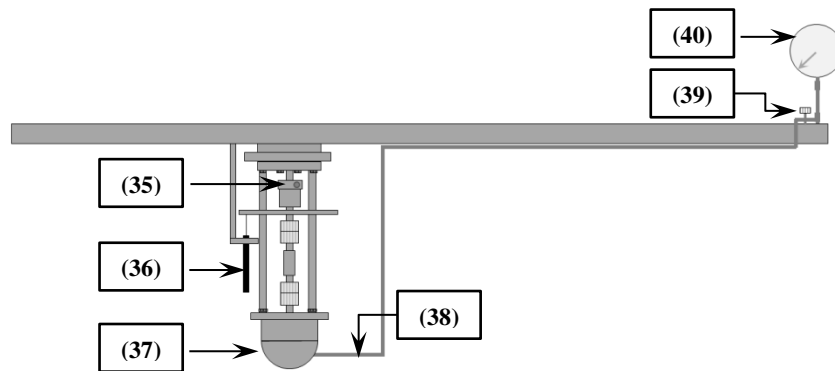


**Figure 3.6 Schematic of Vertical Shaft**

### 3.1.1.1 Transducers and measuring resolutions

The DSS device comprises of four transducers, and they are: (a) vertical load cell; (b) horizontal load cell; (c) horizontal displacement measuring Linear Variable Differential Transformer (LVDT); and (d) Vertical displacement measuring LVDT. Interface 1210 OE load cell which has a capacity of 1000 lb (453 kg) is used to measure the vertical load in DSS device. Sensotec 31 which is used to measure horizontal load has a capacity of 500 lb (226 kg). Both vertical (GCD-SE-2000) and horizontal (GCD-121-1000) LVDTs can measure displacements up to 50 mm and the capacity and measurement resolutions are listed Table 3.1. The “SMC IT2051-N33” type electro pneumatic regulator (EPR) which is capable of delivering 90 kPa full scale pressure output for a 1000 kPa input pressure is used to control the application of shear stresses during the cyclic shear loading phases.

**Table 3.1 Control capacity and measurement resolution of the UBC DSS device**

Measurement	Transducer Capacity	DSS Capacity	Resolution
Vertical / Normal Stress	1150 kPa Interface 1210 OE load cell : 1000 lb	850 kPa Limited by pressure control valve and gauge	0.15 kPa
Static Horizontal / Shear Stress	575 kPa Sensotec 31 load cell : 500 lb	70 kPa Limited by pressure control valve and gauge	0.05 kPa
Cyclic Horizontal / Shear Stress	575 kPa Sensotec 31 load cell : 500 lb	50 kPa Limited by electro pneumatic pressure regulator	0.3 kPa
Vertical Strain	250 % GA-HD GCD-SE-2000 50 mm	200 % Depends on the initial position of the LVDT	0.01 %
Horizontal Strain	$\pm 125$ % GA-HD GCD-121-1000 50 mm	$\pm 125$ % Depends on the initial position of the LVDT	0.005 %

### **3.1.1.2 Loading system and mechanisms of the DSS device**

In the DSS device, required vertical stress or stress increments / decrements on the soil specimen is applied through a single acting pneumatic piston (refer Figure 3.6). Vertical displacement of the specimen is measured using a LVDT. As the wire-reinforced rubber membrane ensures the constant cross sectional area during the testing, volumetric strain can be computed.

A soil specimen in the DSS device can be sheared by monotonic or cyclic variation of horizontal shear stress. The application of monotonic horizontal shear stress is achieved in a strain-controlled manner using a constant shear strain rate. In this, the horizontal shaft in the DSS device is attached to a motomatic motor which runs at a constant speed resulting in a constant strain rate during monotonic shearing (refer Figure 3.4). The cyclic shearing is controlled by an Electro-Pneumatic Regulator (EPR) that could impart changes in air pressure (on the one side of a double acting piston) in a sinusoidal manner so that the required amplitude and period of cyclic shear stress would be applied to the specimen. The horizontal displacement of the specimen is continuously monitored and measured during testing. As the height of the specimen is also continuously measured, shear strain of the soil specimen at any instant during the test can be computed.

### **3.1.2 Data Acquisition and Control System (DACS) of DSS Device**

DACS of the UBC.DSS device has four major components as (i) Signal / data conditioning unit, (ii) Signal / data acquisition unit, (iii) Computation unit and (iv) Display panels and are depicted in Figure 3.1. The signal / data conditioning unit, which was designed and produced by the UBC Civil Engineering workshop, consists of six analog input channels and two analog output channels. Four input channels are used for the vertical load cell, horizontal load call, vertical

displacement measuring LVDT and horizontal displacement measuring LVDT. Two output channels are for amplified horizontal LVDT signals and EPR signals. In signal conditioning unit, input signals can be amplified individually and all input channels are equipped with 50 Hz low pass filters in order to reduce the electrical noise. National Instruments USB 6341 X Series data acquisition (DAQ) unit which comprises 16 analog inputs with a sample rate of 500 kS/s, 16-bit resolution, voltage range of  $\pm 10$  V and two analog outputs with a sample rate of 900 kS/s, 16-bit resolution, voltage range of  $\pm 10$  V is connected to the signal conditioning unit. In the computation unit, acquired data are refined by averaging 100 readings for each channel prior to the computation. The computation unit houses the operating program which performs the tasks such as controlling the device, processing of acquired data, computing stress and strain state of the specimen, instantaneous and continuous displaying of stress and strain state plots during the testing period and recording of data. Further, two display panels provide GUIs to operate / control the DSS device in a more systematic, efficient and user friendly manner.

### **3.1.3 Graphical User Interface (GUI) of the DACS**

The GUI provides convenient platform to interact with the DSS device both in conducting the test and identifying the stress and strain levels of the tested specimen. Dedicated tabs for baselines values / measurements, consolidation, static bias, cyclic shear and monotonic shear phases ensure the systematically guidance for the user to conduct the DSS tests in methodologically manner. The indication of instantaneous stress-strain state of the test specimen continuously throughout the test provides a convenient atmosphere in the laboratory. Figure 3.7 Figure 3.8 and Figure 3.9 illustrate the GUI when ‘Consolidation’, ‘Cyclic shear’ and ‘Monotonic Shear’ tabs are active respectively.

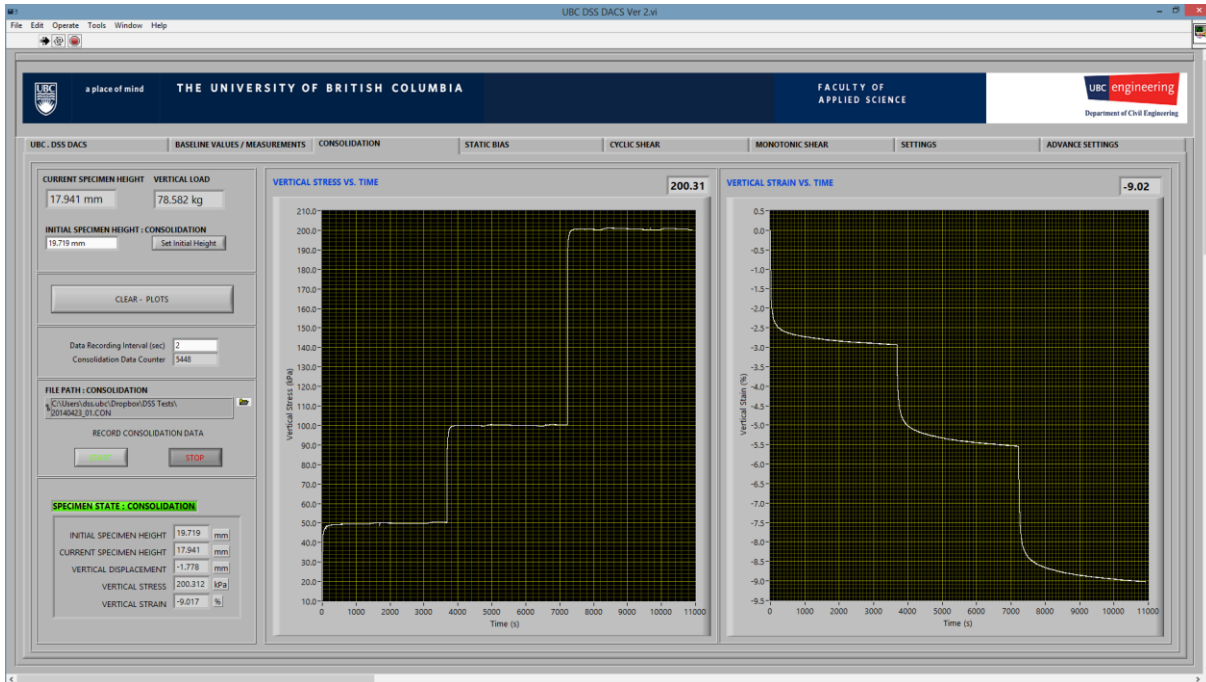


Figure 3.7 GUI of DACS during a typical incremental loading consolidation phase

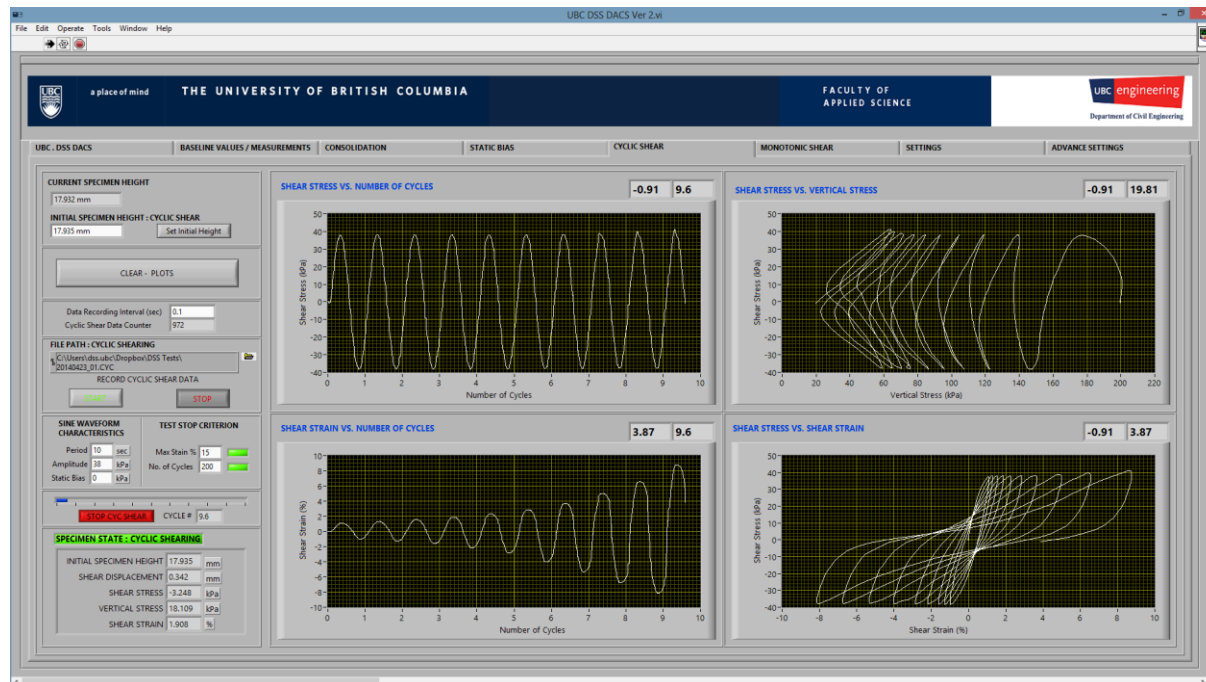
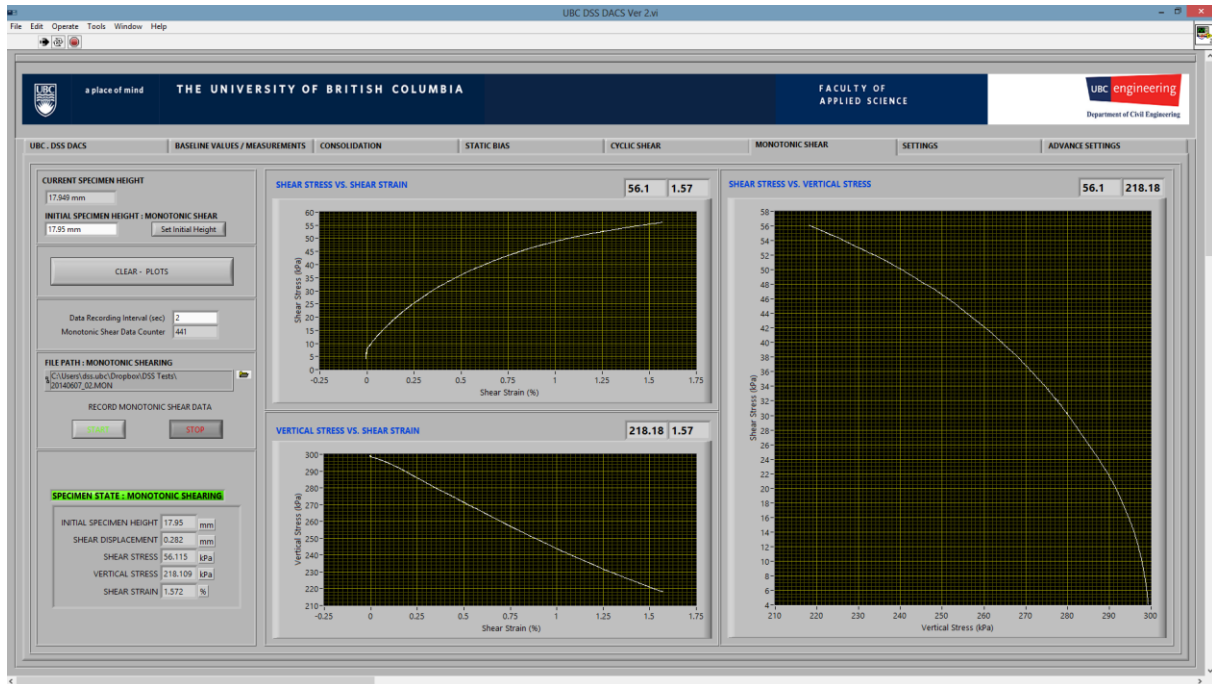


Figure 3.8 GUI of DACS during a typical cyclic shearing phase



**Figure 3.9 GUI of DACS during a typical monotonic shearing phase**

Additionally, it provides the freedom to change setting of the computation process such as calibration factors, data refreshing intervals, data acquiring frequency and etc. in the ‘Setting’ and ‘Advanced settings’ tabs.

### 3.2 Material Tested

As indicated in the introductory chapters, testing of relatively undisturbed fine-grained soil retrieved using thin-walled steel tube samplers was considered for this study. Additionally, a series of tests was conducted with reconstituted specimens in order to enhance the comparison with the response observed from relatively undisturbed specimens. This section presents the selection of location and method for soil sample retrieval including the initial analysis and characterization of the retrieved soil samples through x-ray radiography and soil index tests.

### 3.2.1 Background

The soil tested in this study originates from the Lower Mainland of British Columbia, Canada, and the location details (Figure 3.10) of the subject sites are presented in Table 3.2. The Fraser River Delta extends over a distance up to 23 km from a narrow gap in the Pleistocene uplands East of Vancouver, BC, and meets the sea (Strait of Georgia) along a perimeter of about 40 km (Luternauer et al., 1993). The deposits of the Fraser River Delta are Holocene in age and have a maximum known thickness of 305 m (Clague et al., 1996). These deposits can be subdivided into topset, foreset and bottomset units (Monahan et al., 1997), and the upper part of the topset comprises flood-plain silts and peat (Monahan et al., 2000).

**Table 3.2 Location details of subject sites**

<b>Site #</b>	<b>Location</b>	<b>Geographic Details</b>
Site #1 [CT]	Vulcan Way, Richmond, BC	South bank of the North arm of Fraser River (near Mitchell Island)
Site #2 [JS]	160 <sup>th</sup> Street, Surrey, BC	South bank of the Nicomekl River
Site #3 [MD]	Telegraph Trail, Surrey, BC	South bank of the Fraser River prior to the confluence with Pitt River (near Barnston Island)

The site #1 is at the south bank of the North arm of Fraser River. According to Armstrong & Hicock (1979), the site #1 area comprises shallow lake, salish delta sediments and lowland peat, underlying by overbank sandy to silt loam. The site #2, which is within the past river flooded area of Nicomekl River (Armstrong & Hicock, 1980) comprise shallow lake sediments and lowland peat overlying by sandy to silt loam, deltaic and distributary channel fill. At site #3, which is located on the south bank of Fraser River upstream of the confluence with Pitt River, is underlain by overbank marine silt and silty clay (Armstrong & Hicock, 1980).

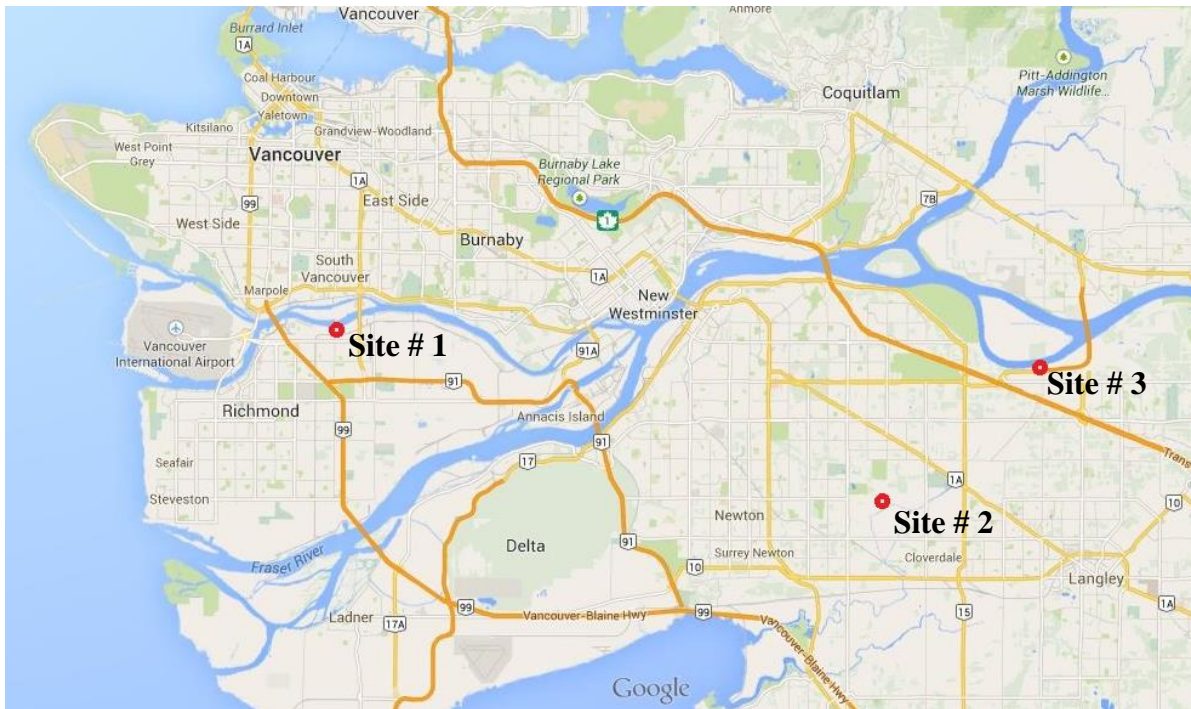


**Figure 3.10 Locations of subject sites in the Lower Mainland BC over-layer with Map data ©2014 Google**  
 Extracted from: <https://www.google.ca/maps/@49.1950801,-122.96154,11z>

In order to understand the soil stratigraphy and groundwater conditions at the site, a geotechnical investigation involving cone penetration testing (CPT) and mud-rotary drilling and sampling was undertaken at the three sites between February 06, 2013 and February 08, 2013. Mud-rotary test holes allowed thin-walled tube sampling to obtain thin-walled tube soil samples. The data from CPT tests allowed determining the optimum depth levels for soil sampling using thin-walled steel tube. Details related to CPT testing and mud-rotary drilling and sampling are given in the next two sub-sections.



### 3.2.2 Cone Penetration Testing

The corrected tip resistance for pore water pressure effects ( $Q_t$ ), friction sleeve stress ( $F_s$ ), friction ratio ( $R_f$ ), equilibrium (in-situ) pore water pressure ( $U_0$ ) and pore water pressure (behind the tip of cone) ( $U_2$ ) readings obtained from the CPT with respect to the depth below ground level are presented in Figure 3.11, Figure 3.12 and Figure 3.13 for Sites #1, #2 and #3 respectively. The interpreted soil behavior types based on the CPT data are also mentioned in those figures and the CPT interpretations are detailed in below.

The interpretations based on CPT data revealed the presence of silt with occasional inter-bedded sandy silt and sand layers from about 2 m to 7 m depth below the ground level at the site #1. Following that, CPT data suggested the existence of silty sand and sand mixtures beyond 7 m depth level. Hence, the silt deposit in-between the depth levels of 5 m to 6.8 m below the ground level were considered as the source of test material from site #1 for the study. In site #2, CPT data suggested that the relatively uniform silt can be found from about 1 m up to 12 m depth level below the ground level. Therefore, silt retrieved from 4.2 m to 5.5 m depth below the ground level at the site #2 was used for the current study. Apart from the top fill layer which was suggested to comprise gravel and sand up to about 4 m depth below the ground level at site #3, the interpreted soil behavior based on the CPT data revealed uniform silt to clayey silt deposit. Hence, for the present study, silt retrieved from depth levels of 4.4 m to 5.5 m was considered. The ground water levels and depth ranges of the material studied under this study from all three sites are indicated as shaded strips in Figure 3.11, Figure 3.12 and Figure 3.13.

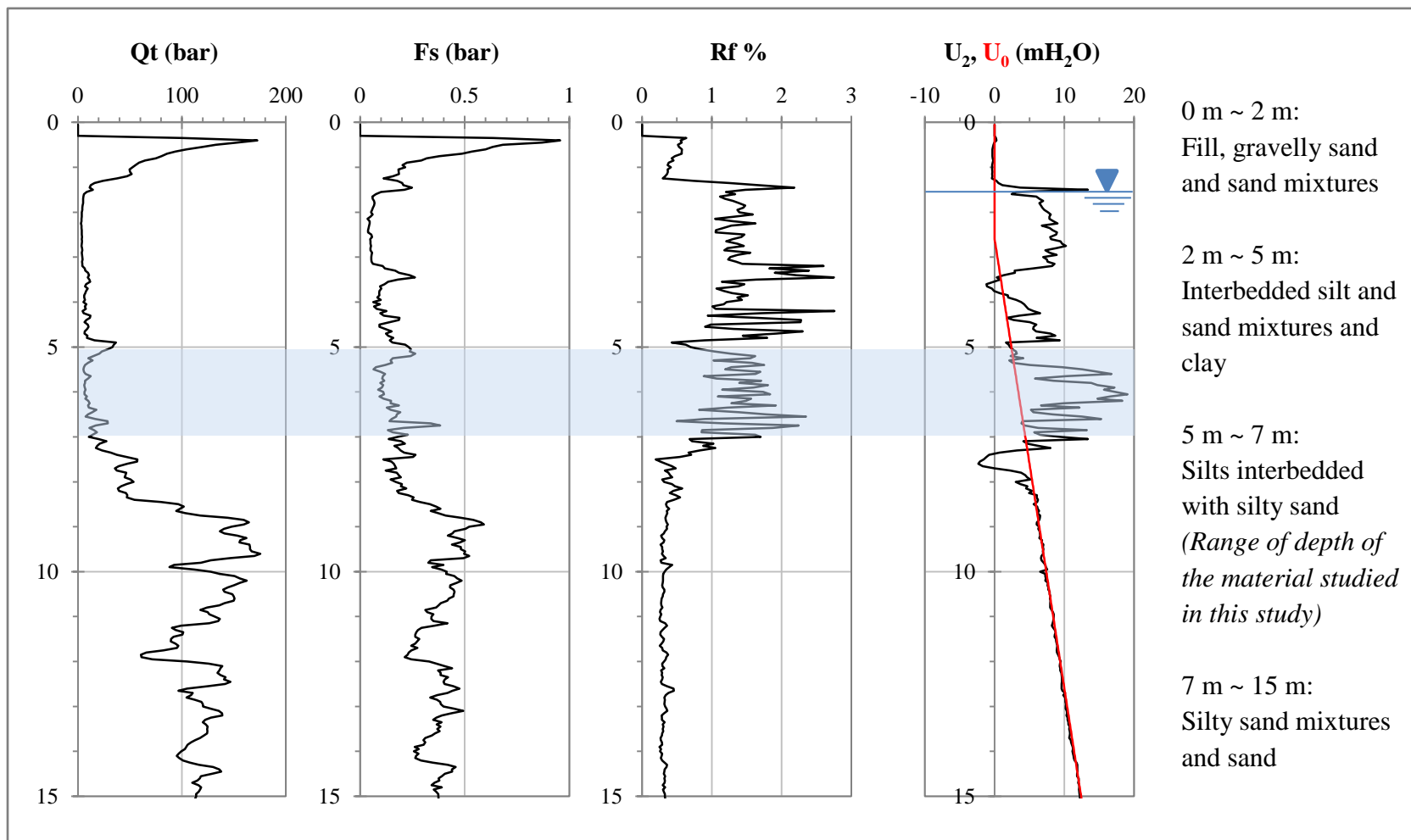


**Figure 3.11 Cone penetration test profiles at Site #1, Vulcan Way, Richmond BC**  
Range of depth of the material studied in this study is highlighted

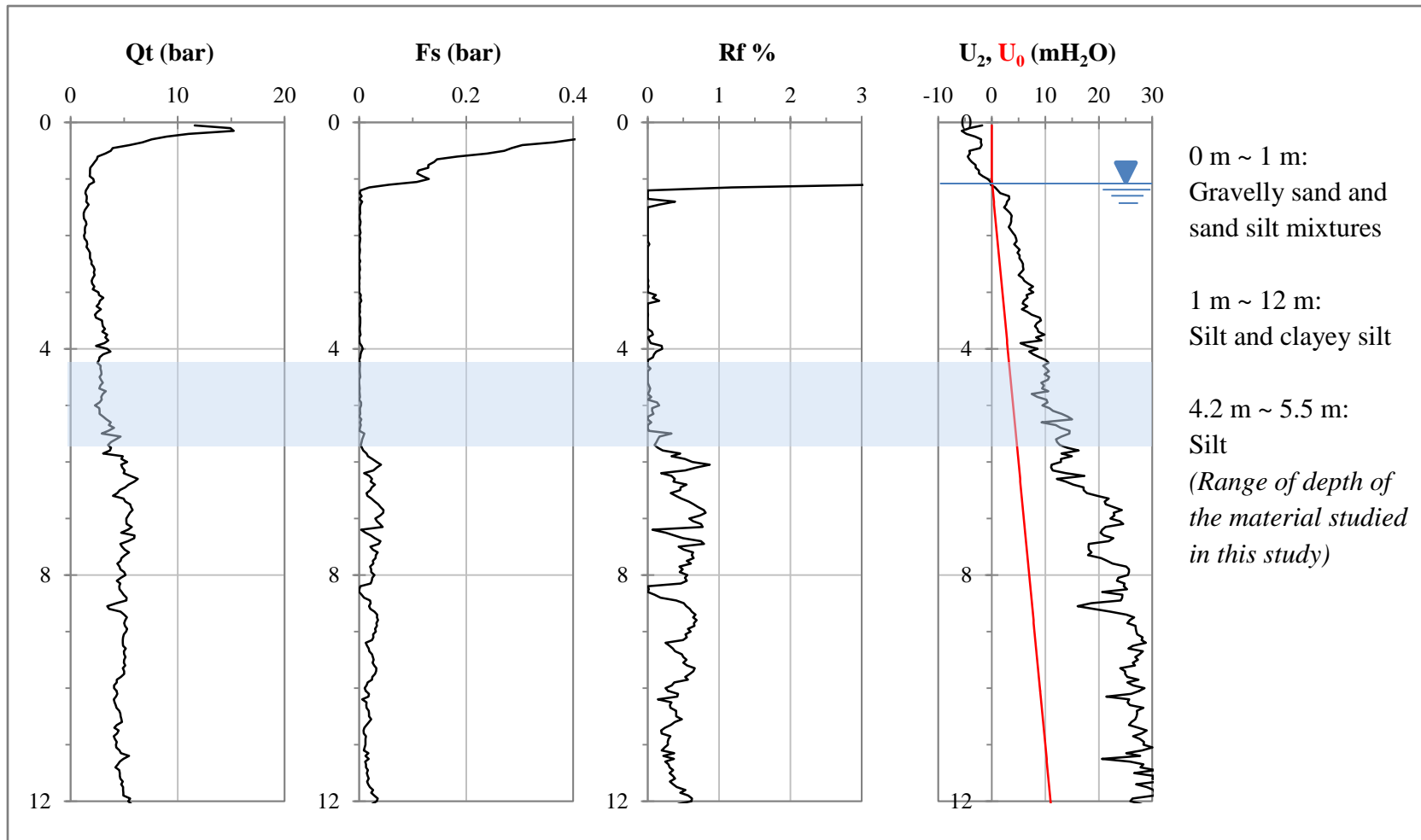


**Figure 3.12 Cone penetration test profiles at Site #2, 160th Street, Surrey, BC**  
Range of depth of the material studied in this study is highlighted

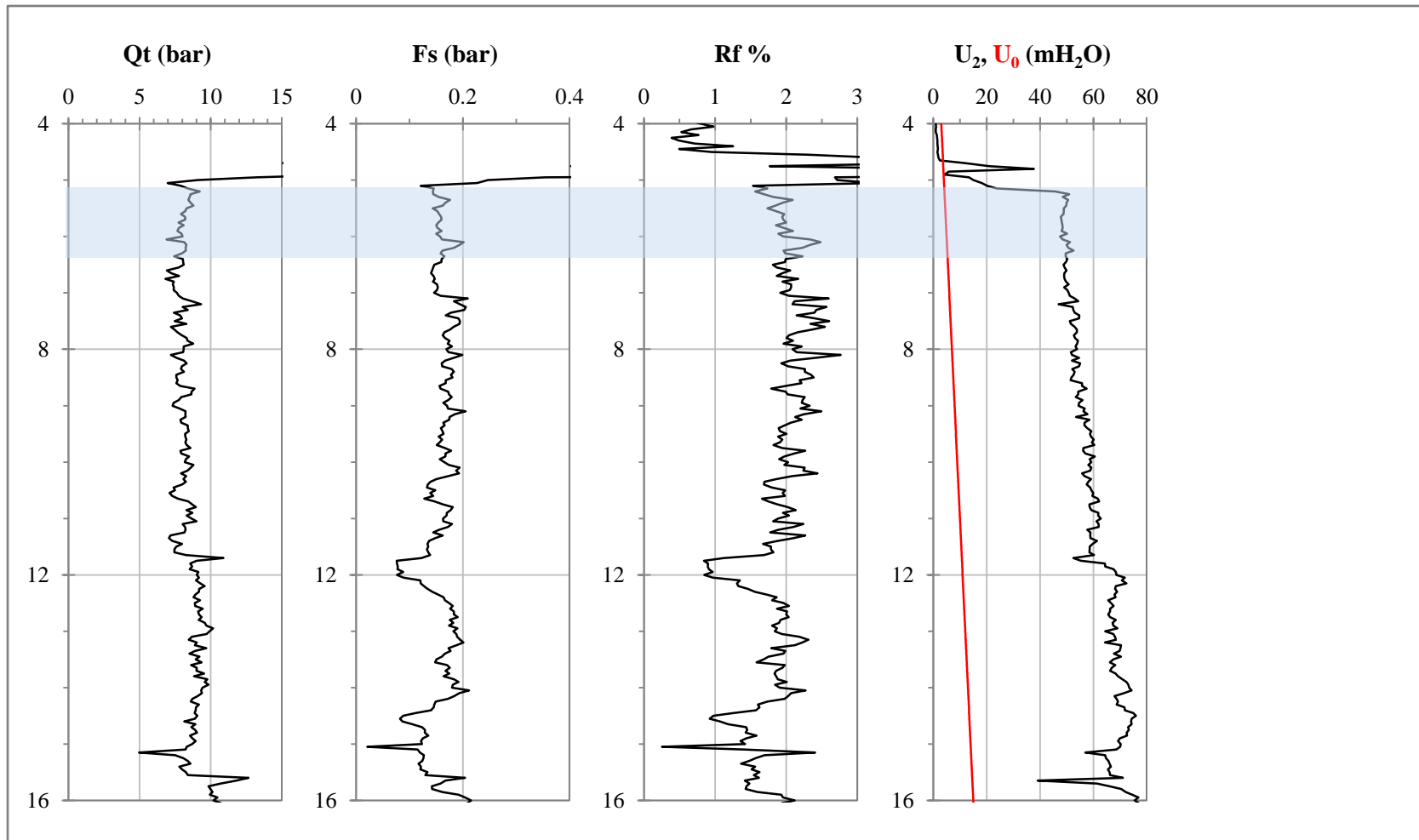


**Figure 3.13 Cone penetration test profiles at Site #3, Telegraph Street, Surrey, BC**  
 Range of depth of the material studied in this study is highlighted

### 3.2.3 Soil Sample Retrieval

Specially fabricated stainless-steel tubes having an outer diameter of 76.2 mm, with no inside clearance, sharpened ( $5^\circ$ -beveled) cutting edge, and 1.5 mm wall thickness, as shown in Figure 3.14, were used to retrieve relatively undisturbed soil samples from the test holes put down using conventional mud-rotary drilling (Figure 3.15) .

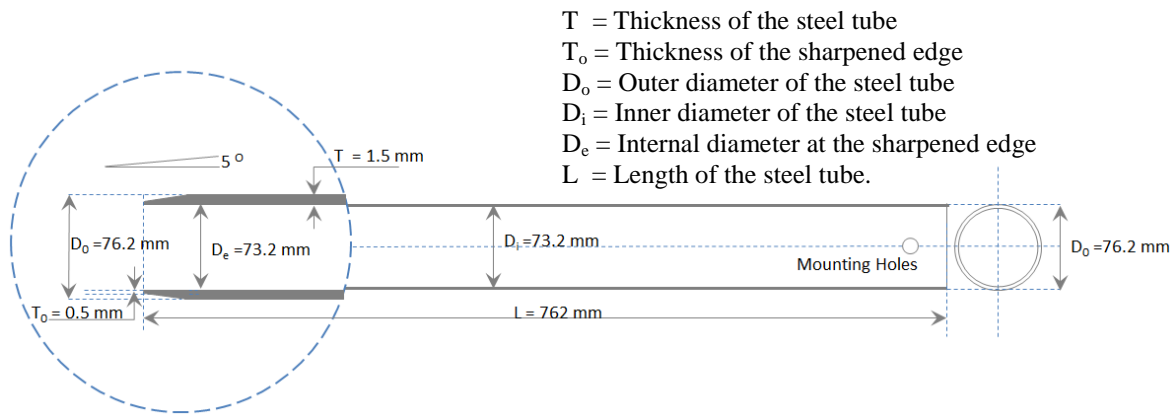


**Figure 3.14 Dimension details of the specially fabricated thin walled samplers with no insider clearance**

Upon retrieval from test holes, the thin-walled samples were sealed at the ends using rubber expansion plugs (“packers”) and wax to preserve the natural water content during transportation and storage. Except at the time of testing and extrusion, the soil samples were stored and secured in a vertical position in a “moist room” (which is maintained at high humidity by automatic spraying of water) in the UBC Geotechnical Research Laboratory.



**Figure 3.15 Conventional rotary mud drilling at Site #1, # 2, and #3 for obtaining relatively undisturbed soil samples**

### **3.2.4 X-Ray Radiographic Analysis**

To determine the quality of the soil retrieved from thin-walled steel tube samplers in a non-destructive manner, x-ray radiography was conducted in accordance to the D4452 -06 (ASTM, 2006) using the custom-designed cabinet x-ray system at the geotechnical research laboratory in UBC. The details of the x-ray radiography conducted for the thin-walled samplers which were used for this study are presented in Appendix A. The x-ray radiography analysis suggested that no evidence of shear fractions, calcareous concretions, shells and invertebrates. However, in certain cases, existence of voids, organic matters and roots and natural fissures could be interpreted based on the x-ray radiography. More importantly, no traceable turning edges were observed therefore, it has indicated proper or good quality sampling during sample retrieving procedure. It is to be noted that the above interpretations were made based on the guideline that

were presented in D4452 -06 (ASTM, 2006) therefore the actual conditions of the retrieved soil samples may be different from the those interpreted above.

### 3.2.5 Soil Grain Size Distribution and Index Testing

Representative soil portions obtained from thin walled samplers were used for evaluating the soil grain size distributions and other soil indices employing standard test methods [i.e. specific gravity D854-10 (ASTM, 2010b), particle size analysis D422-63 (ASTM, 2007) and plasticity index of soil D4310-10 (ASTM, 2010a)]. The lower and upper bound of the ranges of gradation curves for the soil obtained from three sites are indicated in Figure 3.16. The complete set of gradation curves with respect to different depth levels from each site are presented in Appendix B.

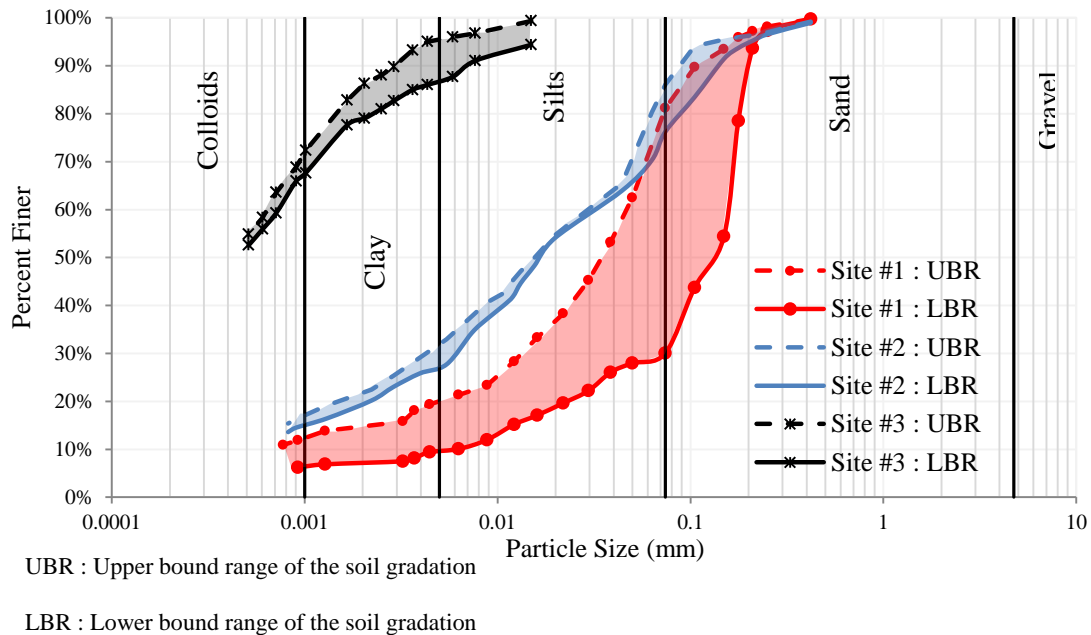


**Figure 3.16 Particle size distribution: Upper and lower bound range of soil gradation curves for Site #1, #2 and #3**

The results from these tests are summarized in Table 3.3. Some of the parameters obtained from CPT testing for these soils area also included in the same table. On average, clay percent were 18 % and 30 % in soil from Site #1 and #2, while the soil from Site #3 contains 70 % of colloids. However, the gradation curves for Site #1 presented in Appendix B in the Section of Appendices indicate a variation of the coarser fraction from 20% to 70 %. Hence, with the presented grain gradation soil samples from Site #1 can be classified as a range from silt with little sand to sandy silt in according to D2488-09a (ASTM, 2009). Unlike for the Site #1, variations of the upper and lower bound ranges of gradation curves for Site #2 and #3 shown in Figure 3.16 are not significant. In general, soil retrieved from Site #1, #2 and #3 can be classified as silt with slight plasticity, low plasticity and high plasticity respectively.

**Table 3.3 Soil properties and index parameters**

Parameter	Value(s)		
	Site #1 (CT)	Site #2 (JS)	Site #3 (MD)
Depth level (m)	5 ~ 7	4.2 ~ 5.5	4.9 ~ 6.2
In-situ water content ( $WC_i$ -%)	35 ~ 44	38 ~ 53	58 ~ 69
Pre-consolidation stress ( $\sigma_{pc}$ kPa)	100 ~ 125	35 ~ 45	75 ~ 85
Specific gravity ( $G_s$ )	2.70	2.77	2.75
Plastic limit (PL- %)	29 <sup>a</sup> (6.9) <sup>s</sup>	34 <sup>a</sup> (3.9) <sup>s</sup>	42 <sup>a</sup> (5.5) <sup>s</sup>
Liquid limit (LL- %)	34 <sup>a</sup> (6.7) <sup>s</sup>	41 <sup>a</sup> (4.7) <sup>s</sup>	76 <sup>a</sup> (9.9) <sup>s</sup>
Plastic index (PI)	5 <sup>a</sup> (0.7) <sup>s</sup>	7 <sup>a</sup> (2.2) <sup>s</sup>	34 <sup>a</sup> (3.8) <sup>s</sup>
Unified soil classification D2487-11 (ASTM, 2011)	ML	ML	MH
Estimated in-situ effective overburden stress ( $\sigma'_{vo}$ kPa)	70 ~ 77	42 ~ 49	44 ~ 51
CPT, cone penetration resistance ( $Q_t$ -MPa)	0.9 ~ 1.6	0.3 ~ 0.45	0.6 ~ 0.8
CPT, friction sleeve stress ( $F_s$ kPa)	15 ~ 35	4 ~ 8	15 ~ 20

a = average value, s = standard deviation



### 3.2.6 Assessment of Sample Quality

One-dimensional (1-D) consolidation tests were conducted in order to assess the compressibility characteristics of the soil, and in turn, the sample quality in terms of disturbance. Void ratio versus vertical effective stress obtained from 1-D consolidation tests are presented in Figure 3.17. Pre-consolidation stress values inferred from these compressibility characteristics in according to Casagrande (1936), Becker et al. (1987) and (Janbu, 1969) methods are tabulated in Table 3.4 and they were in the range of 100 kPa~125 kPa, 35 kPa~45 kPa and 75 kPa~85 kPa for the soil samples retrieved from Site #1, #2 and #3 respectively. Detailed procedures of the estimated pre-consolidation stresses are presented in Appendix C. When these pre-consolidation stresses are compared with the in-situ effective overburden stress shown in Table 3.3, soil retrieved from Site #1 and #3 seems to be in slightly over-consolidated state whereas soil from Site #2 indicates that they were in normally consolidated state.

Despite the careful attention paid during sampling, transportation, storage and extrusion, sample disturbance is inevitable. The change in void ratio ( $\Delta e$ ) at the initial stage in the 1-D consolidation tests with respect to the void ratio observed at estimated in-situ stress condition was examined to assess the sample disturbance according to Lunne et al. (2006) which suggests that the specimens could be considered ‘good to fair’ in terms of sample disturbance if  $\Delta e/e_0$  (normalized void ratio)  $\leq 0.07$ , and the specimens are to be classified as ‘poor’ if  $\Delta e/e_0$  is greater than 0.07. The  $\Delta e/e_0$  values from the present testing are presented in Table 3.4. As may be noted, in most cases, the  $\Delta e/e_0$  values are lesser than 0.07, indicating ‘good to fair’ in terms of sample disturbance according to Lunne et al. (2006).

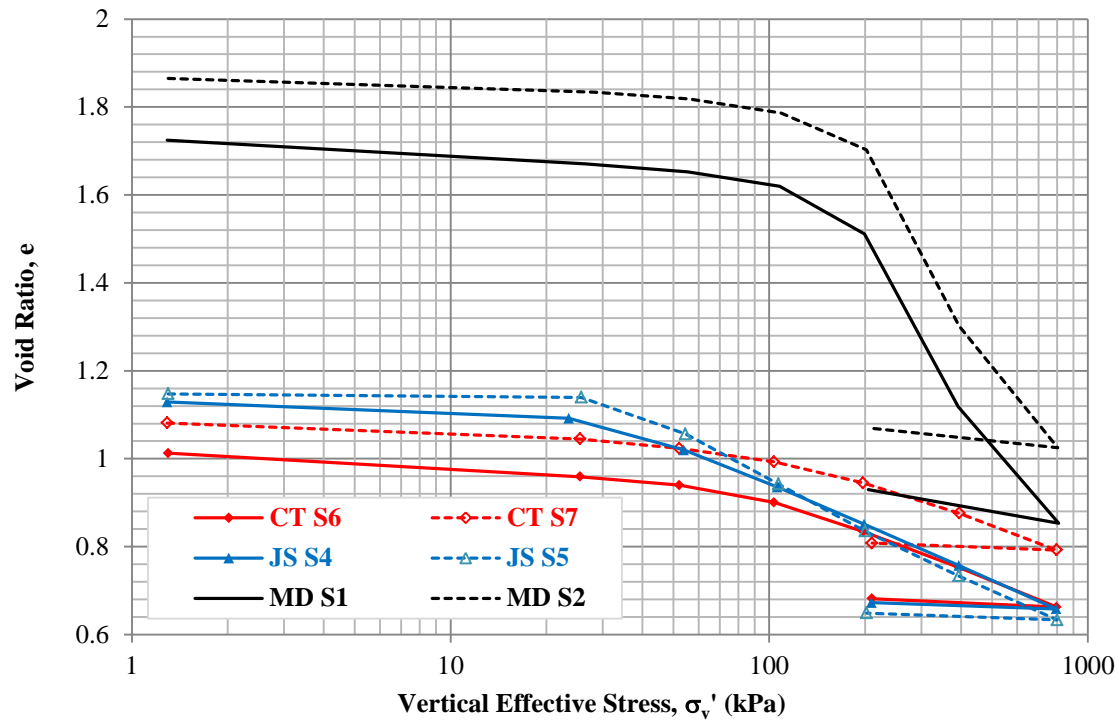


Figure 3.17 Compression characteristics from 1-D consolidation tests

Table 3.4 Assessment of sampling quality and estimation of pre-consolidation stresses from 1-D consolidation test results

Sample ID (Site-Thin walled sampler no.)	Sampling quality classification according to Lunne et al. (2006)		Estimation of Pre-consolidation Stresses in kPa according to		
	$e_o$	$\Delta e/e_o$	Casagrande (1936)	Becker et al. (1987)	Janbu (1969)
CT-S6	1.012	0.081	100	102	105
CT-S7	1.081	0.066	120	125	140
JS-S4	1.129	0.070	35	40	60
JS-S7	1.148	0.068	40	45	70
MD-S1	1.724	0.037	80	75	80
MD-S2	1.865	0.030	85	75	75

$e_o$  = Initial void ratio,  $\Delta e$  = Change in void ratio in between the initial stage and loading up to in-situ stress level

### **3.3 Specimen Preparation and Test Procedure for DSS Testing**

#### **3.3.1 Specimen Preparation**

In this study, most of the DSS tests were conducted using relatively undisturbed specimens prepared from the soil samples extruded from the thin-walled tube samplers. Limited amount of DSS tests were also conducted on reconstituted specimens. The following sections describe the preparation procedure of those test specimens.

##### **3.3.1.1 Preparation of relatively undisturbed specimens**

The soil samples were extruded using an upright extruder as depicted in Figure 3.18. When the extruded portion was approximately 40 mm in height, it was trimmed at the bottom with a wire saw so that the plane of cut is flush with the brass plate attached to the extruder (refer Figure 3.18).

The soil specimens for DSS testing were produced by pushing a sharpened-edge polished stainless steel ring (having a diameter of about 70 mm) vertically downwards on to the extruded soil samples. Since the extruded sample had a diameter of ~73 mm, the pushing process of the stainless steel ring caused the vertical cylindrical face of the sample to be subjected to a minor trimming leading to a sample with a diameter of about 70 mm which is ready for accommodation in the DSS device. The sample which was secured in the steel ring was then trimmed at the top and the bottom sides using a wire saw, leading to a specimen with a height of about 20 mm having smooth top and bottom surfaces as shown in Figure 3.19. DSS device was prepared in advance to accommodate the trimmed specimen inside the steel ring.

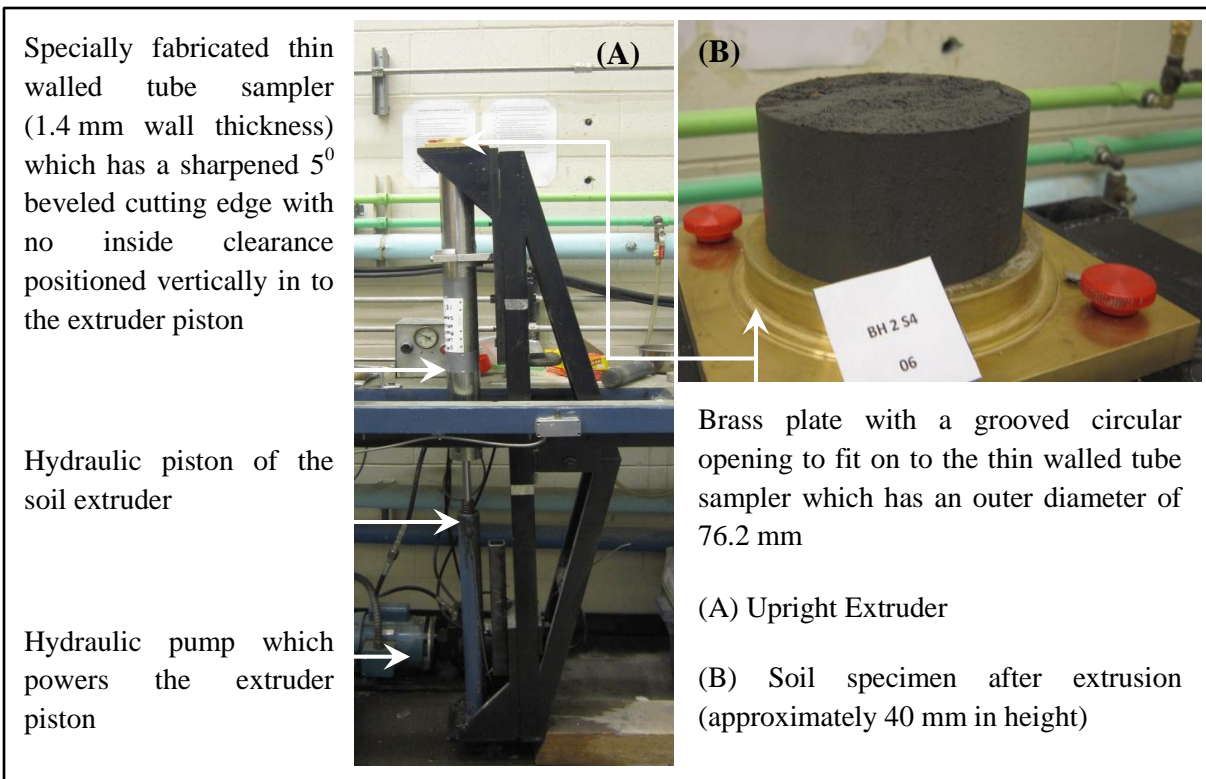


**Figure 3.18 Extrusion of soil specimen from thin-walled steel tube sampler**

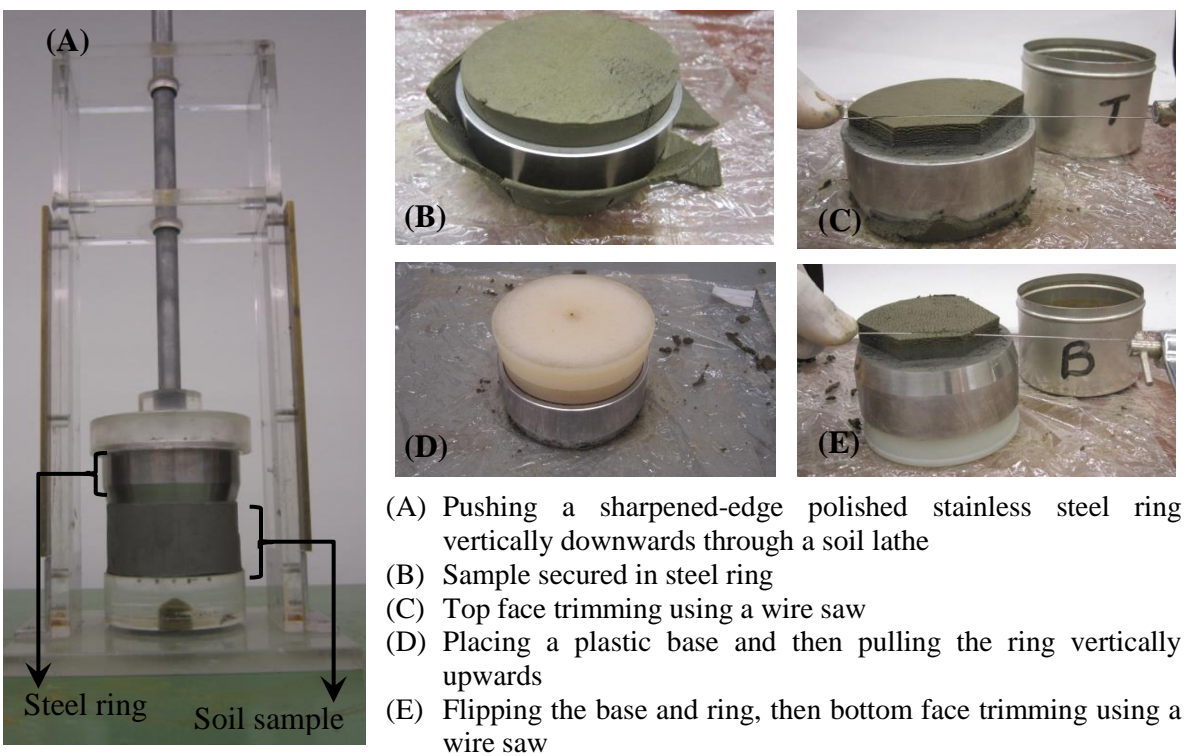


**Figure 3.19 Preparation of relatively undisturbed specimen**

### 3.3.1.2 Reconstituted specimen

The reconstituted specimens tested in this study were prepared from a saturated slurry and the preparation steps for the reconstituted specimens are as follows. The approach is essentially identical to that developed by Sanin (2010).

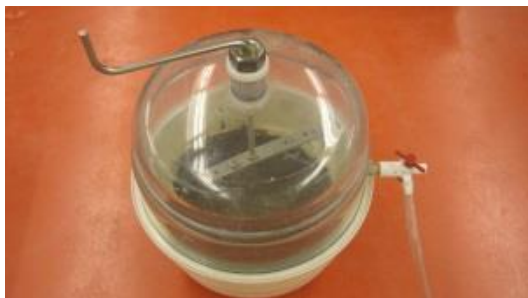
Initially, the soil was dried, and then any clumps of soil were broken down using a pestle, and then de-aired water was added with mixing until a slurry was formed as shown in Figure 3.20-(B). The slurry was kept under vacuum for 24 hours. The sample was stirred, re-mixed and shaken occasionally while it was under vacuum, in order to minimize the entrapped air bubbles inside the slurry.



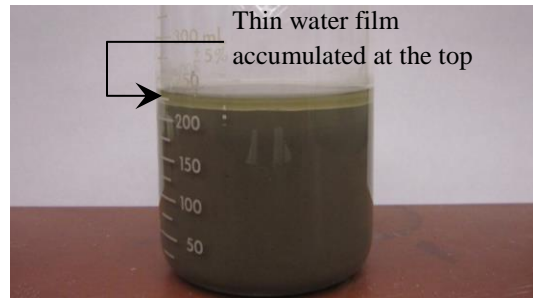
(A) Breaking down soil clumps



(B) Mixing of soil with de-aired water



(C) Soil kept under vacuum with occasionally stirring and re-mixing.



(D) Slurry in the 300 ml beaker just before the thin-clear water film is removed by suction

**Figure 3.20 Preparation of reconstituted specimen**

The slurry was then transferred to 300 ml beakers and allowed to consolidate under its own weight for about 24 hours; at this point, thin-clear water film formed at the top of the slurry was carefully removed by applying suction. Remaining material was stirred once again and ready to be spooned when the DSS device was prepared to accommodate the soil as described in Section 3.3.2.

### 3.3.2 Set up of DSS device

Two porous plates were boiled in water to make them saturated prior to placing them in the recesses at the bottom and top platens which are connected to saturated drainage lines (see Figure 3.5). Steel-reinforced wire membrane was placed on the recess at the bottom platen and followed by sealing the bottom of the membrane by a placement of an O-ring as shown in Figure 3.21-(A).

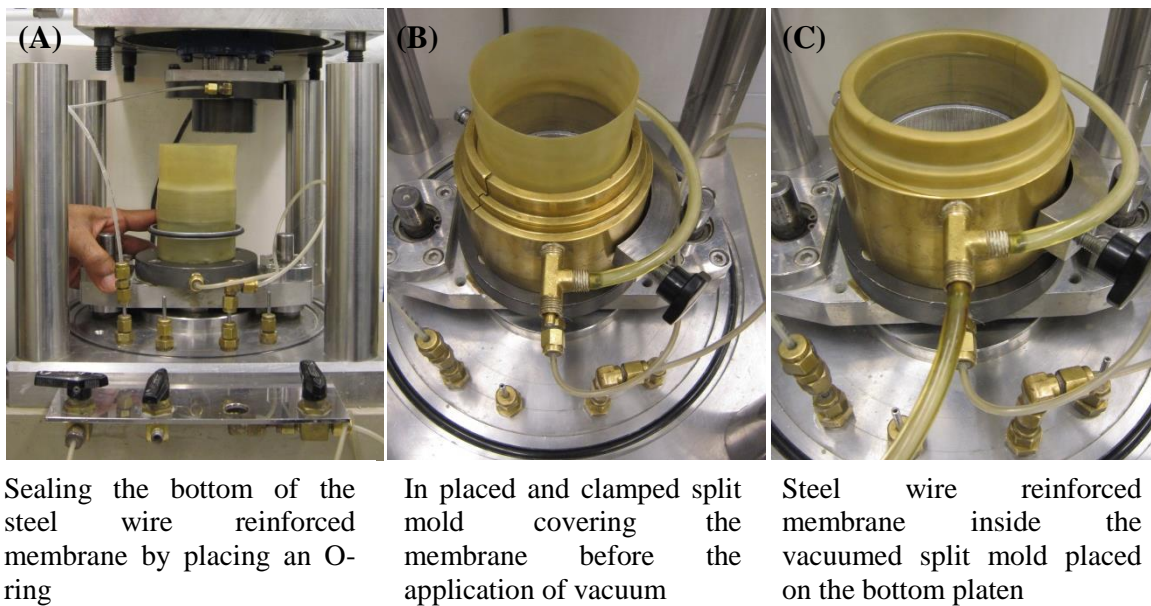


**Figure 3.21 Preparation of the DSS device to receive a soil specimen**



The split mold is then placed in clamped such that it covers the membrane. Application of vacuum and neatly placing the excess top portion of the membrane over the split mold as shown in Figure 3.21-(C) creates a cavity to receive the prepared DSS specimen inside the steel ring for relatively undisturbed specimens, or to place the soil-slurry for reconstituted specimens.

### 3.3.3 Placement of the Specimen in DSS Device

The DSS device is set up as detailed in Section 3.3.2 allows the specimen to be placed in the cavity surrounded by the steel wire reinforced rubber membrane. Following sections describe the procedure of specimen placement for relatively undisturbed specimens and reconstituted specimens.

#### 3.3.3.1 Placement of relatively undisturbed specimen

The trimmed specimen in the steel ring as described in Section 3.3.1.1 was carefully placed on the cavity surrounded by the split mold and the wire-reinforced membrane.

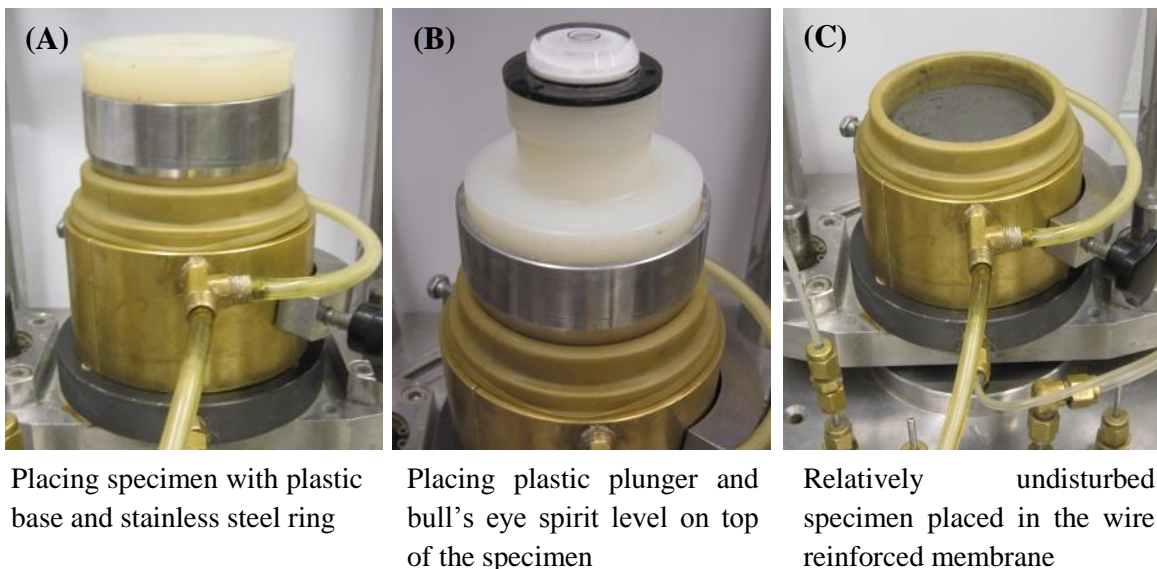


**Figure 3.22 Placing relatively undisturbed specimen in DSS device**

Using a plastic plunger the specimen was smoothly and gradually pushed downwards ensuring an uniform movement by observing the horizontality of the top surface of the plunger as shown in Figure 3.22 (B).

### 3.3.3.2 Reconstituted specimen

Soil slurry prepared as described in Section 3.3.1.2, was gently placed in the cavity surrounded by the wire reinforced membrane as shown in Figure 3.23. Efforts were made during placement to minimize the formation of entrapped air in the reconstituted specimen. At this point, a portion of slurry was sampled for the determination of moisture content. Reconstituted specimen prepared and placed in the DSS device according to the method described herein would not allow controlling the as placed density; therefore, densities obtained from this slurry deposition method were difference from the densities noted in relatively undisturbed specimens. Furthermore, fabric, aging and other related aspects of the reconstituted specimens differs from those of relatively undisturbed specimens.



(A) Spooning the slurry to the cavity surrounded by the wire reinforced membrane



(B) Reconstituted specimen placed in the wire reinforced membrane

**Figure 3.23 Placing reconstituted specimen in DSS device**



After the reconstituted or relatively undisturbed specimens were placed in the DSS device, top platen of the DSS device was lowered and positioned. A seating pressure of about 10 kPa was applied to the specimen in order to make sure that top and bottom platens were firmly intact with the specimen. Membrane was then sealed with the top O-ring as shown in Figure 3.24 (A) and then the specimen was ready to test in consolidating phase.

### **3.3.4 Loading Phases**

This section describes the application of loading during consolidation, cyclic and monotonic shear loading and post cyclic consolidation loading phases.

#### **3.3.4.1 Consolidation phase**

Upon the completion of specimen setup, the vertical load on the specimen was increased to meet the required effective consolidation stress level as required by the test parameters in the test. Target consolidation stress value was achieved by incremental loading method. Using the measurements taken from the vertical load cell and LVDT during the application of consolidation loading, vertical stress level and vertical strain (change of height of the specimen with respect to the initial height of the specimen when it was under a seating load of about 10 kPa) were computed and recorded through the DACS. Specimens were kept at the consolidation test phase for a duration of 1800 seconds (30 minutes) to 10,000 seconds (~3 hours), depending on the time duration required for the test specimen to gain approximately constant vertical strain with respect to time for the applied consolidation stress (i.e. sufficient time for the completion of primary consolidation of the test specimens). In order to achieve a test specimen with a required over consolidation ratio, prior to the shear loading phase, specimens were initially consolidated to a pre-determined stress value as per above and then unloaded to a

required stress level. Again, specimens were kept under the unloaded stress level for a sufficient time (1000 seconds to 15000 seconds) to gain approximately constant vertical strain after swelling.

#### **3.3.4.2 Shear loading phase**

Two types of shear loading phases, monotonic or cyclic shear loading, are generally used in DSS testing. In the present test program, both monotonic and cyclic shear loading phases were conducted under constant volume condition; thus, the vertical shaft was clamped (refer vertical shaft locker pin in Figure 3.6) so that the consolidated specimen was restrained against vertical strains during the shear loading phase.

##### Monotonic Shear Loading Phase

Monotonic shear was applied by connecting the horizontal shaft to a motomatic motor which runs at a constant speed, and it resulted in constant shear strain rate during monotonic shearing (refer Figure 3.4).

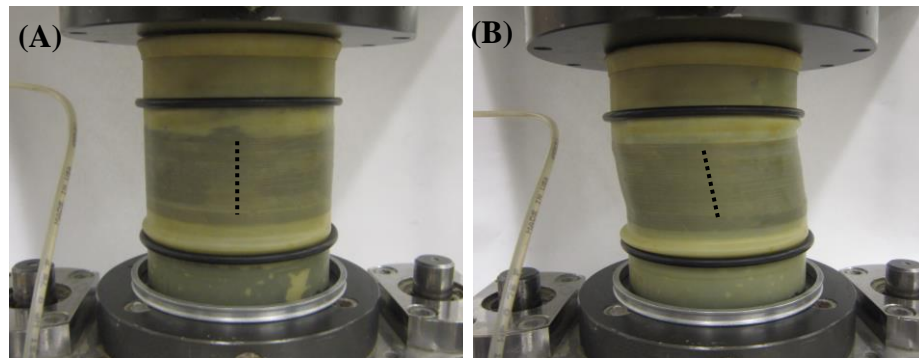


**Figure 3.24 Photos of typical specimen state: (A) after the applied seating pressure prior to consolidation phase (B) after monotonic shearing upto approximately 20 % shear strain**

Centerline of the specimen is indicated as black lines on the photos for the purpose of clarity

In the present test program, a shear strain rate of approximately 10% shear strain per hour was deployed. Monotonic shear loading tests were conducted until the specimen suffered approximately 20% of shear strain. Typical deformed configuration of a specimen after a DSS test subjected to constant-volume monotonic shearing is shown in Figure 3.24 (B) for illustration purposes.

#### Cyclic Shear Loading Phase

Constant amplitude, sinusoidal shear stress is applied to the consolidated specimen during constant-volume cyclic shearing phase. This stress controlled mechanism for the cyclic shear loading was achieved by periodically varying the pneumatic pressure of a chamber in the double acting pneumatic cylinder as a constant amplitude sinusoidal wave through an EPR (refer Figure 3.4). In the testing program herein, the frequency of this constant amplitude sinusoidal wave was 0.1 Hz (Period = 10 s). As constant volume condition was enforced to the test specimen by controlling its external boundaries during direct simple shearing, in this test program, shear induced pore water pressure does not play a role in the volumetric variations. Further, vertical effective stress applied on the specimen is distinguished by the measurements taken from the load cell at the vertical stress boundary. Therefore, the consideration of adequate time for pore water pressure equalization during cyclic shearing was not a necessity. The cyclic shearing test phases were conducted until the test specimens reach a single amplitude shear strain of ~12%.

#### **3.3.4.3 Post-cyclic consolidation phase**

At the end of the final loading cycles during the cyclic shear loading phase which was continued till the specimens reach ~12% of shear strain, the specimens generally had residual shear strains; as such, the specimens were manually repositioned to zero strain level by moving the top platen

back to the initial location (refer Figure 3.4). The specimens were then re-consolidated to the initial vertical consolidation stress achieved during the consolidation phase. This was achieved by simply unclamping the vertical shaft locker pin (refer Figure 3.6; note the shaft had been kept clamped during the constant volume cyclic shear loading phase). Vertical effective stress and volumetric strain were computed based on the measurement recorded from the vertical load cell and vertical LVDT during the re-consolidation phase in order to assess the post cyclic re-consolidation settlements of the test specimens. Again, in the reconsolidation phase, specimens were kept under the stress level for sufficient time (1000 seconds to 12000 seconds) to gain approximately constant vertical strain.

### **3.4 Test Program**

As indicated earlier, the focus of the experimental laboratory study herein is to characterize the mechanical behavior of a range of natural silts with varying plasticity using the DSS device. A systematic testing program that was undertaken, while varying key parameters are presented in Table 3.5. In summary, the following facets were investigated:

- Effect of confining stress and over-consolidation ratio (OCR) on monotonic shear response of natural silt;
- Effect of confining stress on cyclic shear and post cyclic consolidation response of natural silt;
- Effect of coarser fraction on monotonic and cyclic shear response of natural silt;

- Effect of particle structure / fabric on the monotonic and cyclic shear and post cyclic consolidation response of silt by comparing the response for natural silt and reconstituted silt; and
- Effect of plasticity on monotonic, cyclic shear and post cyclic consolidation response of natural silt.

**Table 3.5 Test Program**

Test Case		Test Material	Investigation	Vertical Stress (kPa)	Cyclic Stress Ratio	No of Tests
I	A	Slightly plastic natural silt	Effect of coarser fraction and confining stress on monotonic shear response	150, 300, 600	-	9
	B		Effect of OCR on monotonic shear response	150 : OCR of 2-4	-	2
	C		Effect of coarser fraction on cyclic shear response and post cyclic reconsolidation response	150, 200, 300	0.1 – 0.2	13
	D	Slightly plastic reconstituted silt	Effect of particle structure and confining stress on monotonic shear response	150, 300, 600	-	3
	E		Effect of particle structure on cyclic shear response and post cyclic reconsolidation response	150	0.1 – 0.15	3
II	A	Low plastic natural silt	Effect of confining stress on monotonic shear response	100, 200, 400	-	3
	B		Effect of OCR on monotonic shear response	100 :OCR of 2-4	-	2
	C		Effect of confining stress on cyclic shear response and post cyclic reconsolidation response	100, 150, 200	0.12 – 0.2	14
	D	Low plastic reconstituted silt	Effect particle structure and confining stress on monotonic shear response	100, 200, 400	-	3
	E		Effect of particle structure on cyclic shear response and post cyclic reconsolidation response	100	0.1 – 0.15	3
III	A	High plastic natural silt	Effect of confining stress on monotonic shear response	100, 150, 200, 400	-	4
	B		Effect of OCR on monotonic shear response	100 :OCR of 2-4	-	2
	C		Effect of confining stress on cyclic shear response and post cyclic reconsolidation response	75, 150, 200	0.15 – 0.4	13
	D	High plastic reconstituted silt	Effect particle structure and confining stress on monotonic shear response	75, 100, 200	-	3
	E		Effect of particle structure on cyclic shear response and post cyclic reconsolidation response	75	0.15 – 0.25	3
Total number of tests						80

## **Chapter 4: Mechanical Response of Natural Silts**

The results derived from the DSS test program described in Table 3.5 on natural silt are presented herein from the view point of characterizing the mechanical response of natural silt in monotonic, cyclic shear loading, and post cyclic consolidation stages. Specific focus was paid to investigate the influence of the effects coarse-grained fraction and particle-fabric. In addition, effect of plasticity on the shear loading response of silts was also explored from the limited amount of data arising from this study. Furthermore, observations with respect to the effect of the confining stress and OCR on the response of silt are also presented herein.

Monotonic shear loading response observed from DSS tests conducted on natural silt and reconstituted silt specimens are presented in Section 4.1, whereas their cyclic shear response are presented in Section 4.2. Using the data derived from cyclic shear tests, cyclic shear resistance observed from the different types of silts originating from the three test sites (refer Figure 3.10) are presented in Section 4.3. Finally, the post-cyclic consolidation responses are presented in Section 4.4. A summary of test parameters and results are presented in Table 4.1 at the outset so that reference to that could be made as the results are presented in the following sections.

**Table 4.1 Test parameters and summary of test results**

Test Case		Test ID	WC <sub>I (avg)</sub>	e <sub>i</sub>	σ' <sub>vc</sub> : kPa	OCR	e <sub>c</sub>	Cyclic Shearing				PCC	
								CSR τ <sub>cyc</sub> / σ' <sub>vc</sub>	γ <sub>max</sub> (%)	r <sub>u-max</sub>	N <sub>cyc</sub> [γ=3.75%]	e <sub>pcc</sub>	ε <sub>v-pcc</sub> (%)
I-A	a	CT 150 MA	0.4392	1.12	147.04	1	0.99	Monotonic shear loading					
		CT 300 MA	0.4110	1.07	297.20	1	0.87						
		CT 600 MA	0.3404	1.02	599.15	1	0.76						
	b	CT 150 MB	0.4105	1.08	148.52	1	0.94						
		CT 300 MB	0.3323	0.87	301.93	1	0.76						
		CT 600 MB	0.3722	0.87	598.52	1	0.75						
	c	CT 150 MC	0.3448	0.89	150.89	1	0.77						
		CT 300 MC	0.3571	0.98	303.08	1	0.79						
		CT 600 MC	0.3753	0.98	600.90	1	0.72						
I-B	CT 150 M OCR2		0.3753	1.02	154.52	2	0.86						
	CT 150 M OCR4		0.3450	0.95	146.90	4	0.70						
I-C	CT 150 45		0.4420	1.19	149.69	1	1.03						
	CT 150 30		0.4320	1.15	148.38	1	1.01	0.203	33.08	0.95	4.8	0.91	4.65
	CT 150 22.5		0.4053	1.02	149.29	1	0.91	0.151	16.92	0.98	24.3	0.83	4.44
	CT 150 20		0.4040	1.17	147.64	1	1.00	0.135	19.78	0.97	169.3	0.88	5.85
	CT 150 18.75		0.3622	1.07	147.34	1	0.93	0.126	17.28	0.98	82.8	0.82	5.50
	CT 200 40		0.3886	1.09	196.43	1	0.92	0.210	18.19	0.89	0.9	0.83	4.58
	CT 200 36		0.3736	0.91	197.18	1	0.81	0.181	26.71	0.98	1.2	0.74	3.74
	CT 200 30		0.3792	1.01	195.86	1	0.93	0.151	16.49	0.99	2.8	0.85	3.85
	CT 200 22		0.3968	1.06	199.54	1	0.94	0.108	16.19	0.99	36.8	0.84	4.75
	CT 300 39		0.3550	0.96	300.77	1	0.83	0.131	17.98	0.98	12.8	0.74	5.04



Test Case	Test ID	WC <sub>I (avg)</sub>	e <sub>i</sub>	$\sigma'_{vc}$ : kPa	OCR	e <sub>c</sub>	Cyclic Shearing				PCC	
							CSR $\tau_{cyc} / \sigma'_{vc}$	$\gamma_{max}$ (%)	r <sub>u-max</sub>	N <sub>cyc</sub> [ $\gamma=3.75\%$ ]	e <sub>pcc</sub>	$\varepsilon_{v-pcc}$ (%)
	CT 300 36	0.3505	0.92	300.09	1	0.79	0.121	12.95	0.99	25.3	0.71	4.72
	CT 300 45	0.4040	1.19	300.69	1	0.93	0.153	13.85	0.91	8.8	0.81	5.87
	CT 300 30	0.3849	1.05	300.39	1	0.87	0.100	15.30	0.97	166.8	0.76	5.75
I-D	CT R150M	0.3668	0.78	148.88	1	0.63	Monotonic shear loading					
	CT R300M	0.3573	0.77	299.12	1	0.57						
	CT R600M	0.3499	0.76	602.56	1	0.53						
I-E	CT R150 22.5	0.4057	0.75	150.09	1	0.64	0.150	17.08	0.98	5.8	0.56	4.66
	CT R150 18.75	0.3843	0.77	150.45	1	0.65	0.126	16.97	0.96	14.8	0.57	4.81
	CT R150 16.5	0.4025	0.75	149.06	1	0.63	0.111	15.20	0.98	30.3	0.55	4.85
II-A	JS 100 M	0.4694	1.28	101.18	1	1.06	Monotonic shear loading					
	JS 200 M	0.5280	1.45	199.88	1	1.06						
	JS 400 M	0.4147	1.21	396.02	1	0.91						
II-B	JS 100 M OCR 2	0.3816	1.12	98.95	2	0.92						
	JS 100 M OCR 4	0.4130	0.99	103.77	4	0.80						
II-C	JS 100 20	0.4502	1.44	101.03	1	1.15	0.196	22.09	0.93	1.8	1.04	4.90
	JS 100 17	0.4600	1.21	99.28	1	0.99	0.168	18.30	0.95	5.8	0.89	4.96
	JS 100 16	0.4298	1.19	101.28	1	1.02	0.165	16.59	0.96	13.8	0.92	4.59
	JS 100 15	0.5454	1.69	98.07	1	1.33	0.155	20.08	0.95	30.3	1.19	5.75
	JS 100 13	0.4685	1.54	99.73	1	1.25	0.132	16.29	0.99	91.8	1.12	5.60
	JS 150 30	0.4583	1.20	150.34	1	0.96	0.199	21.09	0.93	2.8	0.86	5.07
	JS 150 25	0.4231	1.21	149.32	1	0.96	0.167	16.13	0.98	13.8	0.87	4.75
	JS 150 22.5	0.4263	1.23	150.02	1	0.97	0.150	15.50	0.96	16.8	0.86	5.45
	JS 150 20	0.4277	1.31	150.09	1	1.01	0.133	16.20	0.97	47.8	0.90	5.41
	JS 150 18	0.4151	1.17	149.94	1	0.95	0.120	15.83	0.97	92.8	0.85	5.46
	JS 200 38	0.3808	1.08	199.39	1	0.89	0.191	10.10	0.91	5.8	0.80	4.76

Test Case	Test ID	WC <sub>I (avg)</sub>	e <sub>i</sub>	$\sigma'_{vc}$ : kPa	OCR	e <sub>c</sub>	Cyclic Shearing				PCC	
							CSR $\tau_{cyc} / \sigma'_{vc}$	$\gamma_{max}$ (%)	r <sub>u-max</sub>	N <sub>cyc</sub> [ $\gamma=3.75\%$ ]	e <sub>pcc</sub>	$\varepsilon_{v-pcc}$ (%)
	JS 200 34	0.3762	1.08	201.17	1	0.88	0.169	15.14	0.97	12.8	0.80	4.42
	JS 200 30	0.3837	1.11	203.37	1	0.91	0.149	15.27	0.97	37.8	0.81	4.82
	JS 200 28	0.3859	1.13	199.75	1	0.89	0.141	15.66	0.95	56.8	0.79	5.38
II-D	JS R100M	0.4176	0.96	98.47	1	0.72	Monotonic shear loading					
	JS R200M	0.4029	0.95	201.05	1	0.68						
	JS R400M	0.3488	0.86	399.32	1	0.58						
II-E	JS R200 30	0.4295	0.95	198.77	1	0.67	0.152	26.53	0.96	7.3	0.60	4.24
	JS R200 26	0.4265	0.99	200.91	1	0.66	0.130	18.46	0.95	19.7	0.57	5.10
	JS R200 20	0.4258	0.96	199.16	1	0.68	0.106	16.95	0.97	86.7	0.58	5.39
III-A	MD 100 M	0.6946	1.85	102.04	1	1.77	Monotonic shear loading					
	MD 150 M	0.6759	1.90	149.60	1	1.78						
	MD 200 M	0.6854	1.97	202.05	1	1.76						
	MD 400 M	0.6333	1.70	398.34	1	1.14						
III-B	MD 100 M OCR 2	0.6634	1.82	104.69	2	1.65						
	MD 100 M OCR 4	0.6782	1.68	104.08	4	1.16						
III-C	MD 075 30	0.6335	1.75	76.80	1	1.70	0.385	25.00	0.76	0.8	1.67	0.89
	MD 075 25	0.6407	1.75	76.01	1	1.70	0.327	15.97	0.61	7.8	1.68	0.56
	MD 075 20	0.6293	1.91	75.61	1	1.84	0.261	26.46	0.69	15.8	1.82	0.82
	MD 075 18	0.6195	1.73	75.14	1	1.67	0.238	22.84	0.74	106.8	1.63	1.16
	MD 075 15	0.6570	1.71	76.22	1	1.64	0.202	0.92	0.45	NA	1.62	0.47
	MD 150 39	0.6450	1.81	151.84	1	1.69	0.259	25.00	0.64	8.8	1.64	1.63
	MD 150 36	0.6469	1.81	152.23	1	1.68	0.238	25.00	0.96	17.8	1.61	2.56
	MD 150 34	0.6529	1.79	153.25	1	1.66	0.222	25.00	0.96	42.8	1.60	2.43
	MD 150 30	0.6495	1.79	151.16	1	1.67	0.199	25.00	0.93	113.8	1.59	3.09
	MD 200 40	0.5755	1.53	201.78	1	1.32	0.204	25.00	1.03	6.8	1.19	5.35

Test Case	Test ID	WC <sub>I (avg)</sub>	e <sub>i</sub>	$\sigma'_{vc}$ : kPa	OCR	e <sub>c</sub>	Cyclic Shearing				PCC	
							CSR $\tau_{cyc} / \sigma'_{vc}$	$\gamma_{max}$ (%)	r <sub>u-max</sub>	N <sub>cyc</sub> [ $\gamma=3.75\%$ ]	e <sub>pcc</sub>	$\epsilon_{v-pcc}$ (%)
	MD 200 36	0.6543	1.86	199.78	1	1.61	0.181	25.00	1.03	26.8	1.47	5.07
	MD 200 34	0.6436	1.61	201.08	1	1.35	0.169	21.18	0.91	17.8	1.21	6.09
	MD 200 30	0.6396	1.70	200.75	1	1.47	0.150	25.00	0.86	139.8	1.34	5.41
III-D	MD R75 M	1.1880	2.92	69.99	1	1.34	Monotonic shear loading					
	MD R100 M	0.9631	2.50	100.21	1	1.30						
	MD R200 M	0.9039	2.45	199.36	1	1.13						
III-E	MD R75 18	0.8817	2.42	70.81	1	1.41	0.248	17.11	1.03	1.3	1.28	5.35
	MD R75 15	0.9177	2.45	72.25	1	1.21	0.208	17.11	0.87	7.8	1.28	5.46
	MD R75 10	0.8663	2.36	73.54	1	1.41	0.151	9.01	0.90	161.8	1.27	5.80
<p>WC<sub>I (avg)</sub> = Average water content of the test specimen computed from the available trimmings from undisturbed specimens and sample portions from reconstituted specimen.</p> <p>e<sub>i</sub> = Initial void ratio after the application of the seating pressure of about 10 kPa</p> <p><math>\sigma'_{vc}</math> = Vertical consolidation stress prior to the application of shearing</p> <p>e<sub>c</sub> = Post-consolidation void ratio prior to the application of shearing</p> <p>CSR [<math>\tau_{cyc} / \sigma'_{vc}</math>] = Cyclic stress ratio, (cyclic shear stress / initial effective vertical stress at the start of cyclic shearing)</p> <p><math>\gamma_{max}</math> (%) = Maximum shear strain during the cyclic shear loading phase.</p> <p>r<sub>u-max</sub> = Maximum pore water pressure ratio during the cyclic shear loading phase.</p> <p>N<sub>cyc</sub> [<math>\gamma=3.75\%</math>] = Number of uniform loading cycles to reach double amplitude shear strain of 3.75 %</p> <p>PCC = Post cyclic consolidation</p> <p>e<sub>pcc</sub> = Void ratio of the specimen after the post cyclic consolidation phase</p> <p><math>\epsilon_{v-pcc}</math> (%) = Volumetric strain during post cyclic consolidation phase</p>												

## **4.1 Monotonic Shear Loading Response**

Constant-volume, monotonic DSS tests were conducted on undisturbed and reconstituted test specimens prepared from the silt retrieved from the Sites #1, #2 and #3 (refer Table 3.2); the objective was to study the influence of initial confining stress, OCR, coarse-grained fraction, plasticity and particle-fabric on the monotonic shear loading response. The monotonic DSS tests presented herein were conducted at a shear strain rate of approximately 10% per hour.

### **4.1.1 Effect of Initial Effective Confining Stress on Monotonic Shear Loading Response**

The monotonic shear loading response observed from the test series I-A(a), II-(A), and III-(A) (refer Table 4.1) were used to study the effect of initial effective confining stress on the monotonic shear loading response of natural silt. Carefully considering the values of the pre-consolidation stresses estimated from 1-D consolidation odometer tests (see Table 3.3), the specimens prepared from silt samples retrieved from Sites #1, #2 and #3 for test series I-A(a), II-A and III-A, respectively, were initially consolidated to vertical effective stress levels so as to ensure that shearing phase of all tests are commenced from a normally consolidated stress state.

Figure 4.1 through Figure 4.4 display the typical shear stress-strain curves,  $r_u$  development curves, stress path curves and normalized stress path curves of constant-volume monotonic DSS tests performed on relatively undisturbed specimens of natural silt retrieved from the Site #1 [Series I-A(a)], Site #2 [Series II-A] and Site #3 [Series III-A], respectively, at normally consolidated stress state at varying confining stress levels.

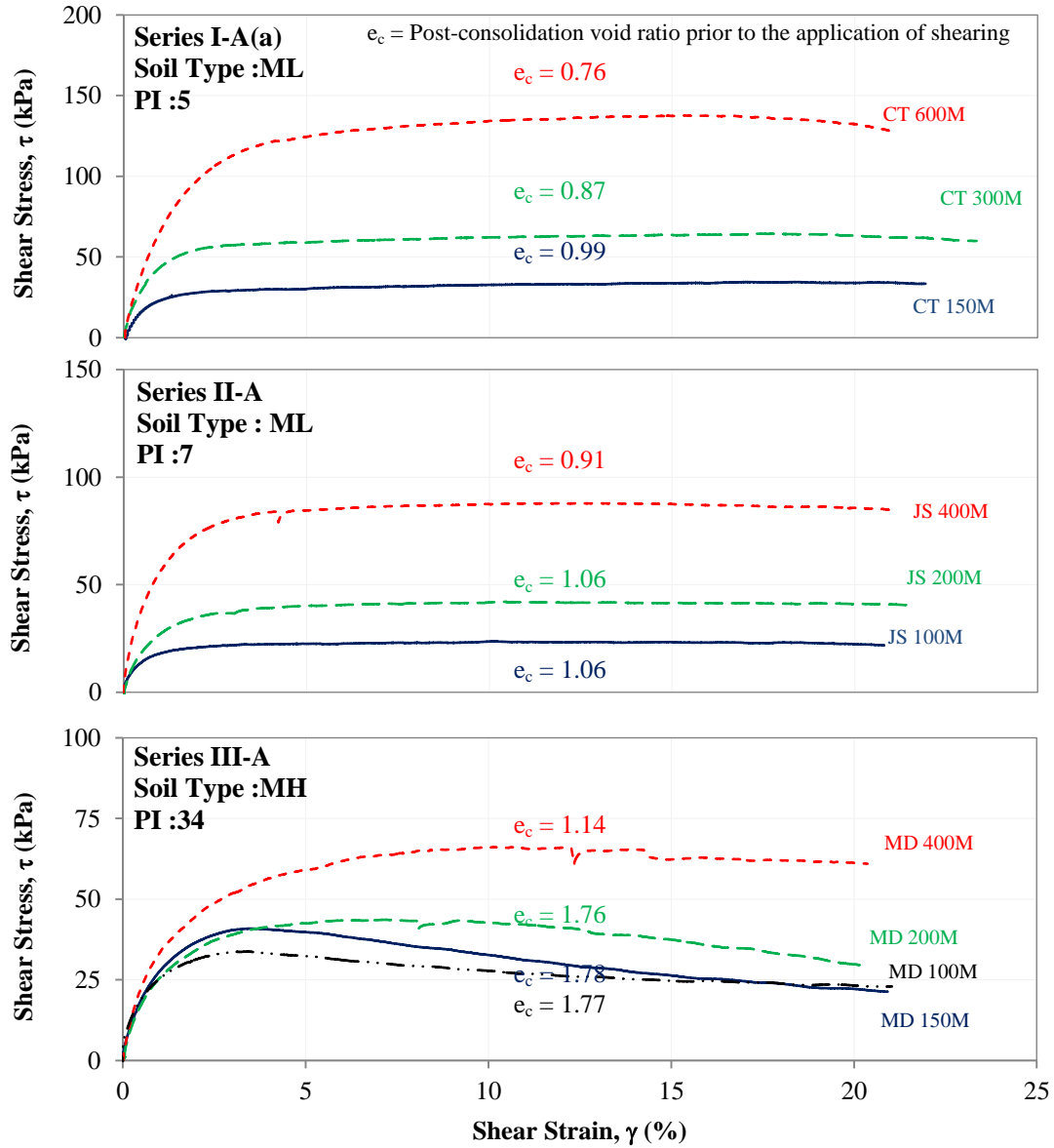


**Figure 4.1** Shear stress-strain curves of constant-volume monotonic DSS tests on relatively undisturbed specimens of natural silt retrieved from the Site #1 [Series I-A(a)], Site #2 [Series II-A] and Site #3 [Series III-A] at normally consolidated stress state at varying confining stress levels (Refer Table 4.1 for test details and parameters)

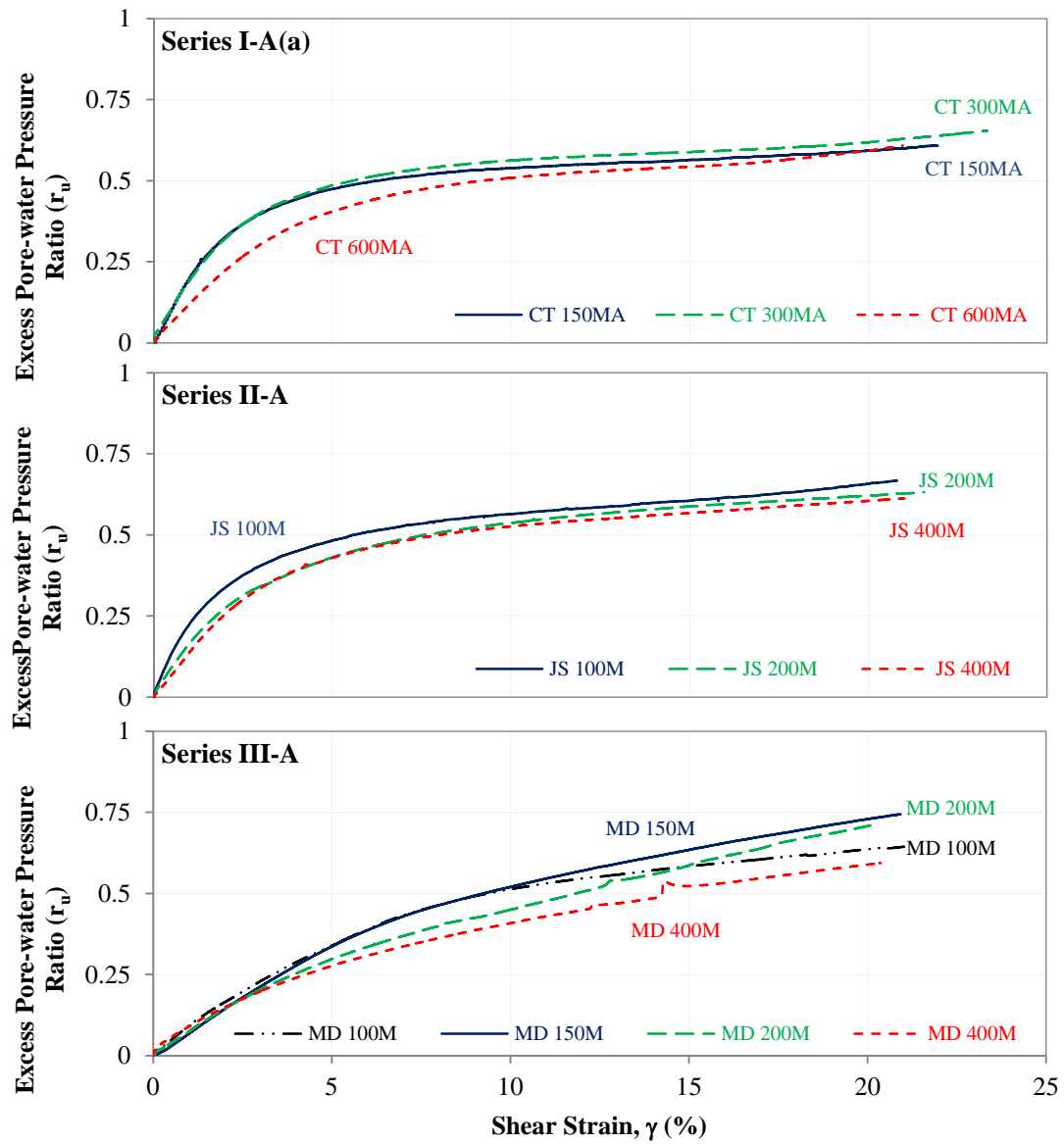


**Figure 4.2** Development of excess pore-water pressure with increasing shear strain during constant-volume monotonic DSS tests on relatively undisturbed specimens of natural silt retrieved from the Site #1 [Series I-A(a)], Site #2 [Series II-A] and Site #3 [Series III-A] at normally consolidated stress state at varying confining stress levels (Refer Table 4.1 for test details and parameters)

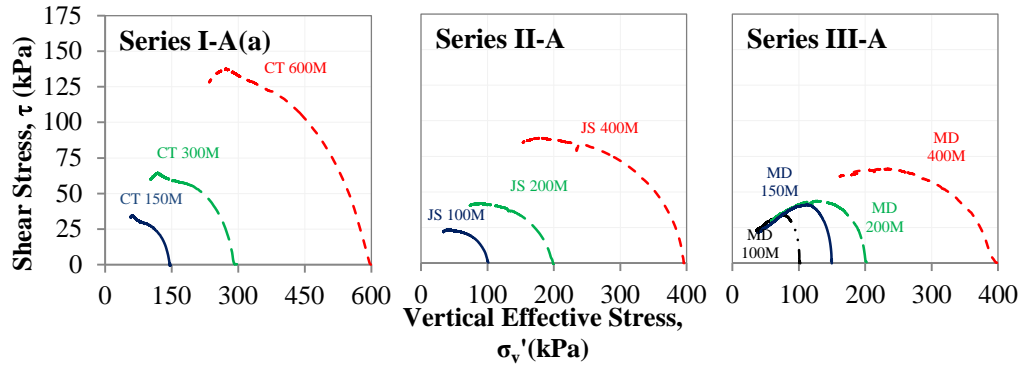


**Figure 4.3 Stress path curves of constant-volume monotonic DSS tests on relatively undisturbed specimens of natural silt retrieved from the Site #1 [Series I-A(a)], Site #2 [Series II-A] and Site #3 [Series III-A] at normally consolidated stress state at varying confining stress levels**  
(Refer Table 4.1 for test details and parameters)

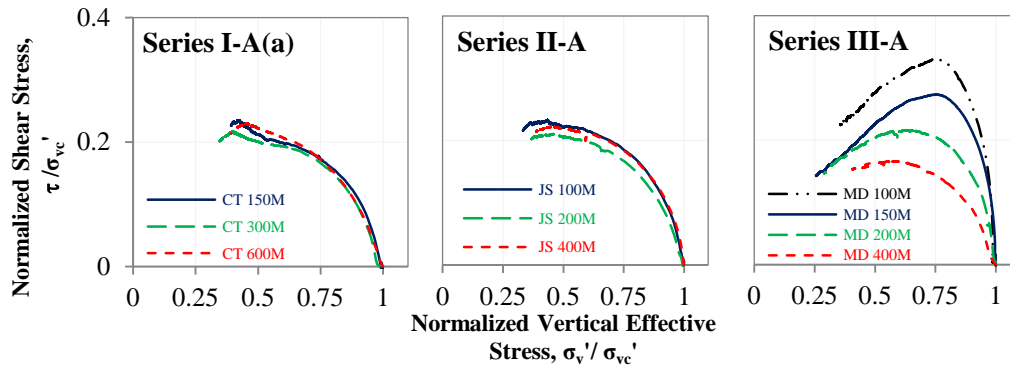


**Figure 4.4 Normalized stress path curves of constant-volume monotonic DSS tests on relatively undisturbed specimens of natural silt retrieved from the Site #1 [Series I-A(a)], Site #2 [Series II-A] and Site #3 [Series III-A] at normally consolidated stress state at varying confining stress levels**  
(Refer Table 4.1 for test details and parameters)

#### 4.1.1.1 Test Series I-A(a)

The shear stress-strain response of normally consolidated, slightly plastic ( $PI = 5$ ) natural silt retrieved from Site #1 observed during the constant-volume monotonic shearing tests conducted at effective vertical stress levels of 150 kPa, 300 kPa and 600 kPa are presented at Series I-A(a) in Figure 4.1. The results for Series I-A(a) shown in Figure 4.1 indicates that shear resistance

initially increases as the shear strain increases until a maximum shear stress is reached, and then that would remain at almost same magnitude, if not for potential decreases observed at larger strain level for some of the tests. Furthermore, increased shear resistances are mobilized for the specimens sheared at higher confining stress levels where the void ratio at higher consolidated stresses ( $e_c$ ) are comparatively lesser as indicated in the Figure 4.1. Relatively rapid development of  $r_u$  can be seen in increasing shear strain up to about 5% for Series I-A(a) shown in Figure 4.2 and followed by gradual increment of  $r_u$  for further increment in shear strain. Stress path for Series I-A(a) shown in Figure 4.3, indicated that specimens have deformed in a contractive manner and behavior of natural silt from Site #1 are found to be stress-history-normalizable as normalized stress path for all tests in Series I-A(a) tends to fall within a narrow range in Figure 4.4 .

#### **4.1.1.2 Test Series II-A**

The shear stress-strain response of normally consolidated, low plastic ( $PI = 7$ ) natural silt retrieved from Site #2 observed during the constant-volume monotonic shearing tests conducted at effective vertical stress levels of 100 kPa, 200 kPa and 400 kPa are presented at Series II-A in Figure 4.1. Similar to the response of Series I-A(a), shear stress –strain characteristics and stress paths with contractive response can be observed for Series II-A as shown in Figure 4.1 and Figure 4.3. Further, mobilized, normalized shear stresses at large strain levels for Series II-A are similar to those in Series I-A(a). When stress path responses obtained from constant-volume monotonic DSS tests conducted for natural silt from Site #2 are normalized to initial confining stress, they were also found to be stress-history-normalizable similar to that observed for the silt from Site #1 as shown in Figure 4.4. Similar stress-history-normalizability have been previously



noted by Sanin & Wijewickreme (2006b) for relatively undisturbed, normally consolidated, recently deposited Fraser river silt and by Seidalinova (2014) for reconstituted, normally consolidated gold tailings. From triaxial tests results on low-plastic Alaskan silts, Fleming & Duncan (1990) demonstrated that the undrained strength of low-plasticity Alaskan silts can be normalized to consolidation stress with relatively small variations. Ladd (1964) observed similar stress-history-normalizability of clay from isotropically consolidated undrain triaxial tests.

#### **4.1.1.3 Test Series III-A**

The shear stress-strain response of normally consolidated, high plastic ( $PI = 34$ ) natural silt retrieved from Site #3, observed during the constant-volume monotonic shearing tests conducted at effective vertical stress levels of 100 kPa, 150 kPa, 200 kPa and 400 kPa are presented as Series III-A in Figure 4.1. It can be seen for Series III-A from Figure 4.1, that shear resistance initially increased as the shear strain increases until a peak is reached, then followed by a decrease with further increase in strain level. As may be notable from the stress path for Series III-A in Figure 4.3, the normally consolidated, high plastic silt specimens from Site #3 deformed in a contractive manner during the monotonic shear loading. It is of interest to note that, unlike the normalized stress path of tests in Series I-A(a) and Series II-A, the normalized stress paths for tests in Series III-A did not exhibit coincidence as presented in Figure 4.4.

One-dimensional consolidation tests conducted for the silt specimen from the Site #3 revealed that when the consolidation stress is increased beyond the estimated pre-consolidation stress, significant amount of vertical strain develops that results in notable reduction of void ratio (refer Appendix C); this observation suggests ‘destruction’ in the soil specimen when the confining stress increases. The disturbance of the soil fabric, breaking of cementation, and other inter-

particle bonds that give rise to microstructure is termed as ‘destruction’ by Hight & Leroueil (2003) and Ladd & Degroot (2003). The alterations of the soil response to shearing based on the degree of destruction have been previously noted for clay by Leroueil et al. (1979), Santagata & Germaine (2002), Lunne et al. (2006) and Zapata-Medina et al. (2014). The weaker shear resistance observed for the monotonic shear loading conducted at higher confining stress levels (compared to that at low confining stress levels) as shown in normalized stress paths in Figure 4.4 for the test Series III-A for the high plastic natural silt, are in accord with the above typical behaviors noted by others. In essence, possible soil destruction occurred when consolidating to higher stress levels above the pre-consolidation stress level, in turn, causing the fabric of the silt specimen to behave in a comparatively weaker manner during monotonic shear loading.

#### **4.1.2 Effect of Over-Consolidation Ratio (OCR) on Monotonic Shear Loading Response**

The monotonic shear loading response of mechanically over-consolidated natural silts prepared from the retrieved silt samples from Site #1, #2 and #3, observed from the Test series I-B, II-B and III-B (refer Table 4.1) respectively are presented herein along with the normally consolidated response to investigate the effect of over-consolidation. Shear stress-strain curves,  $r_u$  curves, stress path curves and normalized stress path curves of constant-volume monotonic DSS tests performed on relatively undisturbed silt specimens which were consolidated to OCR levels of 1 (normally consolidated), 2 and 4 are presented in Figure 4.5 through Figure 4.8, respectively, with post-consolidated void ratios of the specimens prior to monotonic shearing are also indicated in the figures.

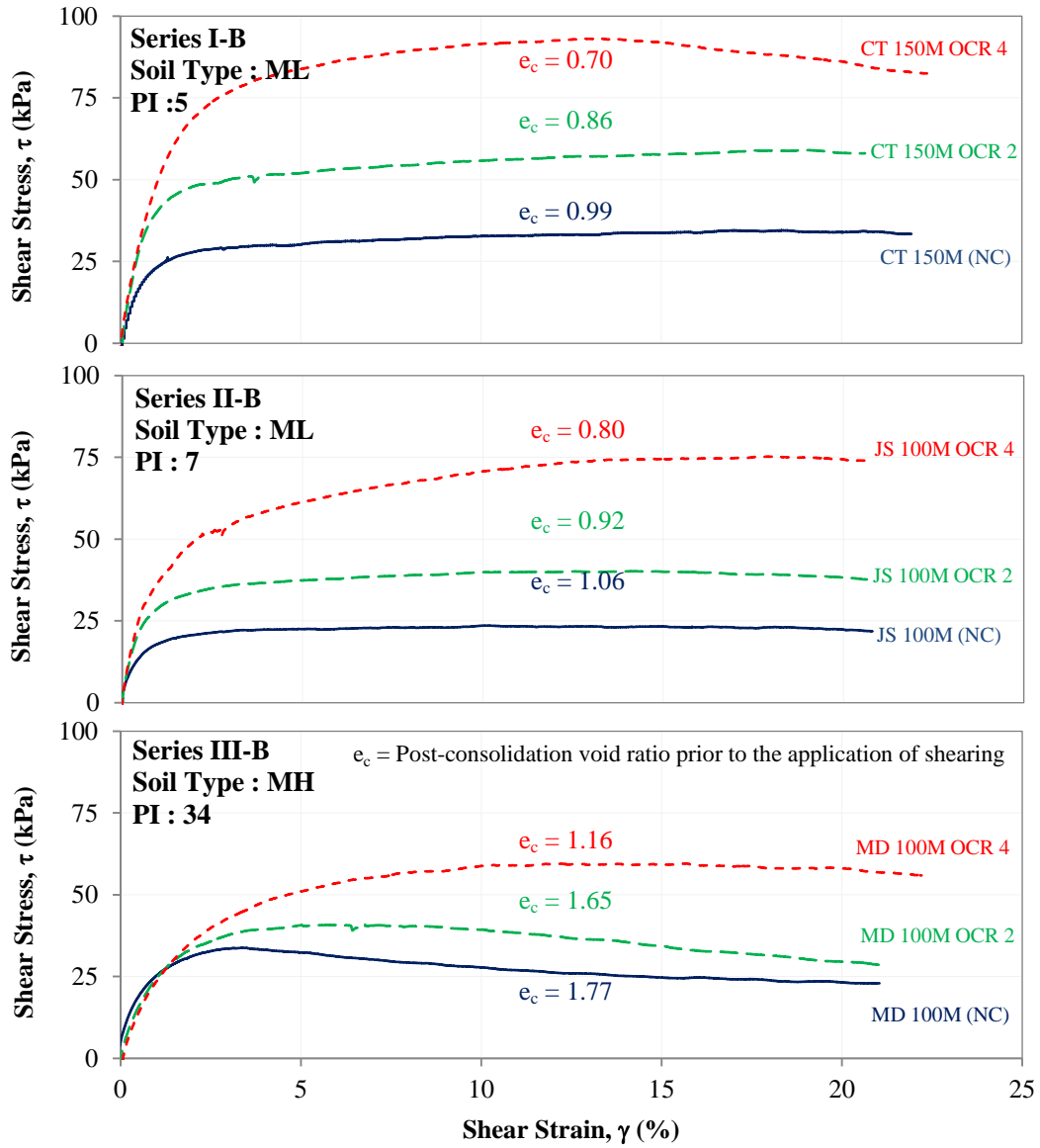


**Figure 4.5** Shear stress-strain curves of constant-volume monotonic DSS tests on relatively undisturbed specimens of natural silt retrieved from the Site #1 [Series I-B], Site #2 [Series II-B] and Site #3 [Series III-B] at confining stress levels of OCR 1 (NC), 2 and 4 (Refer Table 4.1 for test details and parameters)

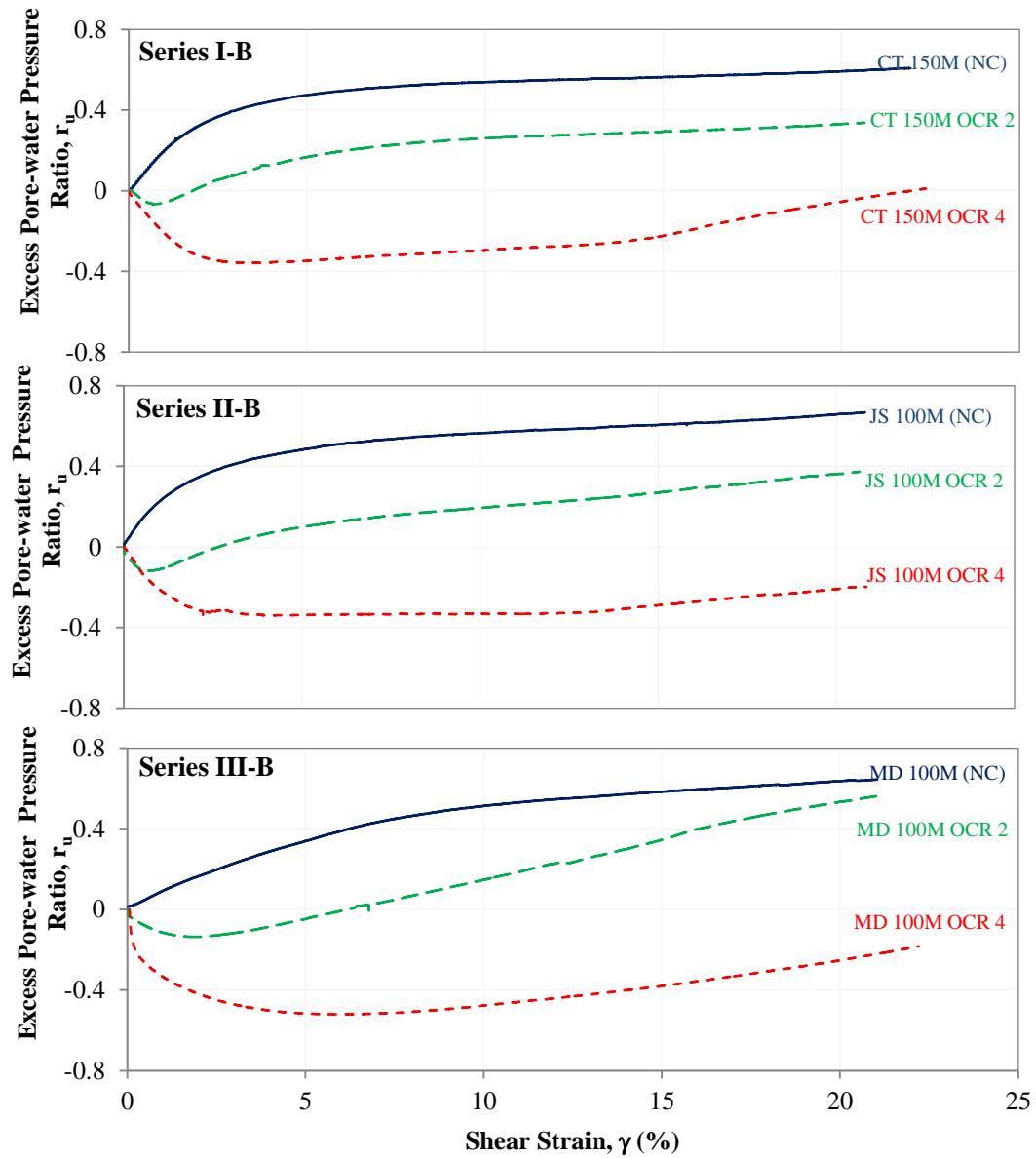


**Figure 4.6** Development of excess pore-water with increasing shear strain during constant-volume monotonic DSS tests on relatively undisturbed specimens of natural silt retrieved from the Site #1 [Series I-B], Site #2 [Series II-B] and Site #3 [Series III-B] at confining stress levels of OCR 1 (NC), 2 and 4  
(Refer Table 4.1 for test details and parameters)

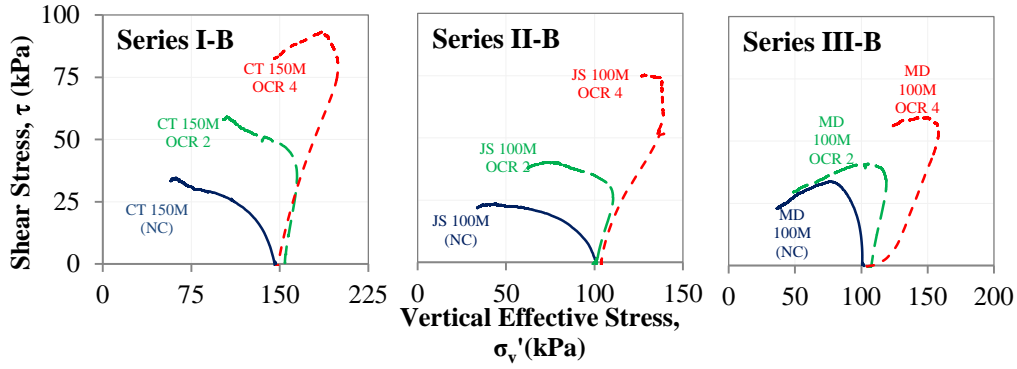


**Figure 4.7** Stress path curves of constant-volume monotonic DSS tests on relatively undisturbed specimens of natural silt retrieved from the Site #1 [Series I-B], Site #2 [Series II-B] and Site #3 [Series III-B] at confining stress levels of OCR 1 (NC), 2 and 4 (Refer Table 4.1 for test details and parameters)

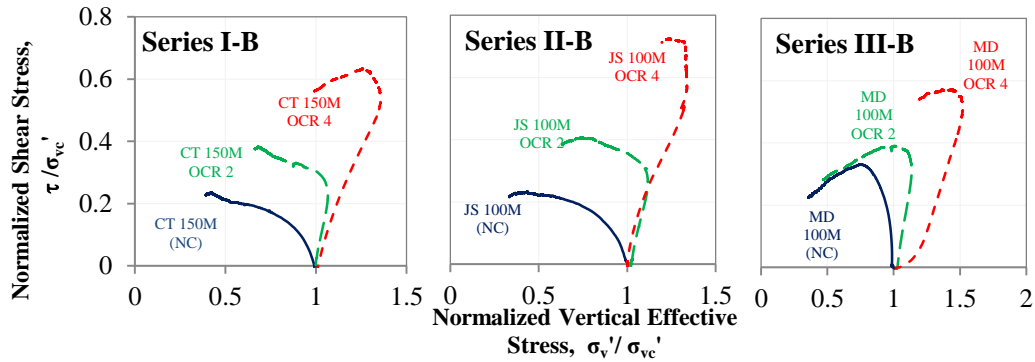


**Figure 4.8** Normalized stress path curves of constant-volume monotonic DSS tests on relatively undisturbed specimens of natural silt retrieved from the Site #1 [Series I-B], Site #2 [Series II-B] and Site #3 [Series III-B] at confining stress levels of OCR 1 (NC), 2 and 4 (Refer Table 4.1 for test details and parameters)

#### 4.1.2.1 Test Series I-B

The shear resistance is observed to increase with increasing OCR, in the Test Series I-B during constant-volume monotonic shear loading (see Figure 4.5) of soils from Site #1 ( $PI = 5$ ). Stress paths and normalized stress paths for Series I-B shown in Figure 4.7 and Figure 4.8 indicate contractive deformation of the normally consolidated specimen opposed to the initial dilative deformation followed by contractive deformation of over-consolidated specimens. Interpreted pore-water pressure developments (as described in Section 3.1.1) during constant-volume

monotonic shear loading are presented in Figure 4.6. The over-consolidated specimens showed increment in negative pore-water pressure and higher the OCR, the greater negative pore-water pressure were developed during shearing. As a result of higher OCR, void ratios of the over-consolidated specimens are lesser compared to the normally consolidated specimens as indicated in Figure 4.5, and this results the dilative deformation of the over-consolidated specimen during shearing.

#### **4.1.2.2 Test Series II-B**

The response of soil specimens in Series II-B for soils from Site #2 ( $PI = 7$ ) observed in constant-volume DSS loading are similar to the response observed in Series I-B as described in Section 4.1.2.1. In the normalized stress space in Figure 4.8, specimens with greater OCR resulted in more dilative response, and the effect OCR significantly enhances the monotonic shear stress-strain response of natural silt as shown in Figure 4.5. Wang & Luna (2011) and Seidalinova & Wijewickreme (2013) observed similar stress-strain response and trends in development of negative pore-water pressure for low-plastic Mississippi river valley silt during triaxial compression tests and for low-plastic gold tailings during DSS tests.

#### **4.1.2.3 Test Series III-B**

Constant-volume monotonic shear stress-strain response observed for high plastic, mechanically over-consolidated silt specimens in Series III-B [for soils from Site #3 ( $PI = 34$ )] shown in Figure 4.5 also indicate higher mobilized shear stress at higher OCR. Greater shear response could be observed for over-consolidated silt specimen than that of normally consolidated silt specimen retrieved from the Site #3, despite the destructuration (discussed in Section 4.1.1.3)

occurred in specimens when the specimens are consolidated beyond the pre-consolidation stress level.

#### **4.1.3 Effect of Coarse-grained Fraction on Monotonic Shear Loading Response**

As discussed in Section 3.2.2, due to the interbedded sand layers interpreted from the CPT results (Figure 3.11), silt retrieved from Site #1 indicated an increase in coarse-grained fraction with increasing depth from the ground surface. This provided an opportunity to investigate the effect of coarse-grained fraction of natural silt on its response in monotonic shear loading. Constant-volume DSS tests were performed on natural silt with different coarse-grained fraction obtained from Site #1 in Test Series I-A(a), (b), and (c) where specimens were consolidated to more than or approximately equal to the in-situ stress levels. The variation of the particle size distribution of the natural silts retrieved from Site #1, and used in the Test Series I-A(a), (b), and (c) are presented in Appendix C. The coarse-grained fractions of specimens tested in Series I-A(a), (b), and (c) are found to be 31%, 70% and 23%, respectively. Hence, responses of natural silt with different coarse-grained fractions in constant-volume monotonic DSS shear loading are examined herein using the observed stress path curves (Figure 4.9) and stress-strain response (Figure 4.10) during the test Series I-A(a), (b) and (c).

Specimens prepared from the soil retrieved from the Site #1 containing natural silt with 31%, 70 % and 23 % of sand were tested in constant-volume monotonic DSS shearing [Test series I-A(a), (b) and (c) respectively] to assess the effect of coarser-grained fraction as well as associated arising from the confining stress.. Each test series for specimen with three different coarse-grained fractions comprised three monotonic DSS tests performed different confining

stress levels. Effect of confining stress for the monotonic shear response observed from Test series I-A(a), (b) and (c) is discussed and followed by the effect of coarse-grained fraction.

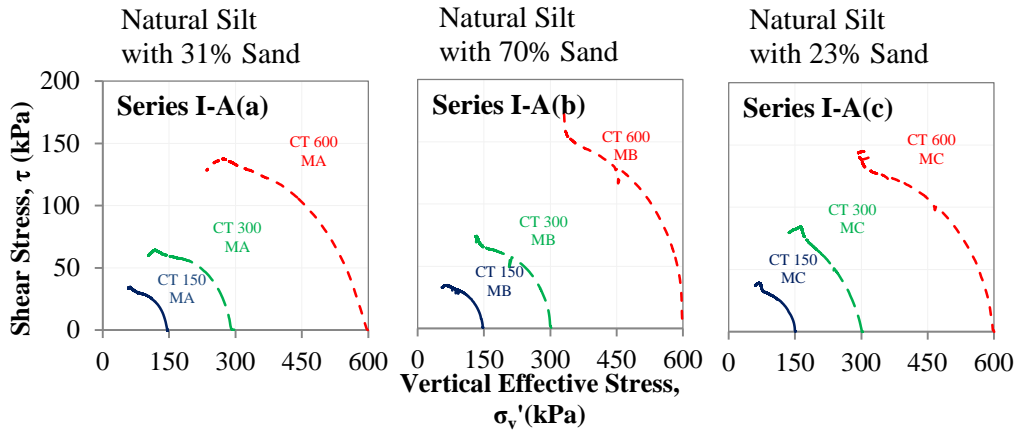


**Figure 4.9 Stress path curves of constant-volume monotonic DSS tests on relatively undisturbed specimens of natural silt with 31 %, 70 % and 23 % coarser-grained fraction respectively in Series I-A(a), I-A(b)] and I-A(c) at normally consolidated stress state at confining stress levels of 150 kPa, 300 kPa and 600 kPa (Refer Table 4.1 for test details and parameters)**

Stress path response (Figure 4.9) and shear stress-strain responses (Figure 4.10) of the silt specimens with varying coarse-grained fraction during constant-volume monotonic DSS loading which were initially normally consolidated to 150 kPa, 300 kPa and 600 kPa stress levels are compared. As discussed in the section 4.1.1.1, contractive responses were observed (Figure 4.9) during constant volume monotonic DSS shear loading and higher shear strength could be noted with higher confining stress regardless the variation of coarse-grained fraction of the test specimens.

The shear stress-strain responses of natural silt specimens [A : 31% of sand, B : 70% of sand and C : 23% of sand] that were initially normally consolidated to 150 kPa indicate that comparatively



higher shear resistance was mobilized for the silt specimen with 23% of sand (lowest coarse-grained fraction out of A, B, and C). However, specimen B which had 70% of sand showed slightly higher shear resistance in comparison with the response of specimen C which had only 31% of sand.

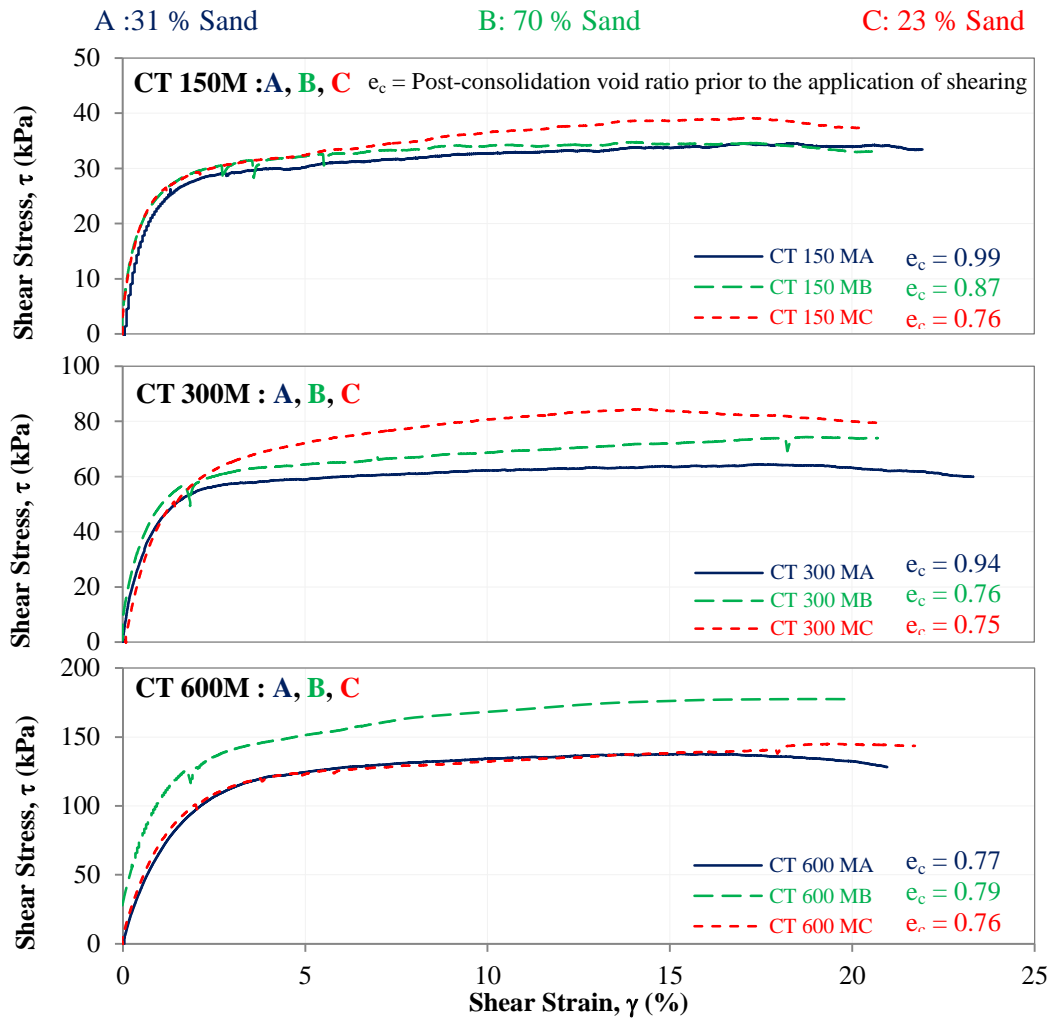


**Figure 4.10 Stress-strain curves of constant-volume monotonic DSS tests on relatively undisturbed specimens of natural silt with 31 %, 70 % and 23 % coarser-grained fraction respectively at normally consolidated stress state of 150 kPa, 300 kPa and 600 kPa**  
(Refer Table 4.1 for test details and parameters)

Similar trend could be observed for the three tests conducted at a normally consolidated stress level of 300 kPa as mobilized shear stress for specimen B (70 % sand) was in between the values for specimen A and C (23 % and 31 % of sand). The post-consolidation void ratios just prior to the application of shearing ( $e_c$ ) shown in Figure 4.10 are in-line with the observed response as lower the void ratio (more denser), higher the mobilized shear resistance during constant volume monotonic DSS tests conducted at 150 kPa and 300 kPa consolidation stress levels. It should be noted that as relatively undisturbed specimens are used for DSS tests, post consolidation void ratio at a given consolidation stress value cannot be controlled. However, in the case of tests conducted in normally consolidated stress level of 600 kPa, highest shear resistance was observed for the specimen B (70% of sand,  $e_c = 0.79$ ), despite the highest content of coarse-grained fraction and greatest void ratios in comparison with specimen A (31% of sand,  $e_c = 0.77$ ) and specimen C (23% of sand,  $e_c = 0.76$ ).

With the limited number of test performed in Test series I-A(a), (b) and (c) and appreciating the variation of coarse-grained fraction of natural silt retrieved from the Site #1, results and observation based on above-mentioned monotonic DSS tests do not show any consistence and conclusive trend for the influence on monotonic shear response with respect to coarse-grained fraction.

#### **4.1.4 Effect of Plasticity on Monotonic Shear Loading Response**

As mentioned in Table 3.3, plasticity indices of the material retrieved from Site #1, #2 and #3 are found to be about 5, 7 and 34 respectively. Therefore, the monotonic shear loading response of normally-consolidated natural silts samples, from Site #1, #2 and #3 having different plasticity, observed during constant-volume monotonic DSS loading creates the opportunity to investigate

the effect of plasticity on monotonic shear loading response. Selected, normalized shear stress-strain curves and normalized stress path curves of constant-volume monotonic DSS tests performed on relatively undisturbed silt specimens with plasticity indices of 5, 7, and 34 are shown in Figure 4.11 and Figure 4.12, respectively; the results suggest that the shear strength would increase with increasing plasticity.

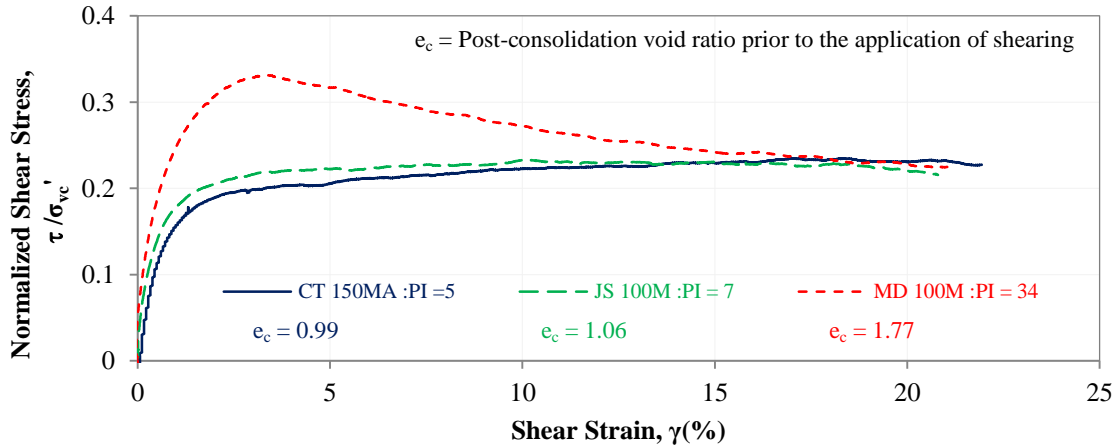


Figure 4.11 Normalized shear stress-strain curves of constant-volume monotonic DSS tests on relatively undisturbed specimens of natural silt with different plasticity indices

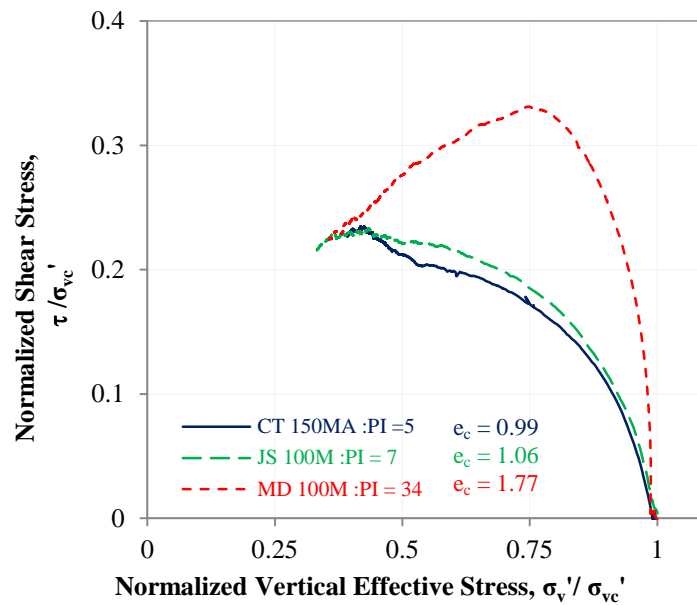


Figure 4.12 Normalized stress path curves of constant-volume monotonic DSS tests on relatively undisturbed specimens of natural silt with different plasticity indices

Contractive response could be seen for all specimens during monotonic shear loading and the peak strength increases significantly with respect to higher plasticity, despite the higher void ratio of the specimens for higher plasticity.

#### **4.1.5 Comparison of Monotonic Shear Loading Response of ‘Relatively Undisturbed’ and ‘Reconstituted’ Specimens**

Constant-volume monotonic shear loading response of reconstituted silts (refer Section 3.3.1.2 and Section 3.3.3.2) prepared from the retrieved silt samples from Site #1, #2 and #3, observed from the tests in test series I-D, II-D, and III-D (refer Table 4.1) respectively are presented with the combination of results for relatively undisturbed silt specimens (refer Section 3.2.3) obtained from test series I-A(a), II-A, and III-A to study the effect of fabric and microstructure.

Figure 4.13 indicates the shear stress-strain curves of constant-volume monotonic DSS tests on relatively undisturbed and reconstituted specimens from the Site #1 [Series I-A(a), I-D], Site #2 [Series II-A, II-D] and Site #3 [Series III-A, III-D] at normally consolidated stress state at varying confining stress levels. Post-consolidation void ratios of the specimens in each case are also presented in the Figure 4.13 for the comparison of packing of the particles in relatively undisturbed and reconstituted specimens prior to constant-volume monotonic shearing. Comparisons of the stress paths of relatively undisturbed and reconstituted specimens from Site #1 (Figure 4.14), Site #2 (Figure 4.15) and Site #3 (Figure 4.16) are also presented where continuous lines represents the response of relatively undisturbed specimens while dashed lines represents the response of reconstituted specimens.

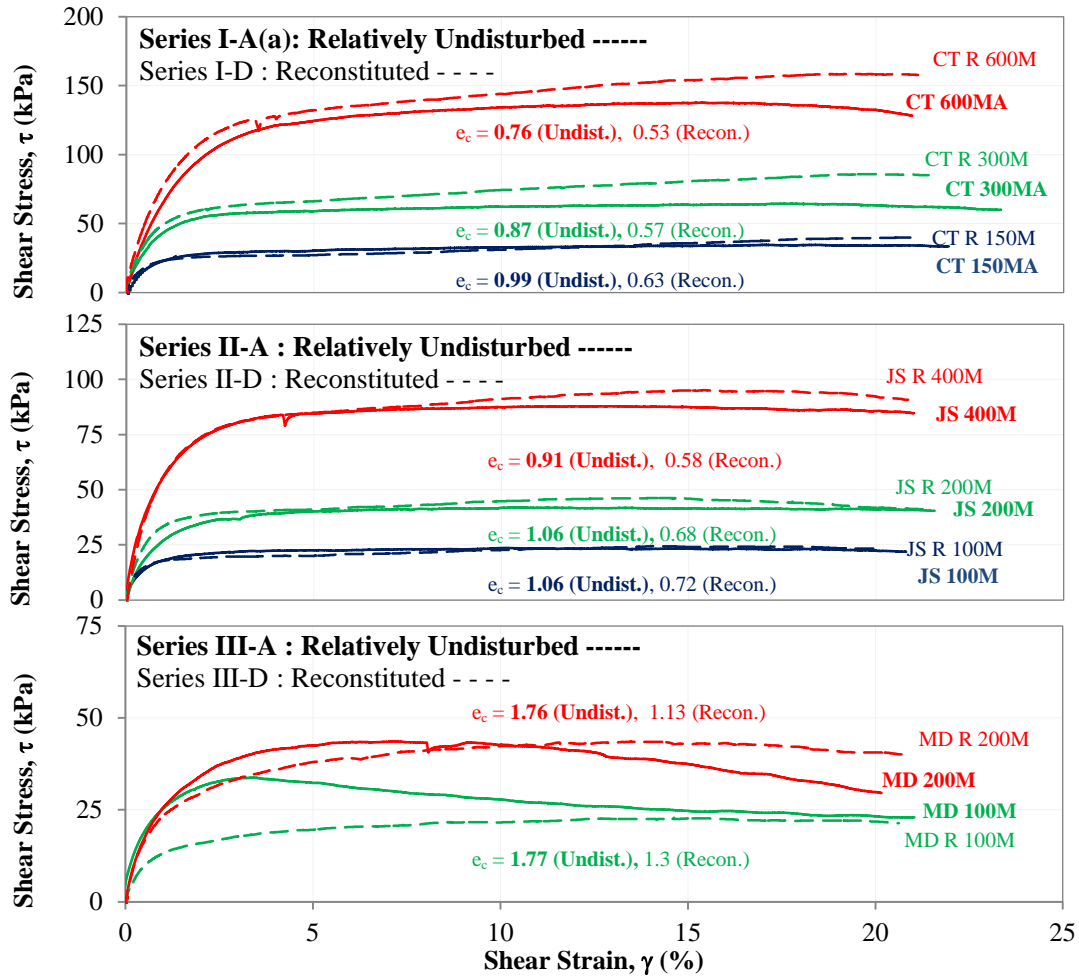


**Figure 4.13** Shear stress-strain curves of constant-volume monotonic DSS tests on relatively undisturbed and reconstituted specimens from the Site #1 [Series I-A(a), I-D], Site #2 [Series II-A, II-D] and Site #3 [Series III-A, III-D] at normally consolidated stress state at varying confining stress levels (Refer Table 4.1 for test details and parameters)

#### 4.1.5.1 Test Series I-A(a) and I-D

From the stress-strain responses of silt ( $PI=5$ ) from Site #1 in series I-A(a) and I-D shown in Figure 4.13, reconstituted specimens indicate comparatively stiffer response than the relatively undisturbed specimens at all tested consolidation stress levels. Accordingly, post consolidation void ratios of the reconstituted specimens are comparatively lesser than that of relatively

undisturbed specimens. Stress path responses of silt tested in series I-A(a) and I-D are shown in Figure 4.14. The results indicate that the shear resistances of the reconstituted specimens are generally higher than the shear resistance observed for the relatively undisturbed specimens at large strain during monotonic shearing.

#### **4.1.5.2 Test Series II-A and II-D**

The stress-strain responses and stress path responses of silt ( $PI = 7$ ) from the Site #2 in series II-A and II-D shown in Figure 4.13 and Figure 4.15 are very much similar to the responses observed for the silt ( $PI = 5$ ) from the Site#1, as stiffer response could be noted in reconstituted specimens comparatively over the relatively undisturbed specimens. Similar responses have been observed by Fleming & Duncan (1990) for Alaskan silt, when undrained shear strength of undisturbed specimen were compared with that of the specimen. From the results of isotropically consolidated undrained triaxial tests on Alaskan silt, Fleming & Duncan (1990) noted that remolded and reconsolidated specimens showed an increased undrained shear strength of 25 % to 40 % compared to undisturbed specimens.

Typically, comparatively lesser void ratio (denser particle arrangement) results an increase in shear stiffness and strength, whereas destructuration of natural fabric causes a decrease in shear stiffness and strength. The competitive performance arising from these factors would determine the observed behavior of a given reconstituted specimen. It appears that in the observed monotonic shear loading response of reconstituted specimens from Site #1 and #2, the effect from change in void ratio has over-shadowed the influence due to the change in fabric and micro-structure.

### 4.1.5.3 Test Series III-A and III-D

Figure 4.13 and Figure 4.16 present the stress-strain and stress path responses of series III-A and III-D where high plastic silt (PI = 34) from the Site #3 are monotonically sheared in constant-volume condition. Unlike the observed responses for comparatively low plastic silt from the Site #1, and #2, relatively undisturbed specimens from the Site #3 showed stiffer shear response than that of reconstituted specimen. The peak shear strength observed for relatively undisturbed specimens were greater than that of reconstituted specimens.

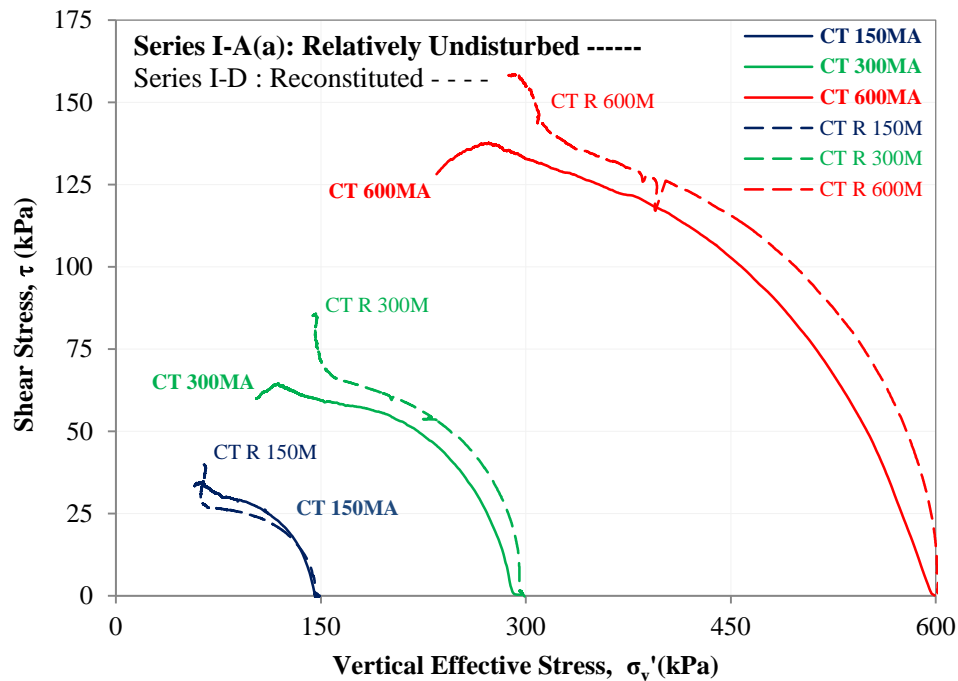


**Figure 4.14 Stress path curves of constant-volume monotonic DSS tests on relatively undisturbed and reconstituted specimens from the Site #1 [Series I-A(a), I-D] at normally consolidated stress levels of 150 kPa, 300 kPa and 600 kPa**

At large strain levels, relatively undisturbed specimens indicated a significantly low shear resistance compared to its peak shear resistance, whereas the reconstituted specimens did not exhibit such a significant degradation of post-peak shear resistance.

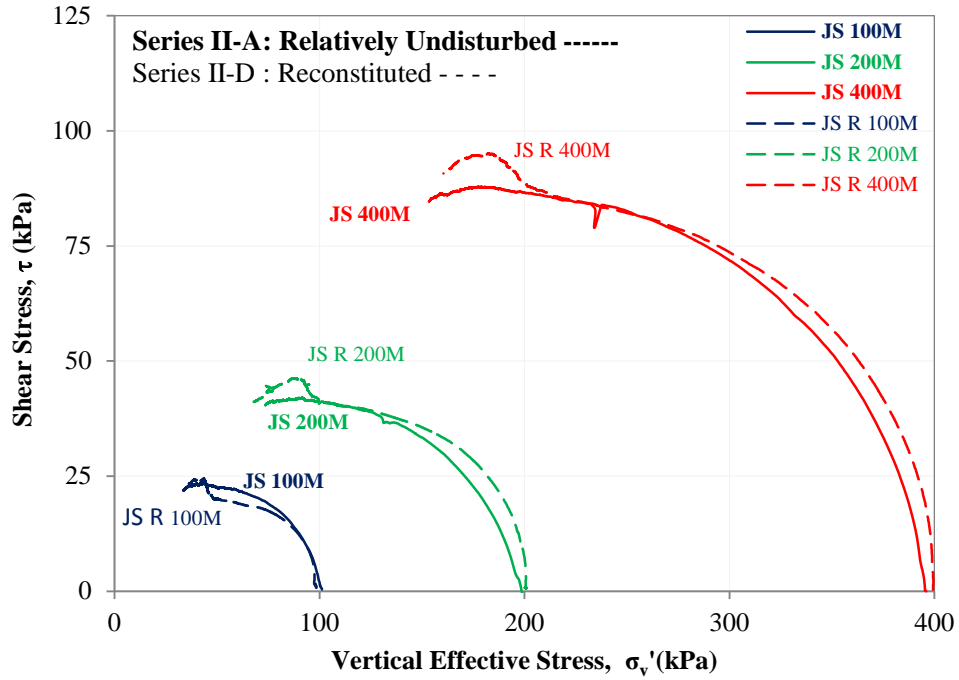


Figure 4.15 Stress path curves of constant-volume monotonic DSS tests on relatively undisturbed and reconstituted specimens from the Site #2 [Series II-A, II-D] at normally consolidated stress levels of 100 kPa, 200 kPa and 400 kPa

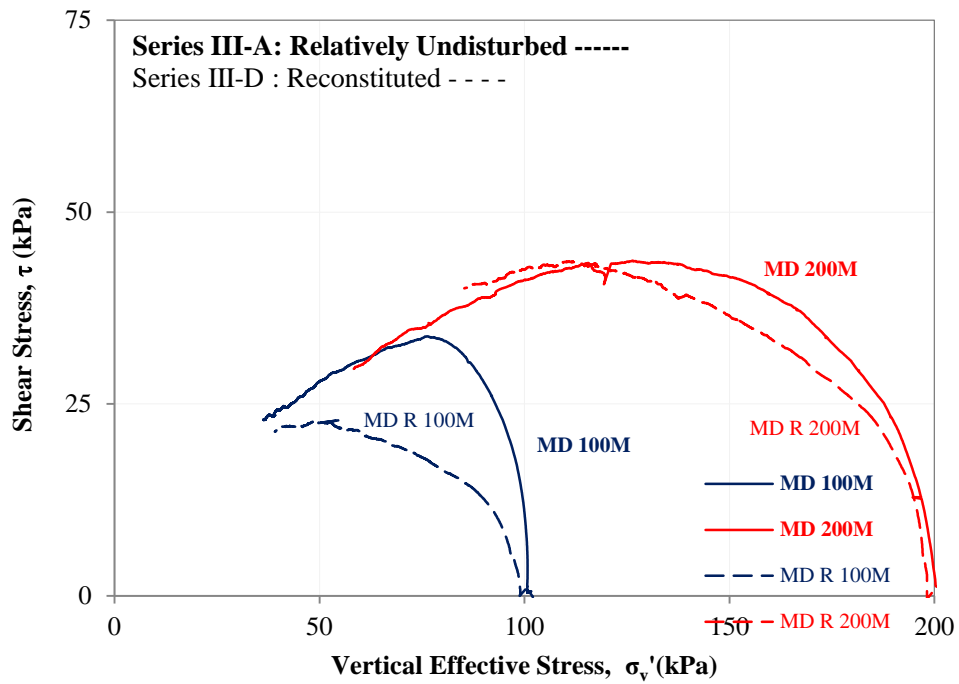


Figure 4.16 Stress path curves of constant-volume monotonic DSS tests on relatively undisturbed and reconstituted specimens from the Site #3 [Series III-A, III-D] at normally consolidated stress levels of 100 kPa and 200 kPa



The microstructure due to high plasticity and the comparatively higher clay content in the silt from the Site #3 may have contributed to the relatively stiffer shear response and the difference in shear peak and large-strain shear resistances of relatively undisturbed specimens, as opposed to the reconstituted specimens prepared by slurry deposition method. When undrained strength of stiff clays such as London and Todi clays were investigated by Burland (1990), it was concluded that various factors such as depositional conditions, ageing cementation have influenced the differences in soil structure (both with respect to fabric and bonding) between natural soils and the corresponding reconstituted material. Similarly, higher shear strengths have also been noted for natural clay over the re-sedimented / reconstituted clay by Santagata (1999) for Boston blue clay and by Callisto & Calabresi (1998) for Pisa clay. The observations from the current work are in accord with these observations.

## **4.2 Cyclic Shear Loading Response**

The results of the constant-volume, CDSS tests conducted on undisturbed test specimens prepared from the silt retrieved from Site #2 (refer Table 3.2) are presented in this section. Development of cyclic strain and excess pore-water pressure during constant-volume CDSS tests are examined and typical responses observed for the tests specimens that were normally consolidated to different stress levels are discussed in Section 4.2.1. The observed cyclic stress strain response and stress path response of the specimen in CDSS loading are presented in Section 4.2.2, while Section 4.2.3 focuses on the effect of confining stress on the cyclic shear loading response. The CDSS tests presented herein are conducted (refer Section 3.3.4.2) under symmetrical sinusoidal cycles of loadings having the desired constant CSR amplitude at a frequency of 0.1 Hz.

### 4.2.1 Cyclic Strain Accumulation and Pore-water Pressure Development

Accumulation of cyclic strains of the silt specimens that were normally consolidated to 100 kPa prior to the application of constant-volume cyclic shear loading with CSR of 0.196, 0.168, 0.155 and 0.132 are presented in Figure 4.17. The results indicate that the process of cyclic strain accumulation for the tested silt is gradual, with higher CSR resulting in an increased potential for shear strain development with number of loading cycles.

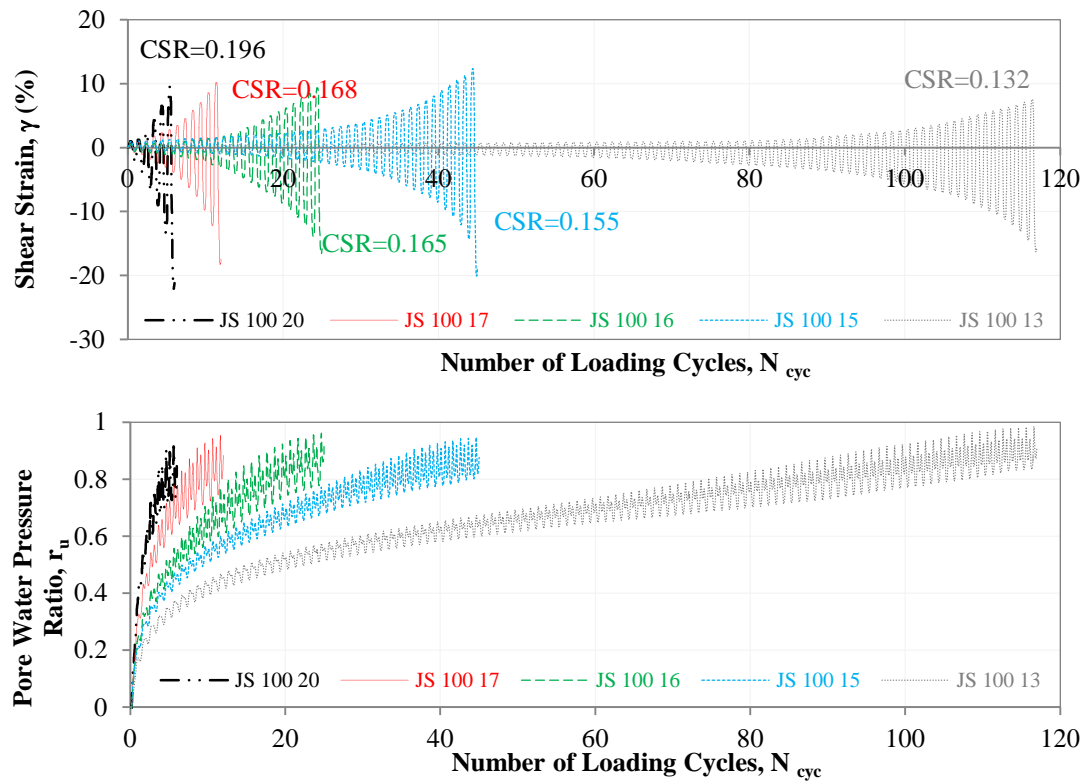


**Figure 4.17** Accumulation of shear strain and development of pore water pressure ratio with respect to loading cycles in constant -volume CDSS test on relatively undisturbed specimen from the Site #2 [PI =7], normally consolidated t 100 kPa with different CSRs  
(Refer Table 4.1 for test details and parameters)

The gradual strain accumulation due to cyclic shear loading is associated with cumulative pore water pressure development. For instance, specimen that was subjected to cyclic shear loading

with a CSR of 0.196 developed  $r_u$  of about 80% in 5 cycles, whereas, the specimen tested with a CSR of 0.132 withstood more than 80 loading cycles before reaching  $r_u$  of about 80%. Figure 4.17 indicates the gradual development of pore water pressure for the tested silt, however, it can be seen that excess pore water pressures did not equal to the confining stresses (i.e.  $r_u = 1$ ) even at the point of the termination of the test, when the test specimens surpassed single-amplitude shear strain level of 12 %.

#### **4.2.2 Typical Cyclic Stress-strain and Stress Path Response**

The cyclic stress-strain and stress path curves derived from the tests reported in the previous section [i.e., silt specimen from the Site #2 ( $PI = 7$ ) tested in constant-volume CDSS loading at normally consolidated effective stress level of 100 kPa with CSR of 0.196, 0.168, 0.155 and 0.132] are shown in Figure 4.18 through Figure 4.21. It can be seen that all specimens display initial contractive behavior during the initial loading cycles in CDSS testing. This is followed by dilative and contractive responses during unloading and loading portions of cyclic shear stress, respectively. In addition to the gradual accumulation of shear strain discussed in Section 4.2.1, degradation of shear stiffness with increasing number of loading cycles can be identified in Figure 4.18 through Figure 4.21. Furthermore, it can be noted that in a given cycle, when the applied shear stress is close to zero, the shear stiffness of the silt specimens undergoes its transient minimum. The observed gradual development of pore pressure and accumulation of shear strain, combined with the progressive stiffness degradation without entailing a significant loss in shear stiffness during constant-volume CDSS for the tested silt is similar to the ‘cyclic mobility’ mode of strain development which has been observed for tailings sand (Chern, 1985),

for clay (Zergoun & Vaid, 1994), for silt (Hyde et al. 2006; Sanin & Wijewickreme, 2006a), for dense sand (Sriskandakumar, 2004).

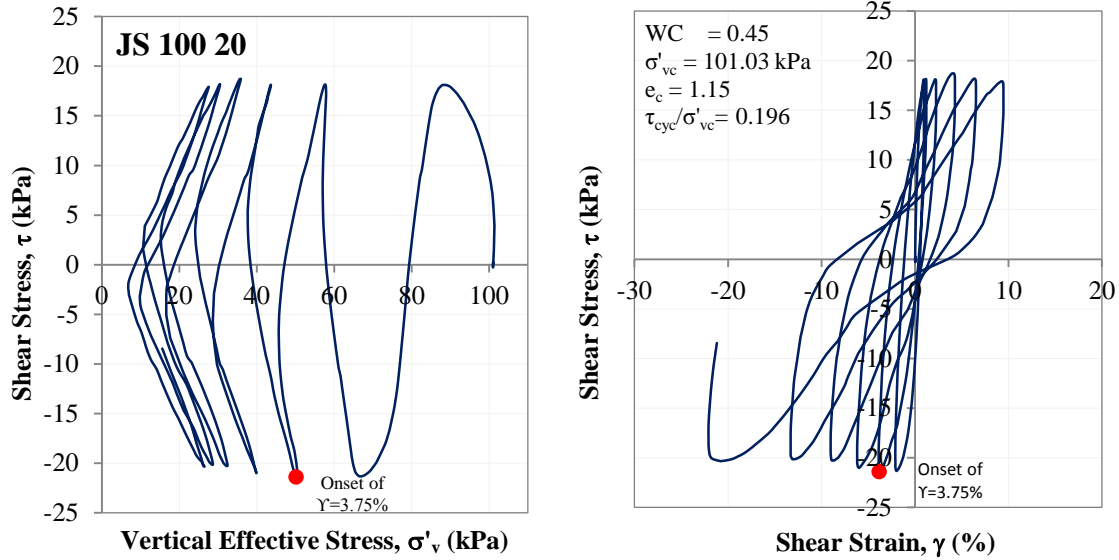


Figure 4.18 Stress path and shear stress-strain curves of constant-volume CDSS test on relatively undisturbed specimen from the Site #2 [PI = 7], normally consolidated to  $\sigma'_{vc} = 100$  kPa and CSR of 0.196

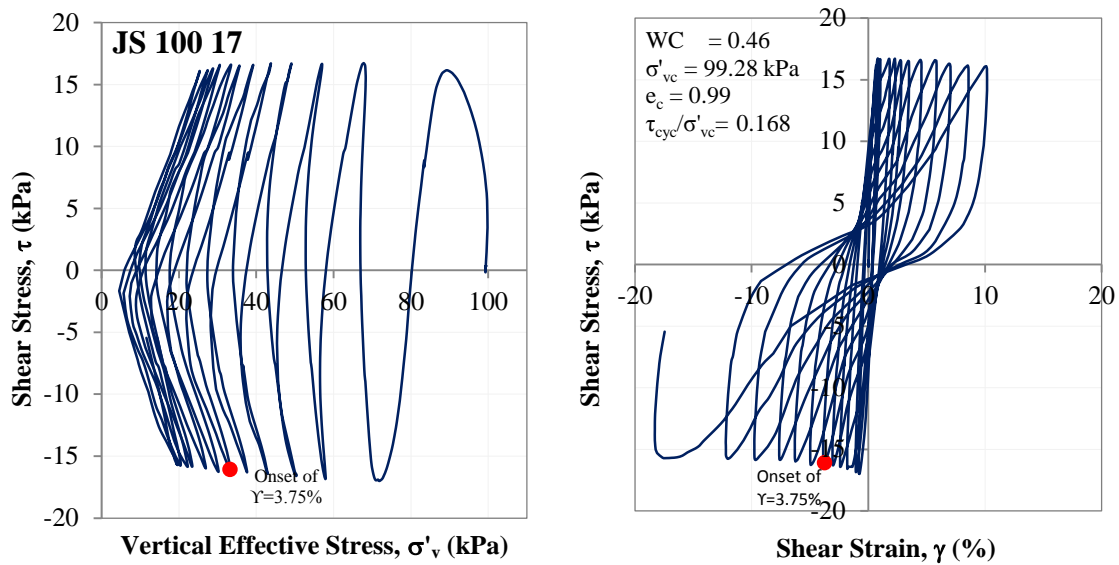


Figure 4.19 Stress path and shear stress-strain curves of constant-volume CDSS test on relatively undisturbed specimen from the Site #2 [PI = 7], normally consolidated to  $\sigma'_{vc} = 100$  kPa and CSR of 0.168

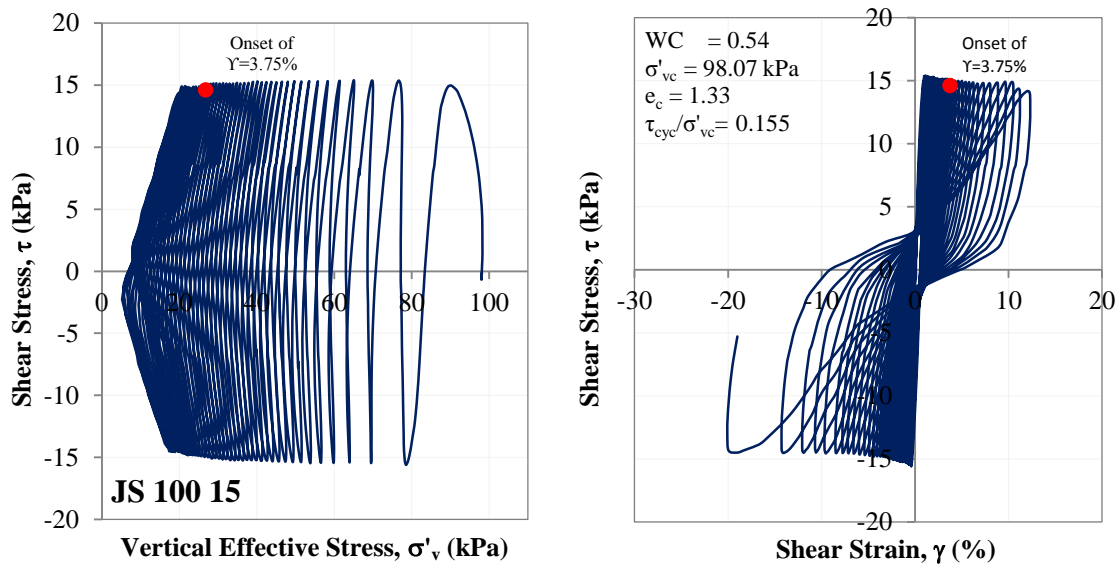


Figure 4.20 Stress path and shear stress-strain curves of constant-volume CDSS test on relatively undisturbed specimen from the Site #2 [PI=7], normally consolidated to  $\sigma'_{vc} = 100$  kPa and CSR of 0.155

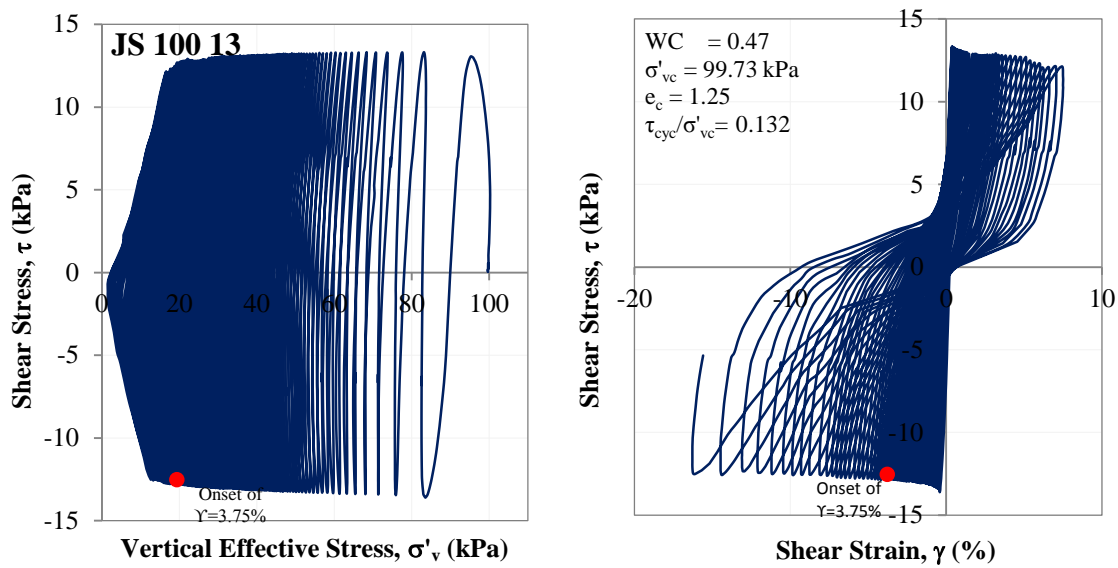


Figure 4.21 Stress path and shear stress-strain curves of constant-volume CDSS test on relatively undisturbed specimen from the Site #2 [PI=7], normally consolidated to  $\sigma'_{vc} = 100$  kPa and CSR of 0.132

### 4.2.3 Effect of Initial Effective Confining Stress

The test series II-C (refer Table 4.1) comprises CDSS tests performed on relatively undisturbed specimens prepared from the silt retrieved from the Site #2 ( $PI = 7$ ) initially normally consolidated to stress levels of 100 kPa, 150 kPa, and 200 kPa. Strain accumulation, pore water development, cyclic stress-strain and stress path curves obtained from the silt specimen tested at 100 kPa with different CSR was shown and discussed in Section 4.2.1 and 4.2.2.

In this section, cyclic stress-strain and stress path responses observed for 150 kPa and 200 kPa are also presented, and Table 4.2 provides an index for the respective figures that depict the shear responses obtained at different consolidation stress levels.

**Table 4.2 Index of Figures for stress path and shear stress-strain curves for silt from the Site #2**

Figure #	Test ID	Consolidation Stress ( $\sigma'_{vc}$ ) kPa	CSR ( $\tau_{cyc} / \sigma'_{vc}$ )
Figure 4.18	JS 100 20	101.03	0.196
Figure 4.19	JS 100 17	99.28	0.168
Figure 4.20	JS 100 15	98.07	0.155
Figure 4.21	JS 100 13	99.73	0.132
Figure 4.22	JS 150 30	150.34	0.199
Figure 4.23	JS 150 25	149.32	0.167
Figure 4.24	JS 150 20	150.09	0.133
Figure 4.25	JS 150 18	149.94	0.120
Figure 4.27	JS 200 38	199.39	0.191
Figure 4.28	JS 200 34	201.17	0.169
Figure 4.29	JS 200 30	203.37	0.149
Figure 4.30	JS 200 28	199.75	0.141

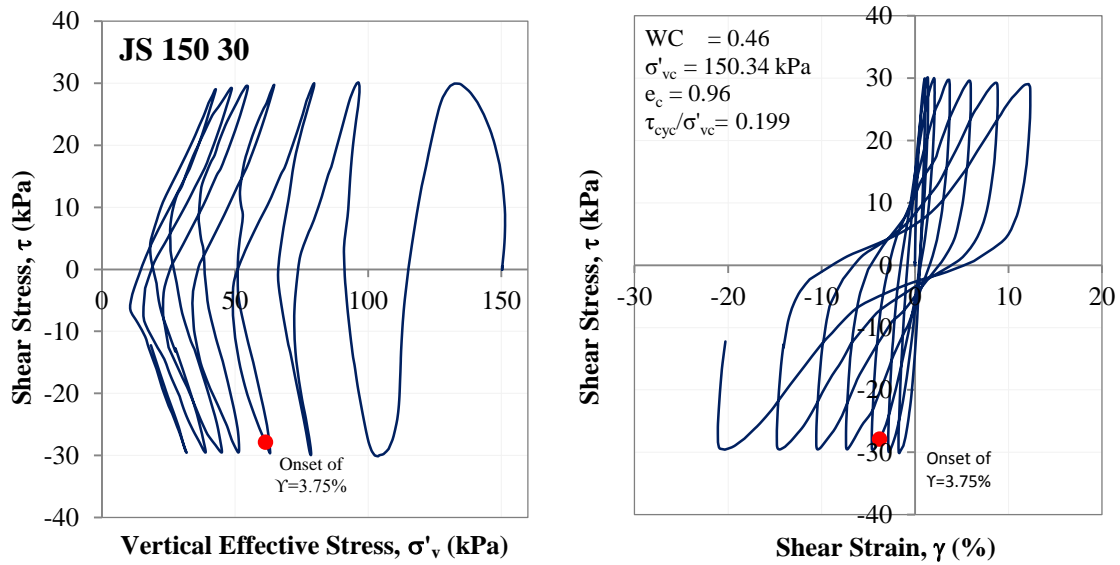


Figure 4.22 Stress path and shear stress-strain curves of constant-volume CDSS test on relatively undisturbed specimen from the Site #2 [PI =7], normally consolidated to  $\sigma'_{vc} = 150$  kPa and CSR of 0.199

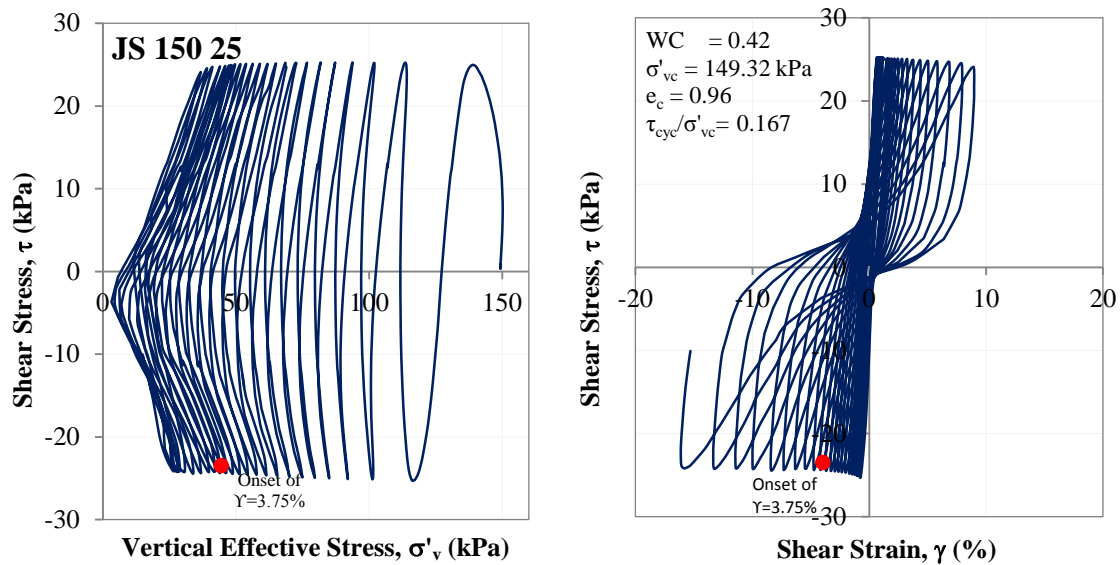


Figure 4.23 Stress path and shear stress-strain curves of constant-volume CDSS test on relatively undisturbed specimen from the Site #2 [PI =7], normally consolidated to  $\sigma'_{vc} = 150$  kPa and CSR of 0.167

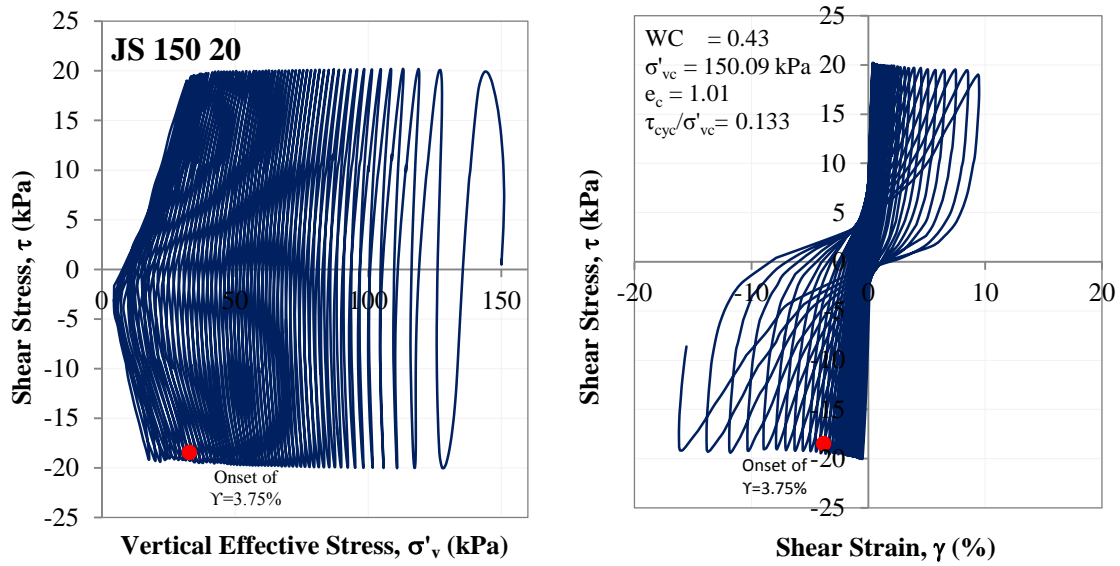


Figure 4.24 Stress path and shear stress-strain curves of constant-volume CDSS test on relatively undisturbed specimen from the Site #2 [PI=7], normally consolidated to  $\sigma'_{vc} = 150$  kPa and CSR of 0.133

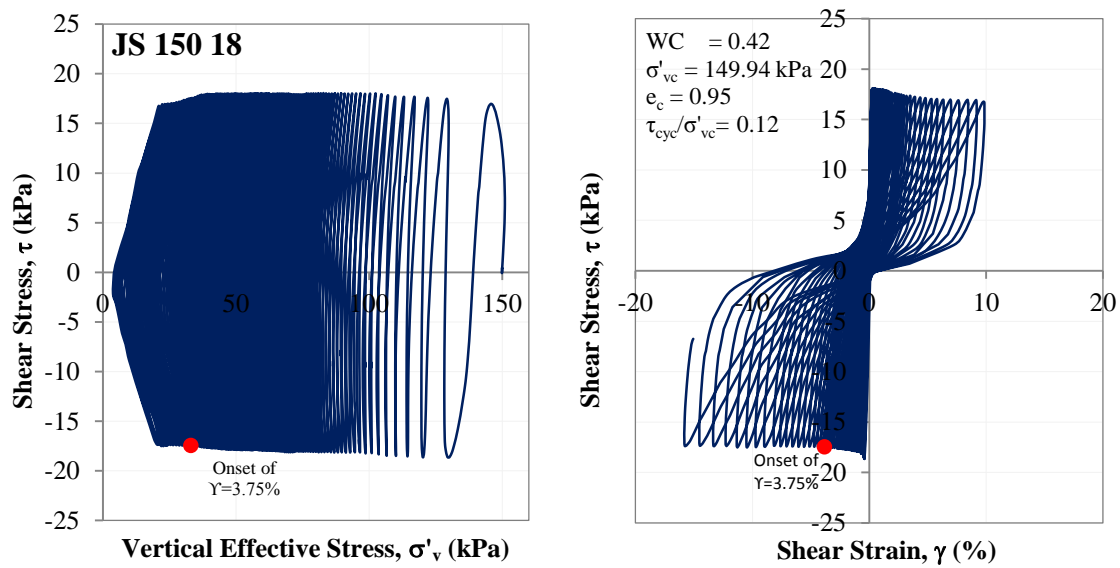
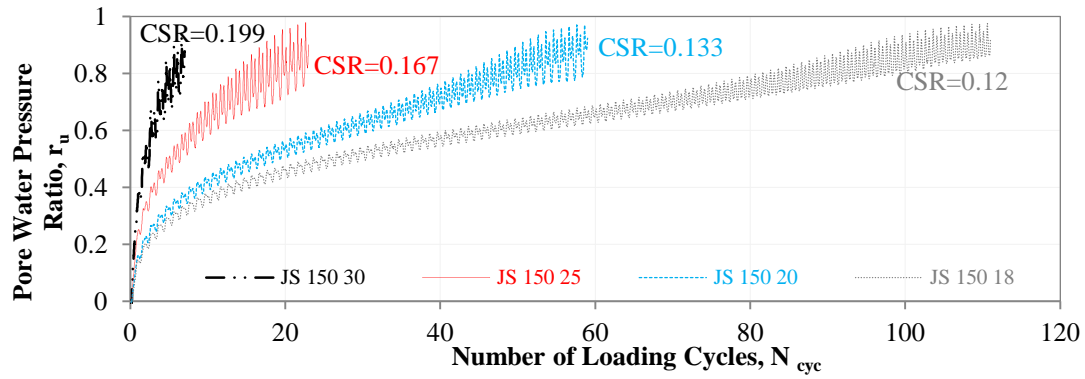
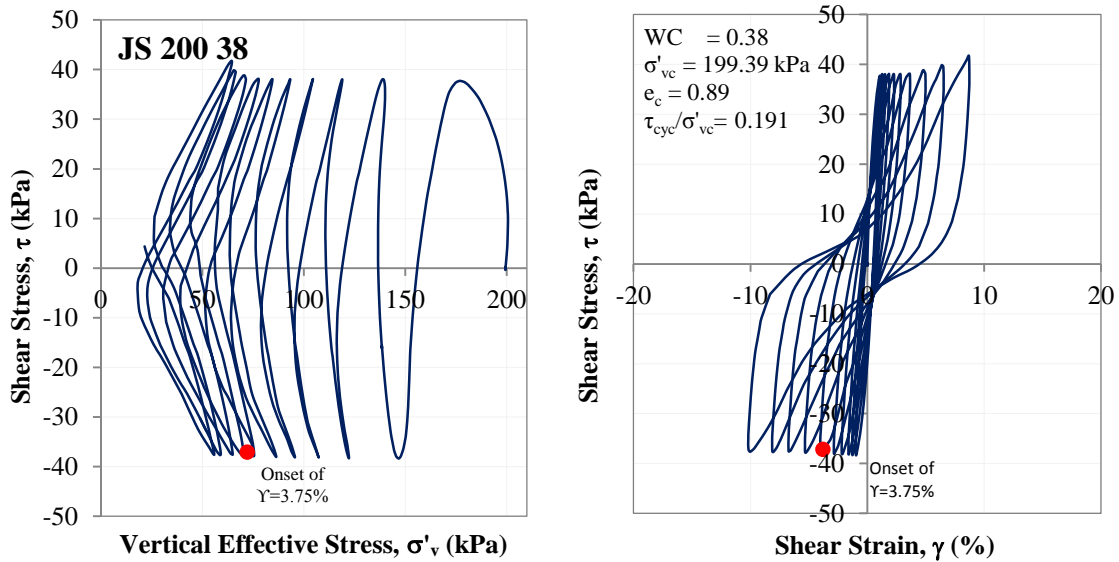


Figure 4.25 Stress path and shear stress-strain curves of constant-volume CDSS test on relatively undisturbed specimen from the Site #2 [PI=7], normally consolidated to  $\sigma'_{vc} = 150$  kPa and CSR of 0.12





**Figure 4.26** Development of pore water pressure ratio with respect to loading cycles in constant -volume CDSS test on relatively undisturbed specimen from the Site #2 [PI =7], normally consolidated to 150 kPa with different CSRs  
(Refer Table 4.1 for test details and parameters)



**Figure 4.27** Stress path and shear stress-strain curves of constant-volume CDSS test on relatively undisturbed specimen from the Site #2 [PI =7], normally consolidated to  $\sigma'_{vc} = 200$  kPa and CSR of 0.191

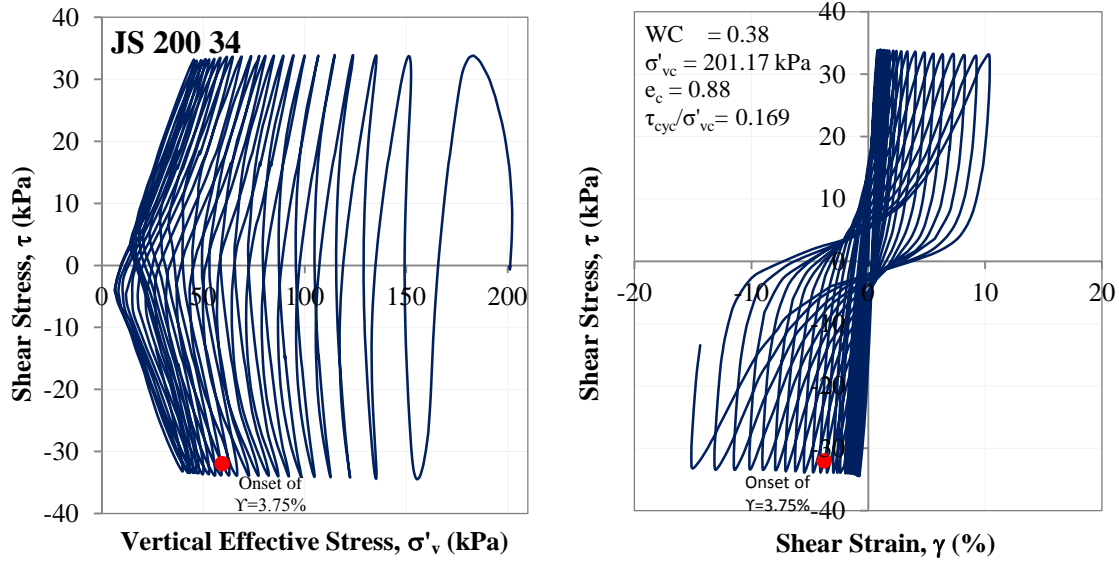


Figure 4.28 Stress path and shear stress-strain curves of constant-volume CDSS test on relatively undisturbed specimen from the Site #2 [PI =7], normally consolidated to  $\sigma'_{vc} = 200$  kPa and CSR of 0.169

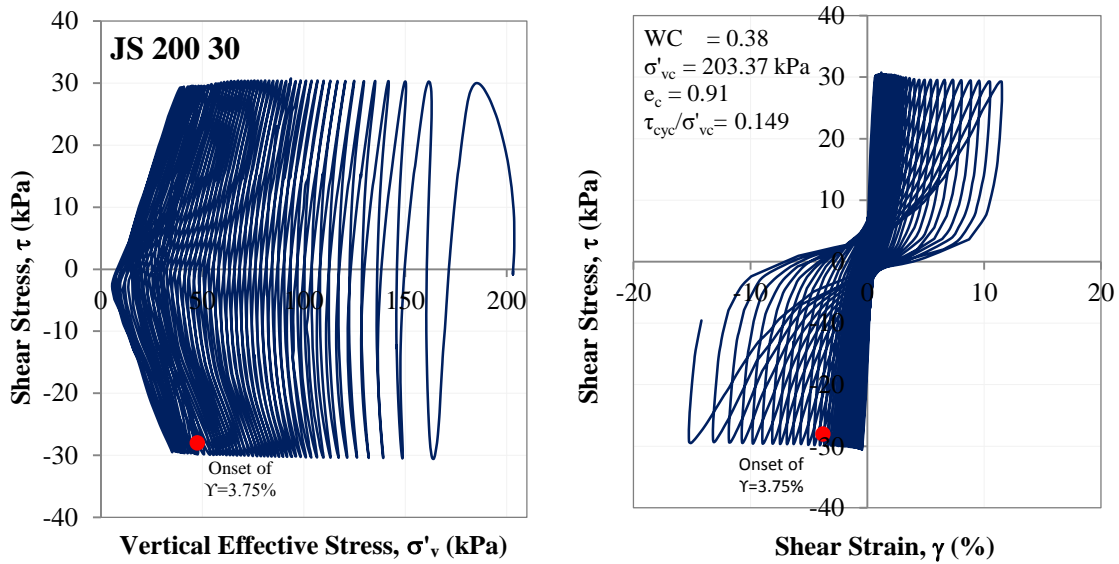
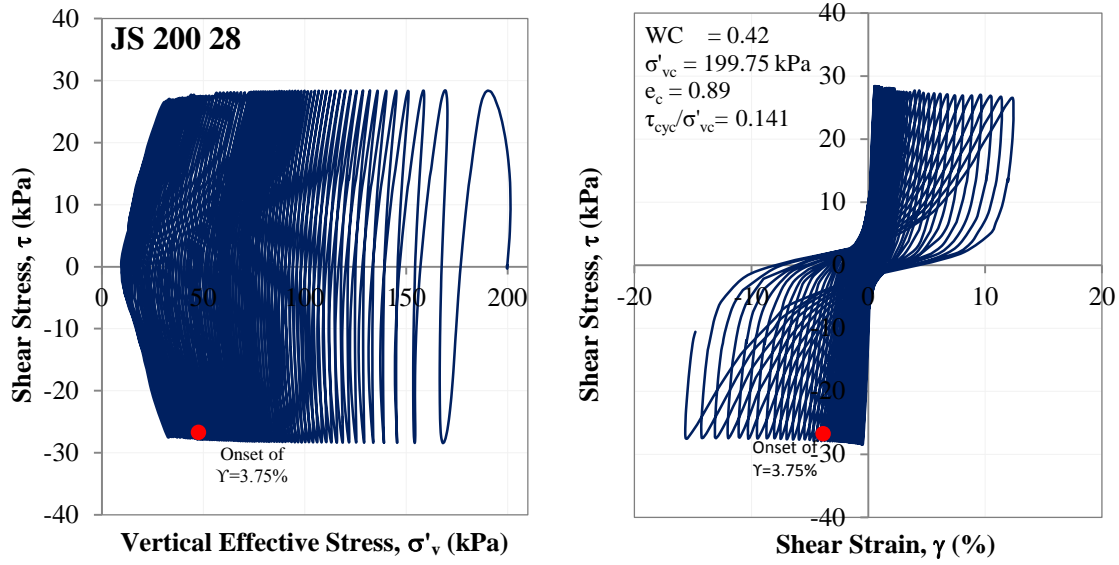
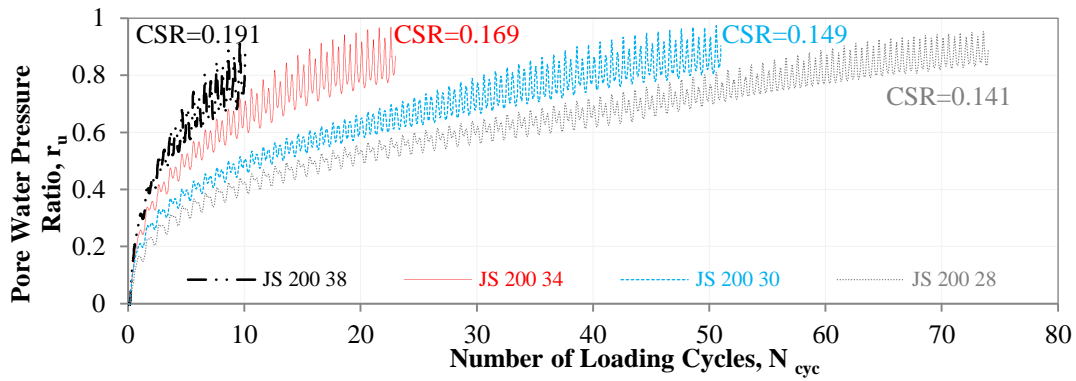


Figure 4.29 Stress path and shear stress-strain curves of constant-volume CDSS test on relatively undisturbed specimen from the Site #2 [PI =7], normally consolidated to  $\sigma'_{vc} = 200$  kPa and CSR of 0.149



**Figure 4.30** Stress path and shear stress-strain curves of constant-volume CDSS test on relatively undisturbed specimen from the Site #2 [PI =7], normally consolidated to  $\sigma'_{vc} = 200$  kPa and CSR of 0.141



**Figure 4.31** Development of pore water pressure ratio with respect to loading cycles in constant - volume CDSS test on relatively undisturbed specimen from the Site #2 [PI =7], normally consolidated to 200 kPa with different CSRs

(Refer Table 4.1 for test details and parameters)

In general, observed gradual accumulation of strain and cumulative development of pore water pressure due to cyclic shear loading are similar for all CDSS tests in Test Series II-C, despite the different consolidation stress levels that the tests were conducted at. Further, all specimens in Test Series II-C displayed initial contractive response followed by progressive degradation of shear stiffness. Moreover,  $r_u$  values (measured when the tests were terminated at a strain limit of 12%) developed due to the cyclic shear loading were about 90%.

### **4.3 Cyclic Shear Resistance**

The examination of the cyclic shear resistance derived from CDSS tests provides an opportunity to identify the parameters influencing the cyclic shear response. The cyclic shear resistance of soil, especially for liquefaction assessment from laboratory tests, is typically described by the number of loading cycles required for the attainment of a threshold cyclic shear strain when a soil specimen is subjected to constant amplitude loading corresponding to a given cyclic stress ratio.

In this regard, the commonly accepted threshold strain criteria is 3.75% of single amplitude shear strain in CDSS tests (equivalent to 5% double amplitude axial strain in cyclic triaxial test). This particular strain criterion can be considered as a result of an evolution from a number of similar criteria developed with attention paid to the approximate strain levels, observed in sand specimens when their  $r_u$  value was approaching the 100% mark during cyclic triaxial tests.

A detailed evolution of this strain based criteria is discussed in the literature review in Section 2.5.2. For the current study, in order to facilitate the comparison of cyclic shear resistance, the number of loading cycles required for the attainment of a single amplitude cyclic shear strain of

3.75% when a soil specimen is subjected to constant amplitude loading corresponding to a given cyclic stress ratio was defined as  $N_{cyc [\gamma=3.75\%]}$  and indicated in Table 4.1. Considering the threshold strain limit of 3.75% as the criterion, this chapter discusses the influence of initial effective confining stress (Section 4.3.1), coarse-grained fraction (Section 4.3.2), plasticity (Section 4.3.3) and fabric change due to reconstitution over the relatively undisturbed condition (Section 4.3.4) on the cyclic shear resistance.

#### **4.3.1 Effect of Initial Effective Confining Stress on Cyclic Resistance**

The cyclic shear resistance derived from tests conducted on normally consolidated silt ( $PI = 7$ ) is shown in Figure 4.32 by plotting the cyclic shear resistance in terms of the variation of CSR versus  $N_{cyc [\gamma=3.75\%]}$ . The data points of CSR versus  $N_{cyc [\gamma=3.75\%]}$  for different confining consolidation stresses seems to fall on a single trend-line as shown in Figure 4.32 implying that the cyclic resistance is not significantly influenced by the confined consolidation pressure, or in spite of the variation in initial void ratio (just prior to cyclic loading) due to different consolidation stress levels.

It should be noted that similar observations are previously discussed in Section 4.1.1.2, where normalized shear strength derived from monotonic DSS tests performed at different consolidated stress levels for the same silt found to fall within a narrow range (refer Series II-A in Figure 4.4). The observation on the effect of confining stress on the cyclic shear resistance from this study are found to be similar to the previous observations by Zergoun & Vaid (1994) for normally consolidated clay and by Sanin (2010) for normally consolidated Fraser River delta silt.

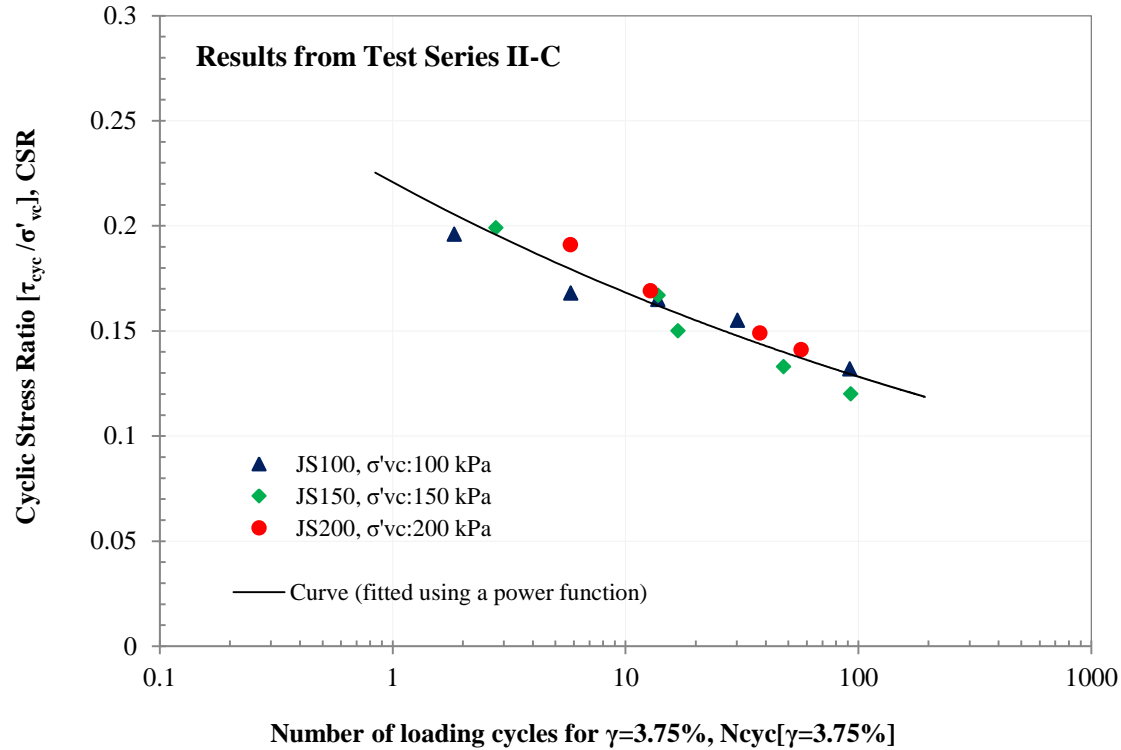


**Figure 4.32 Cyclic Stress Ratio versus Number of loading cycles to reach  $\gamma=3.75\%$  curves from constant-volume CDSS tests on undisturbed silt specimens [Site #2,  $PI=7$ ] at confining consolidation stress levels of 100 kPa, 150 kPa and 200 kPa**

The cyclic shear resistance derived from the test Series III-C (on silt with  $PI = 34$  from Site #3) indicates decreasing cyclic shear resistance in with increasing consolidation stress level. For instance, specimen tested at 75 kPa, 150 kPa and 200 kPa reached 3.75% of strain in similar number of cycles for a CSR of 0.261, 0.238 and 0.169 as shown in Figure 4.33 with stress path and stress-strain plots.

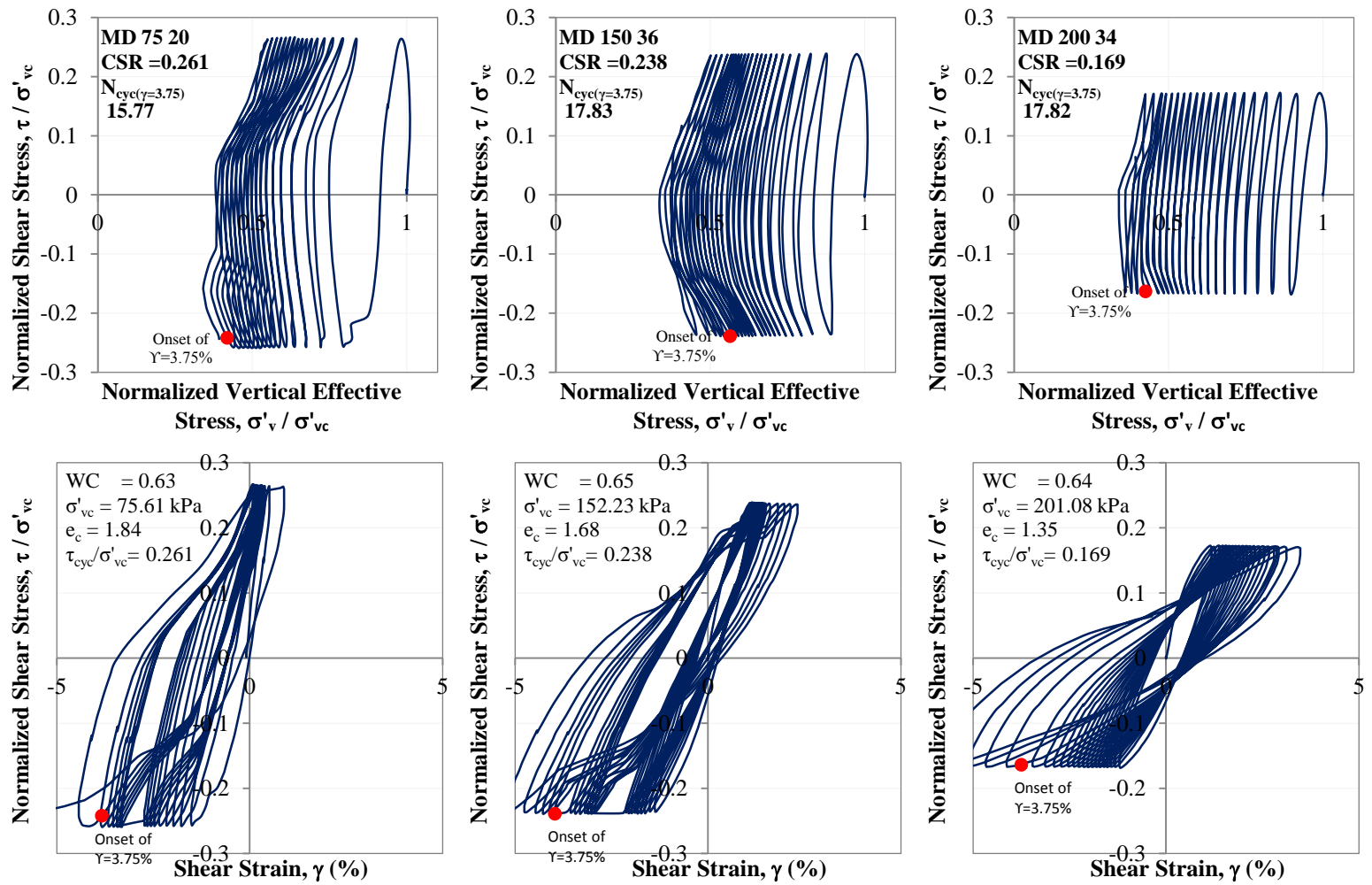
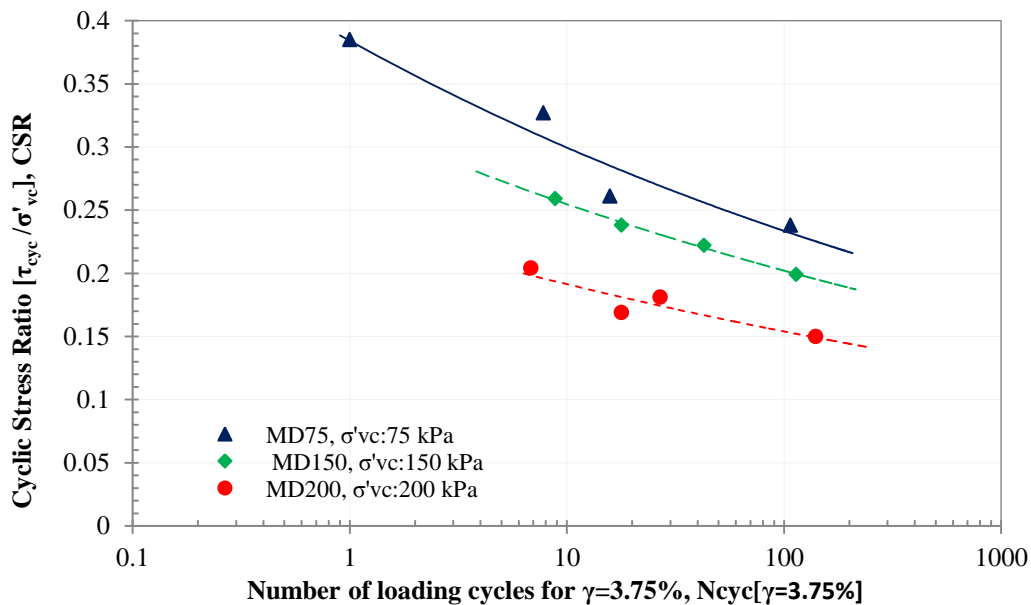


Figure 4.33 Stress path and shear stress-strain curves of constant-volume CDSS test on relatively undisturbed specimen from the Site #3 [PI =34], normally consolidated to  $\sigma'_{vc} = 75$  kPa, 150 kPa and 200 kPa, where  $N_{cyc(\gamma=3.75\%)} = 15.8, 17.8$  and  $17.8$  for different values of CSR

This implies that, unlike in the observed response of cyclic shear resistance with respect to the confining consolidation stress (Figure 4.32) for silt (PI = 7) from the Site #2, possible destructuration may have occurred in the soils from Site #3 when the specimens were consolidated to stress levels above the pre-consolidation stress level; in turn, this destructuration would have caused the fabric of the silt specimen to generate comparatively weaker cyclic shear resistance; this trend is clearly demonstrated in the Figure 4.34, when CSR versus  $N_{cyc} [\gamma=3.75\%]$  for different confining consolidation stresses are plotted together. It appears that the degree of destructuration in a given specimen would increase with increasing margin between the consolidation stress of the specimen and its pre-consolidation stress. This trend is similar to the lower shear strength displayed during monotonic DSS loading by specimens subjected to consolidation stresses higher than the estimated pre-consolidation stress of silt (as discussed in Section 4.1.1.3).



**Figure 4.34** Cyclic Stress Ratio versus Number of loading cycles to reach  $\gamma=3.75\%$  curves from constant-volume CDSS tests on undisturbed silt specimens [Site #3, PI=34] at confining consolidation stress levels of 75 kPa, 150 kPa and 200 kPa



#### **4.3.2 Effect of Coarse-grained Fraction on Cyclic Shear Resistance of Fine-grained Soils**

The interpretation on soil type based on the CPT results (refer Figure 3.11) from the Site #1 revealed the presence of silt, sandy silt, silty sand, and sand within the depth range between 5 m and 8 m. The geotechnical investigation also suggested that the coarser fraction would increase with increasing depth below the ground surface. The water table at the test hole location was about 2.6 m. The coarse-grained fraction determined from grain size analyses conducted on saturated samples collected from the test hole at depths of 5.8 m (Sample A), 6.4 m (Sample B), and 6.7 m (Sample C) below the ground surface were found to be 20%, 30% and 35%, respectively (refer Appendix B) - suggesting an increase in coarse-grained fraction with increasing the depth below ground surface at Site #1. In all specimens, clay content was about 20%. In other words, the soil from sample A can be classified as silt with little sand whereas soil from sample B and C are sandy silt in according to D2488-09a (ASTM, 2009).

This section presents the results of the CDSS tests that were performed on soils from Sample A, B and C, which were retrieved from different depth levels as described above. The variation of the coarse-grained fraction in these samples allowed an investigation of the cyclic shear response of natural silt with increasing coarse-grained fraction. The latter part of this section presents a comparison of the cyclic shear resistance derived from these materials having different coarse-grained fraction with those published by Sanin (2010); Sivathayalan (1994) and Sriskandakumar (2004).

CDSS test specimens prepared from the tube samples obtained from depths of 5.8 m (Sample A), 6.7 m (Sample C), and 6.4 m (Sample B) were initially, normally consolidated to effective stresses of approximately 150 kPa, 200 kPa, and 300 kPa, respectively (Test Series I-C in Table

4.1). It is to be noted that these consolidated stresses are higher than the estimated in-situ overburden stress for the samples which were in the range of 100 kPa to 125 kPa (refer Table 3.3). The tests performed on the specimens prepared from sample A, B, and C are referred as NS20, NS 30, and NS35 in figures for clear identification of natural silt with varying coarser fraction.

The accumulation of shear strain and excess pore water pressure ratio during Tests No. CT150 22.5, CT 200 30 and CT 300 45 are shown in Figure 4.35. The normalized stress path and normalized shear stress-strain plots resulted from the same three CDSS tests are presented in Figure 4.36.

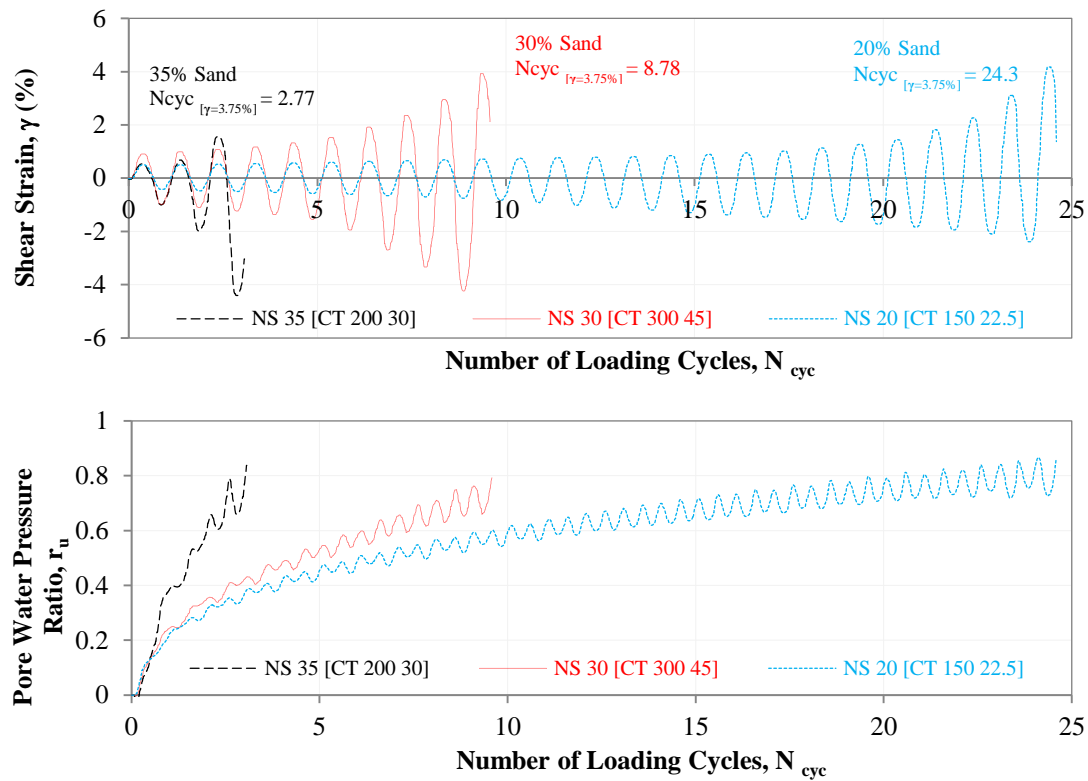


**Figure 4.35** Accumulation of shear strain and development of pore water pressure ratio with respect to loading cycles in constant -volume CDSS test on relatively undisturbed specimen from the Site #1 [PI =5], having coarse-grained fraction of 20%, 30% and 35% when tested for CSR of about 0.15 (Refer Table 4.1 for test details and parameters)

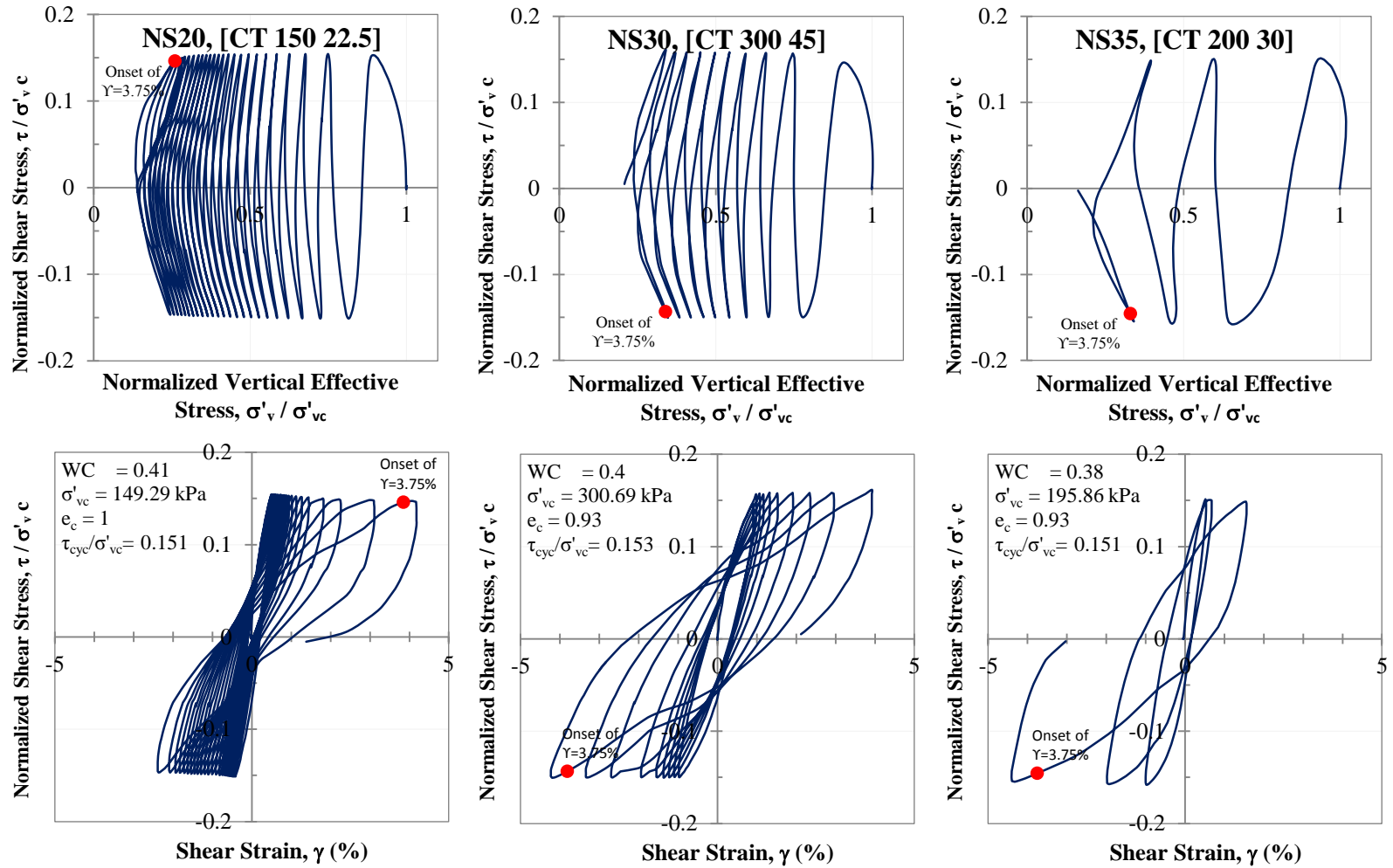
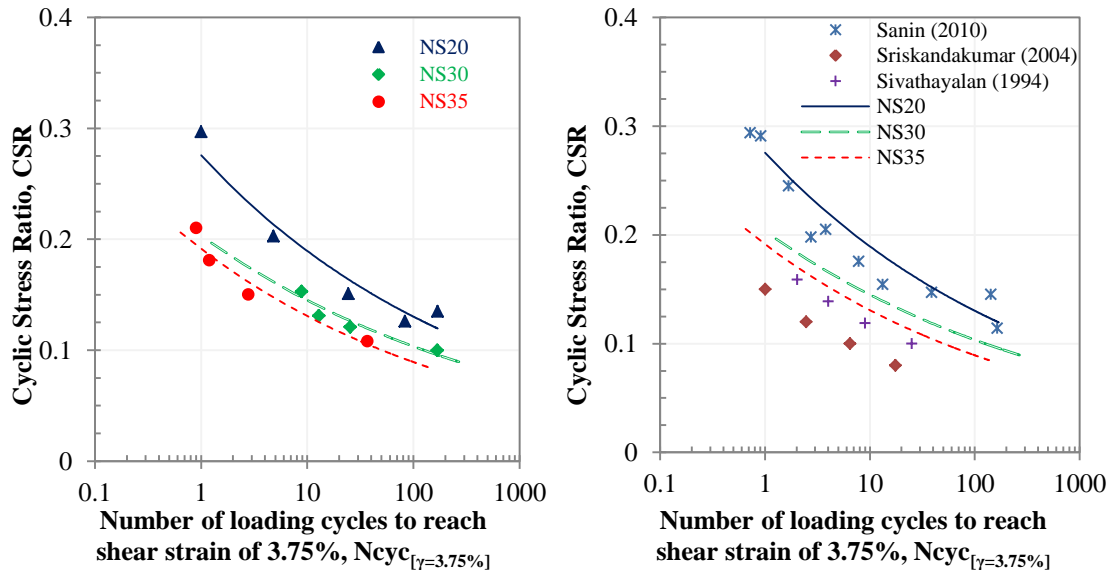


Figure 4.36 Normalized stress path and normalized shear stress-strain curves of constant-volume CDSS test on relatively undisturbed silt specimen from the Site #1 [PI =5], having coarse-grained fraction of 20%, 30% and 35% when tested for CSR of about 0.15

A direct comparison was considered reasonable as the tests were conducted with a CSR of about 0.15 for the silt specimens with different coarse-grained fraction. As may be noted, the rate of shear strain as well as excess pore water pressure development (with respect to number of loading cycles) seems to increase with increasing coarser fraction. The results presented in Figure 4.35 and through Figure 4.36 suggest that the cyclic shear resistance generally weakens with the increasing coarser fraction of the natural silt. The variation of CSR versus  $N_{cyc}$  [ $\gamma=3.75\%$ ] for natural silt with different coarse-grained fractions presented in Figure 4.37 provides further confirmation that the cyclic resistance in natural silt is reduced when coarse-grained fraction increases from 20% to 35%. It is also of general interest to compare the cyclic resistance derived for the natural silts of this with those generated by Sriskandakumar (2004) for air-pluviated Fraser River Sand, and by Sivathayalan (1994) for water-pluviated Fraser River Sand as shown in Figure 4.37.



**Figure 4.37 Cyclic Stress Ratio versus Number of loading cycles to reach  $\gamma=3.75\%$  curves from constant-volume CDSS tests on undisturbed silt specimens [Site #1, PI=5] with different coarse-grained fraction of 20%, 30% and 35% and comparison of cyclic resistance with materials with different coarse-grained fractions**

It is of relevance to note that the natural silt with a sand content of 35% still displays a comparatively higher cyclic resistance than those for both air-pluviated and water-pluviated Fraser River sand. Further, the results for cyclic shear resistance for a low-plastic natural silt ( $PI = 4$ ) from the Fraser River delta observed by Sanin (2010) are also overlain on Figure 4.37 for the purpose of comparison with the present findings. It appears that the cyclic resistance reported for the low-plastic silt having a sand content of about 10%, is similar to the CRR derived from this study for the case with about 20% sand. Although additional research is required to arrive at firm conclusions, it appears that a sand content of at least 20% would be required for the presence of sand content to impact the cyclic resistance.

#### **4.3.3 Effect of Plasticity on Cyclic Shear Resistance**

The following section presents a comparison of the cyclic shear response and resistance observed from constant-volume CDSS tests [the Test Series I-C, II-C and III-C (Table 4.1)] performed on silt specimens prepared from undisturbed samples having different  $PI$  as of 5, 7, and 34 obtained from the Sites #1, #2, and #3 (see Table 3.3). Latter part of this section discuss the effect of plasticity on cyclic shear resistance of fine-grained material combining the test results from this study with a few additional test results reported by Sanin (2005, 2010).

The results of Tests No. CT 200 30, JS 200 30, and MD 200 30 (refer Table 4.1), where undisturbed silt specimens from Site#1 (CT), #2 (JS) and #3 (MD) having  $PI$  of 5, 7, and 34, respectively, are normally consolidated to 200 kPa and cyclic shear loadings were applied with a CSR of about 0.15, are considered herein; these results provide the development of strain accumulation, pore-water pressure development, stress-strain loops during cyclic loading. For example, Figure 4.38 illustrates that all three specimens exhibit progressive shear accumulation

and gradual development of excess pore water pressure with increasing number of loading cycles. It appears that the rate of shear strain accumulation and rate of shear-induced  $r_u$  (with respect to number of loading cycles) decreases with increasing soil plasticity, when all three specimens were tested under similar stress conditions (i.e.  $\sigma'_{vc} = 200$  kPa and  $CSR = 0.15$ ). The specimen with a PI of 5 reached shear strain of 3.75% simply in 2.8 loading cycles and specimen having a PI of 7 took 37.8 loading cycles, whereas, comparatively high plastic specimen (PI=34) survived 139 loading cycles prior to the attainment of same strain level.

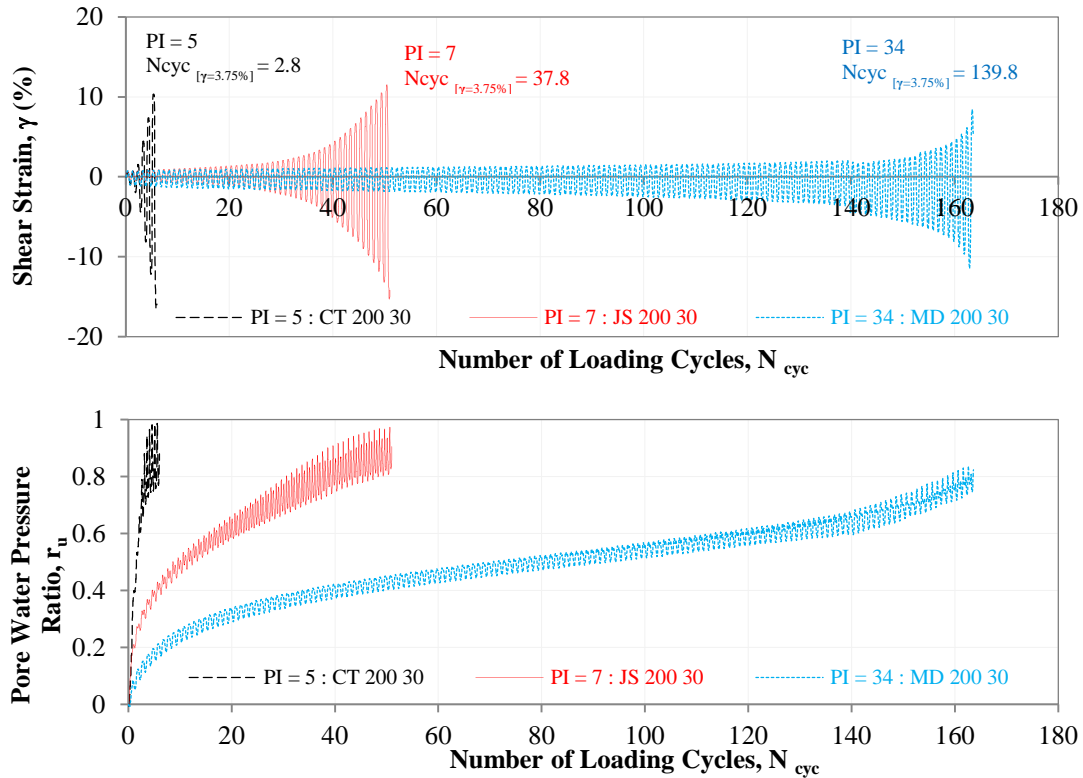


**Figure 4.38 Accumulation of shear strain and development of pore water pressure ratio with respect to loading cycles in constant -volume CDSS test on relatively undisturbed specimen from the Site #1 [PI =5], Site #2 [PI =7], and Site #3 [PI =34], normally consolidated to 200 kPa with a CSR of about 0.15**

Stress path response and shear stress-strain curves for the considered tests cases of CT 200 30, JS 200 30, and MD 200 30 are presented in Figure 4.39 to examine changes in contractive and dilative tendencies during cyclic loading as well as in shear modulus with increasing number of loading cycles. It can be seen that the rate of degradation of shear modulus for the undisturbed silt specimens increases with decreasing plasticity. Since the complete stress path and stress-strain curves for the whole duration of tests are presented in Figure 4.39, the stress path and stress-strain responses only for some selected loading cycles from the same tests are shown in Figure 4.40 for the sake of clarity. It can be seen that in specimens with higher plasticity exhibit lesser reduction of vertical effective stress for the 1<sup>st</sup> loading cycles. When the vertical effective stresses for the three specimens at similar large strain levels due to similar magnitude of cyclic shear loading (CSR of 0.15) are compared (see Figure 4.39), it can be seen that the comparatively higher plasticity specimen (MD 200 30) did not reach zero or near zero margin, whereas comparatively lesser plasticity specimen (CT 200 30) suffered near zero vertical effective stress condition.

Cyclic stress-strain response observed for the three specimens also provides an opportunity to appreciate the differences of the shape of the stress-strain loops at larger strain levels for specimens with different soil plasticity. Some selected stress-strain loops from the tests conducted on specimens having different plasticity are shown in Figure 4.41. It can be noted that the stress-strain responses exhibited broader hysteresis loops with increasing plasticity, and this observation made for natural undisturbed soils is in general accord with the observations made by Romero (1995) for normally consolidated specimens of three blended silt mixtures during undrained cyclic triaxial loading.

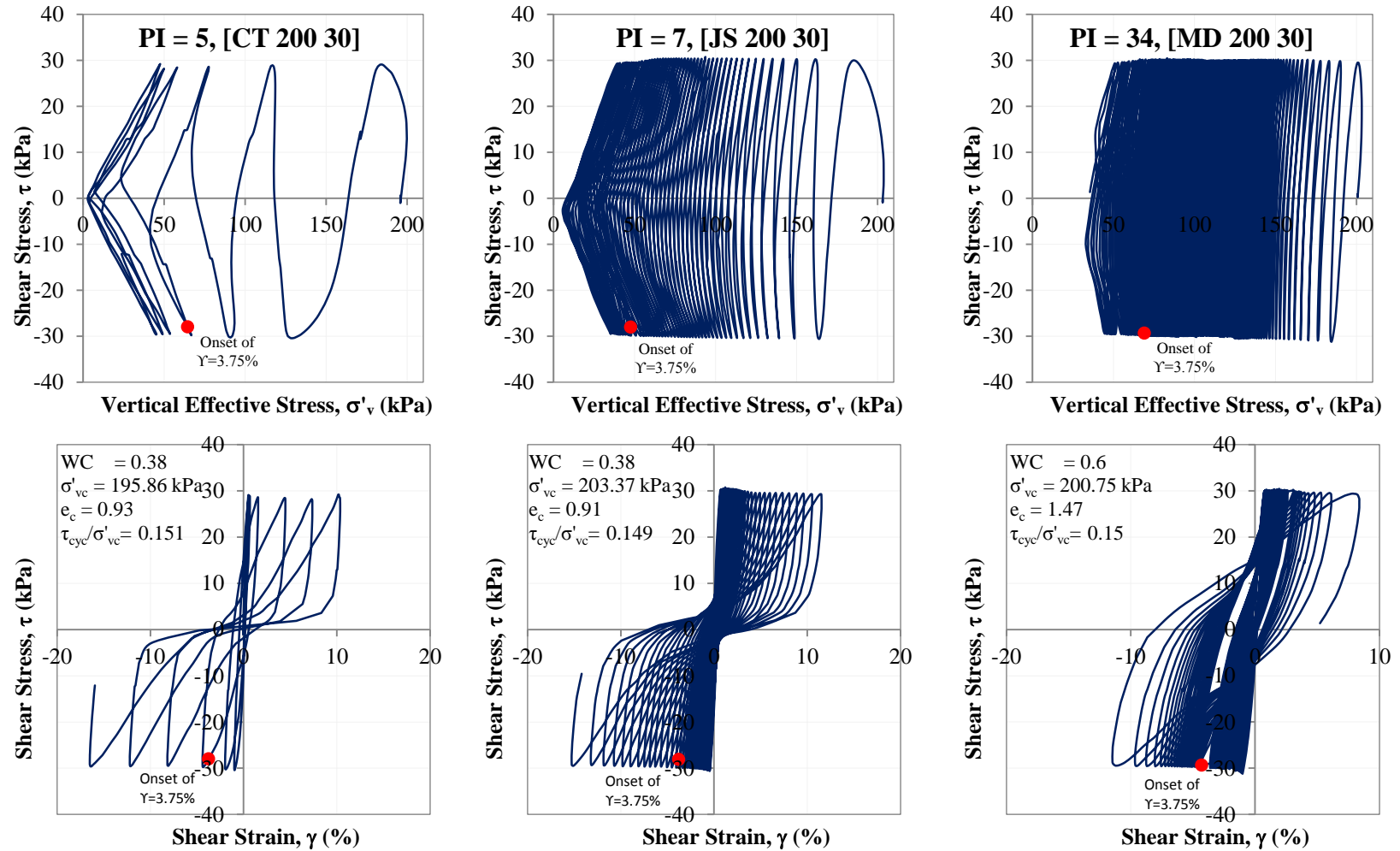


**Figure 4.39 Comparison of stress path and shear stress-strain curves of constant-volume CDSS tests on relatively undisturbed specimen from the Site #1 [PI =5], Site #2 [PI =7], and Site #3 [PI =34], normally consolidated to 200 kPa with a CSR of about 0.15**



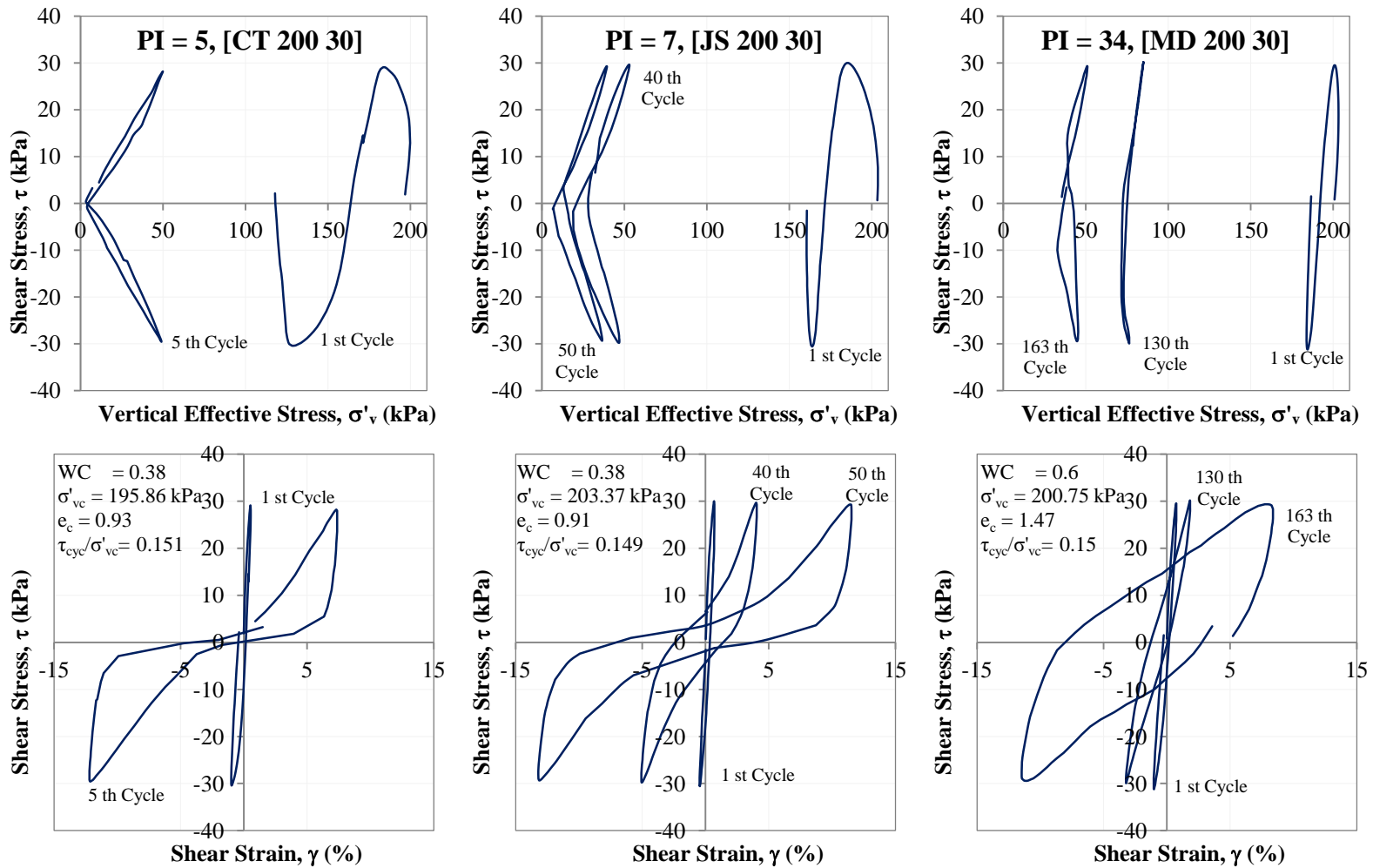


**Figure 4.40 Comparison of stress path and shear stress-strain curves for selected loading cycles during constant-volume CDSS tests on relatively undisturbed specimen from the Site #1 [PI=5], Site #2 [PI=7], and Site #3 [PI=34], normally consolidated to 200 kPa with a CSR of about 0.15**

The variation of cyclic shear resistance in terms of CSR versus  $N_{cyc} [\gamma=3.75\%]$  obtained for the silts considered in this study are presented in Figure 4.42, and compared with those derived for several fine-grained materials with different plasticity by Sanin (2005, 2010). While appreciating the scatter of the experimental test results and possible variation of material from field samples, trend lines generated from the experimental results for relatively undisturbed soil specimens shown in Figure 4.42 reveals that cyclic shear resistances of the fine-grained materials interpreted from the constant volume CDSS tests seem to generally increase with increasing soil plasticity.

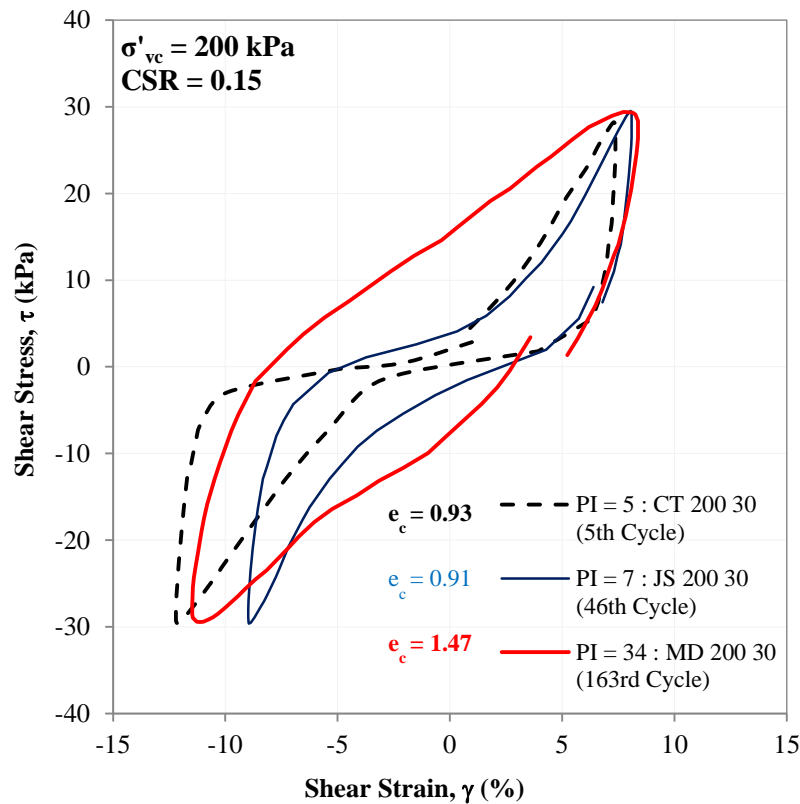


**Figure 4.41 Stress-strain loops for relatively undisturbed, normally consolidated silt specimens with different soil plasticity, at similar strain levels during constant-volume CDSS tests**

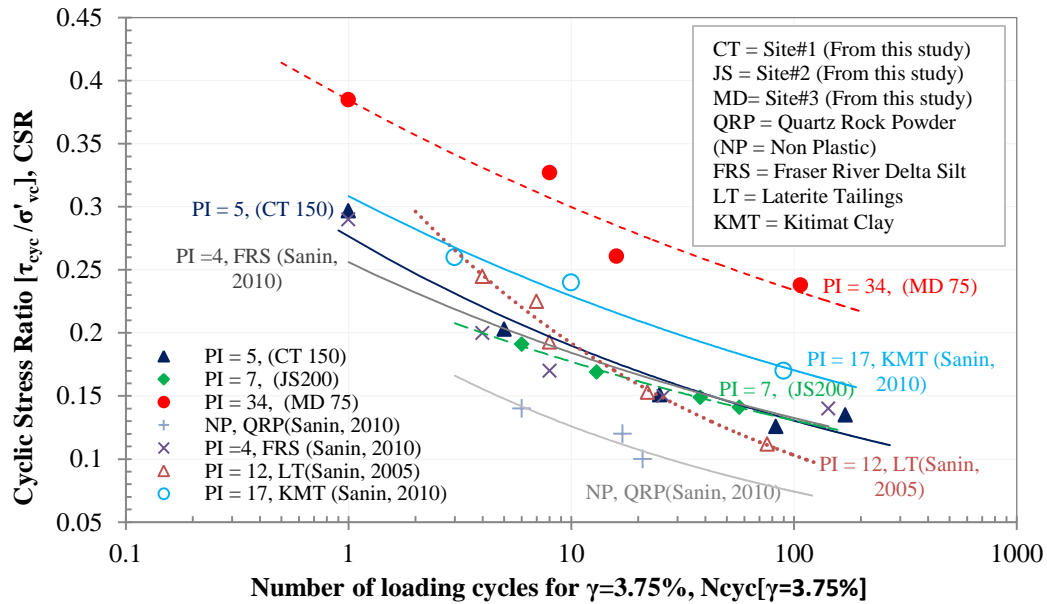


**Figure 4.42** Cyclic Stress Ratio versus Number of loading cycles to reach  $\gamma=3.75\%$  curves from constant-volume CDSS tests on undisturbed specimens of fine-grained materials with different plasticity

#### 4.3.4 Comparison of Cyclic Shear Resistance of ‘Relatively Undisturbed’ and ‘Reconstituted’ Specimens

The constant-volume CDSS response of relatively undisturbed silt specimens retrieved through thin-walled steel tube sampling (as per Section 3.2.3) and reconstituted specimens prepared by slurry deposition method (as per Section 3.3.1.2 and 3.3.3.2) are examined herein. The following section presents a comparison of the results observed from Test Series I-C, I-E, II-C, II-E, III-C and III-E (Table 4.1) to illustrate the differences in cyclic shear response and resistance for the materials obtained from the three sites in the present study. It is to be noted that the material from the relatively undisturbed specimens which were used for the Test Series I-C, II-C and III-C were re-utilized to prepare the reconstituted specimens for Test Series of I-E, II-E and III-E, respectively; since the particle size distribution is unchanged, any differences in the “C” series

and “E” series of tests could be reasonably attributed to the effect of fabric differences between the reconstituted and relatively undisturbed specimens.

During the consolidation phase of reconstituted test specimens prepared by slurry deposition method, specimens were incrementally loaded until the desired consolidation stress levels were reached, and the test specimens were consolidated for durations of ~0.5 hours to ~ 3.5 hours). The key herein was to allow sufficient time duration for the vertical consolidation strain in the test specimen to stabilize under a given applied vertical stress. For example, the initial water content and void ratio before the consolidation phase was more than 85% and about 2.5 respectively for the reconstituted specimens prepared from comparatively high plastic ( $PI=34$ ) material, thus those specimens consumed more than 3.5 hours to the completion of primary consolidation.

The results of selected tests CT 150 18.75, CT R 150 18.75 for the material ( $PI = 5$ ) from the Site #1, JS 200 30, JS R 200 30 for the material ( $PI = 7$ ) from the Site #2 and MD 075 15, MD R 075 15 for the material ( $PI = 34$ ) from the Site #3 are presented herein. Figure 4.43 shows the cyclic strain and pore water pressure development during constant-volume cyclic shear loading for these tests. The cases presented in Figure 4.43 were selected such that the response of relatively undisturbed specimens and reconstituted specimens which were subjected to similar consolidation and cyclic shear stress conditions (i.e.  $\sigma'_{vc}$  and CSR) would be compared. Despite the variance of material from three sites such as the gradation and plasticity, it is clear from the data presented in Figure 4.43 that all reconstituted specimens indicated higher rate in strain accumulation and pore-water pressure development (with respect to number of cycles) compared to those observed in relatively undisturbed specimens.

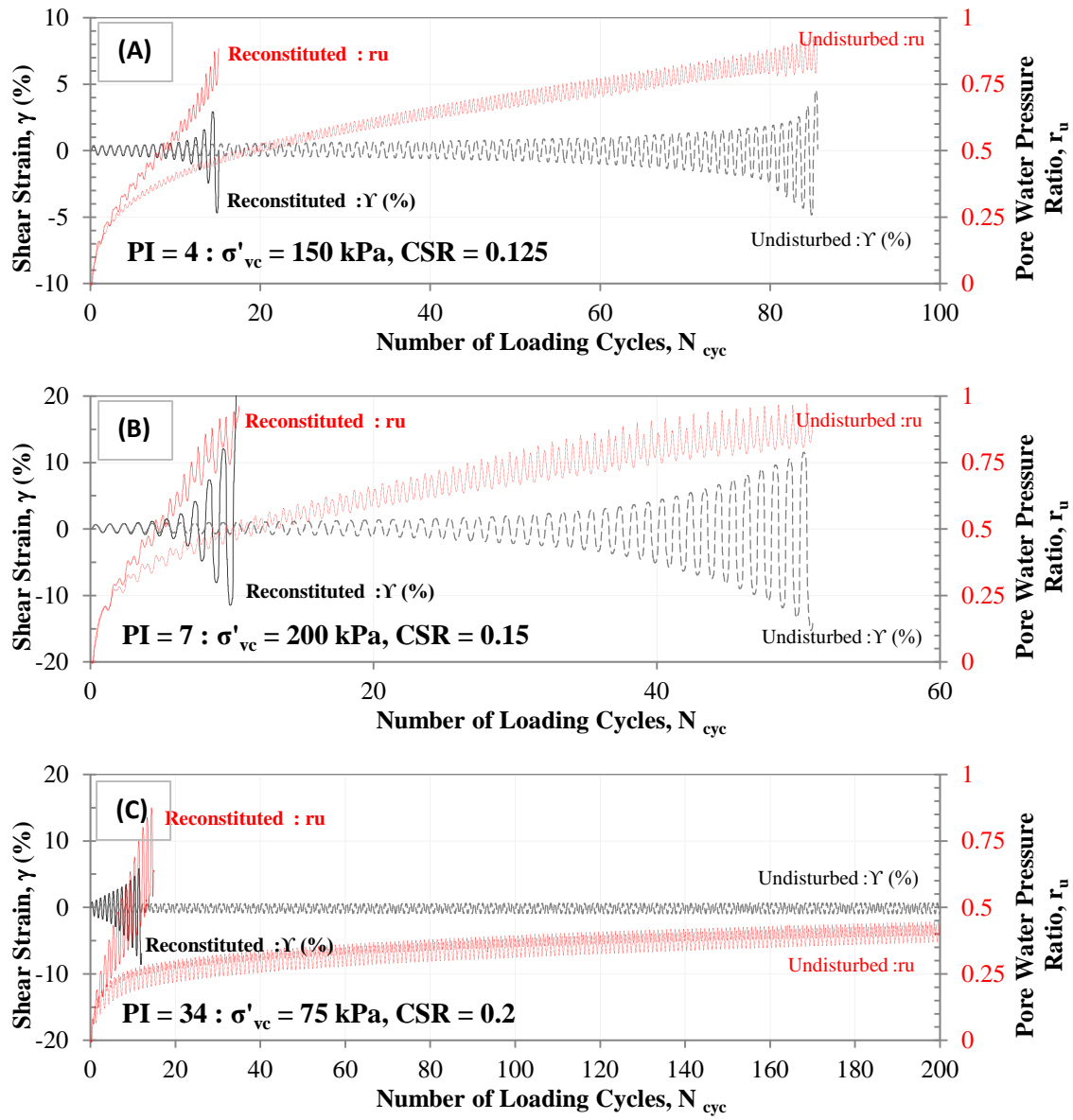


**Figure 4.43 Comparison of the accumulation of shear strain and development of pore water pressure ratio with respect to number of loading cycles in constant -volume CDSS tests of relatively undisturbed and reconstituted specimens**

(A): CT 150 18.75 and CT R 150 18.75

(B): JS 200 30 and JS R 200 30

(C): MD 075 15 and MD R 075 15

(Refer Table 4.1 for test details and parameters)

The stress path and cyclic shear stress-strain curves for the Tests No. CT 150 18.75, CT R 150 18.75 are presented in Figure 4.44, and those of Tests No. JS 200 30, JS R 200 30 are presented in Figure 4.45 to illustrate the difference in shear stiffness degradation of relatively undisturbed and reconstituted specimens during constant-volume CDSS tests.

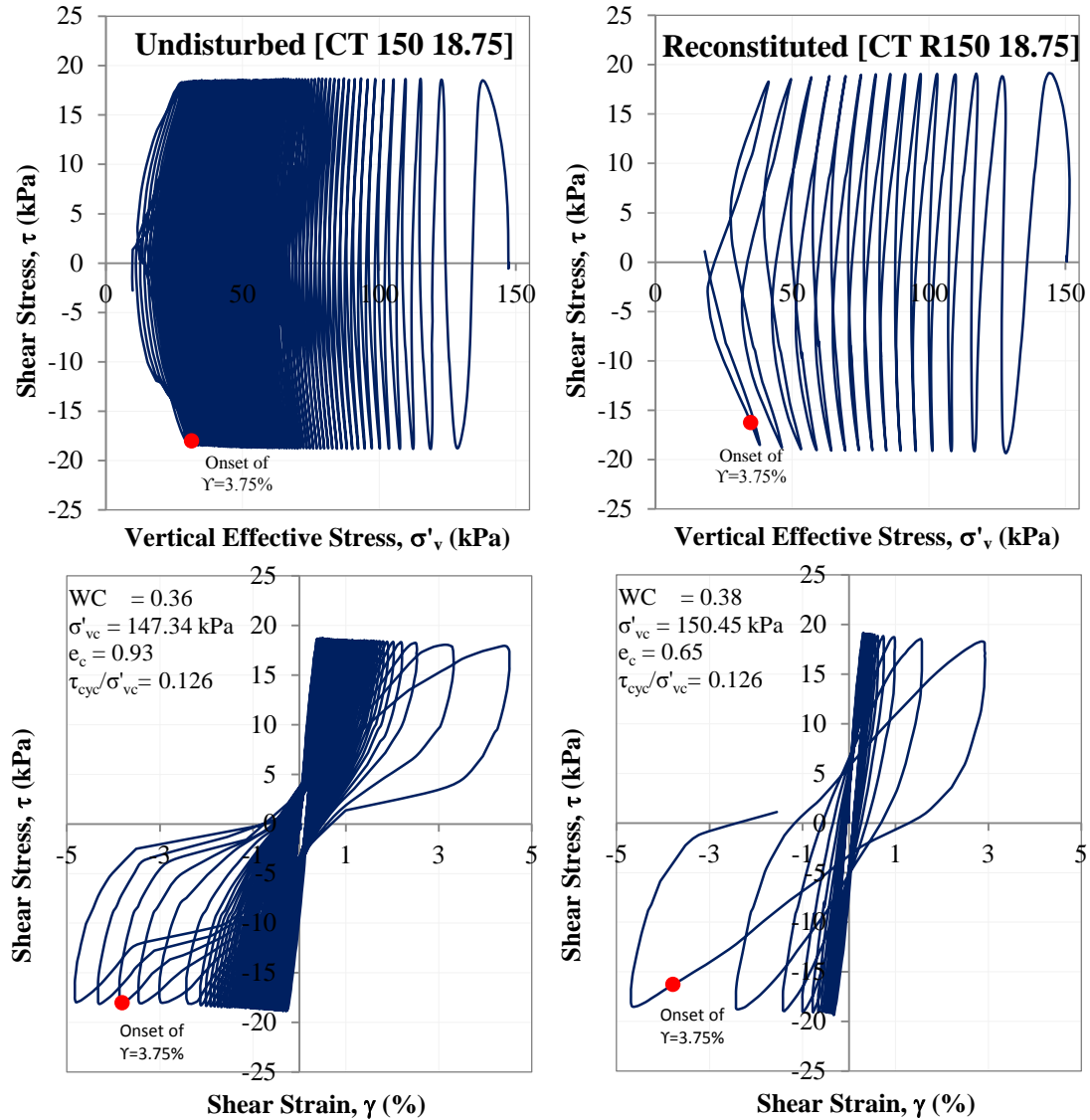


**Figure 4.44 Comparison of stress path and shear stress-strain curves of constant-volume CDSS test on relatively undisturbed (CT 150 18.75) and reconstituted specimen (CT R 150 18.75) from the Site #1 [PI =5], normally consolidated to 150 kPa and CSR of about 0.125**

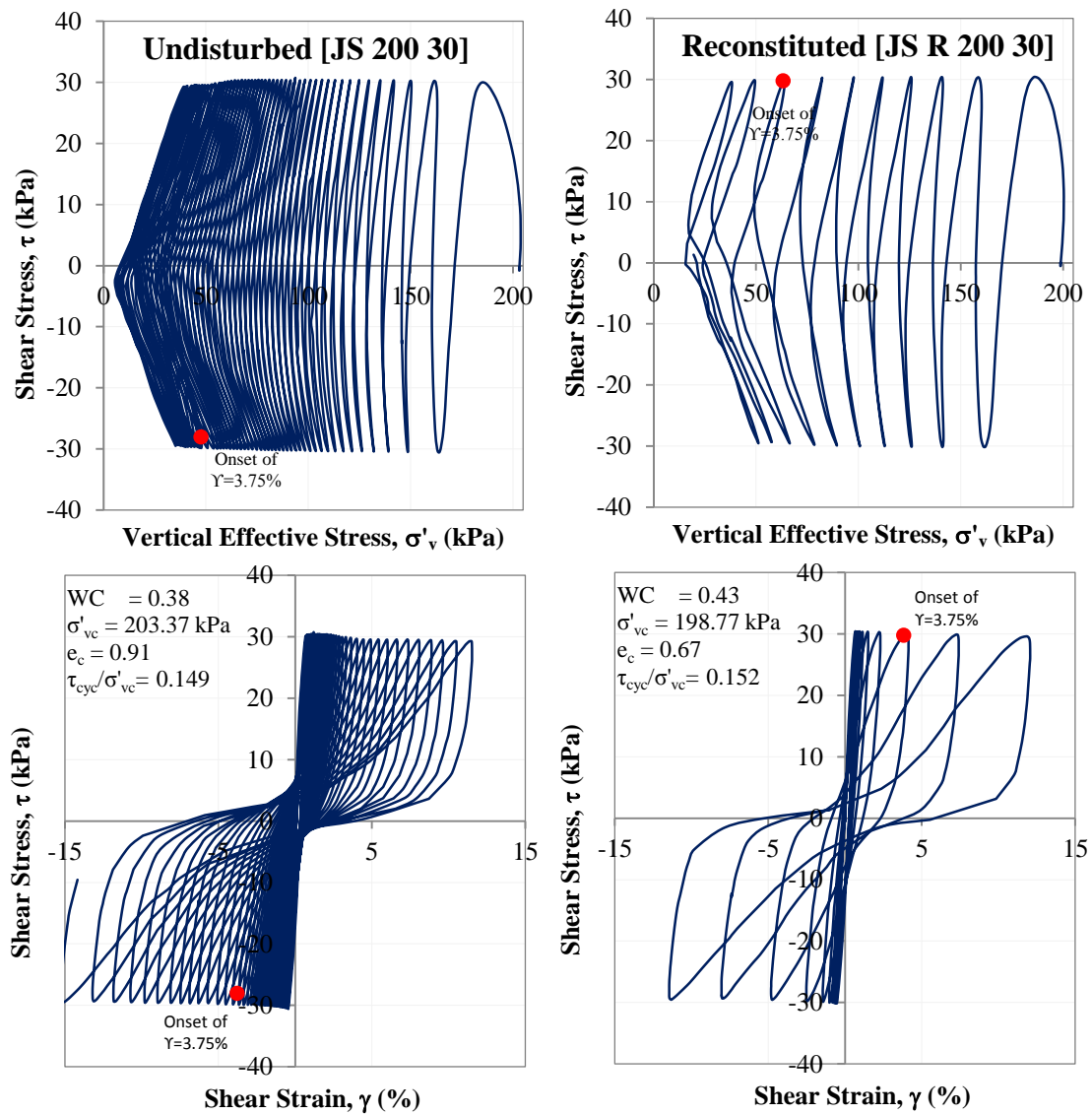


**Figure 4.45 Comparison of stress path and shear stress-strain curves of constant-volume CDSS test on relatively undisturbed (JS 200 30) and reconstituted specimen (JS R 200 30) from the Site #2 [PI=7], normally consolidated to 200 kPa and CSR of about 0.15**

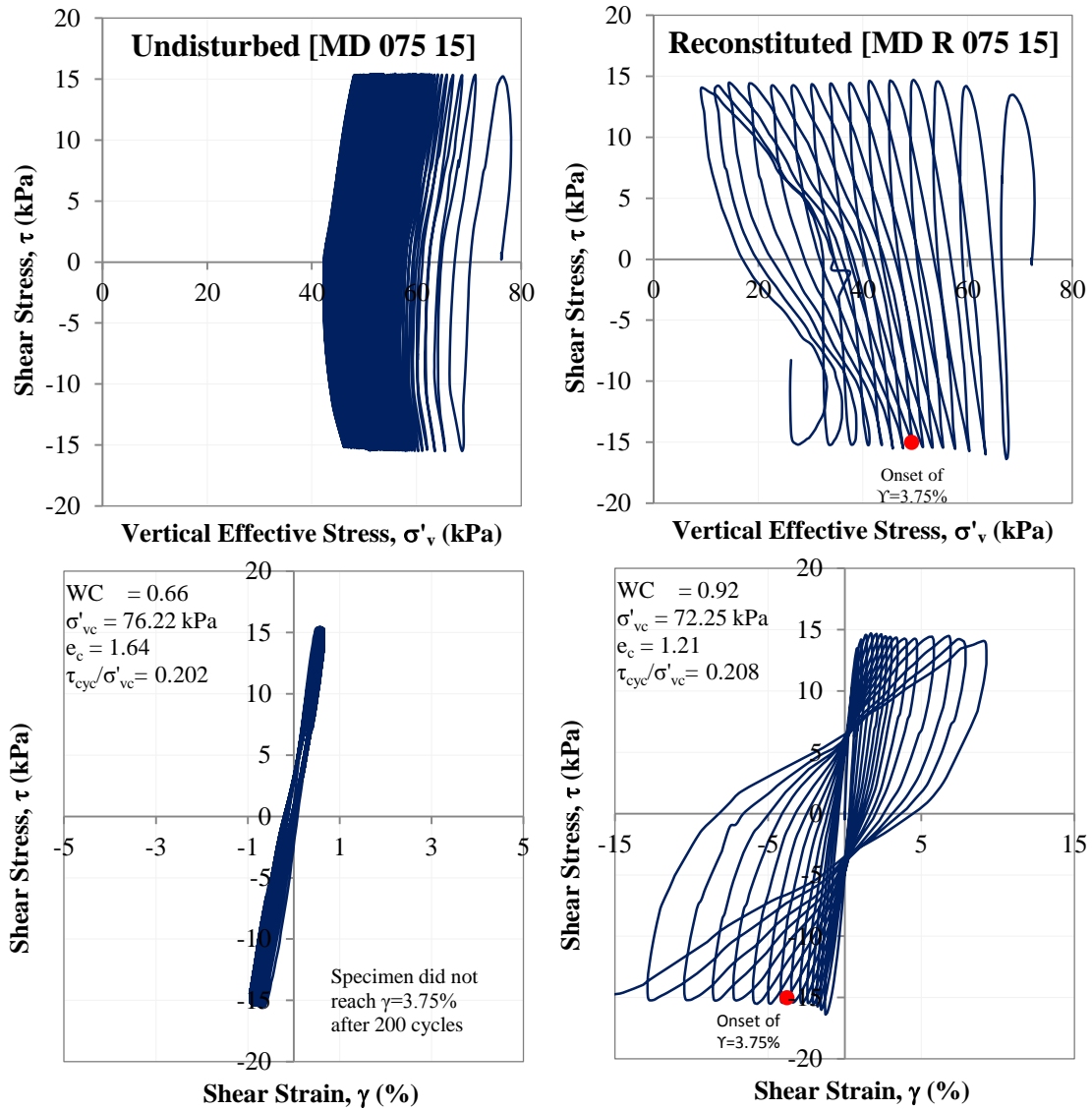


**Figure 4.46 Comparison of stress path and shear stress-strain curves of constant-volume CDSS test on relatively undisturbed (MD 075 15) and reconstituted specimen (MD R 075 15) from the Site #3 [PI =34], normally consolidated to 75 kPa and CSR of about 0.2**



Again, despite the comparatively lesser post consolidation void ratio (i.e., higher density), it can be noted that the reconstituted specimen displayed increased degree of stiffness degradation and potential of strain accumulation compared to the relatively undisturbed specimen. The relatively high plastic material from the Site #3 also exhibit the same comparatively weaker cyclic shear response in reconstituted specimens as opposed to relatively undisturbed specimens, as shown in Figure 4.46 for the tests cases of MD 075 15 and MD R 075 15.

The above relatively weaker response of reconstituted specimens in comparison to that of relatively undisturbed specimens, can be further highlighted when stress path and stress-strain curves for selected loading cycles of reconstituted specimens are plotted in one figure with those of relatively undisturbed specimens as shown in Figure 4.47. As may be noted, during the first cycles, the differences between the stress paths for the reconstituted and relatively undisturbed specimens are not significant. However, this difference becomes quite evident when the stress-strain loops for 15<sup>th</sup> cycles of reconstituted specimen prepared from the material of Site #1 are compared with those for the relatively undisturbed specimen as shown in Figure 4.47. Similar deviation between the results for reconstituted and relatively undisturbed specimens is notable when the results for the materials from the Sites #2 and #3 (at 8<sup>th</sup> and 9<sup>th</sup> loading cycles) are compared.

The cyclic shear response between relatively undisturbed specimens and reconstituted specimens can be further assessed by comparing the cyclic shear resistance in terms of  $N_{cyc [\gamma=3.75\%]}$  versus CSR plots as shown in Figure 4.48. As mentioned in Section 4.1.5, decrease of void ratio and disturbance of natural fabric are two competing factors in governing the cyclic shear resistance of reconstituted material when compared to the cyclic shear resistance of undisturbed specimen.

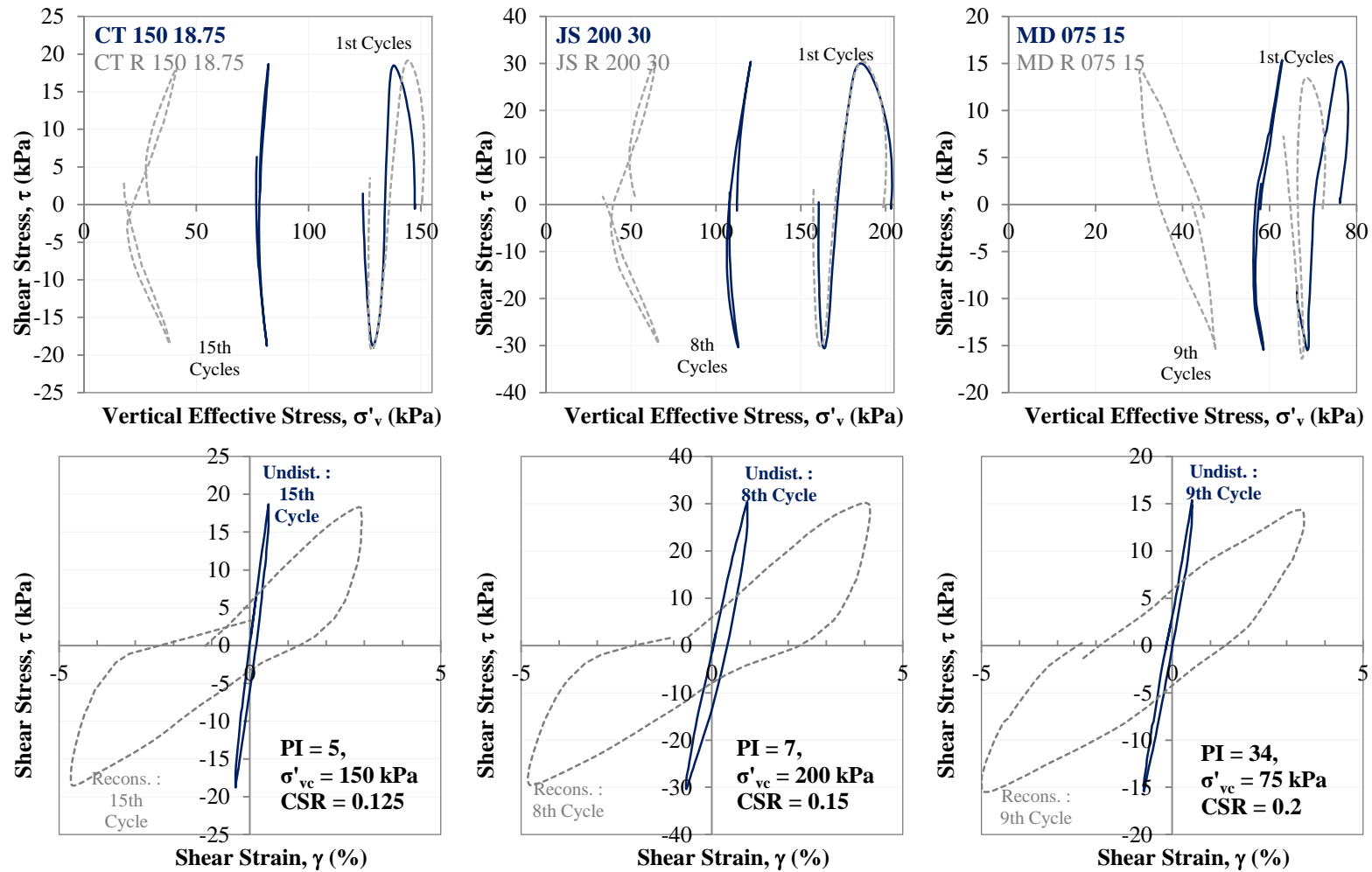
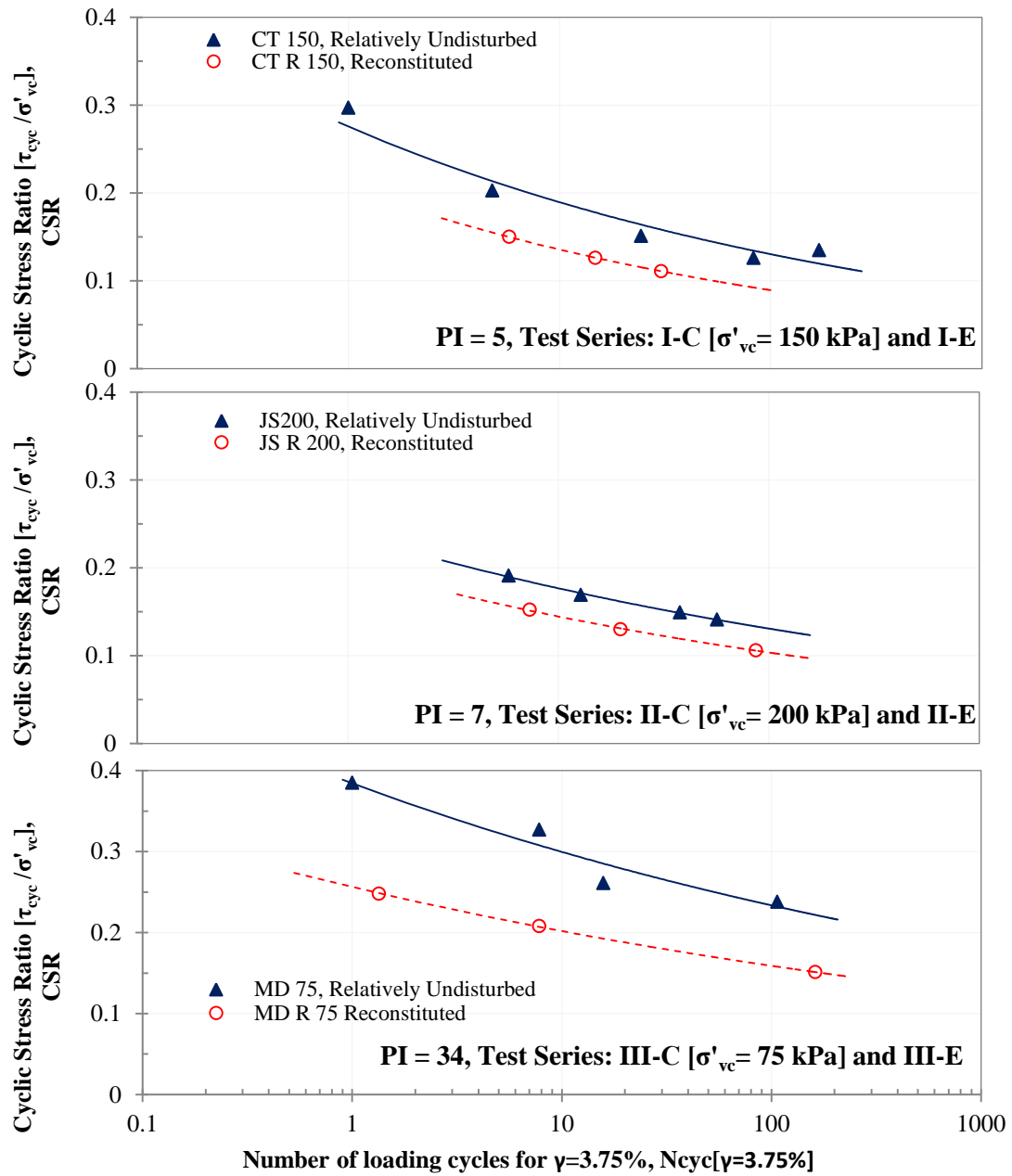


Figure 4.47 Comparison of stress path and shear stress-strain curves of selected loading cycles during constant-volume CDSS test on relatively undisturbed and reconstituted specimen under similar normally consolidated  $\sigma'_{vc}$  and CSR from Site #1 [PI=5], Site #2 [PI=7] and Site #3 [PI=34],



**Figure 4.48 Comparison of Cyclic Stress Ratio versus Number of loading cycles to reach  $\gamma=3.75\%$  curves during constant-volume CDSS test on normally consolidated relatively undisturbed and reconstituted specimen**

(Refer Table 4.1 for test details and parameters of the mentioned test series)

Unlike in the case of monotonic shear loading response discussed in Section 4.1.5, it seems that the influence arising from fabric is predominant in the observed cyclic shear resistance and it has overshadowed the effect due to the change in void ratio of the reconstituted specimens.

The observed relatively weaker response of reconstituted specimens is in accord with the observations of Wijewickreme & Sanin (2008) and Sanin & Wijewickreme (2011) for reconstituted specimens prepared from Fraser River delta silt. The observed reduction of cyclic shear resistance when the specimens are reconstituted are indicated in Figure 4.49 for the material considered in this study along with the data from Sanin (2010) for Fraser River Delta silt and Kitimat clay.

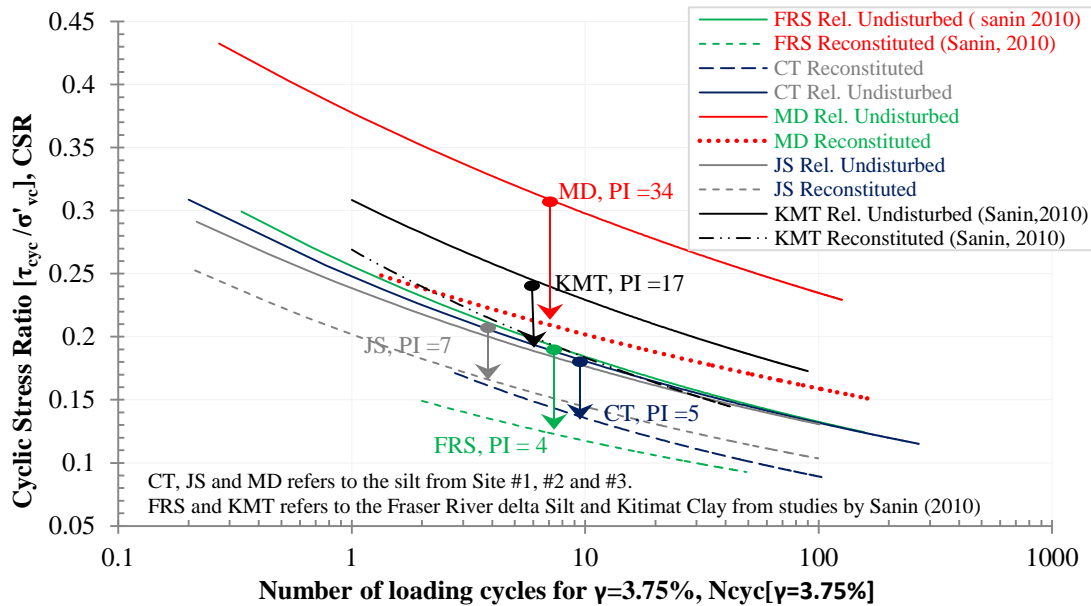


**Figure 4.49 Reduction of cyclic shear resistance of reconstituted specimen with respect to relatively undisturbed specimen of different fine-grained materials**

In an overall sense, the results and observation presented in this section reveals that the reconstituted specimens consistently exhibit higher rates of pore-water pressure development, strain accumulation and shear stiffness degradation under cyclic loading in comparison to those for relatively undisturbed specimens. These observations suggest that the void ratio and confining stress alone are not the only key variables that would control the shear response of fine-grained soils; it appears that the role played by the fabric and microstructure is significant and, it cannot be discounted in predicting the monotonic and cyclic shear loading response of fine-grained materials.

#### **4.4 Post-cyclic Consolidation Response**

In addition to the monotonic and cyclic shear response, it is of interest to evaluate the post cyclic consolidation characteristics of natural silt, as the change of volume in soil masses due to the dissipation of shear induced excess pore water pressure caused by earthquakes often leads to ground settlement and associated failures. As indicated in Table 3.5, each CDSS test conducted in the current test program was followed by a post-cyclic consolidation test phase (refer Section 3.3.4.3). This allowed assessing the post-cyclic consolidation characteristics of both relatively undisturbed and reconstituted specimens prepared from silt originating from all three sites focused in this study. In addition to presenting the experimental observations on post-cyclic consolidation characteristics of silt with different plasticity, the results of this study were used to examine the relationship between post-cyclic volumetric strain ( $\epsilon_{v-pcc}$ ) and maximum cyclic pore-water pressure ratio ( $r_{u-max}$ ) for silts subjected to CDSS loading as proposed by Wijewickreme & Sanin (2010).

Figure 4.50 shows the typical  $\varepsilon_{v-pcc}$  versus consolidation time characteristics of normally consolidated silt (PI=34) from the Site #3. The three curves in Figure 4.50 correspond to the post-cyclic consolidation tests that were conducted on silt specimens which were loaded with different CSRs during CDSS tests and developed different values of  $r_{u-max}$  at the termination of CDSS tests. From Figure 4.50, it can be inferred that higher levels of  $r_{u-max}$  would lead to greater  $\varepsilon_{v-pcc}$ . The  $\varepsilon_{v-pcc}$  versus time curves in Figure 4.51 belong to the post-cyclic consolidation response of relatively undisturbed silts with different plasticity retrieved from the different three test sites employed in this study.

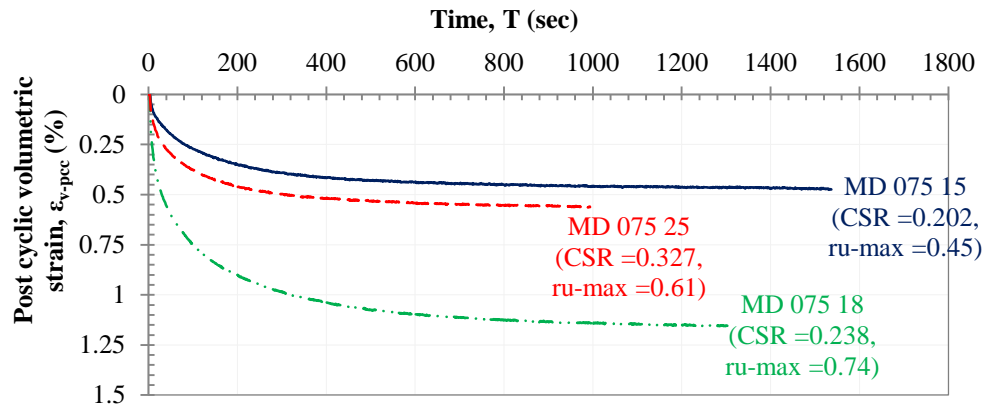


**Figure 4.50 Typical post-cyclic consolidation volumetric strain ( $\varepsilon_{v-pcc}$ ) versus time characteristics of normally consolidated high plastic silt (PI=34) from the Site #3**

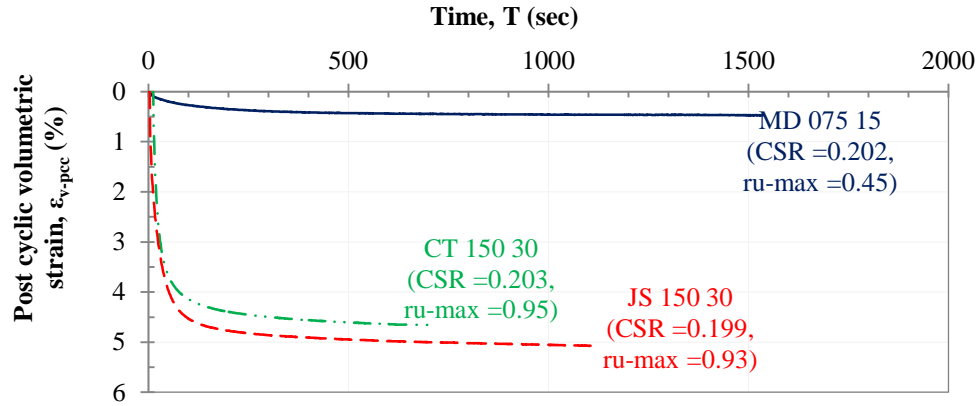


Figure 4.51 Typical post-cyclic consolidation volumetric strain ( $\varepsilon_{v-pcc}$ ) versus time characteristics of normally consolidated silt with different plasticity

Figure 4.51 implies that not only the  $r_{u-max}$ , but also the material type / plasticity influence the post-cyclic response. The  $\varepsilon_{v-pcc}$  and corresponding  $r_{u-max}$  for the relatively undisturbed and reconstituted specimens are plotted in Figure 4.52. The same characteristics for all relatively undisturbed specimens with different plasticity indices that were tested in this study are presented in Figure 4.53.

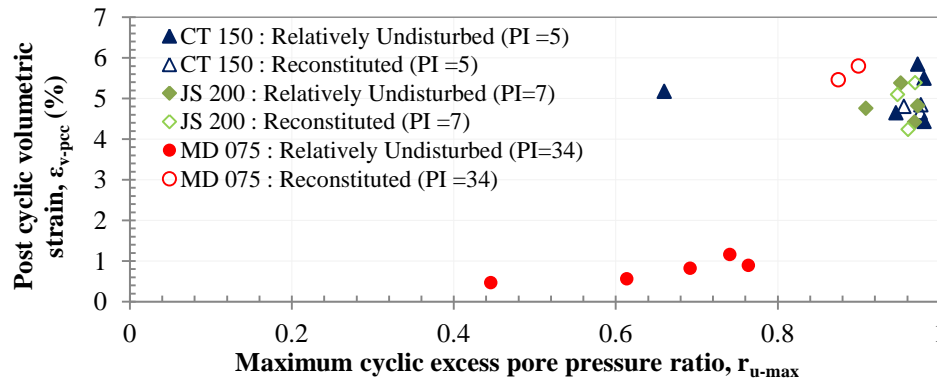
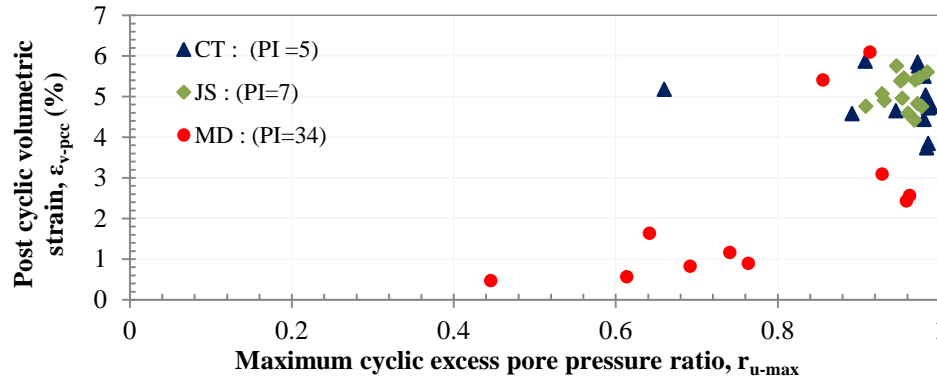
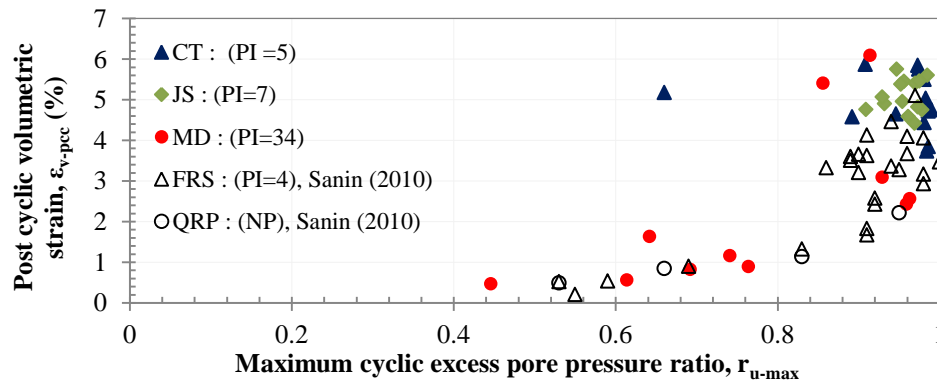


Figure 4.52 Comparison of post-cyclic volumetric strain ( $\varepsilon_{v-pcc}$ ) versus maximum cyclic pore-water pressure ratio ( $r_{u-max}$ ) during CDSS loading of relatively undisturbed and reconstituted silt specimens with different plasticity



**Figure 4.53 Characteristics of post-cyclic volumetric strain ( $\epsilon_{v-pcc}$ ) versus maximum cyclic pore-water pressure ratio ( $r_{u-max}$ ) during CDSS loading of relatively undisturbed silt specimens with different plasticity**

Post cyclic consolidation response data of Fraser river silts and quartz rock powder from Sanin (2010) that were used for the relationship proposed by Wijewickreme & Sanin (2010) is also overlain in Figure 4.54 for comparison. The results from the current testing are in agreement with the trend line suggested by Wijewickreme & Sanin (2010).



**Figure 4.54 Characteristics of post-cyclic volumetric strain ( $\epsilon_{v-pcc}$ ) versus maximum cyclic pore-water pressure ratio ( $r_{u-max}$ ) during CDSS loading from this study over-layed with Fraser River delta Silt (FRS) and Quartz Rock Powder (QRP) data from (Sanin, 2010)**



## Chapter 5: Summary and Conclusions

A systematic laboratory experimental study was performed on saturated natural silt obtained from three different geographic locations within the Fraser River Delta of the Lower Mainland of British Columbia, Canada. The samples were retrieved using thin-walled sharpened-edge tube sampling conducted inside test holes put down using conventional mud-rotary drilling methods. Atterberg limit tests conducted on the silts from the three locations exhibited different plasticity indices, respectively as follows; slightly plastic ( $PI=5$ ), low plastic ( $PI=7$ ), and high plastic ( $PI=34$ ). Series of constant-volume DSS and CDSS tests were performed to investigate the monotonic and cyclic shear response of these natural silts and to enhance the experimental data base of laboratory testing and advance the current understanding of the response of fine-grained natural soil deposits that subjected to seismic loading.

In addition to investigating the fundamental mechanical characteristics of the natural silts, the direct simple shear DSS) test device at UBC was also upgraded as a part of the present thesis work. In particular, a new Data acquisition and Control System (DACS) with a graphical user interface to operate / control the DSS device in a more systematic, efficient and user friendly manner was introduced. The DACS includes: data acquisition, device control, signal conditioning and data processing, computing stress and strain states, and live-graphical-displaying of stress and strain state plots during testing.

This thesis presents the upgrading work undertaken on the UBC-DSS device, experimental procedures used for the testing, and the results of the systematic laboratory experiments conducted on natural silts. Specific impacts arising from parameters such as soil plasticity, coarser-grained fraction, OCR and soil fabric / microstructure on the monotonic and cyclic shear loading response was evaluated. Further post-cyclic consolidation response of these silts was examined to assist understanding post-cyclic settlement characteristics.

This chapter summarizes the key contributions, and presents conclusions and recommendations originating from the research. The Sections 5.1 and Section 5.2 present a summary of the observed monotonic and cyclic shear responses, respectively, for the silts considered during this laboratory experimental study. The post-cyclic consolidation characteristics resulted from this investigation are presented in Section 5.3. Recommendations for future research work on this subject that arose as a result of the present investigation are listed in Section 5.4.

## **5.1 Monotonic Shear Loading Response of Natural Silt**

The normally consolidated, relatively undisturbed specimens indicated generally contractive behavior under constant-volume, monotonic DSS loading. The specimens of silts having relatively low plasticity (i.e.,  $PI = 5$  and  $PI = 7$ ), when normally consolidated to different vertical consolidation stresses and sheared under constant volume conditions, as expected, indicated that the shear stiffness (at a given strain level) and shear strength would increase with increasing initial confining stress level. The observed effective stress paths during these tests for a given material, when normalized with respect to the initial vertical effective stress, were found to fall within a narrow range (i.e., almost coincide); this observed stress-history-normalizability of the

low plastic natural soils are in accord with those observed by Sanin & Wijewickreme (2006) for another low plastic silt obtained from the Fraser River Delta.

In contrast to the above, the results for the relatively high plastic ( $PI = 34$ ) silt revealed that the effective stress paths derived from the experiments are not normalizable with respect to the initial vertical effective confining stress. In essence, the normalized shear strength observed at large strains for high plastic silt specimens were found to reduce with increasing initial vertical effective stress when the specimens are initially consolidated stress levels greater than their pre-consolidation stress. This observation could be explained with respect to the deformation characteristics observed during 1-D consolidation tests of the same relatively high plastic silts; the rate of void ratio reduction with respect to change in vertical effective stress for these silts was found to increase rapidly when the 1-D consolidation stress was increased beyond the estimated pre-consolidation stress. This suggests significant ‘destruction’ in the soil particle structure (or the fabric) of the specimen when the confining stress increases past pre-consolidation stress, and in turn, causing the silt specimen to behave in a comparatively weaker manner during monotonic shear loading.

The over-consolidated specimens initially exhibited dilative shear response with increasing shear strain, which were then followed by contractive response. For the cases of over-consolidated silt specimens, higher shear strengths and stiffness were noted with increasing OCR; this observation is in accord with the generally expected behavior for over-consolidated clay.

The coarse-grained fraction of the slightly plastic ( $PI = 5$ ) natural silt deposit was found to vary with respect to depth. Although the number of samples available for testing was limited, this

was considered an opportunity to examine the effect of coarse-grained fraction on the monotonic shear response for this low plastic material. The results of constant-volume monotonic DSS testing indicated that all specimens exhibit contractive response despite the variation of their coarse-grained fraction. No clear trend on the effects of coarser fraction on the monotonic shear behavior could be found from this limited work; however, the observed differences in monotonic shear loading is attributable to a combination of the effect of the coarser-grained fraction, void ratio, and packing arrangement of the particle.

A comparison of the results from the constant-volume DSS tests on silts with different plastic indices ( $PI = 5, 7, \text{ and } 34$ ) revealed that higher plasticity caused greater peak shear strength.

When shear strength derived from constant-volume DSS tests on relatively undisturbed specimens and reconstituted specimens are compared, reconstituted specimens exhibit slightly higher shear strength than that of relatively undisturbed specimens with  $PI$  5 and 7. Reconstituted specimens in this study were prepared from slurry deposition method, and void ratios of reconstituted specimens were comparatively lesser implying denser than relatively undisturbed specimens. From the observed monotonic shear response in reconstituted specimens, it appears that the effect from change in void ratio has over-shadowed the influence due to the change in fabric and micro-structure.

## **5.2 Cyclic Shear Response of Natural Silt**

All natural silts tested herein under constant-volume cyclic DSS (CDSS) loading indicated gradual accumulation of cyclic shear strain associated with progressive development of excess pore-water pressure, with increasing number of load cycles - despite of their difference in

plasticity. No liquefaction, in the form of  $r_u = 1$  with abrupt loss of shear stiffness or shear modulus was observed in any of the tests. This observed cyclic mobility response suggest that these materials are unlikely to undergo flow failures under earthquake loading. The potential for shear strain and pore-water pressure development with number of loading cycles increased with increasing applied cyclic stress ratio (CSR).

Furthermore, the results obtained for constant-volume CDSS tests performed on low plastic silts ( $PI = 7$ ) revealed that the cyclic resistance ratio (CRR), assessed in the form of number of uniform loading cycles for a specimen to reach single amplitude strain limit of 3.75% for a given CSR, is not significantly influenced by the initial normally consolidated stress levels for the tested initial vertical stress levels between 100 kPa and 200 kPa.

The constant-volume CDSS tests performed on slightly plastic ( $PI = 5$ ) silt with a varying sand fraction from 20% to 35% explicitly indicated that the potential for excess pore water pressure and shear strain development with number of cycles would increase with increasing coarse-grained fraction; this in turn, caused the cyclic shear resistance to decrease with increasing coarse-grained fraction. In other words, it appears that the cyclic shear resistance generally weakens with the increasing coarser fraction (when the coarser fraction is in the range of 20% to 35%) of the natural silt.

The area within hysteresis loops in the stress-strain response curves was noted to increase with increasing plasticity of the tested natural silts – i.e., at a given attained strain level, high plastic silt absorbs a relatively higher amount of energy during cyclic loading compared to that for low

plastic silt. The cyclic resistance ratio (CRR) of the tested silts (i.e.,  $PI = 5, 7$ , and  $34$ ) were found to increase with increasing  $PI$ .

The reconstituted specimens of a given tested silt type consolidated to a given vertical effective stress resulted in a void ratio smaller (i.e., denser) than the void ratio reached by the relatively undisturbed specimens of the same soil when consolidated to the same vertical effective stress. Despite the above relatively denser state of reconstituted specimens in comparison with relatively undisturbed specimens, all reconstituted specimens displayed higher rate in strain accumulation and pore-water pressure development compared to those observed for relatively undisturbed specimens. This resulted in a weaker cyclic shear resistance for the reconstituted specimen in comparison to the relatively undisturbed specimens. This is in contrast to the response observed for the monotonic shear resistance, where reconstituted specimens exhibited slightly higher resistance than that of relatively undisturbed specimens. The observed cyclic shear resistance of reconstituted specimens which had lesser post-consolidation void ratio than the relatively undisturbed specimens suggests that the influence due to the change in fabric and micro-structure has over-shadowed the effect from change in void ratio in reconstituted specimens. These observations suggest that void ratios and corresponding effective confining stresses which have been commonly considered to represent the state of soil are not necessarily sufficient to describe the shear response of soils; it is clear that soil fabric / microstructure and particle arrangement also needs to be concerned in representing the state of soil particularly to understand the response of natural soils.

### 5.3 Post-cyclic Consolidation Response of Natural Silt

The post-cyclic consolidation response of specimens that were initially normally consolidated and subjected to constant-volume CDSS loading were examined. It was noted that the post cyclic consolidation volumetric strain ( $\varepsilon_{v-pcc}$ ) increases with the maximum cyclic pore-water pressure ratio ( $r_{u-max}$ ) developed during constant volume CDSS loading. The values of  $\varepsilon_{v-pcc}$  for both relatively undisturbed and reconstituted silt specimens with different PI and normally consolidated to different consolidation stresses observed from this study seems to be well correlated with the  $r_{u-max}$ , similar to the observed correlation by Wijewickreme & Sanin (2010) for a low plastic silt ( $PI = 4$ ) obtained from another location of the Fraser River delta. The results from this study obtained for silt with different plasticity ( $PI = 5, 7, \text{ and } 34$ ) confirm the validity of the approach presented by Wijewickreme & Sanin (2010) to estimate  $\varepsilon_{v-pcc}$  based  $r_{u-max}$  developed during constant volume CDSS loading.

### 5.4 Recommendations for Future Research

In addition to the above findings and conclusions from the experimental investigations, the work undertaken in thesis so far has also led to identifying a number of additional tasks as given below that could be undertaken in the future to further improve the current understanding of the shear response of natural fine-grained soils:

- The monotonic shear, cyclic shear and post cyclic consolidation responses described in the thesis were merely based on the limited number of constant-volume CDSS conducted on the natural silt retrieved from different three locations in the Fraser River Delta of the Lower Mainland of British Columbia, Canada. Hence, additional tests on natural silt or on fine-

grained material with different index properties should be undertaken for assessing the influence of gradation, coarse-grained fraction, plasticity and soil fabric in order to characterize the general response. The results obtained from the tests under this study were limited to certain range of shear loading conditions and specific initial consolidation stress levels. Testing with enhanced loading range will be useful to estimate or predict the response of soil in higher magnitude of loading.

- The experimental investigation of shear response of fine-grained material is always a challenging task because of the unavoidable constraints and difficulties arising due to the non-homogeneity and variability of natural soils. However, it is still forms an essential part since there is a need to expand the current data base of laboratory tests on fine-grained materials to support effective engineering design works under varying soils conditions, especially those located in areas of seismic activity.

- As noted earlier, the influence of fabric / microstructure is a critical consideration with respect to the understanding of mechanical response of natural silts. As such, further investigations on this subject that has been studied only sparsely would form a very relevant and an essential topic for future research.

- The findings presented in this thesis were based on the test results from constant-volume CDSS tests. As soil response for monotonic and cyclic shearing is governed not only by initial stress state, loading intensity, fabric / microstructure, packing density or void ratio and drainage condition, but also by the loading rate and stress path; therefore, it is important to investigate shear response of fine-grained material through using element test devices such as



triaxial, ring shear, and hollow cylinder tests apparatus that are capable of simulating different shear loading rates and stress paths.

- Obtaining counterpart field test data (e.g., cone penetration tests, CPT) for comparison with the data derived for shear behavior from element tests on relatively undisturbed fine-grained soils would pave the way to developing correlations which would be helpful to assess the shear response of fine-grained material directly from the in-situ tests.

## References

- Andersen, K. H. (2009). Bearing capacity under cyclic loading — offshore, along the coast, and on land. The 21st Bjerrum Lecture presented in Oslo, 23 November 2007. *Canadian Geotechnical Journal*, 46(5), 513–535. doi:10.1139/T09-003
- Andersen, K. H., Pool, J. H., Brown, S. F., & Rosenbrand, W. F. (1980). Cyclic and Static Laboratory Tests on Drammen Clay. *Journal of the Geotechnical Engineering Division, ASCE*, 106(GT5), 499–529.
- Andrews, D. C. A., & Martin, G. R. (2000). Criteria for liquefaction of silty soils. In *Proc., 12th World Conf. on Earthquake Engineering* (pp. 1–8). Auckland, New Zealand. Retrieved from <http://www.iitk.ac.in/nicee/wcee/article/0312.pdf> [accessed January 14, 2014]
- Armstrong, J. E., & Hicock, S. R. (1979). Surficial Geology, Vancouver, British Columbia. Geological Survey of Canada, “A” Series Map 1486A. Retrieved from [http://ftp2.cits.rncan.gc.ca/pub/geott/ess\\_pubs/108/108876/gscmap-a\\_1486a\\_e\\_1979\\_mn01.pdf](http://ftp2.cits.rncan.gc.ca/pub/geott/ess_pubs/108/108876/gscmap-a_1486a_e_1979_mn01.pdf) [accessed April 25, 2014]
- Armstrong, J. E., & Hicock, S. R. (1980). Surficial Geology, New Westminster, West of Sixth Meridian, British Columbia. Geological Survey of Canada, “A” Series Map 1484A. Retrieved from [http://ftp2.cits.rncan.gc.ca/pub/geott/ess\\_pubs/108/108874/gscmap-a\\_1484a\\_e\\_1980\\_mn01.pdf](http://ftp2.cits.rncan.gc.ca/pub/geott/ess_pubs/108/108874/gscmap-a_1484a_e_1980_mn01.pdf) [accessed April 25, 2014]
- ASTM. D4452 - 06, Standard Practice for X-Ray Radiography of Soil Samples (2006). ASTM International, West Conshohocken, PA. doi:10.1520/D4452-06.2
- ASTM. D422 - 63, Standard Test Method for Particle-Size Analysis of Soils (2007). ASTM International, West Conshohocken, PA. doi:10.1520/D0422-63R07.2
- ASTM. D2488 - 09a, Standard Practice for Description and Identification of Soils (Visual-Manual Procedure) (2009). ASTM International, West Conshohocken, PA. doi:10.1520/D2488-09A.
- ASTM. D4310 - 10, Standard Test Methods for Liquid Limit , Plastic Limit , and Plasticity Index of Soils (2010). ASTM International, West Conshohocken, PA. doi:10.1520/D4318-10.
- ASTM. D854 - 10, Standard Test Methods for Specific Gravity of Soil Solids by Water Pycnometer (2010). ASTM International, West Conshohocken, PA. doi:10.1520/D0854-10.

- ASTM. D2487 - 11, Standard Practice for Classification of Soils for Engineering Purposes (Unified Soil Classification System) (2011). ASTM International, West Conshohocken, PA. doi:10.1520/D2487-11.
- Azzouz, A. S., Malek, A. M., & Baligh, M. M. (1989). Cyclic Behaviour of Clays in Underdrained Simple Shear. *Journal of Geotechnical Engineering*, 115(5), 637–657.
- Becker, D., Crooks, J., Been, K., & Jefferies, M.G. (1987). Work as a criterion for determining in situ and yield stresses in clays. *Canadian Geotechnical Journal*, 24 (4), 549-564. Retrieved from <http://www.nrcresearchpress.com/doi/pdf/10.1139/t87-070> [accessed November 14, 2013]
- Bjerrum, L., & Landva, A. (1966). Direct simple-shear tests on a Norwegian quick clay. *Géotechnique*, 16(21), 1–20. doi:10.1680/geot.1966.16.1.1
- Boulanger, R. W., Chan, C. K., Seed, H. B., Seed, R. B., & Sousa, J. B. (1993). A low-compliance bi-directional cyclic simple shear apparatus. *Geotechnical Testing Journal*, 16(1), 36–45.
- Boulanger, R. W., & Idriss, I. M. (2004). *Evaluating the potential for liquefaction or cyclic failure of silts and clays*. Center for Geotechnical Modelling, Department of Civil & Environmental Engineering, University of California, Davis. Retrieved from <http://citeseerx.ist.psu.edu/viewdoc/download?doi=10.1.1.132.3827&rep=rep1&type=pdf> [accessed January 21, 2013]
- Boulanger, R. W., & Idriss, I. M. (2006). Liquefaction susceptibility criteria for silts and clays. *Journal of Geotechnical and Geoenvironmental Engineering*, 132(11), 1413–1426. Retrieved from [http://ascelibrary.org/doi/pdf/10.1061/\(ASCE\)1090-0241\(2006\)132:11\(1413\)](http://ascelibrary.org/doi/pdf/10.1061/(ASCE)1090-0241(2006)132:11(1413)) [accessed November 14, 2013]
- Boulanger, R. W., & Idriss, I. M. (2007). Evaluation of cyclic softening in silts and clays. *Journal of Geotechnical and Geoenvironmental Engineering*, 133(6), 641–652. Retrieved from [http://ascelibrary.org/doi/abs/10.1061/\(ASCE\)1090-0241\(2007\)133:6\(641\)](http://ascelibrary.org/doi/abs/10.1061/(ASCE)1090-0241(2007)133:6(641)) [accessed February 28, 2014]
- Boulanger, R. W., Meyers, M. W., Mejia, L. H., & Idriss, I. M. (1998). Behavior of a fine-grained soil during the Loma Prieta earthquake. *Canadian Geotechnical Journal*, 35(1), 146–158. Retrieved from <http://www.nrcresearchpress.com/doi/abs/10.1139/t97-078> [accessed April 15, 2014]
- Boulanger, R. W., & Seed, R. B. (1995). Liquefaction of sand under bidirectional monotonic and cyclic loading. *Journal of Geotechnical Engineering*, 121(12), 870–878. Retrieved from [http://ascelibrary.org/doi/abs/10.1061/\(ASCE\)0733-9410\(1995\)121:12\(870\)](http://ascelibrary.org/doi/abs/10.1061/(ASCE)0733-9410(1995)121:12(870)) [accessed February 27, 2014]

- Bray, J. D., & Sancio, R. B. (2006). Assessment of the liquefaction susceptibility of fine-grained soils. *Journal of Geotechnical and Geoenvironmental Engineering*, 132(9), 1165–1177. Retrieved from [http://ascelibrary.org/doi/abs/10.1061/\(ASCE\)1090-0241\(2006\)132:9\(1165\)](http://ascelibrary.org/doi/abs/10.1061/(ASCE)1090-0241(2006)132:9(1165)) [accessed November 14, 2013]
- Bray, J. D., Sancio, R. B., Durgunoglu, T., Onalp, A., Youd, T. L., Stewart, J. P., Seed, R.B., Cetin, O.K., Bol, E., Baturay, M.B., Christian, C., & Karadayilar, T. (2004). Subsurface Characterization at Ground Failure Sites in Adapazari, Turkey. *Journal of Geotechnical and Geoenvironmental Engineering*, 130(7), 673–685.
- Budhu, M. (1984). Nonuniformities imposed by simple shear apparatus. *Canadian Geotechnical Journal*, 21(1), 125–137. Retrieved from <http://www.nrcresearchpress.com/doi/abs/10.1139/t84-010> [accessed May 15, 2014]
- Budhu, M. (1985). Lateral stresses observed in two simple shear apparatus. *Journal of Geotechnical Engineering*, 111(6), 698–711. Retrieved from [http://ascelibrary.org/doi/abs/10.1061/\(ASCE\)0733-9410\(1985\)111:6\(698\)](http://ascelibrary.org/doi/abs/10.1061/(ASCE)0733-9410(1985)111:6(698)) [accessed May 15, 2014]
- Burland, J. B. (1990). On the compressibility and shear strength of natural clays. *Géotechnique*, 40(3), 329–378.
- Callisto, L., & Calabresi, G. (1998). Mechanical behaviour of a natural soft clay. *Géotechnique*, 48(4), 495–513.
- Casagrande, A. (1936). The determination of the preconsolidation load and its practical significance. In *Proceedings of the First International Conference on Soil Mechanics and Foundation Engineering, Cambridge, Mass., 22–26 June 1936*. (pp. 60–64). Harvard Printing Office, Cambridge, Mass. Vol. 3.
- Castro, G. (1969). *Liquefaction of sands*. PhD. Thesis, Harvard University, Cambridge, Mass.
- Castro, G. (1975). Liquefaction and Cyclic Mobility of Saturated Sands. *Journal of the Geotechnical Engineering Division, ASCE*, 101(GT6), 551–569.
- Chern, J. C. (1985). *Undrained response of saturated sands with emphasis on liquefaction and cyclic mobility*. The University of British Columbia. Retrieved from [https://circle.ubc.ca/bitstream/id/85493/UBC\\_1985\\_A1\\_C43.pdf](https://circle.ubc.ca/bitstream/id/85493/UBC_1985_A1_C43.pdf) [accessed March 12, 2014]
- Chu, D. B., Stewart, J. P., Lee, S., Tsai, J. S., Lin, P. S., Chu, B. L., Seed, R.B., Hsu, S.C., Yu, M.S., & Wang, M. C. H. (2004). Documentation of soil conditions at liquefaction and non-liquefaction sites from 1999 Chi–Chi (Taiwan) earthquake. *Soil Dynamics and Earthquake Engineering*, 24(9-10), 647–657. doi:10.1016/j.soildyn.2004.06.005

- Clague, J. J., Bobrowsky, P. T., Guilbault, J. P., Linden, R. H., Mathewes, R.W. Naesgaard, E., Shilts, W. W., & Sy, A. (1996). Paleoseismology and Seismic Hazards, Southwestern British Columbia. *Geological Survey of Canada, Bulletin 494*; p.1-88.
- Crawford, C. (1965). The resistance of soil structure to consolidation. *Canadian Geotechnical Journal*, 2(2), 90–97. Retrieved from <http://www.nrcresearchpress.com/doi/abs/10.1139/t65-010> [accessed November 24 , 2014]
- Dabeet, A., Wijewickreme, D., & Byrne, P. M. (2012). Simulation of cyclic direct simple shear loading response of soils using discrete element modeling. In *15th World Conference on Earthquakes Engineering*. Lisboa.
- Davis, A. P., Poulos, S. J., & Castro, G. (1988). Strengths Backfigured from Liquefaction Case Histories. In *Second International Conference on Case Histories in Geotechnical Engineering* (pp. 1693–1701). St. Louis, Missouri.
- De Alba, P., Seed, H. B., & Chan, C. K. (1976). Sand Liquefaction in Large Scale Simple Shear Tests. *Journal of the Geotechnical Engineering Division, ASCE*, 102(GT9), 909–927.
- DeGroot, D. J., Germaine, J. T., & Gedney, R. (1991). An automated electropneumatic control system for direct simple shear testing. *Geotechnical Testing Journal*, 14(4), 339–348.
- Donahue, J. L., Bray, J. D., & Riemer, M. F. (2007). *The liquefaction susceptibility, resistance, and response of silty and clayey soils*. Retrieved from <http://earthquake.usgs.gov/research/external/reports/05HQGR0009.pdf> [accessed February 27, 2014]
- Dyvik, R., Berre, T., Lacasse, S., & Raadim, B. (1987). Comparison of truly undrained and constant volume direct simple shear tests. *Géotechnique*, 37(1), 3–10.
- Finn, W. D. L. (1985). Aspects of Constant Volume Cyclic Simple Shear. In V. Khosla (Ed.), *Advances in the Art of Testing Soils Under Cyclic Conditions, Sponsored by the Geotechnical Engineering Division New York in conjunction with the ASCE Convention* (pp. 74–98). Detroit, Michigan.
- Finn, W. D. L., Bransby, P. L., & Pickering, D. J. (1970). Effect of Strain History on Liquefaction of Sand. *Journal of the Soil Mechanics and Foundations Division, ASCE*, 96(SM6), 1917–1934.
- Finn, W. D. L., Ledbetter, R. H., & Wu, G. (1994). Liquefaction in silty soils: Design and analysis. Ground failures under seismic conditions. *Geotechnical Special Publication, ASCE*, 44, 51–76.

- Finn, W. D. L., Pickering, D. J., & Bransby, P. L. (1971). Sand Liquefaction in Triaxial and Simple Shear Test. *Journal of the Soil Mechanics and Foundations Division, ASCE*, 97(SM4), 639–659.
- Finn, W. D. L., & Vaid, Y. P. (1977). Liquefaction potential from drained constant volume cyclic simple shear tests. In *Proceedings of the 6th World Conference on Earthquake Engineering* (pp. 2157–2162). New Delhi. Retrieved from [http://www.iitk.ac.in/nicee/wcee/article/6\\_vol3\\_2157.pdf](http://www.iitk.ac.in/nicee/wcee/article/6_vol3_2157.pdf) [accessed May 13, 2014]
- Fleming, L. N., & Duncan, J. M. (1990). Stress-deformation characteristics of Alaskan silt. *Journal of Geotechnical Engineering*, 116(3), 377–393. Retrieved from [http://ascelibrary.org/doi/abs/10.1061/\(ASCE\)0733-9410\(1990\)116:3\(377\)](http://ascelibrary.org/doi/abs/10.1061/(ASCE)0733-9410(1990)116:3(377)) [accessed July 30, 2014]
- Geremew, A. M., & Yanful, E. K. (2011). Laboratory Investigation of the Resistance of Tailings and Natural Sediments to Cyclic Loading. *Geotechnical and Geological Engineering*, 30(2), 431–447. doi:10.1007/s10706-011-9478-x
- Gordon, B. B., Dayton, D. J., & Sadigh, K. (1974). Seismic Stability of Upper San Leandro Dam. *Journal of the Geotechnical Engineering Division, ASCE*, 100(GT5), 523–546.
- Graham, J., Crooks, J. H. A., & Bell, A. L. (1983). Time effects on stress-strain behaviour of soft natural clay. *Géotechnique*, 33(3), 327–340.
- Guo, T., & Prakash, S. (1999). Liquefaction of Silts and Silty-Clay Mixtures. *Journal of Geotechnical and Geoenvironmental Engineering*, 5(8), 706–710. Retrieved from [http://dx.doi.org/10.1061/\(ASCE\)1090-0241\(1999\)125:8\(706\)](http://dx.doi.org/10.1061/(ASCE)1090-0241(1999)125:8(706)) [accessed November 14, 2013]
- Hanzawa, H., Nutt, N., Lunne, T., Tang, Y. X., & Long, M. (2007). A comparative study between the NGI direct simple shear apparatus and the Mikasa direct shear apparatus. *Soils and Foundations, Japanese Society of Soil Mechanics and Foundation Engineering*, 47(1), 47–58. Retrieved from [https://www.jstage.jst.go.jp/article/sandf/47/1/47\\_1\\_47/\\_article](https://www.jstage.jst.go.jp/article/sandf/47/1/47_1_47/_article) [accessed May 12, 2014]
- Hazen, A. (1920). Hydraulic Filled Dams. *Transaction of the American Society of Civil Engineers*, LXXXIII(1), 1713–1745.
- Hight, D. W., & Leroueil, S. (2003). Characterisation of soils for engineering purposes. In T. S. Tan, K. K. Phoon, D. W. Hight, & S. Leroueil (Eds.), *Characterisation and Engineering Properties of Natural Soils: Proceedings of the International Workshop, Singapore, 2-4 December 2002* (pp. 255–360). Lisse ; Exton, PA : Balkema.

- Høeg, K., Dyvik, R., & Sandbækken, G. (2000). Strength of undisturbed versus reconstituted silt and silty sand specimens. *Journal of Geotechnical and Geoenvironmental Engineering*, 126(7), 606–617. Retrieved from [http://ascelibrary.org/doi/abs/10.1061/\(ASCE\)1090-0241\(2000\)126:7\(606\)](http://ascelibrary.org/doi/abs/10.1061/(ASCE)1090-0241(2000)126:7(606)) [accessed February 28, 2014]
- Hyde, A. F., Higuchi, T., & Yasuhara, K. (2006). Liquefaction, cyclic mobility, and failure of silt. *Journal of Geotechnical and Geoenvironmental Engineering*, 132(6), 716–735. Retrieved from [http://ascelibrary.org/doi/abs/10.1061/\(ASCE\)1090-0241\(2006\)132:6\(716\)](http://ascelibrary.org/doi/abs/10.1061/(ASCE)1090-0241(2006)132:6(716)) [accessed February 16, 2014]
- Idriss, I. M., & Boulanger, R. W. (2006). Semi-empirical procedures for evaluating liquefaction potential during earthquakes. *Soil Dynamics and Earthquake Engineering*, 26(2-4), 115–130. doi:10.1016/j.soildyn.2004.11.023
- Idriss, I. M., & Boulanger, R. W. (2008). *Soil liquefaction during earthquakes*. Earthquake Engineers Research Institute.
- Ishibashi, I., & Sherif, M. A. (1974). Soil Liquefaction by Torisional Simple Shear Device. *Journal of the Geotechnical Engineering Division, ASCE*, 100(GT8), 871–888.
- Ishihara, K. (1984). Post-earthquake failure of a tailings dam due to liquefaction of the pond deposit. In *Proc. Int. Conf. on Case Histories in Geotechnical Engrg.* (Vol. 3, pp. 1129–1143). St. Louis, Missouri.
- Ishihara, K. (1993). Liquefaction and flow failure during earthquakes. *Géotechnique*, 43(3), 351–415.
- Ishihara, K. (1996). *Soil Behaviour in Earthquake Geotechnics*. Oxford University Press Inc., New York.
- Ishihara, K., & Nagase, H. (1988). Multi-directional irregular loading tests on sand. *Soil Dynamics and Earthquake Engineering*, 7(4), 201–212. doi:10.1016/S0267-7261(88)80004-6
- Ishihara, K., Troncoso, J., Kawase, Y., & Takahashi, Y. (1980). Cyclic strength characteristics of tailings materials. *Soils and Foundations, Japanese Society of Soil Mechanics and Foundation Engineering*, 20(4), 127–142. Retrieved from <http://ci.nii.ac.jp/naid/110003959318/> [accessed May 22, 2014]
- Ishihara, K., & Yamazaki, F. (1980). Cyclic simple shear tests on saturated sand in multi-directional loading. *Soils and Foundations, Japanese Society of Soil Mechanics and Foundation Engineering*, 20(1), 45–59.

- Ishihara, K., & Yasuda, S. (1972). Sand liquefaction due to irregular excitation. *Soils and Foundations, Japanese Society of Soil Mechanics and Foundation Engineering*, 12(4), 65–77.
- Iwasaki, T. (1986). Soil liquefaction studies in Japan: state-of-the-art. *Soil Dynamics and Earthquake Engineering*, 5(1), 2–68. Retrieved from <http://www.sciencedirect.com/science/article/pii/0267726186900242> [accessed February 16, 2014]
- Iwasaki, T., Arakawa, T., & Tokida, K. I. (1984). Simplified procedures for assessing soil liquefaction during earthquakes. *International Journal of Soil Dynamics and Earthquake Engineering*, 3(1), 49–58. Retrieved from <http://www.sciencedirect.com/science/article/pii/0261727784900275> [accessed February 21, 2014]
- Janbu, N. (1969). The resistance concept applied to deformation of soils. In *Proceedings of the 7th International Conference on Soil Mechanics and Foundation Engineering, Mexico City, 25–29 August 1969*. (pp. 191–196). A.A. Balkema, Rotterdam, the Netherlands. Vol. 1.
- Jung, Y. H., Finno, R. J., & Cho, W. (2012). Stress–strain responses of reconstituted and natural compressible Chicago glacial clay. *Engineering Geology*, 129, 9–19. doi:10.1016/j.enggeo.2012.01.003
- Kim, H., Daliri, F., Simms, P., & Sivathayalan, S. (2011). The influence of desiccation and overconsolidation on monotonic and cyclic shear response of thickened gold tailings. In *2011 Pan-Am CGS Geotechnical Conference*. Toronto. Retrieved from <http://geoserver.ing.puc.cl/info/conferences/PanAm2011/panam2011/pdfs/GEO11Paper765.pdf> [accessed May 22, 2014]
- Kishida, H. (1969). Characteristics of Liquefied Sand During Mino-Owari, Tohankai and Fukui Earthquakes. *Soils and Foundations, Japanese Society of Soil Mechanics and Foundation Engineering*, 9(1).
- Kishida, H. (1970). Characteristics of liquefaction of level sandy ground during the Tokachioki earthquake. *Soils and Foundations, Japanese Society of Soil Mechanics and Foundation Engineering*, 10(2). Retrieved from <http://ci.nii.ac.jp/naid/110003899029/> [accessed April 15, 2014]
- Koester, J. P. (1992). The Influence of Test Procedure on Correlation of Atterberg Limits with Liquefaction in Fine-Grained Soils. *ASTM Geotechnical Testing Journal*, 15(4), 352–361.
- Koutsoftas, D. C. (1978). Effect of cyclic loads on undrained strength of two marine clays. *Journal of the Geotechnical Engineering Division, ASCE*, 104(GT5), 609–620.



- Kuerbis, R. H. (1989). *The effect of gradation and fine content on the undrained loading response of sand*. M.ASc. Thesis, The University of British Columbia. Retrieved from <https://circle.ubc.ca/handle/2429/27895> [accessed May 9, 2014]
- Ladd, C. C. (1964). *Stress-strain behavior of saturated clay and basic strength principles : Research in Earth Physics -Research Report R64-17, Massachusetts Institute of Technology*.
- Ladd, C. C., & Degroot, D. J. (2003). Recommended Practice for Soft Ground Site Characterization : Arthur Casagrande Lecture Práctica. In *12th Panamerican Conference on Soil Mechanics and Geotechnical Engineering* (pp. 3–57). Boston, MA.
- Lee, K. L., & Albaisa, A. (1974). Earthquake Induced Settlements in Saturated Sands. *Journal of the Geotechnical Engineering Division, ASCE*, 100(GT4), 387–406.
- Lee, K. L., Makdisi, F. I., Idriss, I. M., & Seed, H. B. (1975). Properties of soil in the San Fernando hydraulic fill dams. *Journal of the Geotechnical Engineering Division, ASCE*, 101(GT8), 801–821.
- Lefebvre, G., & LeBoeuf, D. (1987). Rate Effects And Cyclic Loading of Sensitive Clays. *Journal of Geotechnical Engineering*, 113(5), 476–489. Retrieved from <http://ascelibrary.org/doi/abs/10.1061/%28ASCE%290733-9410%281987%29113:5%28476%29> [accessed November 24, 2013]
- Lefebvre, G., & Pfendler, P. (1996). Strain rate and preshear effects in cyclic resistance of soft clay. *Journal of Geotechnical Engineering*, 122(1), 21–26. Retrieved from [http://ascelibrary.org/doi/abs/10.1061/\(ASCE\)0733-9410\(1996\)122:1\(21\)](http://ascelibrary.org/doi/abs/10.1061/(ASCE)0733-9410(1996)122:1(21)) [accessed February 27, 2014]
- Leroueil, S., & Hight, D. W. (2003). Behaviour and properties of natural soils and soft rocks. In T. S. Tan, K. K. Phoon, D. W. Hight, & S. Leroueil (Eds.), *Characterisation and Engineering Properties of Natural Soils: Proceedings of the International Workshop, Singapore, 2-4 December 2002* (pp. 29–255). Lisse ; Exton, PA : Balkema.
- Leroueil, S., Tavenas, F., Brucy, F., La Rochelle, P., & Roy, M. (1979). Behaviour of destructured natural clays. *Journal of Geotechnical Engineering*, 105(6), 759–778.
- Lucks, A. S., Christian, J. T., Brandow, G. E., & Høeg, K. (1972). Stress condition in NGI simple shear test. *Journal of the Soil Mechanics and Foundations Division, ASCE*, 98(SM1), 155–160.
- Lunne, T., Berre, T., Andersen, K. H., Strandvik, S., & Sjursen, M. (2006). Effects of sample disturbance and consolidation procedures on measured shear strength of soft marine

- Norwegian clays. *Canadian Geotechnical Journal*, 43(0806), 726–750. doi:10.1139/T06-040
- Luternauer, J. L., Clague, J. J., Hunter, J. A. M., Pullan, S. E., Roberts, M. C., Woeller, D. J., Kostaschuk, R.A., Moslow, T.F., Monahan, P.A., & Hart, B. S. (1993). *The Fraser River Delta, British Columbia: architecture, geological dynamics and human impact, Canada. Reprinted from Deltas of the World. Proceedings of the Eighth symposium on Coastal and Ocean Management, New Orleans, Louisiana* (pp. 99–103).
- Martin, G. R., Finn, W. D. L., & Seed, H. B. (1975). Fundamentals of Liquefaction under Cyclic Loading. *Journal of the Geotechnical Engineering Division, ASCE*, 101(GT5), 423–438.
- Martin, G. R., Finn, W. D. L., & Seed, H. B. (1978). Effects of System Compliance on Liquefaction Tests. *Journal of the Geotechnical Engineering Division, ASCE*, 104(GT4), 463–479.
- Martin, J. R., Olgun, C. G., Mitchell, J. K., & Durgunoglu, H. T. (2004). High-Modulus Columns for Liquefaction Mitigation. *Journal of Geotechnical and Geoenvironmental Engineering*, 130(6), 561–571.
- McCarron, W. O., Lawrence, J. C., Werner, R. J., Germaine, J. T., & Cauble, D. F. (1995). Cyclic direct simple shear testing of a Beaufort Sea clay. *Canadian Geotechnical Journal*, 32(4), 584–600. doi:10.1139/t95-061
- Monahan, P. A., Byrne, P. M., Watts, B. D., & Naesgaard, E. (2000). Engineering Geology and Natural Hazards of the Fraser River Delta. Guidebook for geological field trips in Southwestern British Columbia and Northern Washington. In *Annual Meeting of the Cordilleran Section of the Geological Society of America* (pp. 27–47). Vancouver.
- Monahan, P. A., Luternauer, J. L., & Barrie, J. V. (1997). The topset and upper foreset of the modern Fraser River Delta, British Columbia, Canada. In *Wood J, Martindale W, compiled. Core conference, CSPG-SEPM joint convention, Canadian Society of Petroleum Geologists* (pp. 491–517).
- Mullins, J. P., Seed, H. B., Chan, C. K., Mitchell, J. K., & Arulanandan, K. (1977). Effects of Sample Preparation on Sand Liquefaction. *Journal of the Geotechnical Engineering Division, ASCE*, 102(GT3), 91–108.
- Negussey, D., Wijewickreme, D., & Vaid, Y. P. (1986). *Constant-volume Friction Angle of Granular Materials, Soil Mechanics Series No.94, Department of Civil Engineering, The University of British Columbia, BC.*
- NRC. (1985). *Liquefaction of Soils During Earthquakes*. US National Research Council Report, CETS-EE-001, National Academy Press, Washington, D.C.

- Oda, M. (1972). The Mechanism of Fabric Changes During Compressional Deformation of Sand. *Soils and Foundations, Japanese Society of Soil Mechanics and Foundation Engineering*, 12(2).
- Oda, M., Koishikawa, I., & Higuchi, T. (1978). Experimental Study of Anisotropic Shear Strength of Sand by Plain Strain Test. *Soils and Foundations, Japanese Society of Soil Mechanics and Foundation Engineering*, 18(1), 25–38.
- Oda, M., & Konishi, J. (1974). Rotation of principal stresses in granular material during simple shear. *Soils and Foundations, Japanese Society of Soil Mechanics and Foundation Engineering*, 14(4), 39–53.
- Ohsaki, Y. (1966). Niigata earthquakes, 1964 building damage and soil condition. *Soils and Foundations, Japanese Society of Soil Mechanics and Foundation Engineering*, VI(2). Retrieved from <http://ci.nii.ac.jp/naid/110003899118/> [accessed February 23, 2014]
- Peacock, W. H., & Seed, H. B. (1968). Sand Liquefaction under Cyclic Loading Simple Shear Conditions. *Journal of the Soil Mechanics and Foundations Division, ASCE*, 94(SM3), 689–708.
- Porcino, D., Marciano, V., & Granata, R. (2012). Liquefaction and re-liquefaction of a silicate grouted dans due to repeated earthquakes. In *Incontro Annuale dei Ricercatori di Geotecnica* (pp. 2–7). Padova, Italy.
- Poulos, S. J., Castro, G., & France, J. W. (1985). Liquefaction Evaluation Procedure. *Journal of Geotechnical Engineering*, 111(6), 772–792. doi:10.1061/(ASCE)0733-9410(1985)111:6(772)
- Prakash, S., & Sandoval, J. A. (1992). Liquefaction of low plasticity silts. *Soil Dynamics and Earthquake Engineering*, 11(7), 373–379. doi:10.1016/0267-7261(92)90001-T
- Romero, S. (1995). *The behavior of silt as clay content is increased*. MS Thesis, University of California, Davis.
- Roscoe, K. (1953). An apparatus for the application of simple shear to soil samples. In *3rd International Conference on Soil Mechanics* (pp. 186–191). Zurich.
- Sanin, M. V. (2005). *Cyclic Shear Loading Response of Fraser River Delta Silt*. M.ASc. Thesis, The University of British Columbia. Retrieved from [circle.ubc.ca/handle/2429/16928](http://circle.ubc.ca/handle/2429/16928) [accessed November 19, 2012]
- Sanin, M. V. (2010). *Cyclic Shear Loading Response of Fraser River Delta Silt*. PhD Thesis, The University of British Columbia. Retrieved from <http://elk.library.ubc.ca/handle/2429/30064> [accessed November 19, 2012]

- Sanin, M. V., & Wijewickreme, D. (2006a). Cyclic shear response of channel-fill Fraser River Delta silt. *Soil Dynamics and Earthquake Engineering*, 26(9), 854–869. doi:10.1016/j.soildyn.2005.12.006 [accessed November 14, 2013]
- Sanin, M. V., & Wijewickreme, D. (2006b). Influence of Initial Confining Stress on the Mechanical Response of Natural Fraser River Delta Silt. In *59th Canadian Geotechnical Conference* (pp. 252–257). Vancouver, British Columbia. [accessed November 10, 2014]
- Sanin, M. V., & Wijewickreme, D. (2011). Cyclic shear response of undisturbed and reconstituted Fraser River Silt. In *14th Pan-American Conference on Soil Mechanics and Geotechnical Engineering 64th Canadian Geotechnical Conference*. Toronto, Ontario.
- Santagata, M. C. (1999). *Factors affecting the initial stiffness and stiffness degradation of cohesive soils*. Ph.D. Thesis, MIT, Massachusetts. Retrieved from <http://dspace.mit.edu/handle/1721.1/9663> [accessed August 7, 2014]
- Santagata, M. C., & Germaine, J. T. (2002). Sampling disturbance effects in normally consolidated clays. *Journal of Geotechnical and Geoenvironmental Engineering*, 128(12), 997–1006. Retrieved from [http://ascelibrary.org/doi/abs/10.1061/\(ASCE\)1090-0241\(2002\)128:12\(997\)](http://ascelibrary.org/doi/abs/10.1061/(ASCE)1090-0241(2002)128:12(997)) [accessed July 28, 2014]
- Schofield, A., & Wroth, P. (1968). *Critical state soil mechanics*. McGraw-Hill Inc., US.
- Seed, H. B. (1976). Evaluation of soil liquefaction effects on ground during earthquakes. In *Liquefaction problems in geotechnical engineering, ASCE Preprint 2752, presented at the ASCE National Convention*, (pp. 1–104). Philadelphia, Pennsylvania: ASCE, New York.
- Seed, H. B., & Idriss, I. M. (1971). Simplified Procedure for Evaluating Soil Liquefaction Potential. *Journal of the Soil Mechanics and Foundations Division, ASCE*, 97(SM9), 1249–1273.
- Seed, H. B., & Idriss, I. M. (1982). *Ground motions and soil liquefaction during earthquakes*. Earthquake Engineering Research Institute (Monograph).
- Seed, H. B., & Lee, K. L. (1966). Liquefaction of saturated sands during cyclic loading. *Journal of the Soil Mechanics and Foundations Division, ASCE*, 92(SM6), 105–134.
- Seed, H. B., & Lee, K. L. (1967a). Cyclic Stress Conditions Causing Liquefaction of Sand. *Journal of the Soil Mechanics and Foundations Division, ASCE*, 93(SM1), 47–70.
- Seed, H. B., & Lee, K. L. (1967b). Dynamic Strength of Anisotropically Consolidated Sand. *Journal of the Soil Mechanics and Foundations Division, ASCE*, 93(SM5), 169–190.

- Seed, H. B., & Peacock, W. H. (1971). Test Procedures for Measuring Soil Liquefaction Characteristics. *Journal of the Soil Mechanics and Foundations Division, ASCE*, 97(SM8), 1099–1119.
- Seed, H. B., Seed, R. B., Harder, L. F., & Jong, H. (1989). *Re-evaluation of the lower San Fernando Dam - Report 2 Examination of the post-earthquake slide of February 9, 1971*. H.Bolton Seed Inc. Orinda, California.
- Seidalinova, A. (2014). *Monotonic and cyclic shear loading response of fine-grained gold tailings*. M.ASc. Thesis, The University of British Columbia. Retrieved from [circle.ubc.ca/handle/2429/46531](http://circle.ubc.ca/handle/2429/46531) [accessed April 22, 2014]
- Seidalinova, A., & Wijewickreme, D. (2013). Effect of specimen preparation and mechanical overconsolidation on the laboratory monotonic shear response of thickened gold tailings. In *66th Canadian Geotechnical Conference*. Montreal, Quebec.
- Shibata, T., Yukimoto, H., & Miyoshi, M. (1972). Liquefaction process of sand during cyclic loading. *Soils and Foundations, Japanese Society of Soil Mechanics and Foundation Engineering*, 12(1), 1–16. Retrieved from <http://ci.nii.ac.jp/naid/110006151456/> [accessed February 25, 2014]
- Silver, M. L., Chan, C. K., Ladd, R. S., Lee, K. L., Tiedemann, D. A., Townsend, F. C., Valera, J.E., & Wilson, J. H. (1976). Cyclic Triaxial Strength of Standard Test Sand. *Journal of the Geotechnical Engineering Division, ASCE*, 102(GT5), 511–523.
- Silver, M. L., & Seed, H. B. (1971). Deformation characteristics of sands under cyclic loading. *Journal of the Soil Mechanics and Foundations Division, ASCE*, 97(SM8), 1091–1098.
- Sivathayalan, S. (1994). *Static, cyclic and post liquefaction simple shear response of sands*. M.ASc. Thesis, The University of British Columbia. Retrieved from <https://circle.ubc.ca/handle/2429/3527> [accessed May 6, 2014]
- Sriskandakumar, S. (2004). *Cyclic loading response of Fraser River sand for validation of numerical models simulating centrifuge tests*. M.ASc. Thesis, The University of British Columbia. Retrieved from <https://circle.ubc.ca/handle/2429/15189> [accessed November 14, 2013]
- Tanaka, H., & Locat, J. (1999). A microstructural investigation of Osaka Bay clay: the impact of microfossils on its mechanical behaviour. *Canadian Geotechnical Journal*, 36(3), 493–508. doi:10.1139/t99-009
- Tatsuoka, F., Ochi, K., Fujii, S., & Okamoto, M. (1986). Cyclic undrained triaxial and torsional shear strength of sands for different sample preparation methods. *Soils and Foundations, Japanese Society of Soil Mechanics and Foundation Engineering*, 26(3), 23–41.

- Terzaghi, K., & Peck, R. B. (1968). *Soil Mechanics in Engineering Practice*. New York: John Wiley and Sons Inc.
- Thevanayagam, S. (1998). Effect of fines and confining stress on undrained shear strength of silty sands. *Journal of Geotechnical and Geoenvironmental Engineering*, 124(6), 479–491. Retrieved from [http://ascelibrary.org/doi/abs/10.1061/\(ASCE\)1090-0241\(1998\)124:6\(479\)](http://ascelibrary.org/doi/abs/10.1061/(ASCE)1090-0241(1998)124:6(479)) [accessed July 3, 2014]
- Tohno, I., & Yasuda, S. (1981). Liquefaction of the ground during the 1978 Miyagiken-Oki earthquake. *Soils and Foundations, Japanese Society of Soil Mechanics and Foundation Engineering*, 21(3). Retrieved from <http://ci.nii.ac.jp/naid/110003914689/> [accessed April 15, 2014]
- Toki, S., Tatsuoka, F., Miyura, S., Yoshimi, Y., Yasuda, S., & Makihara, Y. (1986). Cyclic undrained triaxial strength of sand by a cooperative test program. *Soils and Foundations, Japanese Society of Soil Mechanics and Foundation Engineering*, 26(3), 117–128.
- Troncoso, J. H. (1986). Critical state of tailing silty sands for earthquake loadings. *Soil Dynamics and Earthquake Engineering*, 5(3), 248–252.
- Troncoso, J., Ishihara, K., & Verdugo, R. (1988). Aging effects on cyclic shear strength of tailings materials. In *Proceedings of 9th world conference on earthquake engineering* (pp. 121–126). Tokyo-Kyoto. Retrieved from [ww.iitk.ac.in/nicee/wcee/article/9\\_vol3\\_121.pdf](http://www.iitk.ac.in/nicee/wcee/article/9_vol3_121.pdf) [accessed May 22, 2014]
- Vaid, Y. P., & Chern, J. C. (1983). Mechanism of deformation during cyclic undrained loading of saturated sands. *International Journal of Soil Dynamics and Earthquake Engineering*, 2(3), 171–177. doi:10.1016/0261-7277(83)90014-1
- Vaid, Y. P., & Chern, J. C. (1985). Cyclic and monotonic undrained response of sands. In V. Khosla (Ed.), *Advances in the Art of Testing Soils Under Cyclic Conditions, Sponsored by the Geotechnical Engineering Division New York in conjunction with the ASCE Convention* (pp. 120–147). Detroit, Michigan.
- Vaid, Y. P., Chung, E. K. F., & Kuerbis, R. H. (1990). Stress path and steady state. *Canadian Geotechnical Journal*, 27(1), 1–7. Retrieved from <http://www.nrcresearchpress.com/doi/abs/10.1139/t90-001> [accessed July 3, 2014]
- Vaid, Y. P., & Finn, W. D. L. (1979). Static Shear and Liquefaction Potential. *Journal of the Geotechnical Engineering Division, ASCE*, 105(GT10), 1233–1246.
- Vaid, Y. P., & Negussey, D. (1988). Preparation of reconstituted sand specimens. In R. T. Donaghe, R. C. Chaney, & M. L. Silver (Eds.), *Advanced triaxial testing of soil and rock, ASTM, STP 977* (pp. 405–417). Philadelphia: American Society for Testing and Materials.

- Vaid, Y. P., Robertson, P. K., & Campanella, R. G. (1979). Strain rate behaviour of Saint-Jean-Vianney clay. *Canadian Geotechnical Journal*, 16(1), 34–42. Retrieved from <http://www.nrcresearchpress.com/doi/abs/10.1139/t79-004> [accessed November 23, 2013]
- Vaid, Y. P., & Sivathayalan, S. (1996). Static and cyclic liquefaction potential of Fraser Delta sand in simple shear and triaxial tests. *Canadian Geotechnical Journal*, 33(2), 281–289. Retrieved from <http://www.nrcresearchpress.com/doi/abs/10.1139/t96-007> [accessed February 24, 2014]
- Vaid, Y. P., Sivathayalan, S., & Stedman, D. (1999). Influence of specimen-reconstituting method on the undrained response of sand. *Geotechnical Testing Journal*, 22(3), 187–195. Retrieved from [http://www.astm.org/DIGITAL\\_LIBRARY/JOURNALS/GEOTECH/PAGES/GTJ11110J.htm](http://www.astm.org/DIGITAL_LIBRARY/JOURNALS/GEOTECH/PAGES/GTJ11110J.htm) [accessed July 3, 2014]
- Wang, S., & Luna, R. (2011). Monotonic behavior of mississippi river valley silt in triaxial compression. *Journal of Geotechnical and Geoenvironmental Engineering*, 138(4), 516–525. doi:10.1061/(ASCE)GT.1943-5606.0000603.
- Wang, W. (1979). *Some findings in soil liquefaction*. Earthquake Engineering Department, Water Conservancy and Hydroelectric Power Scientific Research Institute. Beijing.
- Wijewickreme, D., & Sanin, M. V. (2008). Cyclic Shear Response of Undisturbed and Reconstituted Low-Plastic Fraser River Silt. In *Geotechnical Earthquake Engineering and Soil Dynamics IV* (pp. 1–10). Sacramento, California: American Society of Civil Engineers. doi:10.1061/40975(318)88
- Wijewickreme, D., & Sanin, M. V. (2010). Postcyclic Reconsolidation Strains in Low-Plastic Fraser River Silt due to Dissipation of Excess Pore-Water Pressures. *Journal of Geotechnical and Geoenvironmental Engineering*, 136(10), 1347–1357. Retrieved from [http://ascelibrary.org/doi/pdf/10.1061/\(ASCE\)GT.1943-5606.0000349](http://ascelibrary.org/doi/pdf/10.1061/(ASCE)GT.1943-5606.0000349) [accessed November 14, 2014]
- Wijewickreme, D., Sanin, M. V., & Greenway, G. R. (2005). Cyclic Shear Response of Fine-Grained Mine Tailings. *Canadian Geotechnical Journal*, 42(5), 1408–1421. doi:10.1139/T05-058
- Wong, R. T., Seed, H. B., & Chan, C. K. (1975). Cyclic Loading Liquefaction of Gravelly Soils. *Journal of the Geotechnical Engineering Division, ASCE*, 101(GT6), 571–583.
- Wood, D. M., Drescher, A., & Budhu, M. (1979). On the determination of stress state in the simple shear apparatus. *Geotechnical Testing Journal*, 2(4), 211–221.

- Yamamuro, J. A., & Lade, P. V. (1997). Static liquefaction of very loose sands. *Canadian Geotechnical Journal*, 34(6), 905–917. Retrieved from <http://www.nrcresearchpress.com/doi/pdf/10.1139/t97-057> [accessed August 5, 2014]
- Yoshimi, Y. (1967). An Experimental Study of Liquefaction of Saturated Sands. *Soils and Foundations, Japanese Society of Soil Mechanics and Foundation Engineering*, 7(2), 20–32. Retrieved from <http://ci.nii.ac.jp/naid/110003899131/> [accessed February 22, 2014]
- Yoshimi, Y., & Kuwabara, F. (1973). Effect of subsurface liquefaction on the strength of surface soil. *Soils and Foundations, Japanese Society of Soil Mechanics and Foundation Engineering*, 13(2), 67–81. Retrieved from <http://ci.nii.ac.jp/naid/110003959068/> [accessed February 25, 2014]
- Yoshimi, Y., Tokimatsu, K., Kaneko, O., & Makiyara, Y. (1984). Undrained cyclic shear strength of a dense Niigata sand. *Soils and Foundations, Japanese Society of Soil Mechanics and Foundation Engineering*, 24(4), 131–145. Retrieved from <http://ci.nii.ac.jp/naid/110003983520> [accessed May 10, 2014]
- Youd, T. L. (1972). Compaction of sands by repeated shear straining. *Journal of the Soil Mechanics and Foundations Division, ASCE*, 98(SM7), 709–725.
- Youd, T. L., & Idriss, I. M. (2001). Liquefaction resistance of soils: summary report from the 1996 NCEER and 1998 NCEER/NSF workshops on evaluation of liquefaction resistance of soils. *Journal of Geotechnical and Geoenvironmental Engineering*, 127(4), 297–313. Retrieved from [http://ascelibrary.org/doi/abs/10.1061/\(ASCE\)1090-0241\(2001\)127:10\(817\)](http://ascelibrary.org/doi/abs/10.1061/(ASCE)1090-0241(2001)127:10(817)) [accessed November 14, 2013]
- Youd, T. L., Idriss, I. M., Andrus, R. D., Arango, I., Castro, G., Christian, J. T., Dorby, R., Finn, W.D.L., Harder, L.F., Hynes, M.E., Ishihara, K., Koester, J.P., Liao, S.C., Marcuson, W.F., Martin, G.R., Mitchell, J.K., Moriwaki, Y., Power, M.S., Robertson, P.K., Seed, R.B., & Stokoe, K. H. (2001). Liquefaction resistance of soils: summary report from the 1996 NCEER and 1998 NCEER/NSF workshops on evaluation of liquefaction resistance of soils. *Journal of Geotechnical and Geoenvironmental Engineering*, 127(10), 817–833. Retrieved from [http://ascelibrary.org/doi/abs/10.1061/\(ASCE\)1090-0241\(2001\)127:4\(297\)](http://ascelibrary.org/doi/abs/10.1061/(ASCE)1090-0241(2001)127:4(297)) [accessed November 14, 2013]
- Zapata-Medina, D. G., Finno, R. J., & Vega-Posada, C. A. (2014). Stress history and sampling disturbance effects on monotonic and cyclic responses of overconsolidated Bootlegger Cove clays. *Canadian Geotechnical Journal*, 51(6), 599–609. Retrieved from <http://www.nrcresearchpress.com/doi/abs/10.1139/cgj-2013-0292> [accessed July 28, 2014]
- Zergoun, M., & Vaid, Y. P. (1994). Effective stress response of clay to undrained cyclic loading. *Canadian Geotechnical Journal*, 31(5), 714–727. Retrieved from <http://www.nrcresearchpress.com/doi/abs/10.1139/t94-083> [accessed February 12, 2014]



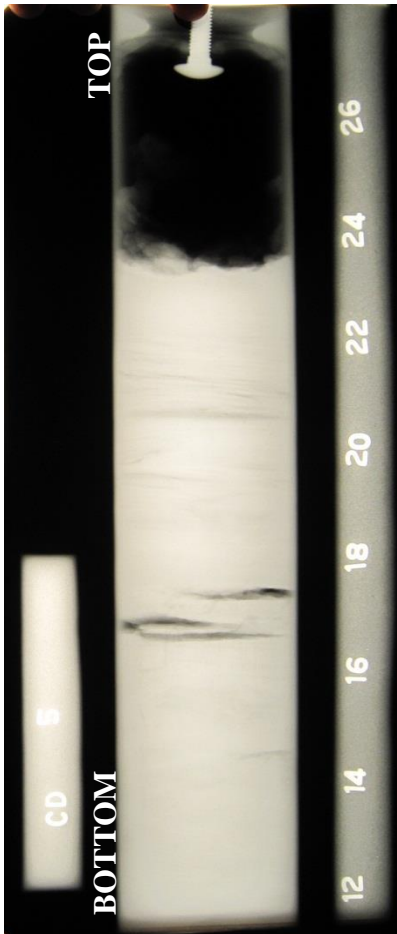
## **Appendices**

### **Appendix A**

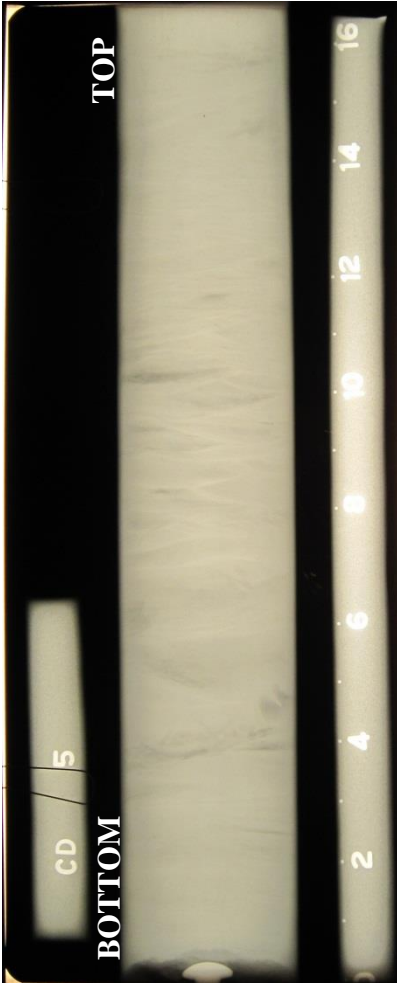
X-ray radiography that was conducted in accordance to the D4452 -06 (ASTM, 2006) using the custom- designed cabinet x-ray system at the Geotechnical laboratory in UBC. The Appendix A provides the details of the x-ray radiography (as referred in Section 3.2.4) conducted for the thin-walled samplers which were used for this research study

## A.1 X-ray Radiograph of Soil Samples from Site #1 [CT]

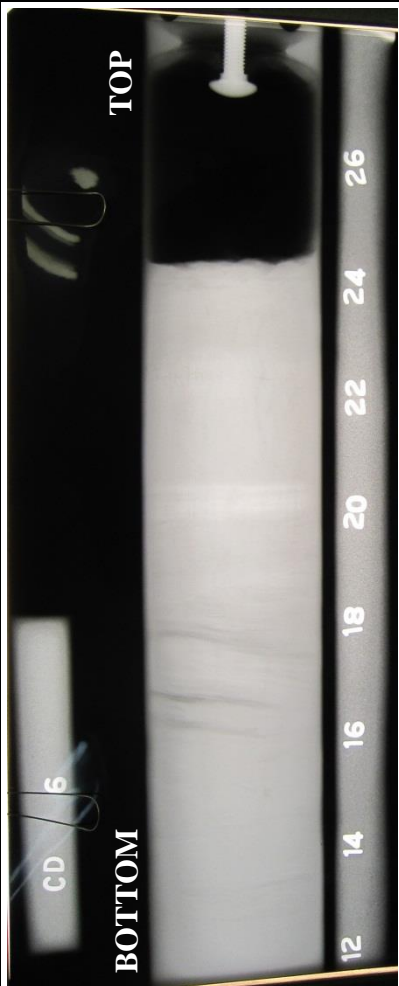
### X-RAY RADIOGRAPH REPORT OF SOIL SPECIMEN

Date	Sample collecting			2/6/2013		
	X-ray imaging			5/8/2013		
	X-ray image processing			5/14/2013		
Sample Collection	Location		Vulcan Way, Richmond			
	Method		Rotary mud drilling Thin walled tube sampler with no inside clearance			
Sample	Number		BH1 S5		Depth	15' - 17'
Specimen	Type	Core in tube	Length	16''	Diameter	3''
	Identification No		CD 5_T	Depth		15' - 16'
Radiography	Radiation period		7 min	Distance source to film		86 cm
	Tube type		Beryllium window	Voltage		120 kVp
				Amperage		3 mA
Attachment		Depth	Interpretation of Radiographic Analysis			
Digital image of processed x-ray film		15'	Voids : Horizontal lines of voids are visible at around 15'6''. It might be an indication of natural fissures.			
			Bedding :Horizontal bedding is visible			
		Disturbance due to Turning of Edges : No traceable turning of edges, hence proper sampling is implied.				
		Peat, Organic Matter and Roots : No significant evidence of peat and organic matter, however, occasional traces for clumps of peat or organic matter are visible at 15'10''. No traceable roots				
		Shells and Invertebrates : No evidence of shells and invertebrates				
		Calcareous Concretions : No evidence of calcareous concretions				
		15'6''	Shear Fractures : No evidence of shear fractures			
		16'				

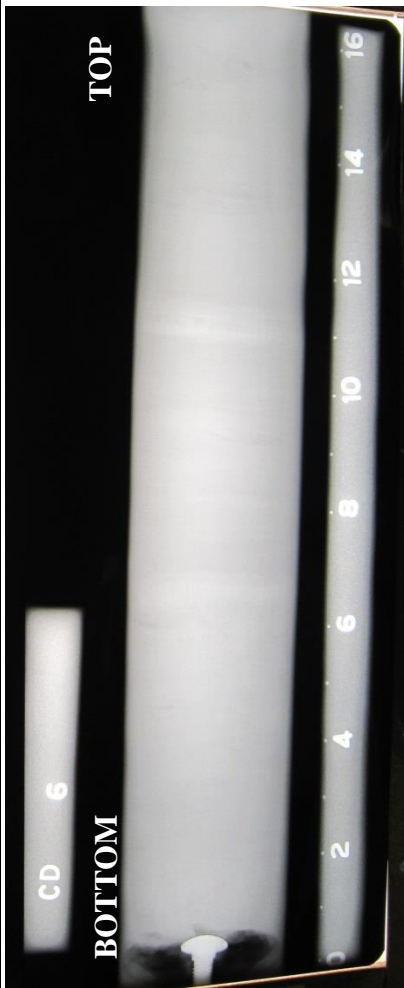
### X-RAY RADIOGRAPH REPORT OF SOIL SPECIMEN

Date	Sample collecting			2/6/2013		
	X-ray imaging			5/8/2013		
	X-ray image processing			5/14/2013		
Sample Collection	Location		Vulcan Way, Richmond			
	Method		Rotary mud drilling Thin walled tube sampler with no inside clearance			
Sample	Number		BH1 S5		Depth	15' - 17'
Specimen	Type	Core in tube	Length	16''	Diameter	3''
	Identification No		CD 5_B	Depth		15'8'' - 17'
Radiography	Radiation period		7 min	Distance source to film		86 cm
	Tube type		Beryllium window	Voltage Amperage		120 kVp 3 mA
Attachment		Depth	Interpretation of Radiographic Analysis			
Digital image of processed x-ray film		15'8''	Voids : No traceable voids			
			Bedding :Horizontal and slightly inclined (14' – 14'2'') bedding are visible			
			Disturbance due to Turning of Edges : No traceable turning of edges, hence proper sampling is implied.			
		16'	Peat, Organic Matter and Roots : No significant evidence of peat and organic matter, however, occasional traces for clumps of peat or organic matter are visible at 16'8''. No traceable roots			
16'6''	Shells and Invertebrates : No evidence of shells and invertebrates					
	17'	Calcareous Concretions : No evidence of calcareous concretions				
Shear Fractures : No evidence of shear fractures						

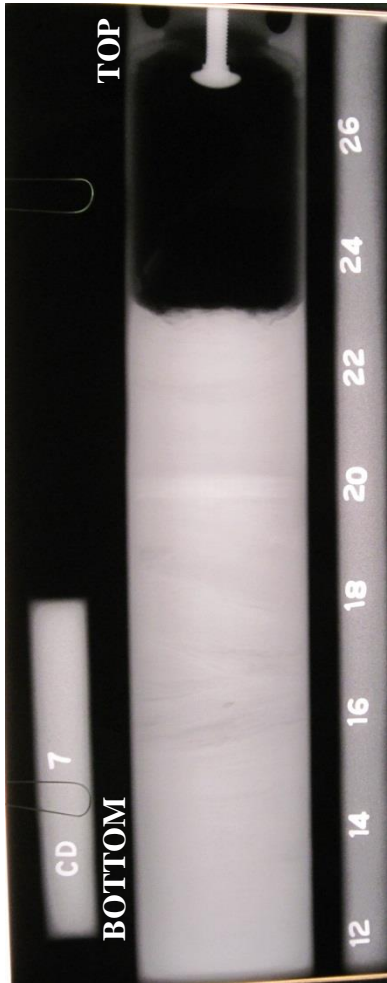
### X-RAY RADIOGRAPH REPORT OF SOIL SPECIMEN

Date	Sample collecting			2/6/2013		
	X-ray imaging			5/14/2013		
	X-ray image processing			5/15/2013		
Sample Collection	Location		Vulcan Way, Richmond			
	Method		Rotary mud drilling Thin walled tube sampler with no inside clearance			
Sample	Number		BH1 S6		Depth	17'6" - 19'6"
Specimen	Type	Core in tube	Length	16"	Diameter	3"
	Identification No		CD 6_T	Depth		17'6" - 18'6"
Radiography	Radiation period		7 min	Distance source to film		86 cm
	Tube type		Beryllium window	Voltage Amperage		120 kVp 3 mA
Attachment		Depth	Interpretation of Radiographic Analysis			
Digital image of processed x-ray film		17'6"	Voids : No traceable voids			
			Bedding :Horizontal and slightly inclined (18' – 18'2") bedding are visible			
			Disturbance due to Turning of Edges : No traceable turning of edges, hence proper sampling is implied.			
		Peat, Organic Matter and Roots : No significant evidence of presence peat and organic matter, however, occasional traces of peat or organic matter are visible at 18'3". No traceable roots				
		18'	Shells and Invertebrates : No evidence of shells and invertebrates			
		Calcareous Concretions : No evidence of calcareous concretions				
		18'6"	Shear Fractures : No evidence of shear fractures			

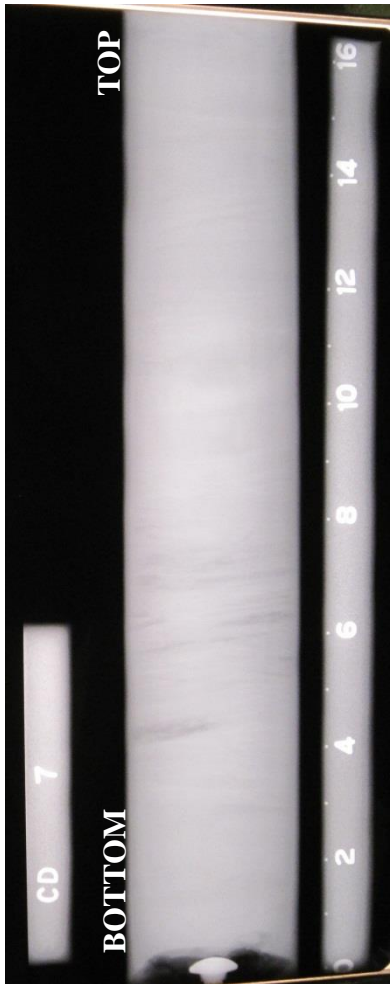
### X-RAY RADIOGRAPH REPORT OF SOIL SPECIMEN

Date	Sample collecting			2/6/2013		
	X-ray imaging			5/14/2013		
	X-ray image processing			5/15/2013		
Sample Collection	Location		Vulcan Way, Richmond			
	Method		Rotary mud drilling Thin walled tube sampler with no inside clearance			
Sample	Number		BH1 S6		Depth	17'6" - 19'6"
Specimen	Type	Core in tube	Length	16"	Diameter	3"
	Identification No		CD 6_B	Depth		18'2" - 19'6"
Radiography	Radiation period		7 min	Distance source to film		86 cm
	Tube type		Beryllium window	Voltage Amperage		120 kVp 3 mA
Attachment		Depth	Interpretation of Radiographic Analysis			
Digital image of processed x-ray film		18'2"	Voids : No traceable voids			
			Bedding :Horizontal bedding is visible			
			Disturbance due to Turning of Edges : No traceable turning of edges, hence proper sampling is implied.			
			Peat, Organic Matter and Roots : No evidence of presence peat organic matter and roots			
		18'6"	Shells and Invertebrates : No evidence of shells and invertebrates			
Calcareous Concretions : No evidence of calcareous concretions						
19'	Shear Fractures : No evidence of shear fractures					
19'6"						

### X-RAY RADIOGRAPH REPORT OF SOIL SPECIMEN

Date	Sample collecting			2/6/2013		
	X-ray imaging			5/14/2013		
	X-ray image processing			5/15/2013		
Sample Collection	Location		Vulcan Way, Richmond			
	Method		Rotary mud drilling Thin walled tube sampler with no inside clearance			
Sample	Number		BH1 S7		Depth	20' - 22'
Specimen	Type	Core in tube	Length	16''	Diameter	3''
	Identification No		CD 7_T	Depth		20' - 21'
Radiography	Radiation period		7 min	Distance source to film		86 cm
	Tube type		Beryllium window	Voltage Amperage		120 kVp 3 mA
Attachment		Depth	Interpretation of Radiographic Analysis			
Digital image of processed x-ray film		20'	Voids : No traceable voids			
			Bedding :Horizontal and slightly inclined (20'5' – 20'9'') bedding are visible			
		Disturbance due to Turning of Edges : No traceable turning of edges, hence proper sampling is implied.				
		Peat, Organic Matter and Roots : No significant evidence of presence peat and organic matter, however, occasional traces of peat or organic matter are visible at 20'8''. No traceable roots				
		Shells and Invertebrates : No evidence of shells and invertebrates				
		Calcareous Concretions : No evidence of calcareous concretions				
		20'6''	Shear Fractures : No evidence of shear fractures			
		21'				


### X-RAY RADIOGRAPH REPORT OF SOIL SPECIMEN

Date	Sample collecting			2/6/2013		
	X-ray imaging			5/14/2013		
	X-ray image processing			5/15/2013		
Sample Collection	Location		Vulcan Way, Richmond			
	Method		Rotary mud drilling Thin walled tube sampler with no inside clearance			
Sample	Number		BH1 S7		Depth	20' - 22'
Specimen	Type	Core in tube	Length	16"	Diameter	3"
	Identification No		CD 7_B	Depth		20'10" - 22'
Radiography	Radiation period		7 min	Distance source to film		86 cm
	Tube type		Beryllium window	Voltage Amperage		120 kVp 3 mA
Attachment		Depth	Interpretation of Radiographic Analysis			
Digital image of processed x-ray film		20'10"	Voids : No traceable voids			
			Bedding :Horizontal and slightly inclined (21'6' – 21'8") bedding are visible			
			Disturbance due to Turning of Edges : No traceable turning of edges, hence proper sampling is implied.			
		21'	Peat, Organic Matter and Roots : No significant evidence of presence peat and organic matter, however, occasional traces of peat or organic matter are visible at 21'6". No traceable roots			
21'6"	Shells and Invertebrates : No evidence of shells and invertebrates					
	Calcareous Concretions : No evidence of calcareous concretions					
	22'	Shear Fractures : No evidence of shear fractures				



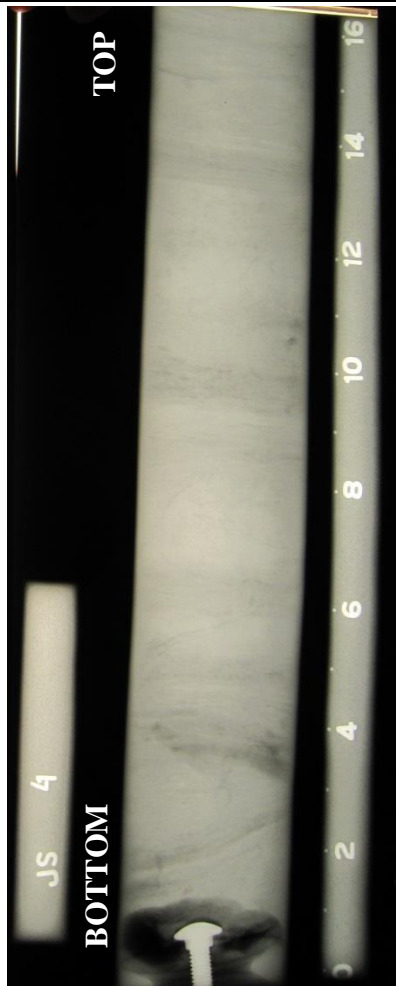
## A.2 X-ray Radiograph of Soil Samples from Site #2 [JS]

### X-RAY RADIOGRAPH REPORT OF SOIL SPECIMEN

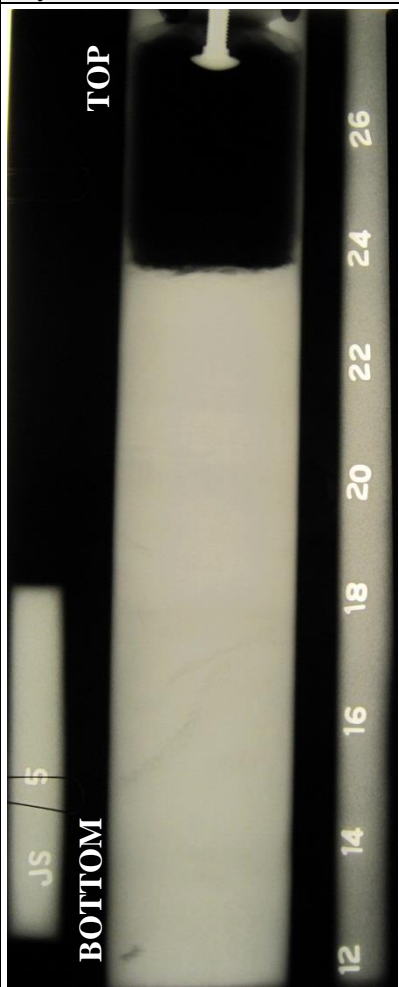
Date	Sample collecting			2/7/2013		
	X-ray imaging			5/15/2013		
	X-ray image processing			5/16/2013		
Sample Collection	Location		160 <sup>th</sup> Street, Surrey			
	Method		Rotary mud drilling Thin walled tube sampler with no inside clearance			
Sample	Number		BH2 S4		Depth	13'6" - 15'6"
Specimen	Type	Core in tube	Length	16"	Diameter	3"
	Identification No		JS 4_T	Depth		13'6" - 14'6"
Radiography	Radiation period		7 min	Distance source to film		86 cm
	Tube type		Beryllium window	Voltage		120 kVp
				Amperage		3 mA
Attachment		Depth	Interpretation of Radiographic Analysis			
Digital image of processed x-ray film		13'6"	Voids : No traceable voids			
			Bedding :Horizontal and slightly inclined (13'10" - 14'4") bedding are visible			
			Disturbance due to Turning of Edges : No traceable turning of edges, hence proper sampling is implied.			
		Peat, Organic Matter and Roots : No evidence of peat, organic matter and roots				
		Shells and Invertebrates : No evidence of shells and invertebrates				
		Calcareous Concretions : No evidence of calcareous concretions				
		14'	Shear Fractures : No evidence of shear fractures			
		14'6"				



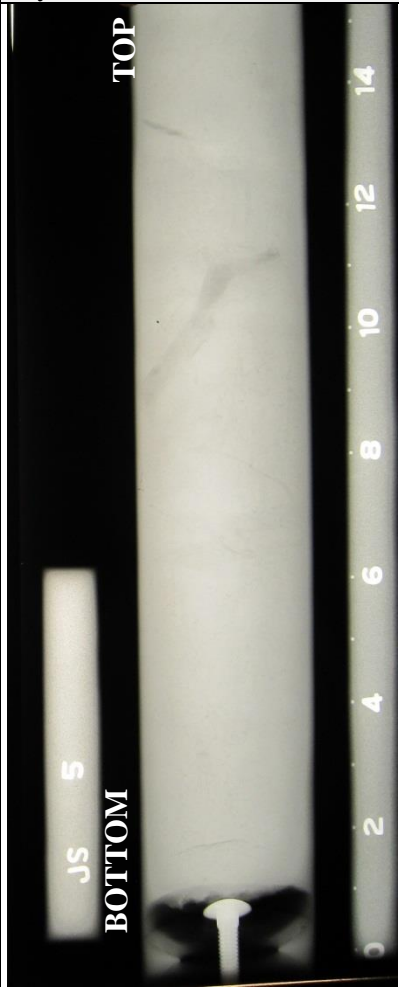
## X-RAY RADIOGRAPH REPORT OF SOIL SPECIMEN

Date	Sample collecting			2/7/2013		
	X-ray imaging			5/15/2013		
	X-ray image processing			5/16/2013		
Sample Collection	Location		160 <sup>th</sup> Street, Surrey			
	Method		Rotary mud drilling Thin walled tube sampler with no inside clearance			
Sample	Number		BH2 S4		Depth	13'6" - 15'6"
Specimen	Type	Core in tube	Length	16"	Diameter	3"
	Identification No		JS 4_B	Depth		14'2" - 15'6"
Radiography	Radiation period		7 min	Distance source to film		86 cm
	Tube type		Beryllium window	Voltage Amperage		120 kVp 3 mA
Attachment		Depth	Interpretation of Radiographic Analysis			
Digital image of processed x-ray film		14'2"	Voids : No traceable voids			
			Bedding :Horizontal and slightly inclined bedding are visible			
			Disturbance due to Turning of Edges : No traceable turning of edges, hence proper sampling is implied.			
			Peat, Organic Matter and Roots : No significant evidence of peat, organic matter and roots, however minor traces of peat or organic matter are visible.			
		14'6"	Shells and Invertebrates : No evidence of shells and invertebrates			
		15'	Calcareous Concretions : No evidence of calcareous concretions			
			Shear Fractures : No evidence of shear fractures			
		15'6"				

## X-RAY RADIOGRAPH REPORT OF SOIL SPECIMEN


Date	Sample collecting			2/7/2013		
	X-ray imaging			5/15/2013		
	X-ray image processing			5/16/2013		
Sample Collection	Location		160 <sup>th</sup> Street, Surrey			
	Method		Rotary mud drilling Thin walled tube sampler with no inside clearance			
Sample	Number		BH2 S5		Depth	16' - 18'
Specimen	Type	Core in tube	Length	16''	Diameter	3''
	Identification No		JS 5_T	Depth		16' - 17'
Radiography	Radiation period		7 min	Distance source to film		86 cm
	Tube type		Beryllium window	Voltage Amperage		120 kVp 3 mA
Attachment		Depth	Interpretation of Radiographic Analysis			
Digital image of processed x-ray film		16'	Voids : No traceable voids			
			Bedding :Horizontal and slightly inclined bedding are visible			
		Disturbance due to Turning of Edges : No traceable turning of edges, hence proper sampling is implied.				
		Peat, Organic Matter and Roots : No significant evidence of peat, organic matter and roots, however, traces of peat or organic matter at a depth of 17' and 16'8'' – 16'10'' are visible.				
		Shells and Invertebrates : No evidence of shells and invertebrates				
		Calcareous Concretions : No evidence of calcareous concretions				
		16'6''	Shear Fractures : No evidence of shear fractures			
		17'				

### X-RAY RADIOGRAPH REPORT OF SOIL SPECIMEN

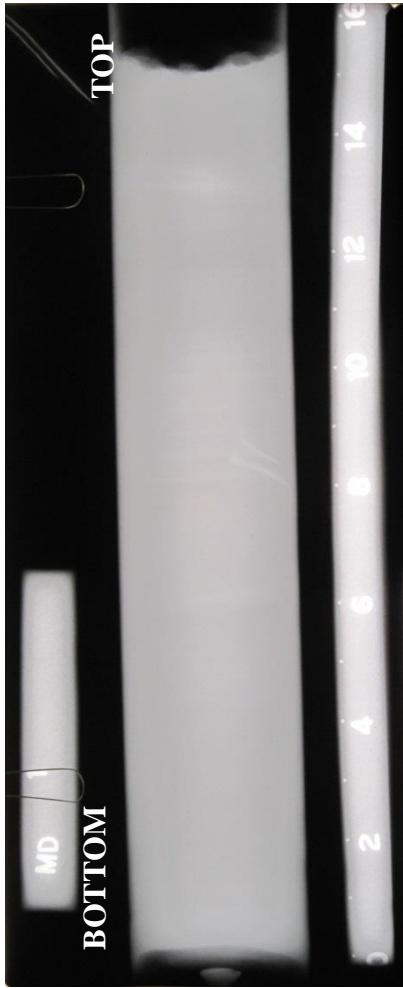
Date	Sample collecting			2/7/2013		
	X-ray imaging			5/15/2013		
	X-ray image processing			5/16/2013		
Sample Collection	Location		160 <sup>th</sup> Street, Surrey			
	Method		Rotary mud drilling Thin walled tube sampler with no inside clearance			
Sample	Number		BH2 S5		Depth	16' - 18'
Specimen	Type	Core in tube	Length	16''	Diameter	3''
	Identification No		JS 5_B	Depth		16'8'' - 18'
Radiography	Radiation period		7 min	Distance source to film		86 cm
	Tube type		Beryllium window	Voltage Amperage		120 kVp 3 mA
Attachment		Depth	Interpretation of Radiographic Analysis			
Digital image of processed x-ray film		16'8''	Voids : No traceable voids			
			Bedding :Horizontal and slightly inclined bedding are visible			
			Disturbance due to Turning of Edges : No traceable turning of edges, hence proper sampling is implied.			
			Peat, Organic Matter and Roots : No significant evidence of peat, organic matter and roots, however, traces of peat or organic matter at a depth of 17' - 17'4'' are visible. Presence of roots is also visible.			
		17'	Shells and Invertebrates : No evidence of shells and invertebrates			
		17'6''	Calcareous Concretions : No evidence of calcareous concretions			
			Shear Fractures : No evidence of shear fractures			
		18'				

### A.3 X-ray Radiograph of Soil Samples from Site #3 [MD]

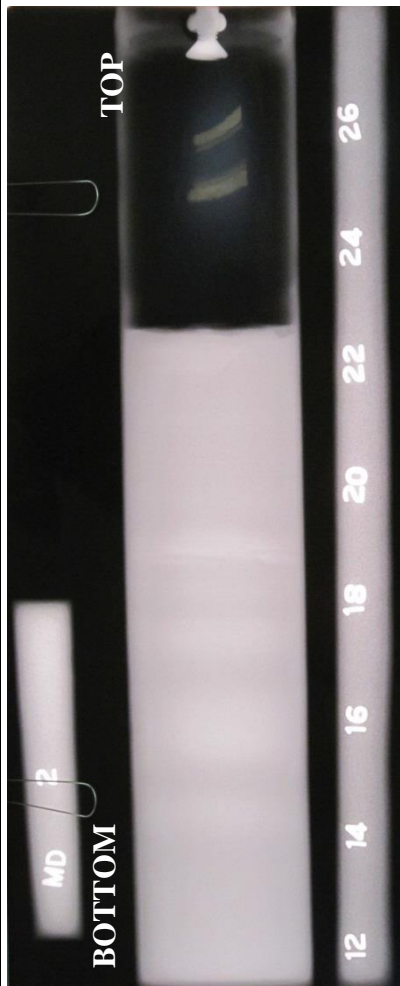
#### X-RAY RADIOGRAPH REPORT OF SOIL SPECIMEN

Date	Sample collecting			2/8/2013		
	X-ray imaging			5/30/2013		
	X-ray image processing			5/31/2013		
Sample Collection	Location		Telegraph Trail, Surrey			
	Method		Rotary mud drilling Thin walled tube sampler with no inside clearance			
Sample	Number		BH3 S1		Depth	15'6" - 17'5"
Specimen	Type	Core in tube	Length	16"	Diameter	3"
	Identification No		MD 1_T	Depth		15'6' - 15'8"
Radiography	Radiation period		7 min	Distance source to film		86 cm
	Tube type		Beryllium window	Voltage Amperage		120 kVp 3 mA
Attachment		Depth	Interpretation of Radiographic Analysis			
Digital image of processed x-ray film			<p><i>Voids</i> : No traceable voids</p> <p><i>Bedding</i> : No bedding is visible</p> <p><i>Disturbance due to Turning of Edges</i> : No traceable turning of edges, hence proper sampling is implied</p> <p><i>Peat, Organic Matter and Roots</i> : No evidence of peat, organic matter and roots</p> <p><i>Shells and Invertebrates</i> : No evidence of shells and invertebrates</p> <p><i>Calcareous Concretions</i> : No evidence of calcareous concretions</p> <p><i>Shear Fractures</i> : No evidence of significant shear fractures.</p>			
						
		15'6"				
		15'8"				

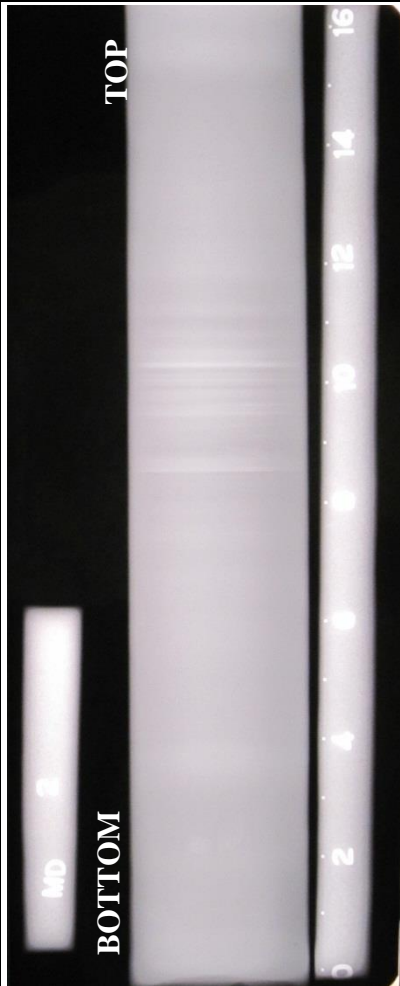
### X-RAY RADIOGRAPH REPORT OF SOIL SPECIMEN

Date	Sample collecting			2/8/2013		
	X-ray imaging			5/30/2013		
	X-ray image processing			5/31/2013		
Sample Collection	Location		Telegraph Trail, Surrey			
	Method		Rotary mud drilling Thin walled tube sampler with no inside clearance			
Sample	Number		BH3 S1		Depth	18' - 20'
Specimen	Type	Core in tube	Length	16"	Diameter	3"
	Identification No		MD 1_B	Depth		15'6' - 16'10"
Radiography	Radiation period		7 min	Distance source to film		86 cm
	Tube type		Beryllium window	Voltage Amperage		120 kVp 3 mA
	Attachment		Depth	Interpretation of Radiographic Analysis		
Digital image of processed x-ray film						
				15'6"	<i>Voids</i> : No traceable voids	
					<i>Bedding</i> : Horizontal (15'8' – 16'2") and slightly inclined (16'4") bedding is visible	
					<i>Disturbance due to Turning of Edges</i> : No traceable turning of edges, hence proper sampling is implied	
				<i>Peat, Organic Matter and Roots</i> : No evidence of peat, organic matter and roots		
			16'	<i>Shells and Invertebrates</i> : No evidence of shells and invertebrates		
				<i>Calcareous Concretions</i> : No evidence of calcareous concretions		
				<i>Shear Fractures</i> : No evidence of significant shear fractures, however, minor shear fracture is visible at 16'10", probably due to the fixing of butterfly nut at the end of the thin-walled tube sampler		
			16'6"			
			16'10"			

### X-RAY RADIOGRAPH REPORT OF SOIL SPECIMEN

Date	Sample collecting			2/8/2013			
	X-ray imaging			5/16/2013			
	X-ray image processing			5/17/2013			
Sample Collection	Location		Telegraph Trail, Surrey				
	Method		Rotary mud drilling Thin walled tube sampler with no inside clearance				
Sample	Number		BH3 S2		Depth	18' - 20'	
Specimen	Type	Core in tube	Length	16''	Diameter	3''	
	Identification No		MD 2_T	Depth		18' - 18'10''	
Radiography	Radiation period		7 min	Distance source to film		86 cm	
	Tube type		Beryllium window	Voltage Amperage		120 kVp 3 mA	
Attachment		Depth	Interpretation of Radiographic Analysis				
Digital image of processed x-ray film							
			18'	<p><i>Voids</i> : No traceable voids</p> <p><i>Bedding</i> :Thin horizontal bedding is visible</p> <p><i>Disturbance due to Turning of Edges</i> : No traceable turning of edges, hence proper sampling is implied.</p> <p><i>Peat, Organic Matter and Roots</i> : No evidence of peat, organic matter and roots.</p> <p><i>Shells and Invertebrates</i> : No evidence of shells and invertebrates</p> <p><i>Calcareous Concretions</i> : No evidence of calcareous concretions</p> <p><i>Shear Fractures</i> : No significant evidence of shear fractures, however minor shear plane is visible at just below 18' depth</p>			
			18'6''				
		18'10''					

### X-RAY RADIOGRAPH REPORT OF SOIL SPECIMEN

Date	Sample collecting			2/8/2013		
	X-ray imaging			5/16/2013		
	X-ray image processing			5/17/2013		
Sample Collection	Location		Telegraph Trail, Surrey			
	Method		Rotary mud drilling Thin walled tube sampler with no inside clearance			
Sample	Number		BH3 S2		Depth	18' - 20'
Specimen	Type	Core in tube	Length	16"	Diameter	3"
	Identification No		MD 2_B	Depth		18'6" - 19'10"
Radiography	Radiation period		7 min	Distance source to film		86 cm
	Tube type		Beryllium window	Voltage Amperage		120 kVp 3 mA
Attachment		Depth	Interpretation of Radiographic Analysis			
Digital image of processed x-ray film		18'6"	<p><i>Voids</i> : No traceable voids</p> <p><i>Bedding</i> :Thin horizontal bedding is visible specially from 18'10" to 19'2"</p> <p><i>Disturbance due to Turning of Edges</i> : No traceable turning of edges, hence proper sampling is implied.</p> <p><i>Peat, Organic Matter and Roots</i> : No evidence of peat, organic matter and roots.</p> <p><i>Shells and Invertebrates</i> : No evidence of shells and invertebrates</p> <p><i>Calcareous Concretions</i> : No significant evidence of calcareous concretions, however, two minor concretions are visible at 19'8"</p> <p><i>Shear Fractures</i> : No evidence of shear fractures</p>			
		19'				
		19'6"				
		19'10"				

## **Appendix B**

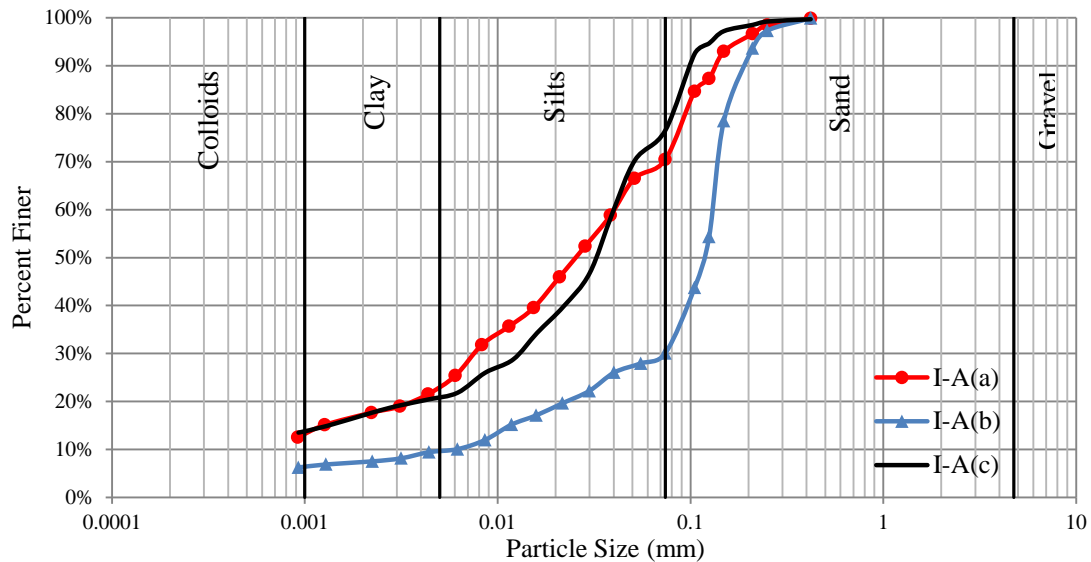
Assessments of particle size gradation that were conducted using sieve analysis and hydrometer analysis in accordance with D422-63 (ASTM, 2007) are presented in Appendix B.

As referred in Section 3.2.5, Appendix B provides the complete set of plots indicating the gradation of soil retrieved from Site #1, #2 and #3.



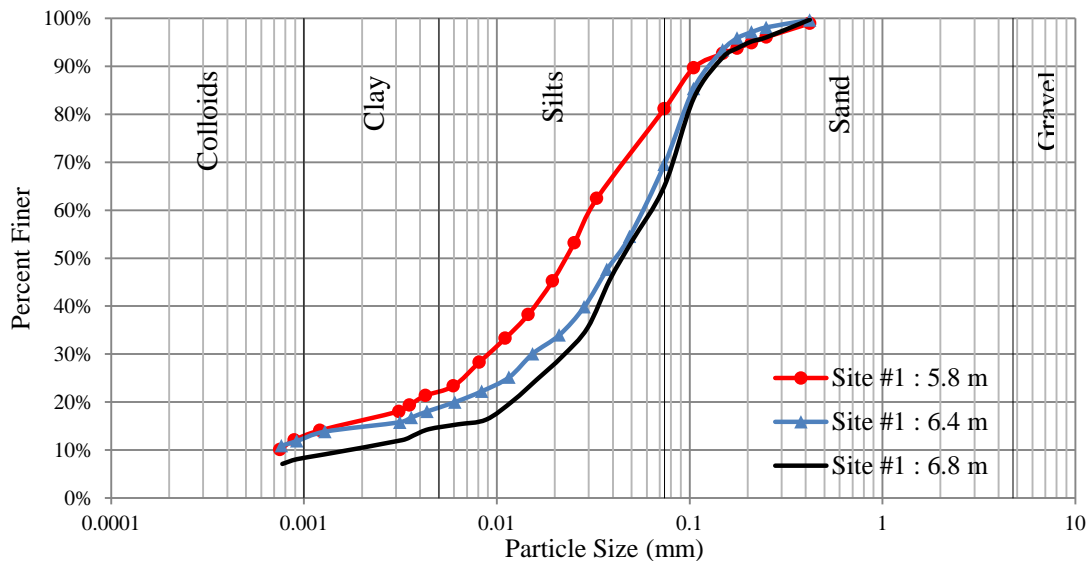
### B.1 Particle Size Analysis of Soil Samples from Site #1 [CT]

Following is a summary of the sieve analysis and hydrometer analysis conducted for three samples which were used for monotonic DSS tests series of I-A(a), I-A(b), and I-A(c)



Particle size	I-A(a)	I-A(b)	I-A(c)
Gravel, passing 3-in. No. 4 sieve %	100	100	100
Sand, passing No. 4 sieve and retained on No. 200 sieve %	31	70	23
<i>Coarse sand, passing No. 4 sieve and retained on No. 10 sieve %</i>	<i>0</i>	<i>0</i>	<i>0</i>
<i>Medium sand, passing No. 10 sieve and retained on No. 40 sieve %</i>	<i>0</i>	<i>0</i>	<i>0</i>
<i>Fine sand, passing No. 40 sieve and retained on No. 200 sieve %</i>	<i>31</i>	<i>70</i>	<i>23</i>
Silt size, 0.074 to 0.005 mm %	47	21	57
Clay size, smaller than 0.005 mm. %	22	9	20
Colloids, smaller than 0.001 mm. %	13	6	14

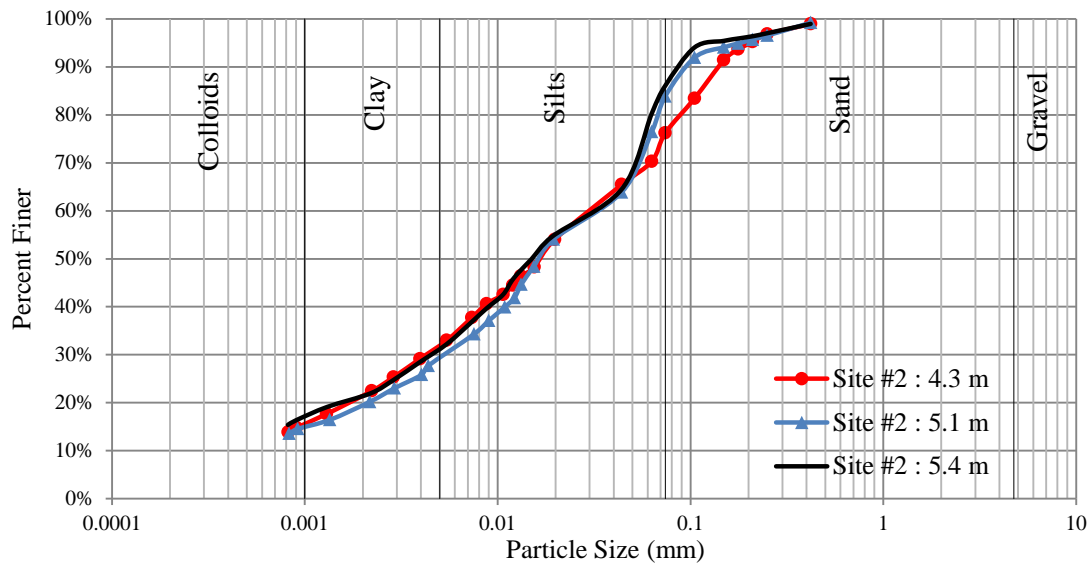
Following is a summary of the sieve analysis and hydrometer analysis conducted for three samples obtained from different depth levels at the Site #1. These samples were used for CDSS tests.



Particle size	At 5.8 m	At 6.4 m	At 6.8 m
Gravel, passing 3-in. No. 4 sieve %	100	100	100
Sand, passing No. 4 sieve and retained on No. 200 sieve %	19	30	35
<i>Coarse sand, passing No. 4 sieve and retained on No. 10 sieve %</i>	<i>0</i>	<i>0</i>	<i>0</i>
<i>Medium sand, passing No. 10 sieve and retained on No. 40 sieve %</i>	<i>1</i>	<i>0</i>	<i>0</i>
<i>Fine sand, passing No. 40 sieve and retained on No. 200 sieve %</i>	<i>18</i>	<i>30</i>	<i>35</i>
Silt size, 0.074 to 0.005 mm %	58	50	50
Clay size, smaller than 0.005 mm. %	23	20	15
Colloids, smaller than 0.001 mm. %	14	13	9

## B.2 Particle Size Analysis of Soil Samples from Site #2 [JS]

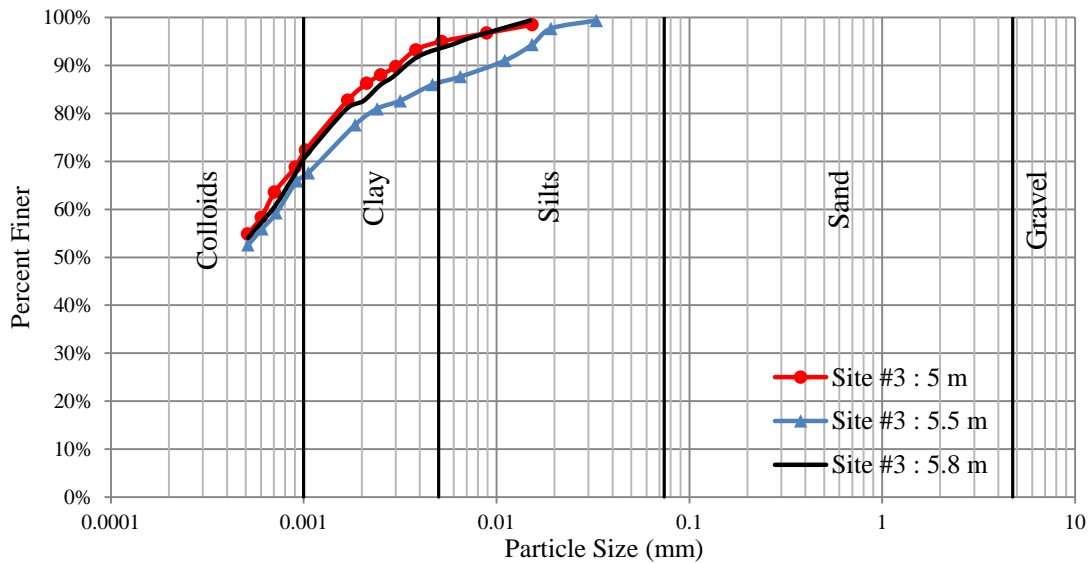
Following is a summary of the sieve analysis and hydrometer analysis conducted for three samples obtained from different depth levels at the Site #2.



Particle size	At 4.3 m	At 5.1 m	At 5.4 m
Gravel, passing 3-in. No. 4 sieve %	100	100	100
Sand, passing No. 4 sieve and retained on No. 200 sieve %	24	16	14
<i>Coarse sand, passing No. 4 sieve and retained on No. 10 sieve %</i>	<i>0</i>	<i>0</i>	<i>0</i>
<i>Medium sand, passing No. 10 sieve and retained on No. 40 sieve %</i>	<i>1</i>	<i>1</i>	<i>1</i>
<i>Fine sand, passing No. 40 sieve and retained on No. 200 sieve %</i>	<i>23</i>	<i>15</i>	<i>13</i>
Silt size, 0.074 to 0.005 mm %	43	56	54
Clay size, smaller than 0.005 mm. %	33	28	32
Colloids, smaller than 0.001 mm. %	17	16	19

### B.3 Particle Size Analysis of Soil Samples from Site #3 [MD]

Following is a summary of the sieve analysis and hydrometer analysis conducted for three samples obtained from different depth levels at the Site #3.



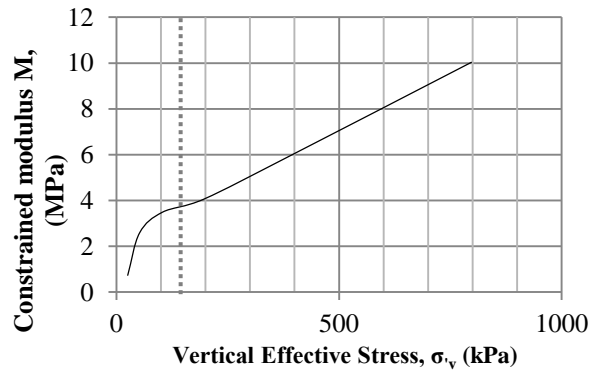
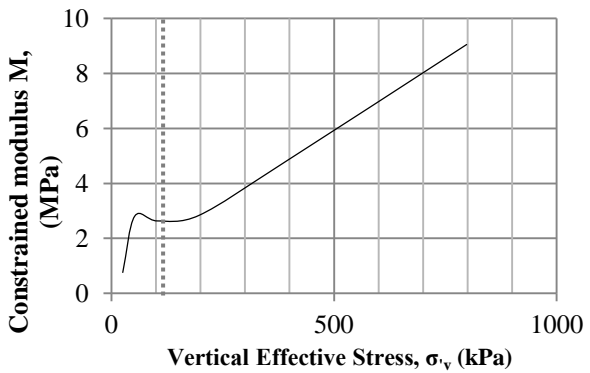
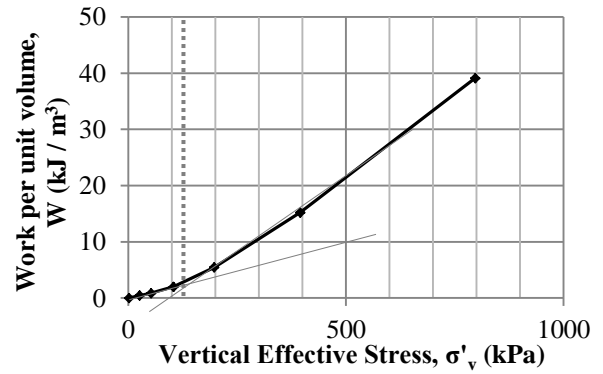
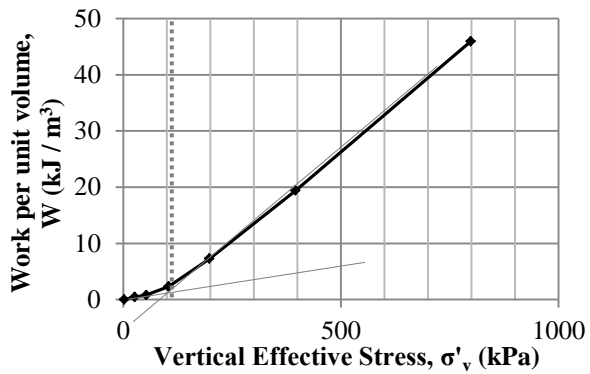
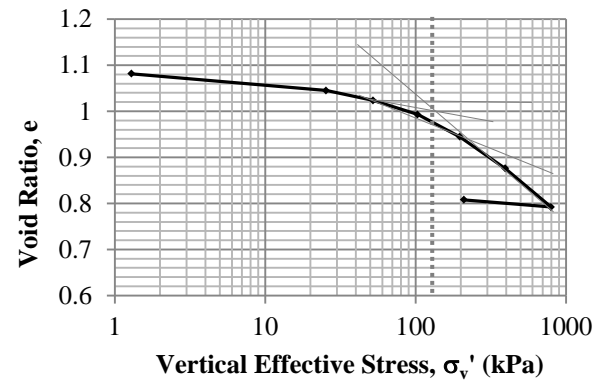
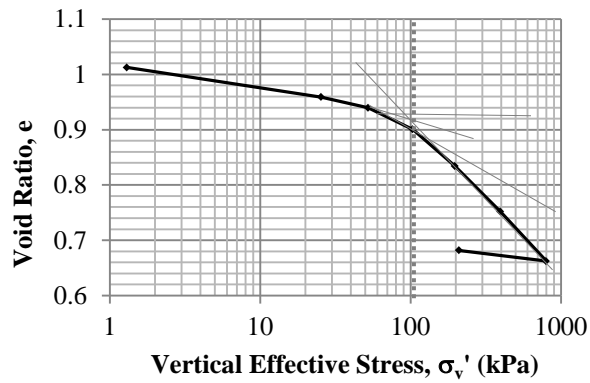
Particle size	At 5.0 m	At 5.5 m	At 5.8 m
Gravel, passing 3-in. No. 4 sieve %	100	100	100
Sand, passing No. 4 sieve and retained on No. 200 sieve %	0	0	0
<i>Coarse sand, passing No. 4 sieve and retained on No. 10 sieve %</i>	<i>0</i>	<i>0</i>	<i>0</i>
<i>Medium sand, passing No. 10 sieve and retained on No. 40 sieve %</i>	<i>0</i>	<i>0</i>	<i>0</i>
<i>Fine sand, passing No. 40 sieve and retained on No. 200 sieve %</i>	<i>0</i>	<i>0</i>	<i>0</i>
Silt size, 0.074 to 0.005 mm %	5	14	7
Clay size, smaller than 0.005 mm. %	95	86	93
Colloids, smaller than 0.001 mm. %	72	67	70

## **Appendix C**

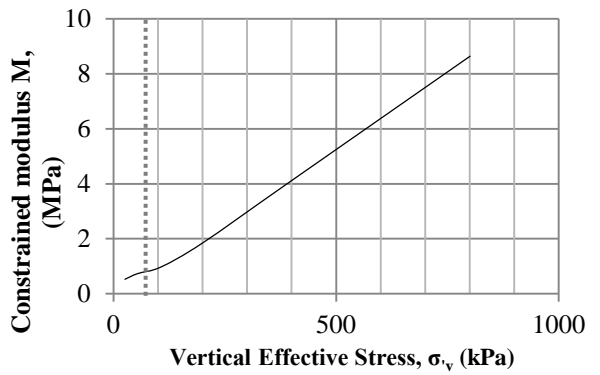
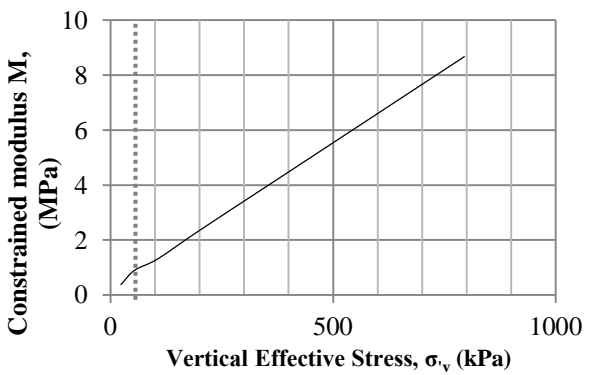
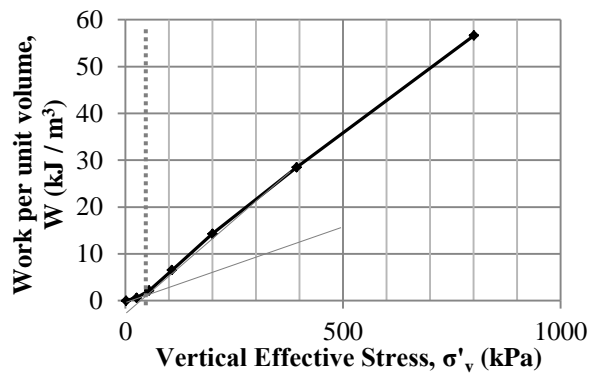
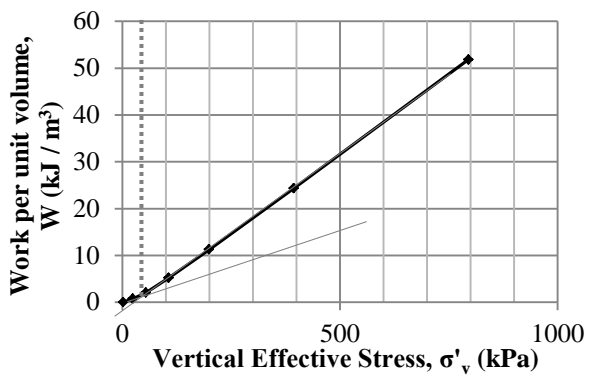
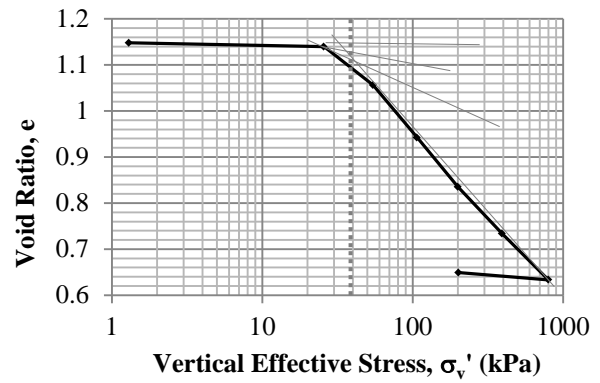
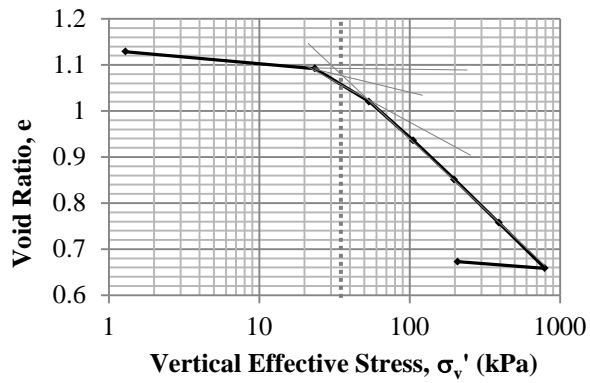
Estimation of pre-consolidation stress for the retrieved soil samples considered in this research study is presented in Appendix C

As referred in Section 3.2.5 and 3.2.6, Appendix C provides the plots in estimating the pre-consolidation stress in accordance with the Casagrande (1936) considering the void ratio and stress relationship, Becker et al. (1987) using the work based approach and Janbu (1969) applying the constrained modulus mechanism.

## C.1 1-D Consolidation Tests on Soil Samples from Site #1 [CT]



## C.2 1-D Consolidation Tests on Soil Samples from Site #2 [JS]



### C.3 1-D Consolidation Tests on Soil Samples from Site #3 [MD]

